EU-MET-EOSMLS-PRECISION
JPL D-16160 / CL#04-2238
EOS MLS DRL 601 (part 4)
ATBD-MLS-04

Earth Observing System (EOS)

Microwave Limb Sounder (MLS)

Precision Estimates for the Geophysical Parameters Measured by EOS MLS

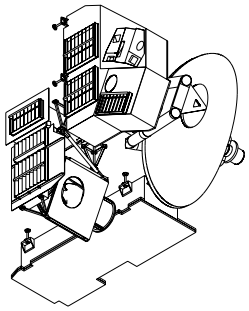

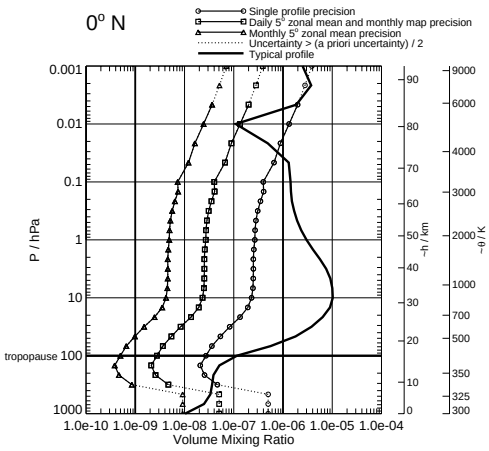

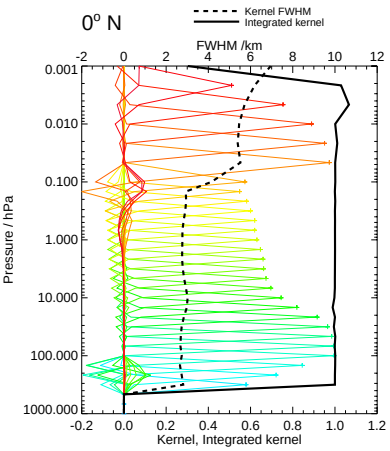

Mark J. Filipiak, Nathaniel J. Livesey and William G. Read

Version 1.4
28 June 2004

University of Edinburgh
King's Buildings
Edinburgh EH9 3JZ, UK

Jet Propulsion Laboratory
California Institute of Technology
Pasadena, California 91109-8099, USA

Release Record

Version	date released	comments
1.0	15 Jan 1999	Initial version
1.1	11 Oct 1999	Released following formal review of Version 1.0 by NASA board reviewing the EOS CHEM Algorithm Theoretical Basis Documents. This document received top grade of 'A' from the review board, but some changes were recommended. The board recommendations which apply to this document are italicised below, followed by the (non-italicised) responses of the MLS team. • *Vertical resolution and the approach to enhancing it should be carefully analysed and validated. Averaging kernels calculated on a high resolution grid (with finer spacing than used in the retrieval if necessary) are critical in this regard. In addition, retrieval simulations on detailed high-resolution synthetic radiance profiles with realistic noise and systematic error values should be studied, the ability to retrieve at higher resolution verified and quantified and constraint effects clearly described. This is critical to low-altitude data quality. Detailed, full, blind retrieval simulations should be done to verify expected performance. It must be demonstrated that the spectral information from well resolved lines provides the additional information necessary to achieve the desired 2 km resolution from a 4–6 km field-of-view.* Averaging kernels have been calculated on a $\sim$0.5 km grid and the high vertical resolution possible for H_2O and temperature in the troposphere verified and analysed (see Section 5). Blind retrieval simulations and detailed sensitivity studies are planned after the operational software is more mature; the results will be documented in later versions of this document. Changes from Version 1.0 are described below. General changes: 1. Scan program updated to conform with that shown in Waters and Froidevaux (2004). 2. Zonal means for HO_2 corrected: these were day+night averages, but HO_2 has a strong diurnal variation. 3. Scene brightness temperature added to T_{sys} to give the total radiance noise. 4. Discussion of the resolution of H_2O and temperature in the troposphere added, including plots of averaging kernels on a 0.5 km grid. Emphasised throughout that reported resolution is *grid* resolution. Additional detailed changes, apart from minor additions/rewordings (in order of appearance in document): 1. Updated Section 2.1 introduction to make plain that profile of radiance and boresight angle is measured. 2. Added Section 2.5 explaining averaging kernels. 3. In Section 3.4 the radiance uncertainty is now computed from a sum of the limb brightness temperature and the system noise temperature. 4. Added Section 3.7 and Table 2 with information on the values of *a priori* used in the averaging kernels. Updated Section 3.6 to emphasise that these *a priori* values were for the precision estimates. 5. Added Section 3.9 on the averaging kernel calculation. 6. In Section 4.1 made explicit that for varying resolution calculations, the resolution was varied only for the measurement shown. 7. Added Section 5 discussing the resolution of H_2O and temperature in the troposphere, and included plots of averaging kernels. 8. Table 3 and all plots updated with results using new formula for radiance uncertainty.

Release Record (continued)

Version	date released	comments
1.2	12 Jan 2003	To be released as 'Version 2.0' following review of draft (especially review of regularisation parameters) by MLS team. Note that the RCS *Revision* number will grow upwards from 1.2 as the document is reviewed and modified, but the *Version* number is put in manually. General changes: 1. Version 1.2 uses the operational retrieval code (including the operational 2D forward model). The discussion of the retrieval is much reduced, since the information is available in other documents. 2. The model atmospheres have been updated. 3. Tikhonov regularisation rather than different grid spacing is used to change the resolution of the retrievals. 4. The precision of derived products (ozone column, relative humidity, geopotential) is calculated from the diagonal elements of the original products (temperature, ozone, water vapor), rather than from their covariance matrices. 5. Estimates for the various retrieval phases/radiometers are included. 6. Averaging kernels are plotted for all products except relative humidity and geopotential. The ones for H2O are a messy and difficult to interpret—may need more work (they are improved with the bug fix for the lower boundary of the regularisation, but other quantities appear to have poorer AKs). 7. The comparison with UARS MLS estimates has been deleted.
1.3	12 Feb 2003	Incorporating Joe's comments, and adjusting some of the L2 configuration to get better averaging kernels. 1. Results updated to use Herb's measured system temperatures and sideband ratios. Regularisation parameters and retrieval ranges made consistent—this removes most of the funny averaging kernels, but there still remain strange oscillations in the water vapour kernels (the kernels for OH and CO with regularisation look strange, but that is because the smoothing is so strong in the upper atmosphere). 2. Minor mishap with the OH vertical regularisation, which should have been a profile like the horizontal regularisation but is 3 pptv everywhere. However, the results look very similar to previous runs with a profile regularisation. Note that the choice of regularisation for OH was experimental, to improve our precision in the lower stratosphere. 3. Added tables for system temperature, sideband ratio, noise bandwidth. These may be condensed to 'typical values', since the actual data will be in a calibration report. 4. Added description of scan program.
1.4 DRAFT	11 June 2004	Updated to the V1.4 configuration. The results should now match the results of the prelaunch simulations, *but there will need to be a further version with all the calibrated system temperatures, etc.* 1. The system temperatures for R5 are changed back to the values used in the simulations. 2. System temperature, etc. tables condensed to typical values. 3. Integrated kernels are now for the 2D integration–they look right now. 4. Several cosmetic changes. 5. Clouds still not included. 6. There is a minor problem with the RHI precision curves: the values are correct, but the *a priori* uncertainty (used *only* to indicate how much information is coming from the measurement) is too small (it does not include the *a priori* temperature uncertainty). This will be corrected before the final version. There is no effect on the actual retrieval.

Release Record (continued)

Version	date released	comments
1.4	28 June 2004	Version corresponding to V1.4 configuration of the retrieval software. Note that the versions of this document are now going to have the same number as the corresponding retrieval software configuration versions, where possible. 1. RHI *a priori* uncertainty now corrected. Note that high resolution RHI is still mainly *a priori*, it is not clear why since the water vapour and temperature are not.

Contents

1 Scope and relation to other documents

This document reports the precision and spatial resolution of EOS MLS measurements, estimated from simulations of the EOS MLS measurement process. The reader is referred to Waters and Froidevaux (2004) for an overview of the EOS MLS experiment.

The simulations use the operational EOS MLS code developed at JPL (Read *et al.* 2004; Schwartz *et al.* 2004; Livesey and Van Snyder 2004) including spectroscopic information and instrument parameters from initial calibration (Jarnot *et al.* 2004). The results are representative of the measurement capabilities of EOS MLS. Clouds *are* included in the operational code (Wu and Jiang 2004) , but have not yet been included in the precision estimates documented here: in the current version a clear atmosphere is assumed. Estimates of the precision of the ice water content (IWC) product for high and low clouds will be included in a future revision. The effects of clouds on the precision of tropospheric H_2O, O_3 and CO are complicated and depend on the type, amount and altitude of the clouds: it is doubtful that simple simulations such as the present will be enough to characterise these effects. Liquid water clouds will not be included: although these absorb strongly in the frequency region used by EOS MLS, they generally occur below the targeted altitude range.

These types of simulations have helped guide some of the EOS MLS instrument design, e.g. feasibility of measuring particular chemical species and placement of spectrometer channels. The current simulations will be useful in planning the scientific exploitation of the EOS MLS data, and serve as a reference to check against the measurement capability in actual operation.

2 Introduction to the simulation model

2.1 EOS MLS

EOS MLS measures electromagnetic radiation emitted from the Earth's atmosphere in the frequency regions 100–600 GHz and 2.5 THz (Waters and Froidevaux 2004). The radiances are measured at a series of boresight angles (equivalent to tangent heights or tangent pressures). The measured radiances as a function of boresight angle can be inverted (Livesey and Van Snyder 2004) to derive profiles of geophysical parameters (the Data Products): chemical mixing ratios, temperature, geopotential height and ice water content (IWC). Tangent pressure and baseline, although not standard geophysical data products, are also produced by the inversion process.

To simulate the EOS MLS measurements, a model atmosphere is used as input to the operational forward model (Read *et al.* 2004), which generates simulated radiances. The other inputs to the forward model are the instrument characteristics (antenna pattern, filter responses, sideband ratios, etc.), spectroscopic data (line strengths, line broadening parameters, continua, extinction, etc.) and the orbit/attitude data, which itself is simulated from Aura and EOS MLS characteristics.

The EOS MLS processing treats the atmosphere as 2D along the orbit track. The geophysical parameters are given as coefficients of a set of triangular basis functions in orbit angle and $\log(\text{pressure})$, to give piecewise bilinear profiles.

2.2 Retrieval process

The method used in EOS MLS to invert the radiances and tangent heights to give geophysical parameters (Livesey and Van Snyder 2004) is optimal estimation (Rodgers 1976), with Tikhonov regularisation applied. One of the products of this method is an estimate of the uncertainty in the geophysical parameters. This uncertainty is given as a covariance matrix $\mathbf{S_x}$, where usually there are correlations between errors at different levels of any one geophysical parameter (because of the limited vertical resolution of EOS MLS), and often there are correlations between errors in different geophysical parameters (e.g. because of overlapping spectral lines). The diagonal elements of $\mathbf{S_x}$ are used as the precision estimates.

The formula for $\mathbf{S_x}$ is

$$\mathbf{S_x} = (\mathbf{S_a}^{-1} + (\Delta^2)^T \mathbf{S_r}^{-1} \Delta^2 + \mathbf{K}^T \mathbf{S_y}^{-1} \mathbf{K})^{-1}, \quad (1)$$

where $\mathbf{S_y}$ is the combined radiance and tangent height uncertainty covariance matrix, $\mathbf{S_a}$ is the *a priori* uncertainty covariance matrix, $\mathbf{S_r}$ is the regularisation 'covariance' matrix, $\mathbf{K}$ is the matrix of sensitivities of radiance and tangent height to changes in geophysical and instrumental parameters, and Δ^2 is a matrix representing the 2nd order central difference operator. In this equation, the measurement process has already been discretised: the radiances (and tangent heights, of course) are measured at discrete tangent heights/orbit angles (integration periods) and the geophysical parameters are given as coefficients of the set of triangular basis functions in orbit angle and $\log(\text{pressure})$.

The radiance uncertainty estimates are based on the initial calibration data (Jarnot *et al.* 2004) for the system temperatures, noise bandwidths and Minor Frame integration times, as processed by the L1B operational code.

The tangent height uncertainty estimates are based on the values given for elevation angle (χ) uncertainties in Waters and Froidevaux (2004). These angles are transformed from χ to tangent height h by scaling with the nominal tangent-point-to-EOSMLS distance for a 16 km tangent height (3062 km). The resulting tangent height uncertainty is then used to construct the tangent height uncertainty covariance matrix.

In simulating the precisions, the model assumes the true atmosphere is the same as that used to calculate sensitivities (or 'derivatives'), so that Equation 1 is valid, i.e., the problem is linear. The method used to calculate the sensitivities $\mathbf{K}$ is described in Read *et al.* (2004). Note that, since the GHz and THz modules have separate scans, there are two separate sets of tangent pressure derivatives.

The *a priori* uncertainty covariance matrix, as its name suggests, is the matrix of the variability of the geophysical or instrumental parameters, derived from climatology or a (large) set of previous measurements. In practice, only limited information is available and the *a priori* can better be considered a stabiliser/regulariser for the inversion of $(\mathbf{K}^T \mathbf{S_y}^{-1} \mathbf{K})$. A very simple *a priori* error covariance matrix is used for the geophysical parameters, with no correlations between parameters, nor between vertical levels or horizontal profiles for each parameter (i.e. the matrix is diagonal). There is a trade-off between stabilising the inversion and biasing the retrieved parameters and uncertainties with the *a priori* values. Generally the *a priori* uncertainty is made large compared with the typical MLS precision so that any bias is small.

Any further stabilisation required is provided by Tikhonov regularisation. The smoothing parameters (regularisation order and weights) are chosen to smooth out unphysical vertical and horizontal oscillations in retrieved geophysical parameters.

The retrieval is done in phases, changing the set of radiometers used at each phase. The final standard product for a species generally comes from one phase (an exception is nitric acid which has the best results using the 190 GHz radiometer (R2) for the upper stratosphere and the 240 GHz radiometer (R3) for the lower stratosphere). Precision and resolution estimates have been made for each of these phases. Each phase corresponds (approximately) to a retrieval using one radiometer plus a 'Core' configuration which includes the 118 GHz radiometer (R1A) and bands in the 190 GHz radiometer to provide temperature and pointing, and several channels from the 190 GHz radiometer (R2) to provide upper-tropospheric water vapour. The results from every phase are also output as diagnostic products.

As a 'touchstone' for the operational results, an estimate of the precision has been calculated using all radiometers (R1A, R2, R3, R4, R5H, R5V), all bands, full ranges, no regularisation, but otherwise with the operational configuration. Further cases, for each phase separately (essentially single radiometer retrievals), have been calculated to compare with the operational diagnostic products.

2.3 Averaging kernels and spatial resolution

The diagonal elements of $\mathbf{S_x}$ give the precision estimates at a specified vertical resolution (set by the basis functions used to represent the geophysical parameters and the regularisation order and weights). Averaging kernels (Rodgers 1990) can be used to estimate the vertical and horizontal resolution. The averaging kernel matrix $\mathbf{A}$ is given by

$$\mathbf{A} = (\mathbf{S_a}^{-1} + (\Delta^k)^T \mathbf{S_r}^{-1} \Delta^k + \mathbf{K}^T \mathbf{S_y}^{-1} \mathbf{K})^{-1} (\mathbf{K}^T \mathbf{S_y}^{-1} \mathbf{K}) \quad (2)$$

The averaging kernel quantifies how the measurement system averages the true values of geophysical parameters (i.e. columns of $\mathbf{A}$) to give the measured values (i.e. rows of $\mathbf{A}$); for an ideal measurement system, $\mathbf{A}$ would be the identity matrix. Although there may be some contribution to the measured value of a 'row' geophysical parameter at a particular level from other ('column') geophysical parameters, the useful quantity for investigating resolution is the averaging kernel for identical 'row' and 'column' geophysical parameters (i.e., on the block diagonal of $\mathbf{A}$)

3 Details of the simulation model

3.1 Introduction

The major part of the simulation is the calculation of the sensitivity matrix $\mathbf{K}$. Calculating $\mathbf{K}$ requires a forward model, which is the model of the first part of the EOS MLS measurement process, from the atmosphere to calibrated radiances. The details and background to the forward model used here and operationally in EOS MLS are given by Read *et al.* (2004).

The full forward model is used to calculate the radiance and the sensitivity matrix at a set of tangent heights (with spacing of approximately 1.3 km from 0–100 km, 5.3 km above 100 km). Then orbit/attitude data is used to interpolate these, using a 2D pointing model, to the measurement tangent positions. At this stage radiance and tangent height uncertainties are calculated. Finally the retrieval code is run to calculate $\mathbf{S_x}$ using Equation 1.

3.2 Input atmosphere

To calculate sensitivities **K** a model atmosphere is required. The EOS MLS model of the atmosphere is 2D along the orbit track. Two typical atmospheres have been chosen for the precision simulations. One is for February at the Equator with tropopause at 100 hPa. This gives a tropical atmosphere near the Equinox. The other is for February at 70N with tropopause at 320 hPa, with unperturbed O_3. This gives a polar winter atmosphere, but with some sunlight for chemical activation.

By experiment it was found that running the models and retrieval with a 5-profile horizontal section was sufficient to give precision estimates consistent with results from longer sections, as long as the results from the centre (i.e. third) profile were used. The input model atmosphere is effectively 1D, spread over the 5 profiles, but the resulting simulations are truly 2D.

Most of the atmospheric parameters (temperature and chemical mixing ratios as a function of pressure) come from a run of the THINAIR model for the year 2003 (see Kinnersley and Harwood (1993) for a description of an earlier version of this model). The THINAIR model produces daylight averaged values, from 1000 to 0.1 hPa. Above 0.1 hPa the parameters are taken from a combination of Shimazaki (1985), AFGL (1985) and Hedin (1990). Some atmospheric parameters have been taken from other sources and combined with the THINAIR model climatology:

- Geopotential height as a function of pressure is calculated using the hydrostatic equation, with reference geopotential height at a reference pressure of 100 hPa set to values from Oort (1983).
- Temperature comes from a UARS Model Climatology [from Grose *et al.*], and in the lower troposphere from the monthly mean values in Oort (1983). The vertical profiles have been smoothed, and the values adjusted in the troposphere to give smooth RH(ice) profiles.
- H_2O comes mainly from a climatology developed from UARS results (Pumphrey *et al.* 1998), with lower tropospheric values from Oort (1983). The values near the tropopause have been calculated directly from SAGE-2 profiles relative to each profile's tropopause. The resulting mean H_2O is then shifted vertically so that the SAGE-2 mean tropopause coincides with the model tropopause. For the February 0N atmosphere, the SAGE-2 profiles from 10S to 10N were averaged, and for the February 70N atmosphere, the SAGE-2 profiles from 50N to 60N were averaged. The vertical profiles have been smoothed, and the values adjusted in the troposphere to give smooth RH(ice) profiles, with values of 35% in the tropical upper troposphere, 70% in the polar upper troposphere.
- O_3 was taken from a variety of sources: Logan (1999) in the troposphere, Wang *et al.* (1995) in the troposphere and stratosphere, a UARS Model Climatology [from Grose *et al.*] in the stratosphere and nighttime results mainly from Cirris measurements (Pumphrey 2002) in the mesosphere and thermosphere. The vertical profiles have been smoothed.
- CO was taken from a variety of sources: a run of the STOCHEM model (Collins *et al.* 1997) in the troposphere, Allen *et al.* (2000) in the stratosphere and mesosphere, ATMOS (1992) in the mesosphere and Solomon *et al.* (1985) in the mesosphere and thermosphere.
- ClO was adjusted to match values from UARS MLS.
- The standard atmospheres have no clouds. In a future version of this document the effect of cirrus clouds on the precision of other tropospheric species (H_2O, O_3 and CO) may be tested using synthetic atmospheres with typical cirrus included.

3.2.1 Magnetic field

Magnetic field effects (Schwartz *et al.* 2004) are included in the simulations for standard resolution (6/decade) but not for high resolution (12/decade), which use an unpolarised model. However, the precisions and averaging kernels for the polarised and unpolarised calculations are very similar, so the results for the high resolution case will be valid.

3.3 Instrument parameters

Sideband fractions (from configuration file
`MLS-Aura_L2Cal-SBFraction_v1-4-1_0000d000.l2cf`),
antenna responses (from
`MLS-Aura_L2Cal-AAAP_v1-4-1_0000d000.txt`,
`MLS-Aura_L2Cal-FOV-Directions_v1-4-0_0000d000.l2cf`),
filter shapes (from
`MLS-Aura_L2Cal-Filters_v1-4-0_0000d000.txt`,
`MLS-Aura_L2Cal-DACSFilters_v1-4-1_0000d000.txt`)
are all taken from pre-calibration results (Jarnot *et al.* 2004). The operational scan program is used (from `MLS-Aura_L1BOA-Full_s6--t_1996d051.h4`).

There are several frequency regions where there are overlapping filters (see Figure 5-3 of Waters and Froidevaux (2004)). These overlaps have been treated by deleting one of the sets of overlapping filters, usually the wider filters, from the simulation (this can result in some very small gaps or some even smaller overlaps remaining). Specifically, the centre filters of each DACS (Digital Auto-Correlator Spectrometer) are used instead of the centre filter of the overlapping 25-filter bank spectrometer.

The 'instrumental' baseline is also retrieved, but this is really a combination of instrument baseline and unmodelled clear-sky radiance, and can be used (as in the operational code) to derive estimates of cloud IWC.

3.4 Spectroscopic data

This comes from
`MLS-Aura_L2Cal-Spectroscopy_v1-4-0_0000d000.l2cf`
which is based on the JPL Catalog (Pickett *et al.* 1992), with line broadening information taken from the literature and a series of measurements made by B.J. Drouin *et al.* at JPL.

Note that the operational retrievals use a reduced version of this file for the non-linear retrievals, but the precisions are expected to be very similar.

3.5 Radiance uncertainty S_y

The radiance uncertainty is taken from simulated L1B outputs, which are calculated from pre-calibration data for system temperature and sideband fraction for each channel (see summaries for the different bands in Table 1), noise bandwidths (see Table 2), and integration times (0.162 s per MIF). In these simulations, the data is from pre-calibration estimates. Calibration T_{sys} is similar ($\pm 20\%$) to the pre-calibration results, except for some R5 filters ($+60\%$) and the wide filters (-60%). However, the improved performance of the wide filters will likely be nullified by the $1/f$ noise which especially affects these filters. It is not clear what the effect will be since the $1/f$ noise is correlated over a radiometer.

Note that the system temperature given in Table 1 should be compared with the atmospheric radiance multiplied by the relevant sideband fraction.

3.6 Tangent height uncertainty S_h

The tangent height uncertainties are based on the values given for elevation angle (χ) uncertainties in Section 5.5 of Waters and Froidevaux (2004). The transformation from χ to tangent height h is approximated by scaling with the nominal tangent-point-to-EOSMLS distance for a 16 km tangent height (3062 km), so that a 1 arcsecond elevation uncertainty is modelled as a 15 metre tangent height uncertainty. The resulting tangent height uncertainty is divided by 3 to convert from 3σ to 1σ errors. This leads to the following values for 1σ tangent height uncertainties: absolute tangent height uncertainty $= 10$ m, tangent height rate uncertainty $= 5\ \mathrm{m\,s^{-1}}$, tangent height jitter $= 10$ m.

In the current version of the precision estimates, the tangent height rate uncertainty is neglected. The absolute tangent height uncertainty and tangent height jitter are combined RSS to give a 14 m tangent height uncertainty, with no correlation between the errors for different integration periods, leading to a diagonal covariance matrix. This uncertainty has been inflated to 30 m in the simulations until there is flight data to confirm the actual performance. The GHz and THz modules have separate scans, so there are two separate covariance matrices for the tangent heights.

3.7 *A priori* uncertainty S_a for the precision estimates

The operational *a priori* uncertainties in the geophysical and instrumental parameters are from configuration file `fillapriori.l2cf`, v1.85. The *a priori* uncertainty is kept the same for varying retrieval grid resolution. The *a priori* uncertainty is assumed uncorrelated, so $\mathbf{S_a}$ is diagonal.

These values are used for both the V1.4 and the Touchstone simulations. The values are deliberately set large to cause as little bias as possible in the results.

Table 1: Typical system noise temperatures and sideband fractions.

Band	Typical T_{sys} /K		Typical sideband fraction	
	Min	Max	lower SB	upperSB
1	1350	1550	1.0	0.0
2	1100	1350	0.5	0.5
3	1150	1250	0.5	0.5
4	950	1250	0.5	0.5
5	1000	1100	0.5	0.5
6	900	1050	0.5	0.5
7	1250	1550	0.5	0.5
8	1550	1650	0.5	0.5
9	1100	1200	0.5	0.5
10	5600	6900	0.5	0.5
11	5800	7000	0.5	0.5
12	5600	6900	0.5	0.5
13	5300	6500	0.5	0.5
14	5400	6900	0.5	0.5
15	17000	17000	0.95	0.05
16	15000	15000	0.8	0.2
17	20000	20000	0.4	0.6
18	15000	15000	0.95	0.05
19	12000	12000	0.8	0.2
20	14000	14000	0.4	0.6
21	1350	1550	1.0	0.0
22	1350	1350	1.0	0.0
23	1100	1100	0.5	0.5
24	1300	1300	0.5	0.5
25	1100	1100	0.5	0.5
26	1400	1400	0.5	0.5
27	1000	1050	0.5	0.5
28	5800	6100	0.5	0.5
29	5800	6000	0.5	0.5
30	5500	5800	0.5	0.5
31	5600	5800	0.5	0.5
32	3600	6000	1.0	0.0
33	3500	4600	0.5	0.5
34	4300	6200	1.0	0.0

Table 2: Noise bandwidth.

channel no.		1	2	3	4	5	6	7	8	9	10
		11	12	13	14	15	16	17	18	19	20
		21	22	23	24	25					
Spectrometer type	no. of channels	Noise bandwidth /MHz									
standard	25	110.000 14.000 74.000	110.000 9.200 74.000	110.000 7.200 110.000	74.000 9.200 110.000	74.000 14.000 110.000	74.000 18.400	55.000 28.000	37.000 37.000	28.000 55.000	18.400 74.000
DACS	129	all channels: 0.097									
narrow	11	37.000 37.000	28.000	18.400	14.000	9.200	7.200	9.200	14.000	18.400	28.000
wide (B32)	4	500.000	500.000	500.000	400.000						
wide (B33)	4	450.000	500.000	500.000	450.000						
wide (B34)	4	500.000	500.000	500.000	400.000						

3.8 Regularisation parameters

The operational (V1.4) regularisation parameters for the geophysical and instrumental parameters are from configuration file `fillapriori.l2cf`, v1.85. The parameters are the costs for the second order central difference of the profile or section in the retrieval (note that the regularisation is based on differences, not derivatives, so varying the grid resolution has an effect on the smoothing). The Touchstone simulations are not regularised (i.e., the resolution is the finest that can be expected from EOS MLS using this retrieval grid).

3.9 Precision estimate calculation

The uncertainties for space/time averages (e.g. zonal means) are calculated by scaling from the single profiles values.

The standard grid resolution is 6/decade ($\sim$2.67 km) from 100 hPa to 0.1 hPa, 3/decade ($\sim$5.33 km) above 0.1 hPa. Some species measurements (H_2O, O_3 and temperature) have sufficient precision and resolution that they are also planned to be retrieved on a finer, 12/decade ($\sim$1.33 km) grid from 1000 to 22 hPa. The actual resolution of the retrieval is controlled by the regularisation parameters.

Some products are derived from the retrieved profiles of mixing ratio, temperature, etc. These products are the stratospheric/mesospheric O_3 column (the column above the tropopause), the profiles of relative humidity with respect to ice, and the geopotential height profile. The O_3 column precision is derived from the O_3 profile precision (with uncertainties in the tropopause height being neglected), the relative humidity profile precision is derived from the H_2O and temperature precision, and the geopotential height profile precision is derived from the reference geopotential precision and the temperature precision (the small effect of H_2O variations being neglected). The derivation is based on the diagonal of the covariance matrix, as is done in the operational retrieval. The actual precision will be slightly better, since there are correlations which average out. However, it is likely that the natural atmospheric variability will mask any differences between the reported and actual precisions.

3.9.1 O_3 column

The stratospheric O_3 column (the column above the tropopause) is a weighted sum of the O_3 profile, the weights being the integrated air number density (converted to Dobson units (DU)) of each triangular basis function above the tropopause, with corrections at the tropopause for part-triangles. If the weights are represented by a matrix $\mathbf{L}$, and the O_3 profile covariance matrix by $\mathbf{S_{O_3}}$, then the stratospheric O_3 column uncertainty $\mathbf{S}_{\mathrm{O_3column}}$ is given by,

$$\mathbf{S}_{\mathrm{O_3column}} = \mathbf{L}^T \mathbf{S_{O_3}} \mathbf{L} \tag{3}$$

and this is approximated in the code by

$$\mathbf{S}_{\mathrm{O_3column}} = \mathbf{L}^T \mathrm{diag}(\mathbf{S_{O_3}}) \mathbf{L}, \tag{4}$$

which will slightly overestimate the uncertainty. In fact, the code calculates

$$\sqrt{\mathbf{S}_{\mathrm{O_3column}}} = \sum \mathbf{L}^T \sqrt{\mathrm{diag}(\mathbf{S_{O_3}})} \tag{5}$$

i.e., sum rather than RSS—this will cause the uncertainty to be further overestimated and will be corrected in a future version of the code.

In these precision estimate simulations, the tropopause is fixed at 320 hPa for February 70N and 100 hPa for February 0N. So the 'stratospheric' O_3 column is really the O_3 column above a specified *pressure*. Operationally, the tropopause pressure will be calculated from the retrieved temperature profiles, using the WMO definition, and the uncertainty in this tropopause pressure will result in the precision of the O_3 column being worse than that reported below in Tables 4 and 3. To set the scale for the contribution of the tropopause pressure (or height) uncertainties, at the tropopause the O_3 concentration is $\sim$4 DU/km, and the uncertainty in the tropopause height will be no larger than 1 km, increasing (RSS) the uncertainty from $\sim$13 DU to $\sim$14 DU.

3.9.2 Relative humidity

The precision of the profile of relative humidity with respect to ice (RHI) is treated similarly to the O_3 column. At H_2O profile level m, RHI is a function g of the H_2O mixing ratio, pressure and temperature, and the RHI covariance matrix $\mathbf{S}_{\mathrm{RHI}_m}$ is given by

$$\mathbf{S}_{\mathrm{RHI}_m} = \mathbf{L}_m^T \mathbf{S}_{\mathrm{H_2O}_m,\mathrm{T}_m} \mathbf{L}_m \tag{6}$$

and approximated by

$$\mathbf{S}_{\mathrm{RHI}_m} = \mathbf{L}_m^T \mathrm{diag}(\mathbf{S}_{\mathrm{H_2O}_m,\mathrm{T}_m}) \mathbf{L}_m, \tag{7}$$

where $\mathbf{L}_m$ is the matrix of $\partial g/\partial \mathrm{H_2O}_m$ and $\partial g/\partial \mathrm{T}_m$ at level m, and $\mathbf{S}_{\mathrm{H_2O}_m,\mathrm{T}_m}$ is the covariance matrix for H_2O and temperature at level m only.

3.9.3 Geopotential height

The geopotential height at pressure p is the sum of the reference geopotential height (refGPH) and a weighted sum of the temperature profile, the weights being the contribution of each triangular basis function (of the temperature profile) to the integral of the hydrostatic equation between the reference pressure and p. If the weights are represented by a matrix $\mathbf{L}$ with weight $= 1$ for the reference geopotential height, and the combined T and reference geopotential height covariance matrix by $\mathbf{S}_{\mathbf{T},\mathrm{refGPH}}$, then the geopotential height covariance matrix $\mathbf{S}_{\mathrm{GPH}}$ is given by,

$$\mathbf{S}_{\mathrm{GPH}} = \mathbf{L}^T \mathbf{S}_{\mathbf{T},\mathrm{refGPH}} \mathbf{L}, \tag{8}$$

approximated by

$$\mathbf{S}_{\mathrm{GPH}} = \mathbf{L}^T \mathrm{diag}(\mathbf{S}_{\mathbf{T},\mathrm{refGPH}}) \mathbf{L}. \tag{9}$$

4 Precision estimates

4.1 General description of plots

In Figures 1 to 133, plots of estimated precision *vs.* pressure and vertical and horizontal averaging kernels are given. Tables 4 and 3 give the estimated precision of the stratospheric O_3 column measurements, neglecting the contribution due to the uncertainty in knowledge of the tropopause pressure (which will increase the uncertainty by approximately 1 DU).

The horizontal grid spacing is 1.5° along the orbit track. The vertical grid spacing varies: 6/decade from 100 hPa to 0.1 hPa, 3/decade above 0.1 hPa. For the species retrieved at high resolution, the grid spacing between 1000 and 22 hPa is 12/decade. The vertical grid points are marked by the symbols on the precision curves and by the + marks on the averaging kernels. The actual resolution of the measurement is controlled by the regularisation, and should be read off from the averaging kernel plots.

The operational retrieval is done in phases (the standard products are taken from a combination of phases, in most cases just from one phase). Precision and resolution estimates have been made for each of these for the V1.4 (with regularisation, selected bands and channels) and Touchstone (without regularisation, maximal channels/bands in R1A and the relevant radiometer) configurations. The phases are:

InitPtan Retrieves temperature, reference geopotential height, and tangent pressure, and relevant baselines. Uses R1A (B1, B32).

UpdatePtan Retrieves temperature, reference geopotential height, and tangent pressure, ozone, and relevant baselines. Uses R1A (B1, B22, B32). Radiance noise is inflated to 2 K in B1 and B32.

InitUTH Retrieves H_2O in troposphere and stratosphere, and relevant baselines. Uses R1A (B1, B32).Uses R2 (B2, B3, B4, B5, B6). Radiance noise is inflated to 2 K in B3, B4 and B6 (since interfering species are not retrieved). Note that tangent pressure and temperature are not retrieved: results from InitPtan and UpdatePtan are used. The a priori uncertainty for H_2O is reduced by a factor of 10 in the troposphere for this phase.

Core This isn't actually a phase, it is the combination of InitPtan, UpdatePtan and InitUTH.

CorePlusR2 Retrieves temperature, reference geopotential height, tangent pressure, CH_3CN, ClO, HCN, HNO_3, H_2O, N_2O, O_3, and relevant baselines. Uses R1A and R2.

CorePlusR3 Retrieves temperature, reference geopotential height, tangent pressure, CO, O_3, and relevant baselines. Uses R1A and R3.

CorePlusR4 Retrieves temperature, reference geopotential height, tangent pressure, BrO, CH_3CN, ClO, HNO_3, HCl, HO_2, HOCl, N_2O, O_3, and relevant baselines. Uses R1A and R4.

CorePlusR5 Retrieves temperature, reference geopotential height, tangent pressure (for both the GHz and THz modules), O_3, OH, and relevant baselines. Uses R1A (B1 and B22 only), R5H and R5V.

The HiRes 'phase' is rather different for V1.4 and Touchstone:

HiRes/V1.4 Retrieves high resolution temperature, reference geopotential height, tangent pressure, high resolution H_2O and relevant baselines. Uses R1A (B1 and B32 only), R2 (B2, B3, B4, B5) and B8 in R3.

HiRes/Touchstone Retrieves high resolution temperature, reference geopotential height, tangent pressure, high resolution H_2O, high resolution O_3, all other species at standard resolution and relevant baselines. Uses all bands in all radiometers.

For each geophysical parameter there are several figures each containing several plots. There are a pair of figures for each phase, with and without regularisation, and, for H_2O, O_3 and temperature, figures for the high resolution grid. Except for geopotential height and relative humidity, in each figure there are six plots, three (precision, vertical averaging kernel, horizontal averaging kernel) for each of the February 70N and February Equator atmospheres. Geopotential height and relative humidity are derived from other products and averaging kernels have not been generated for them.

On each plot the left vertical axis is pressure in hPa. On the precision plots the right axes give approximate height and potential temperature. The vertical range of the plots is from 1000 to 0.001 hPa to correspond to the nominal scan pattern.

On the precision plots the horizontal axis is the estimated precision, which is the square root of the diagonal elements of the covariance matrix $\mathbf{S_x}$.

The precision estimates are for various space/time averages:

single profile no averaging, derived from one radiance profile,

daily zonal mean 5° zone, diurnally-varying species split into day and night, non-diurnally-varying species averaged over day and night, this is equivalent to

monthly map approximately 5° latitude, 20° longitude resolution at mid-latitudes for diurnally-varying species, 5° latitude, 10° longitude resolution at mid-latitudes for non-diurnally-varying species,

monthly zonal mean 5° zone, diurnally-varying species split into day and night, non-diurnally-varying species averaged over day and night.

The lines are dotted where the estimated uncertainty is more than half the *a priori* uncertainty, indicating that retrieved values will be mainly *a priori*. Note, however, that when regularisation is applied, the comparison is still with the unsmoothed *a priori*, and the averaging kernel should be used to indicate the retrieval range (where the peak value of the kernel is greater than 0.75).

A typical profile (the one in the model atmosphere) is also plotted to set the scale.

In the vertical averaging kernel plots, the lower horizontal axis is the kernel value and the integrated kernel value, and the upper axis is the FWHM (in km). The kernels are plotted for each retrieval level (indicated by the + sign on the curve and color-coded). The resolution is plotted as the full width at half-maximum (FWHM) and is at the grid resolution for effectively δ-function kernels. The integrated kernel (integrated in the horizontal and vertical, since the system is two dimensional) will be 1 in regions where the information from the EOS MLS measurements dominates that from the *a priori*.

Since the model atmosphere is homogeneous in the horizontal direction (but the the retrieval *is* two dimensional) only one horizontal averaging kernel need be plotted for each vertical level. The color coding is the same as for the vertical kernels. The FWHM and integrated kernel are plotted as a function of pressure—there is no variation in the horizontal. The integrated kernel and the full-width at half-maximum (FWHM) are not accurate in regions where the kernels are very wide since the chunk size is only 5 profiles. Note that profile -2 is closer to the spacecraft than profile 2.

4.2 Configuration version used

The configurations used to generate these estimates were

v1-3-8-l2pc01-f02-06 for the V1.4 results

v1-3-8-l2pc01-f02-07 for the Touchstone results (no regularisation, all radiances used at once, no optical depth cutoff)

v1-3-8-l2pc01-f02-08 for the results of separate V1.4 phases

v1-3-8-l2pc01-f02-09 for the results of separate V1.4 phases, but with Touchstone configuration.

4.3 Stratospheric O_3 Column

Table 3: Stratospheric O_3 column precision, for varying space/time averages, with typical values and sensitivity to changes in tropopause and stratopause heights. V1.4 results. The precision values do not include any contribution from uncertainties in the tropopause height: the tropopause is fixed at 320 hPa for February 70N and 100 hPa for February 0N. Note that these values are from the L2 code, and so over-estimate the uncertainty

	Stratospheric O_3 Column					
	precision /DU				typical	tropopause height
	single profile	daily zonal mean	monthly map	monthly zonal mean	value /DU	sensitivity /(DU/km)
February 70N	14.6	1.4	1.6	0.3	413	4
February 0N	12.0	1.2	1.3	0.2	247	4

4.4 Plots of estimated precision and averaging kernels

Plots of the precision estimates and averaging kernels are given on the following pages. The plots are in alphabetical order of the parameter name.

Table 4: As Table 4, but Touchstone (no regularisation) results.

	Stratospheric O_3 Column					
	precision /DU				typical	tropopause height
	single profile	daily zonal mean	monthly map	monthly zonal mean	value /DU	sensitivity /(DU/km)
February 70N	13.5	1.3	1.5	0.2	413	4
February 0N	9.9	1.0	1.1	0.2	247	4

Blank page

BrO

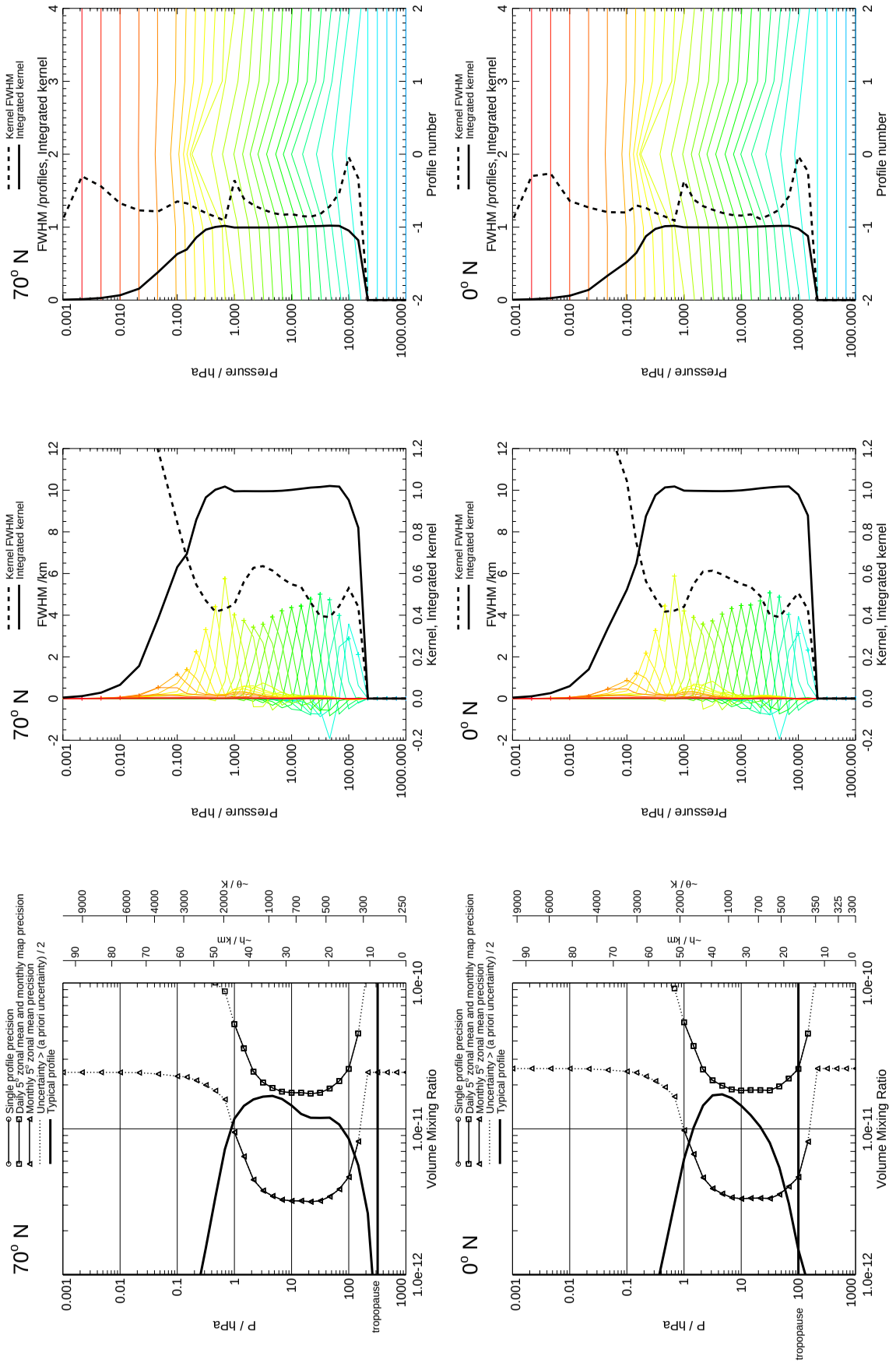

Figure 1: BrO precision and averaging kernels, with V1.4 regularisation. V1.4 phased retrieval.

BrO

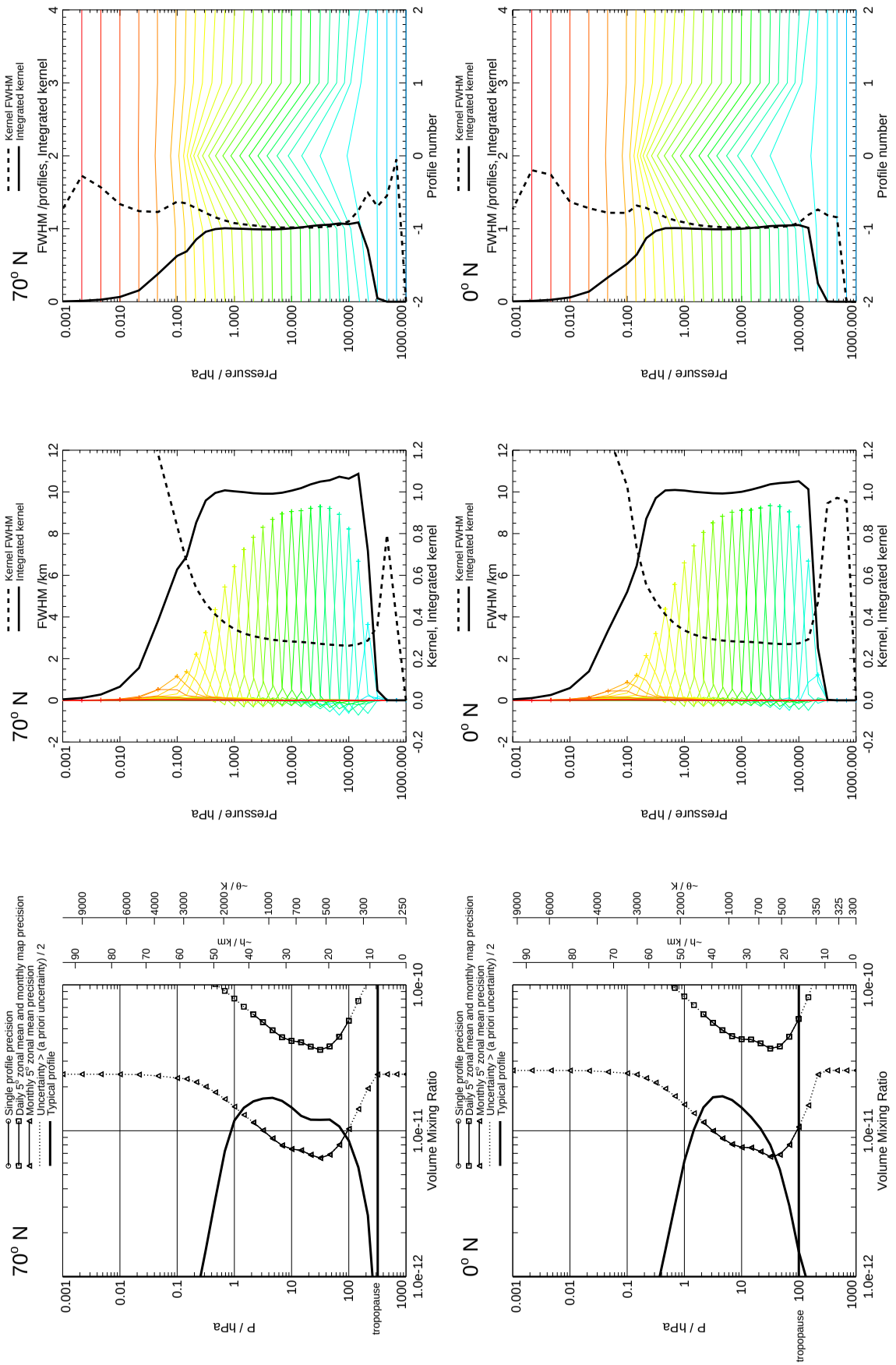

Figure 2: BrO precision and averaging kernels, with no regularisation. Touchstone retrieval.

BrO

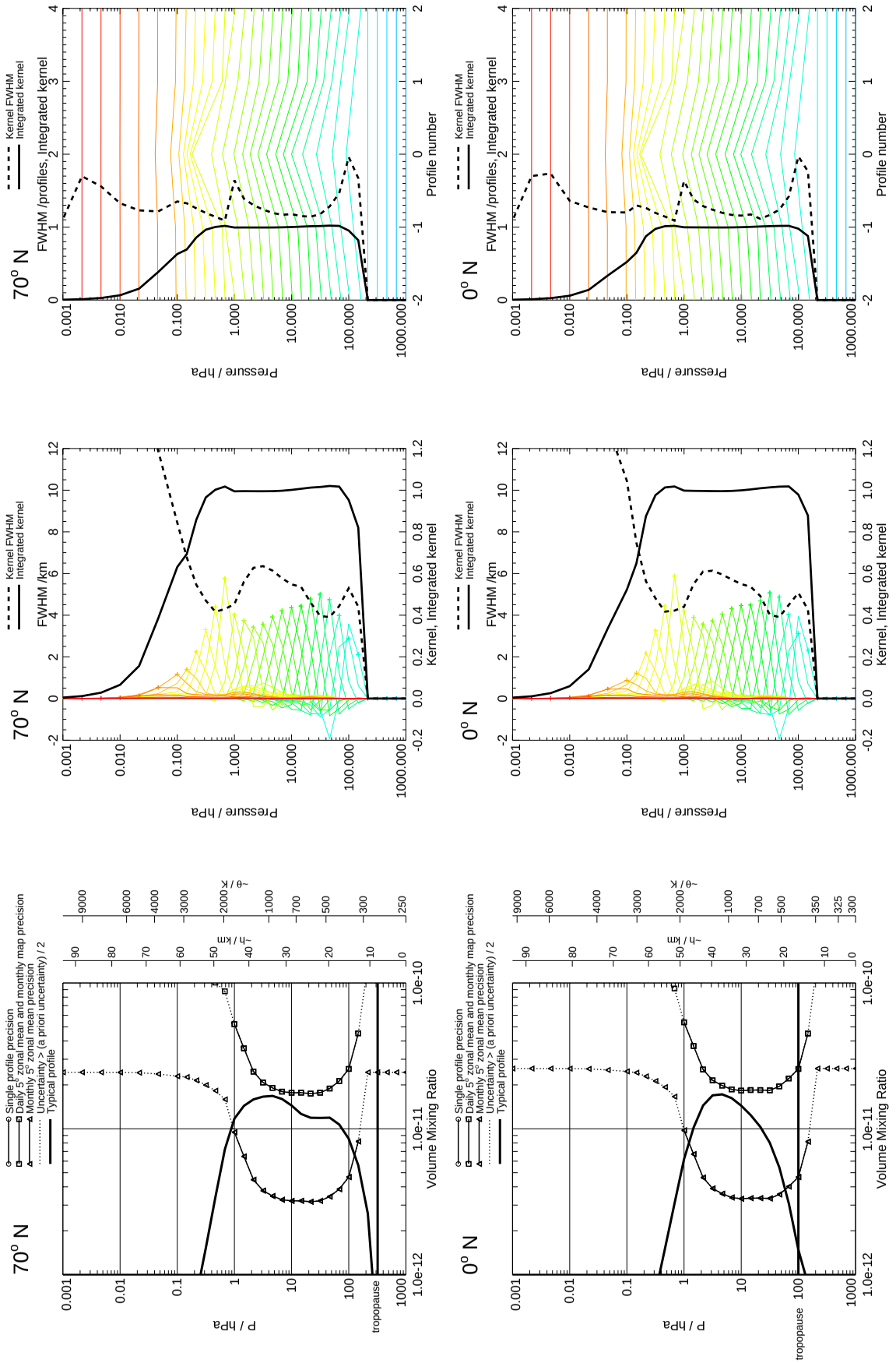

Figure 3: BrO precision and averaging kernels, with V1.4 regularisation. V1.4 phase CorePlusR4.

BrO

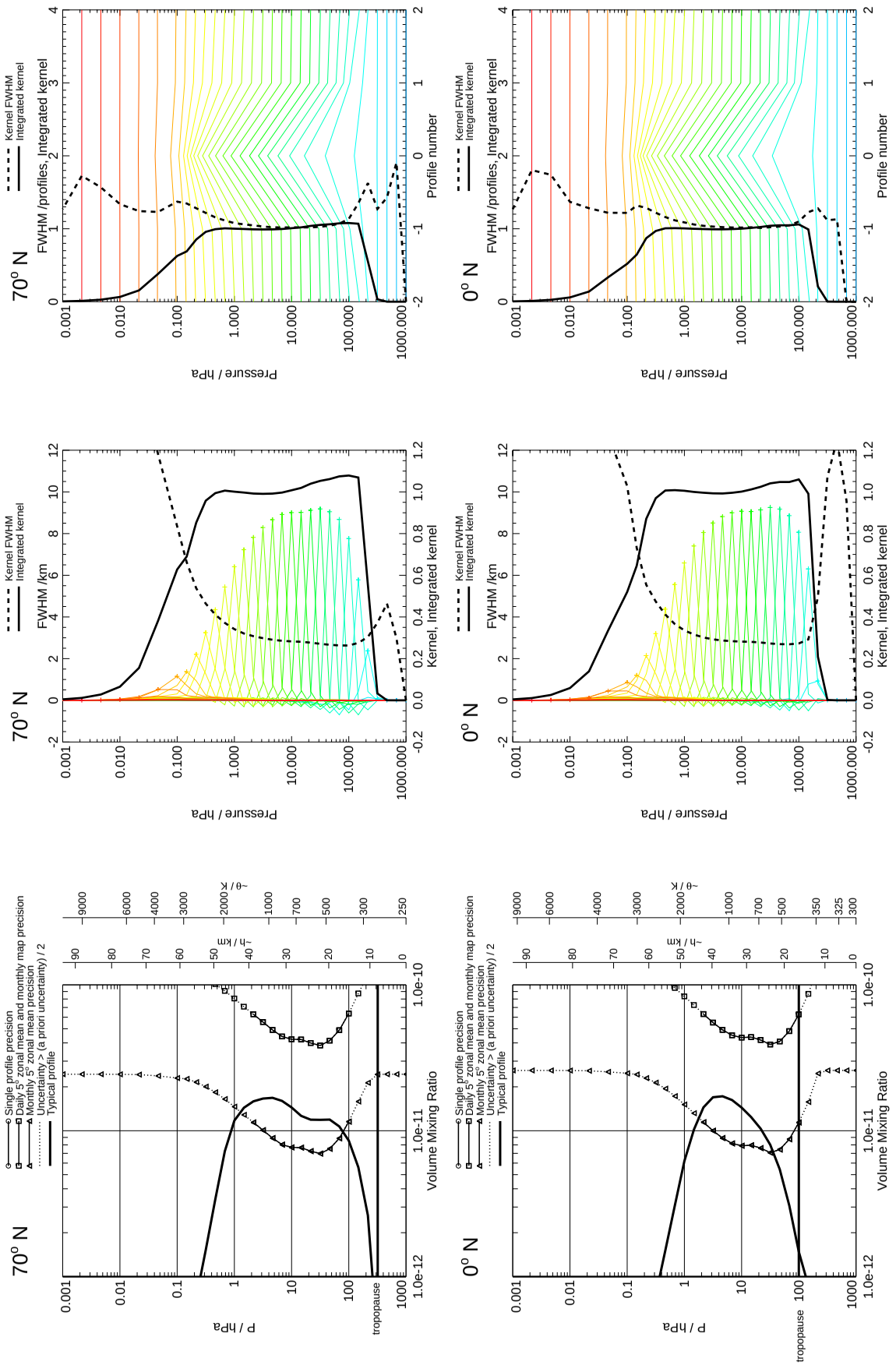

Figure 4: BrO precision and averaging kernels, with no regularisation. Touchstone phase CorePlusR4.

CH_3CN

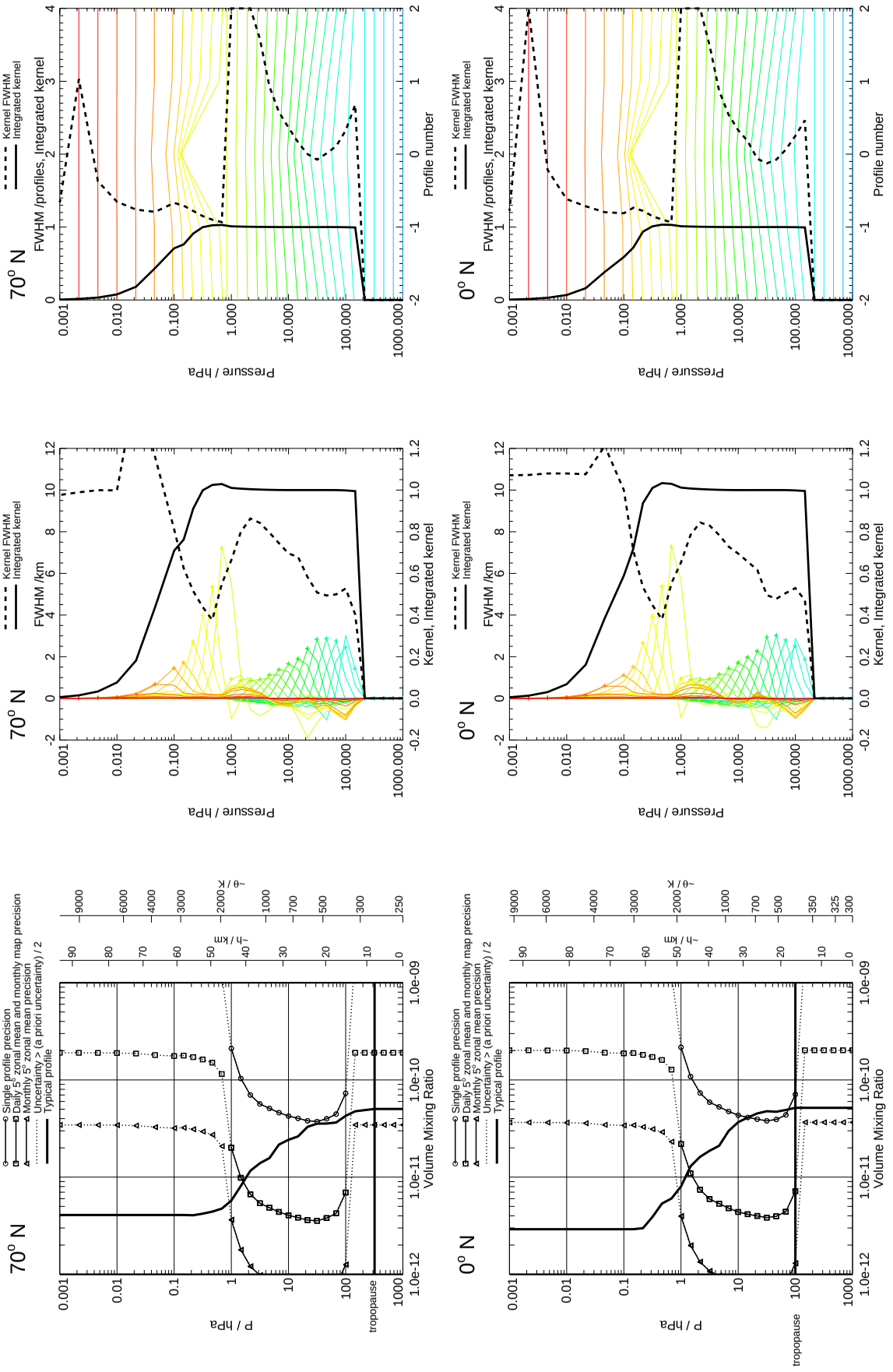

Figure 5: CH_3CN precision and averaging kernels, with V1.4 regularisation. V1.4 phased retrieval.

CH_3CN

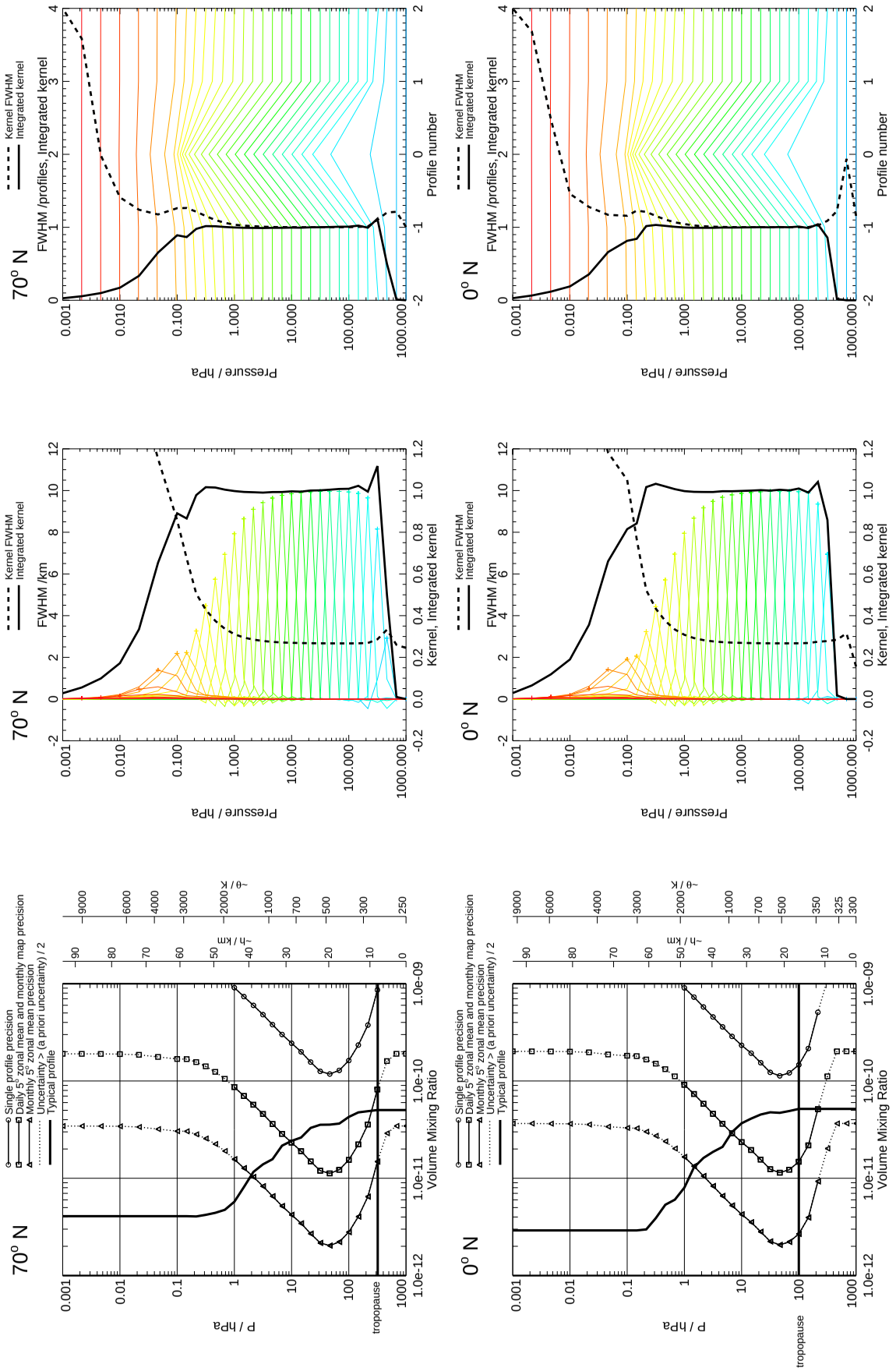

Figure 6: CH_3CN precision and averaging kernels, with no regularisation. Touchstone retrieval.

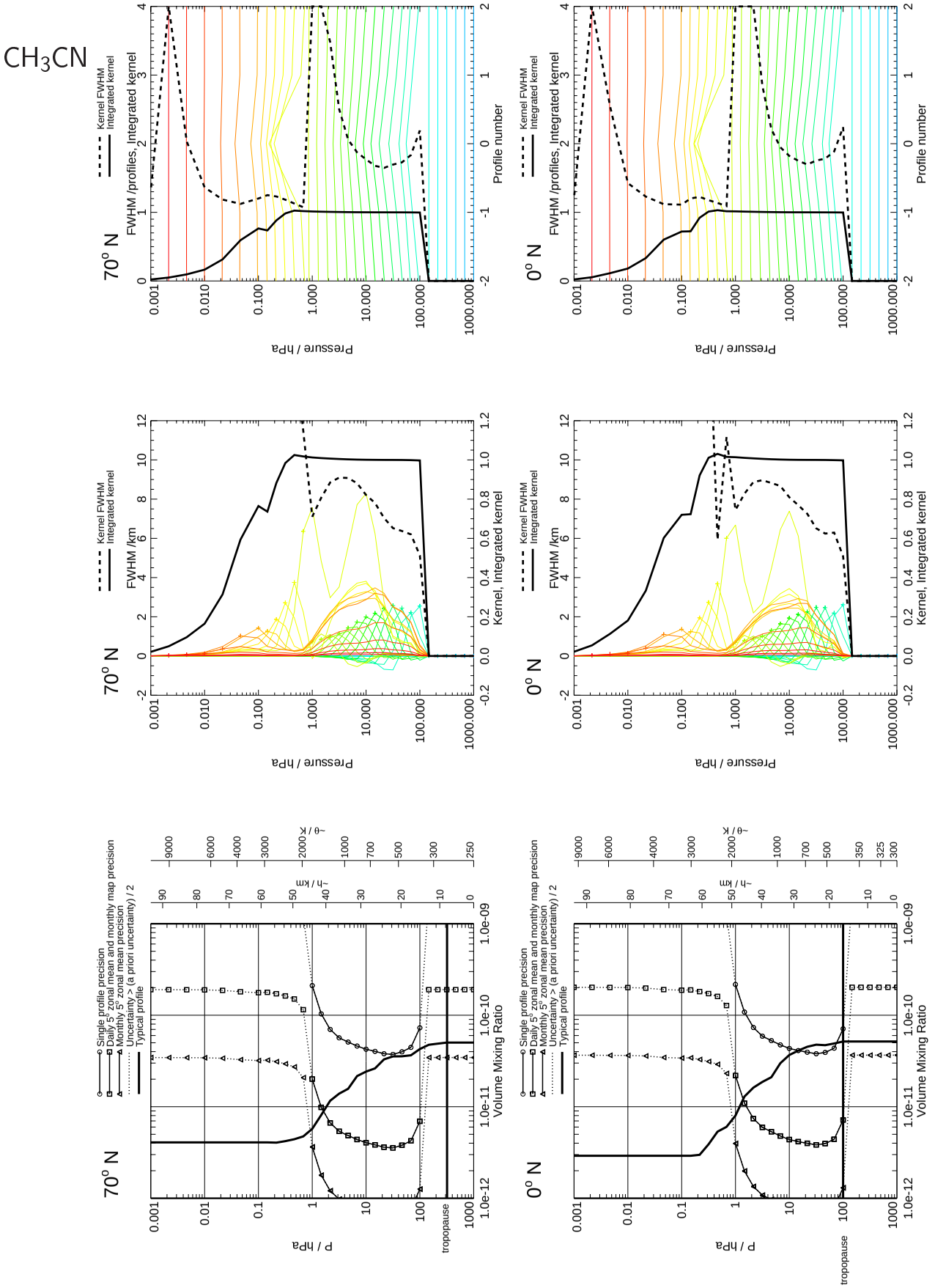

Figure 7: CH_3CN precision and averaging kernels, with V1.4 regularisation. V1.4 phase CorePlusR2.

CH_3CN

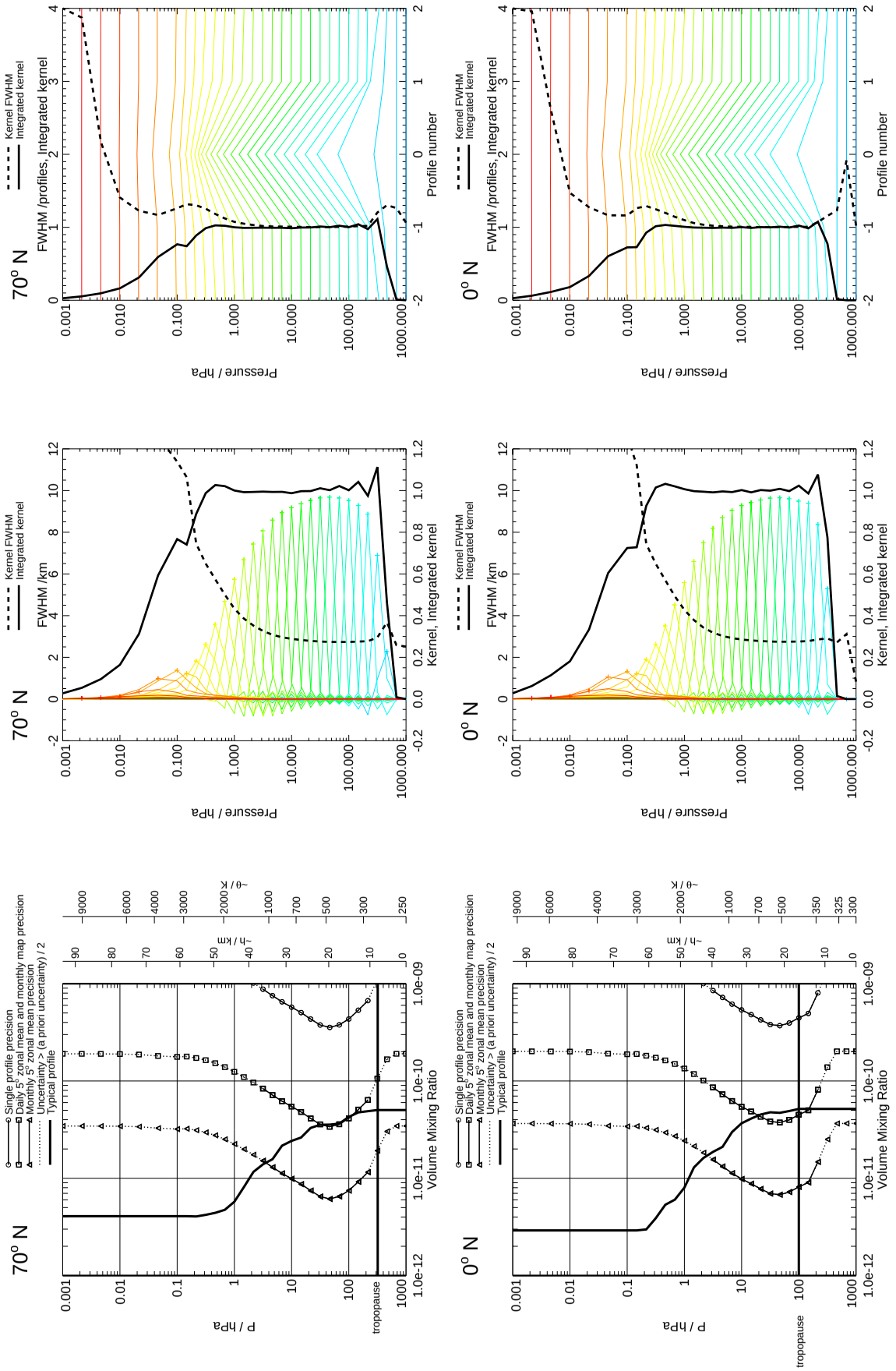

Figure 8: CH_3CN precision and averaging kernels, with no regularisation. Touchstone phase CorePlusR2.

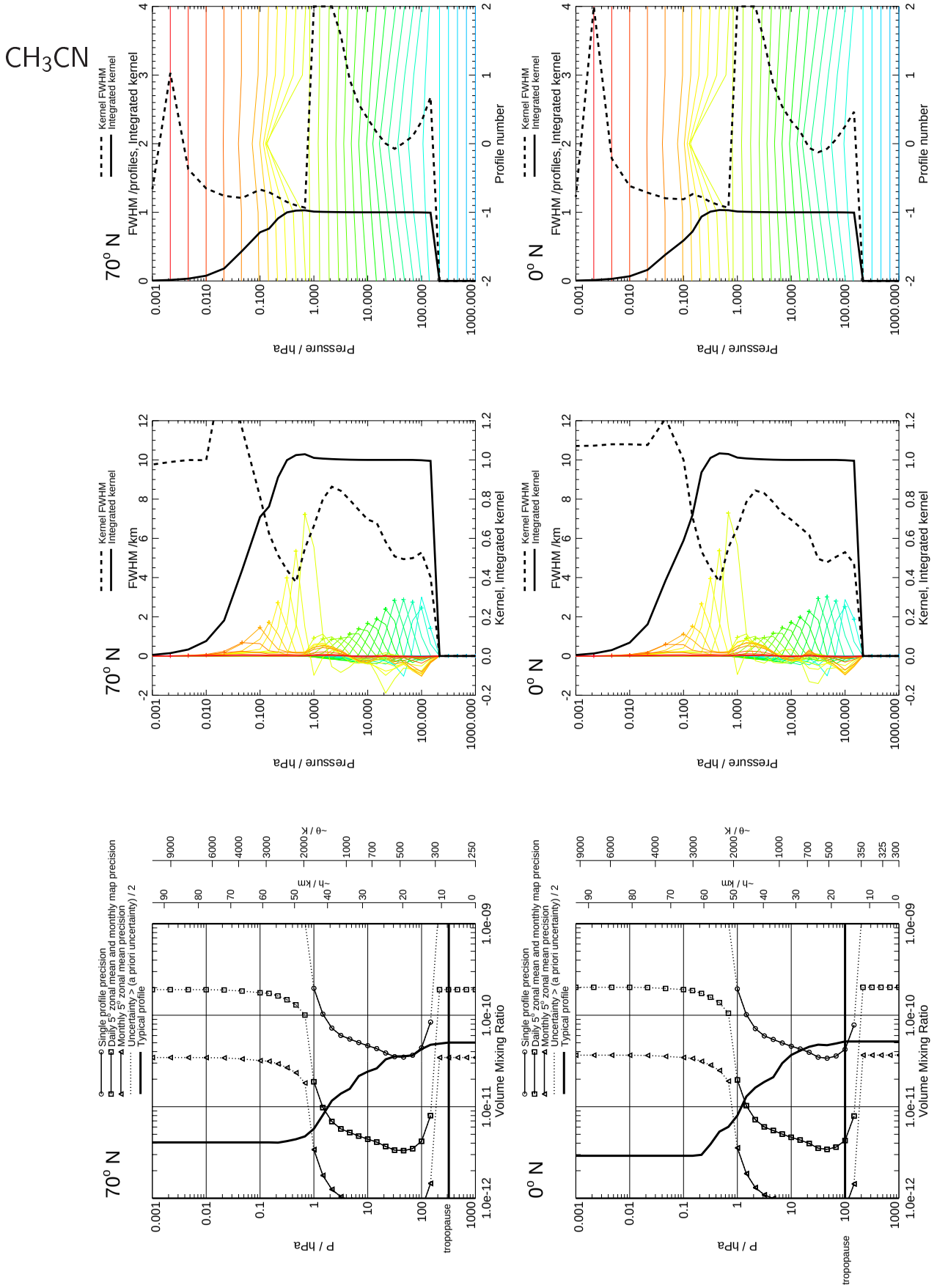

Figure 9: CH_3CN precision and averaging kernels, with V1.4 regularisation. V1.4 phase CorePlusR4.

CH_3CN

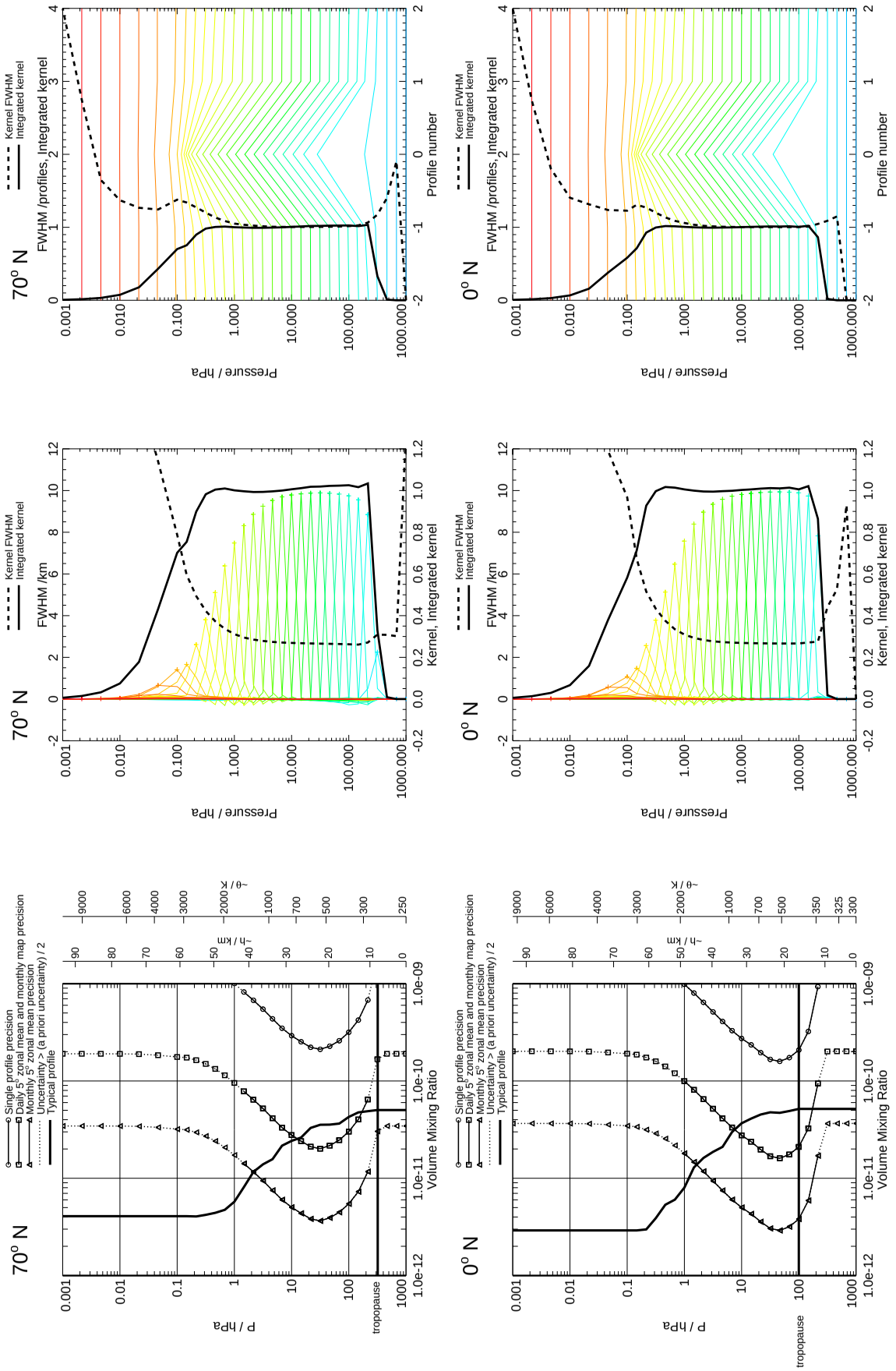

Figure 10: CH_3CN precision and averaging kernels, with no regularisation. Touchstone phase CorePlusR4.

ClO

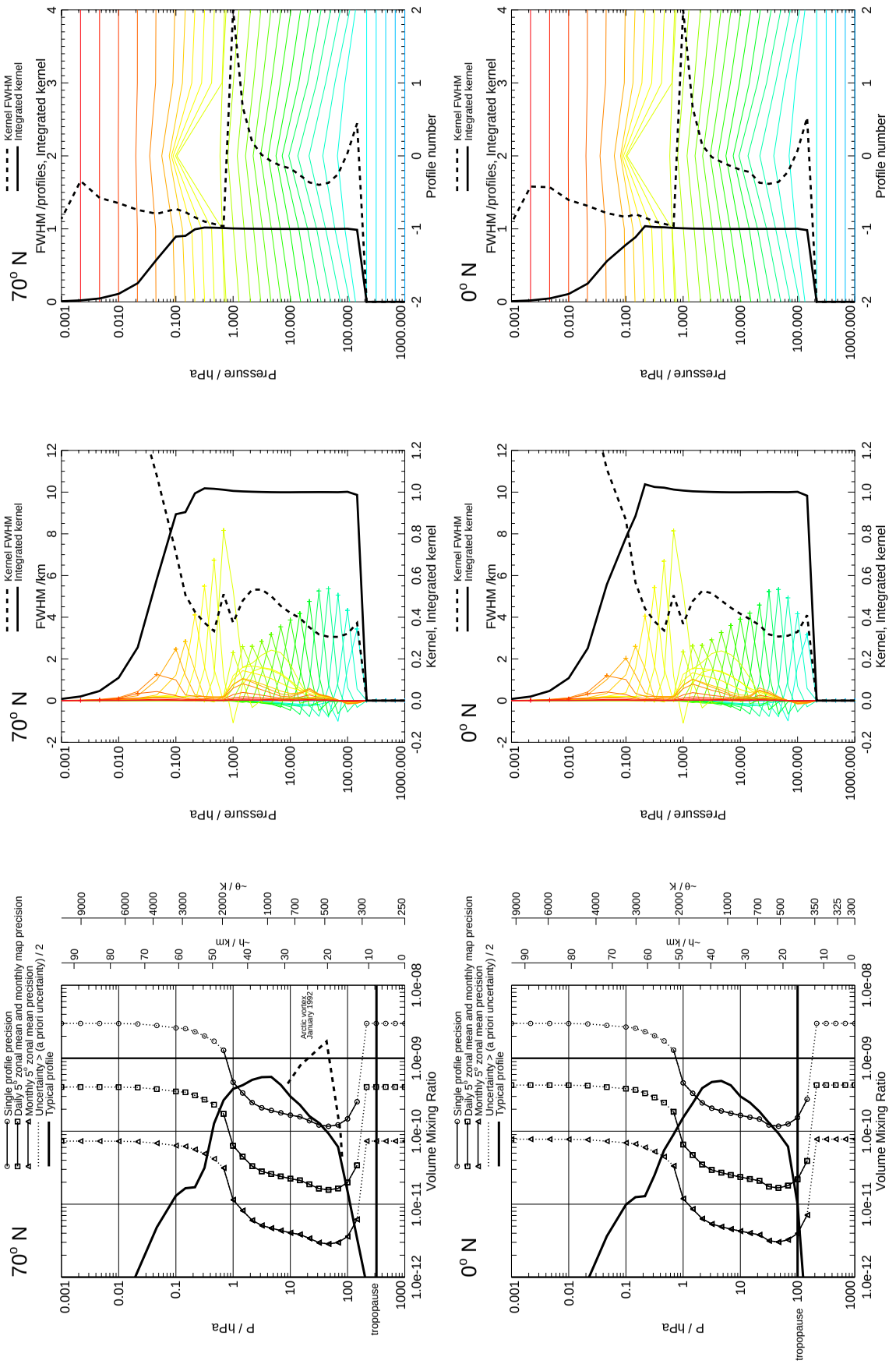

Figure 11: ClO precision and averaging kernels, with V1.4 regularisation. V1.4 phased retrieval. The enhanced ClO profile comes from UARS MLS measurements for January 1992, averaged over the Arctic vortex (Waters *et al.* 1996).

ClO

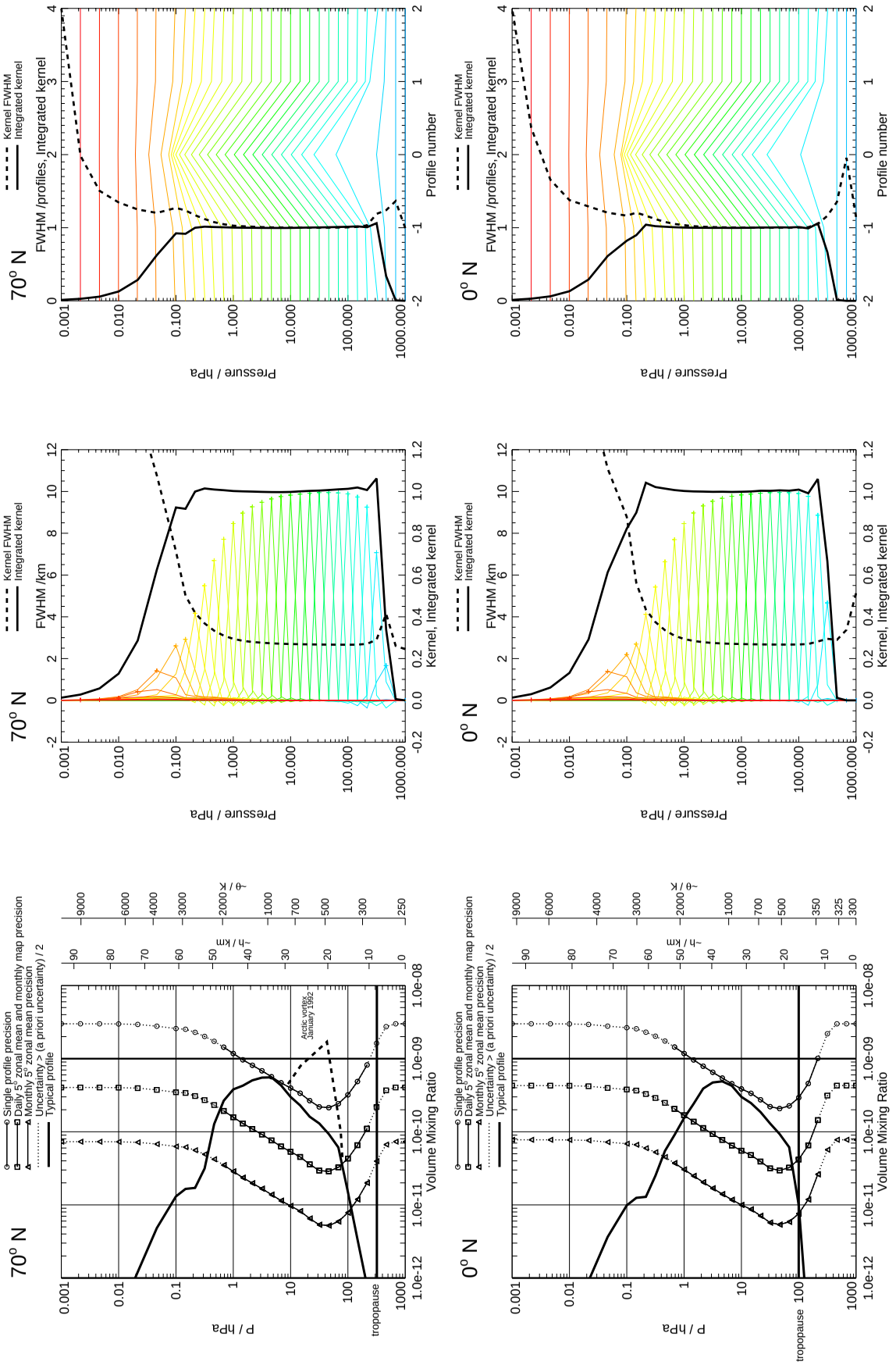

Figure 12: ClO precision and averaging kernels, with no regularisation. Touchstone retrieval. The enhanced ClO profile comes from UARS MLS measurements for January 1992, averaged over the Arctic vortex (Waters *et al.* 1996).

ClO

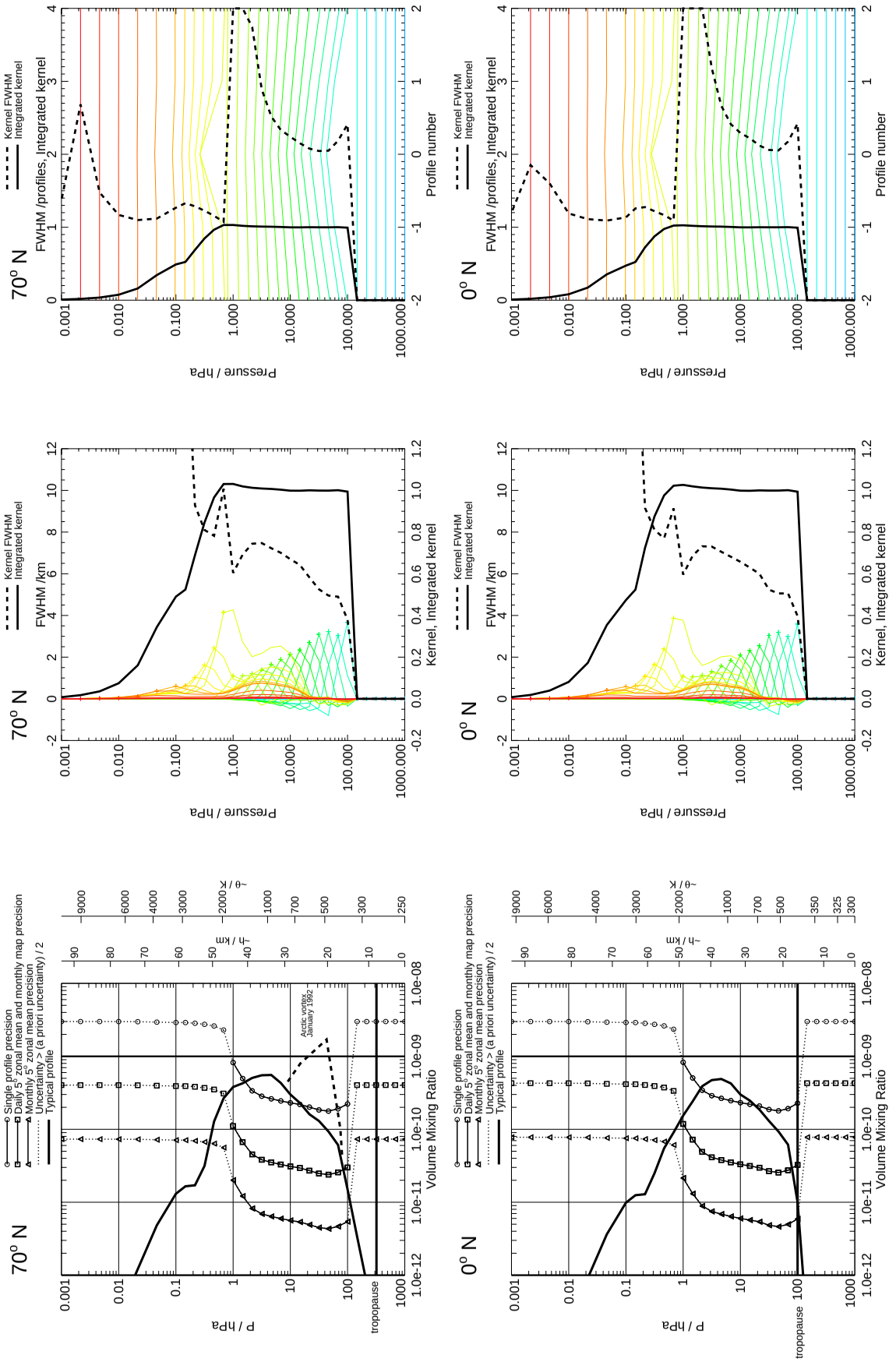

Figure 13: ClO precision and averaging kernels, with V1.4 regularisation. V1.4 phase CorePlusR2. The enhanced ClO profile comes from UARS MLS measurements for January 1992, averaged over the Arctic vortex (Waters *et al.* 1996).

ClO

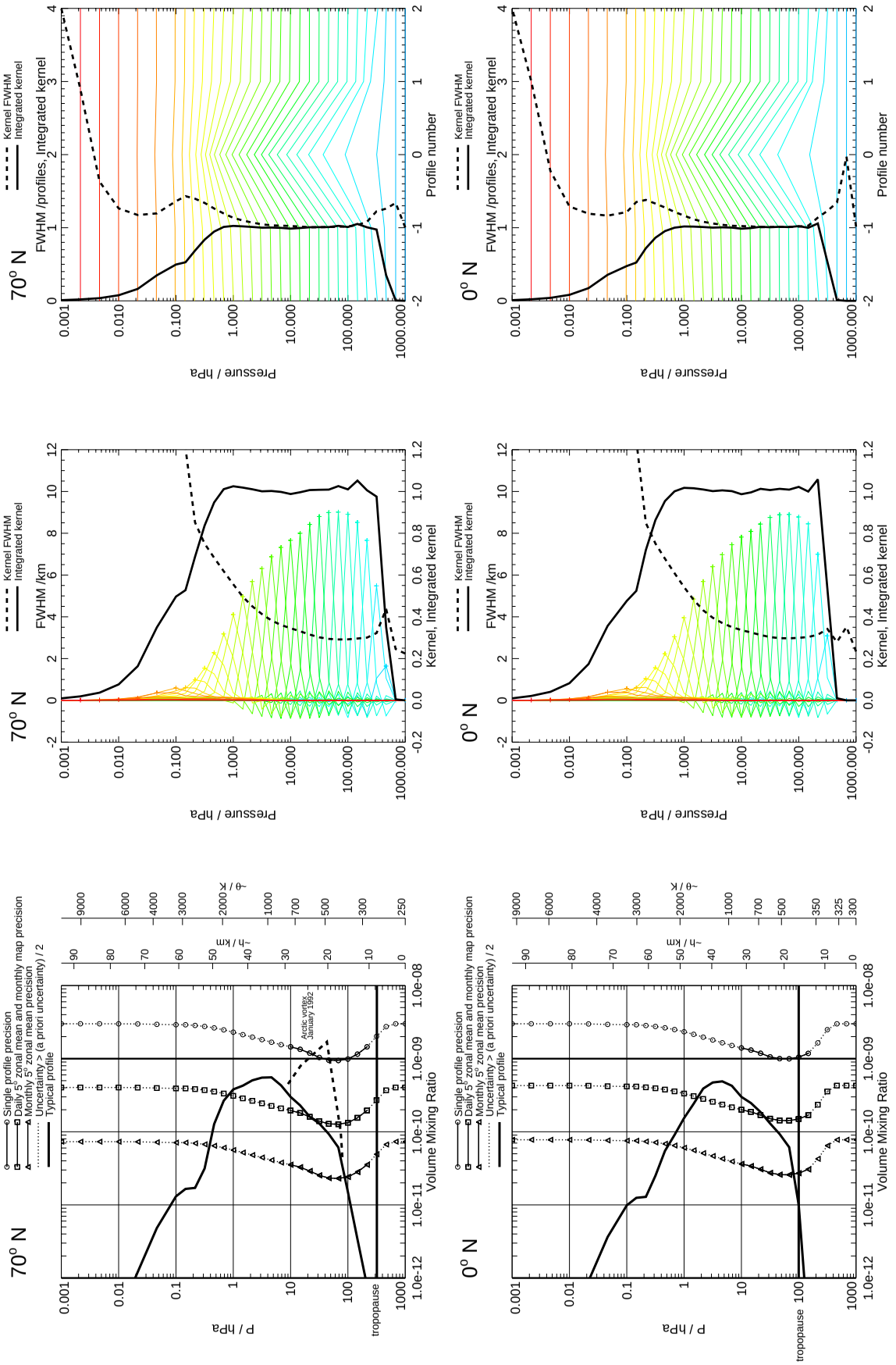

Figure 14: ClO precision and averaging kernels, with no regularisation. Touchstone phase CorePlusR2. The enhanced ClO profile comes from UARS MLS measurements for January 1992, averaged over the Arctic vortex (Waters *et al.* 1996).

ClO

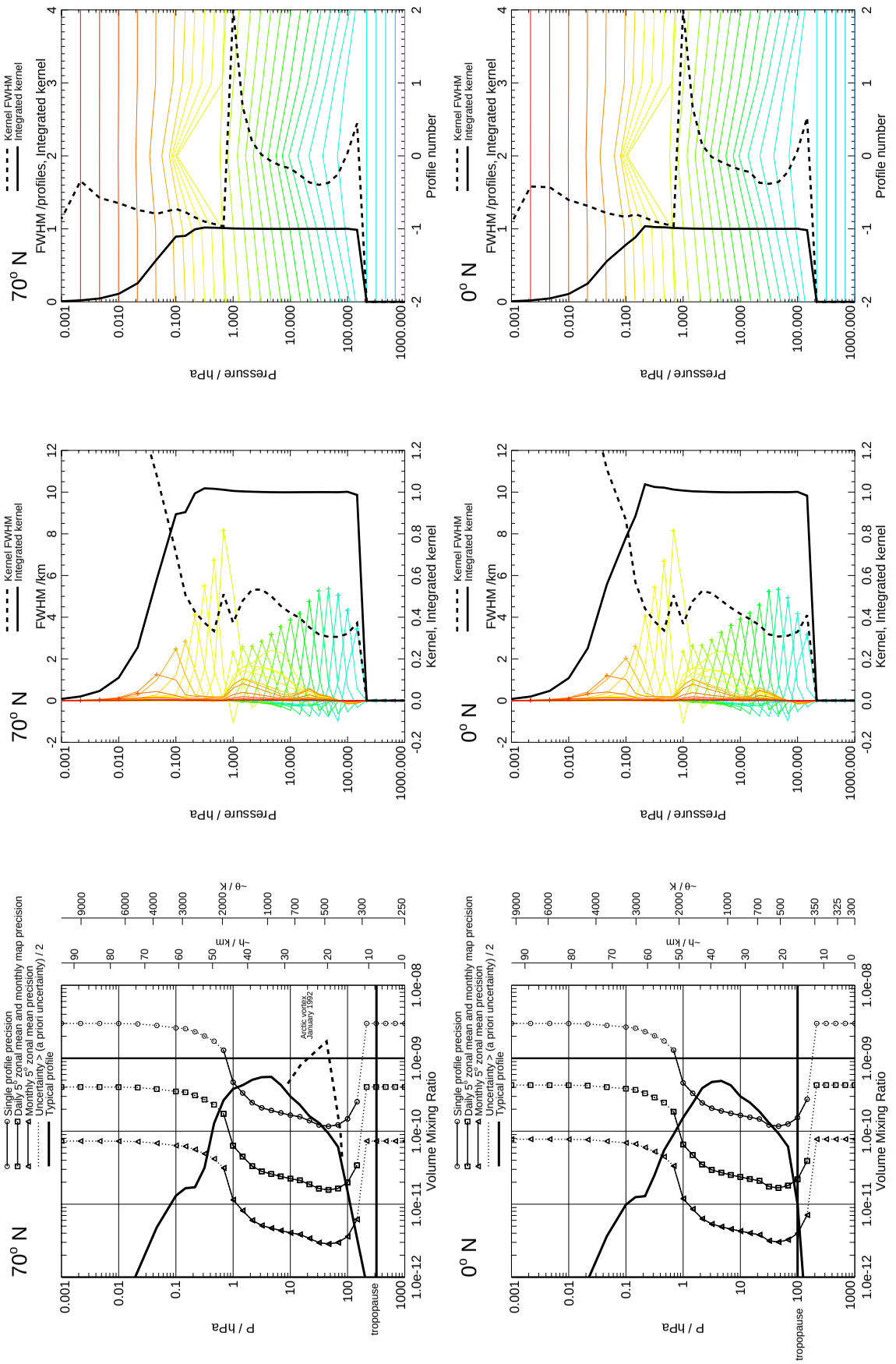

Figure 15: ClO precision and averaging kernels, with V1.4 regularisation. V1.4 phase CorePlusR4. The enhanced ClO profile comes from UARS MLS measurements for January 1992, averaged over the Arctic vortex (Waters *et al.* 1996).

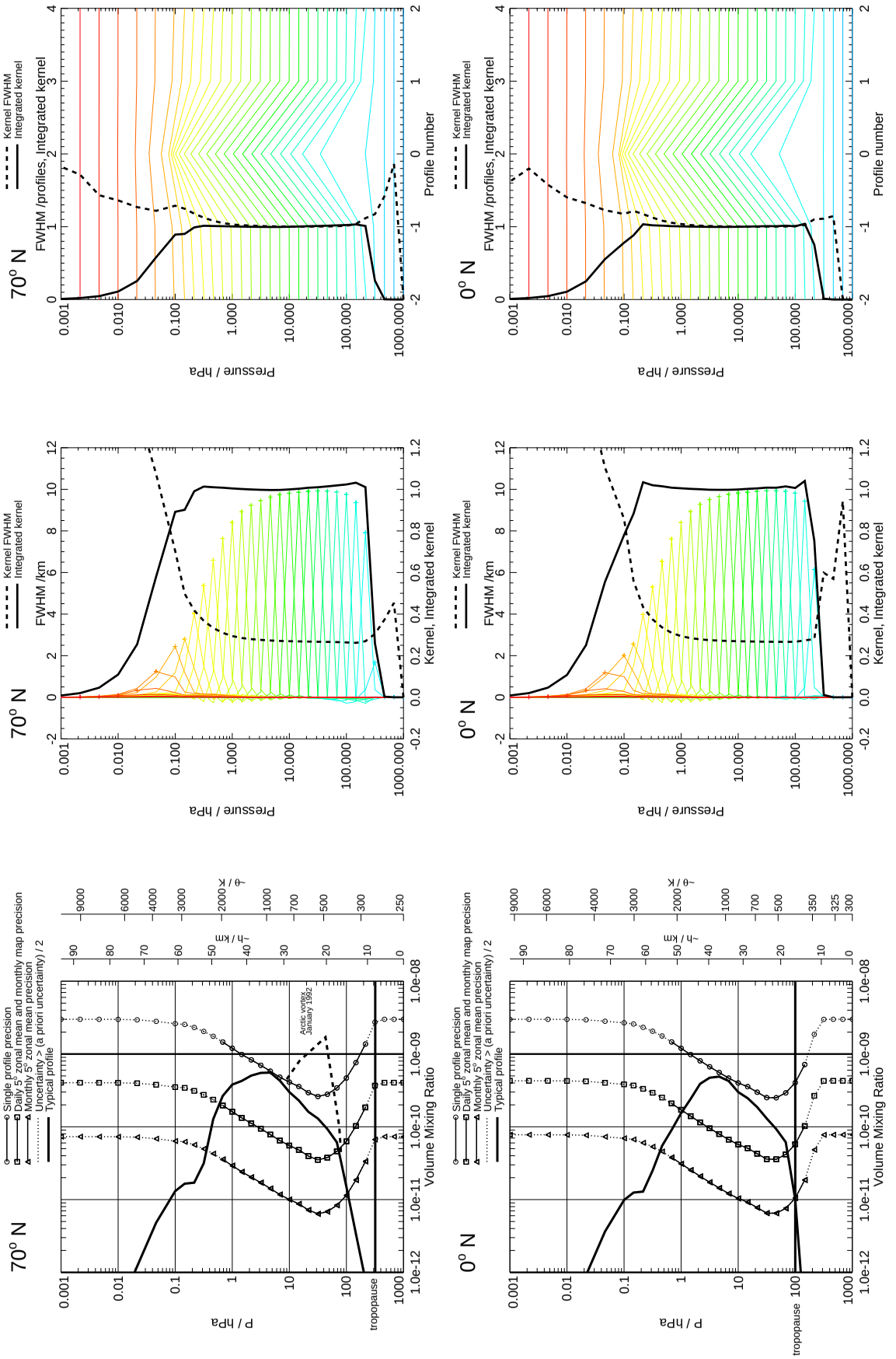

Figure 16: ClO precision and averaging kernels, with no regularisation. Touchstone phase CorePlusR4. The enhanced ClO profile comes from UARS MLS measurements for January 1992, averaged over the Arctic vortex (Waters *et al.* 1996).

CO

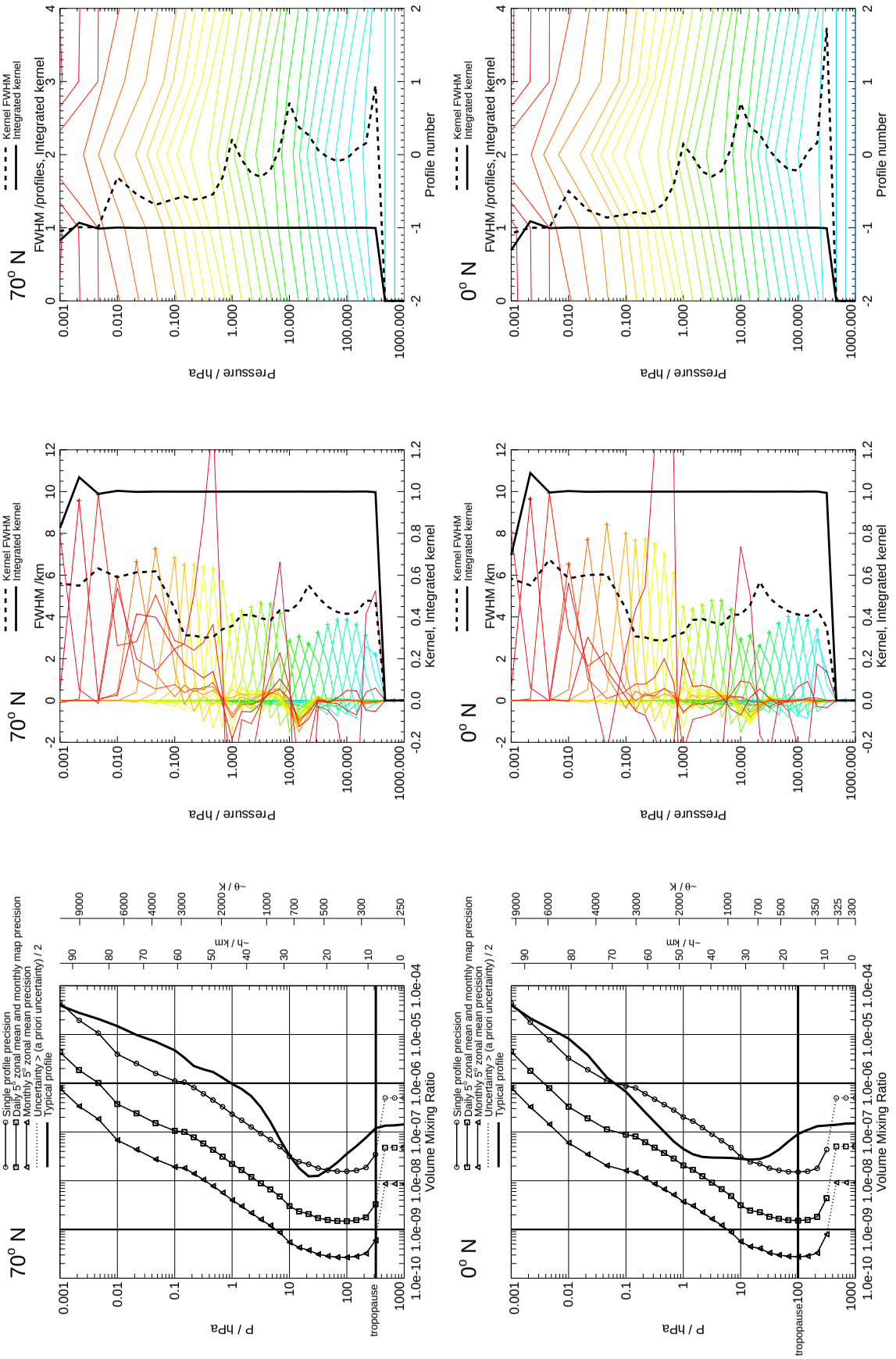

Figure 17: CO precision and averaging kernels, with V1.4 regularisation. V1.4 phased retrieval.

CO

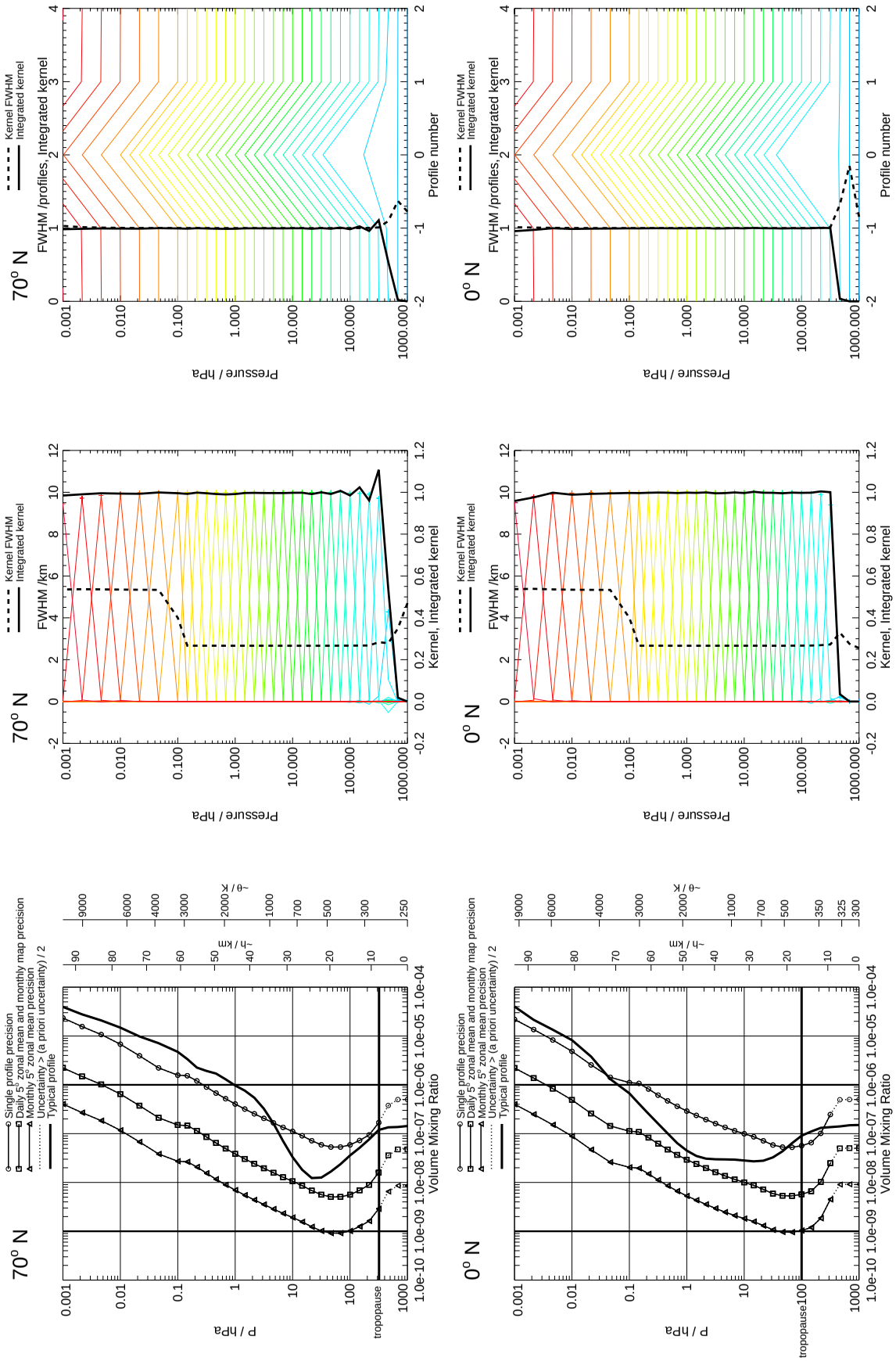

Figure 18: CO precision and averaging kernels, with no regularisation. Touchstone retrieval.

CO

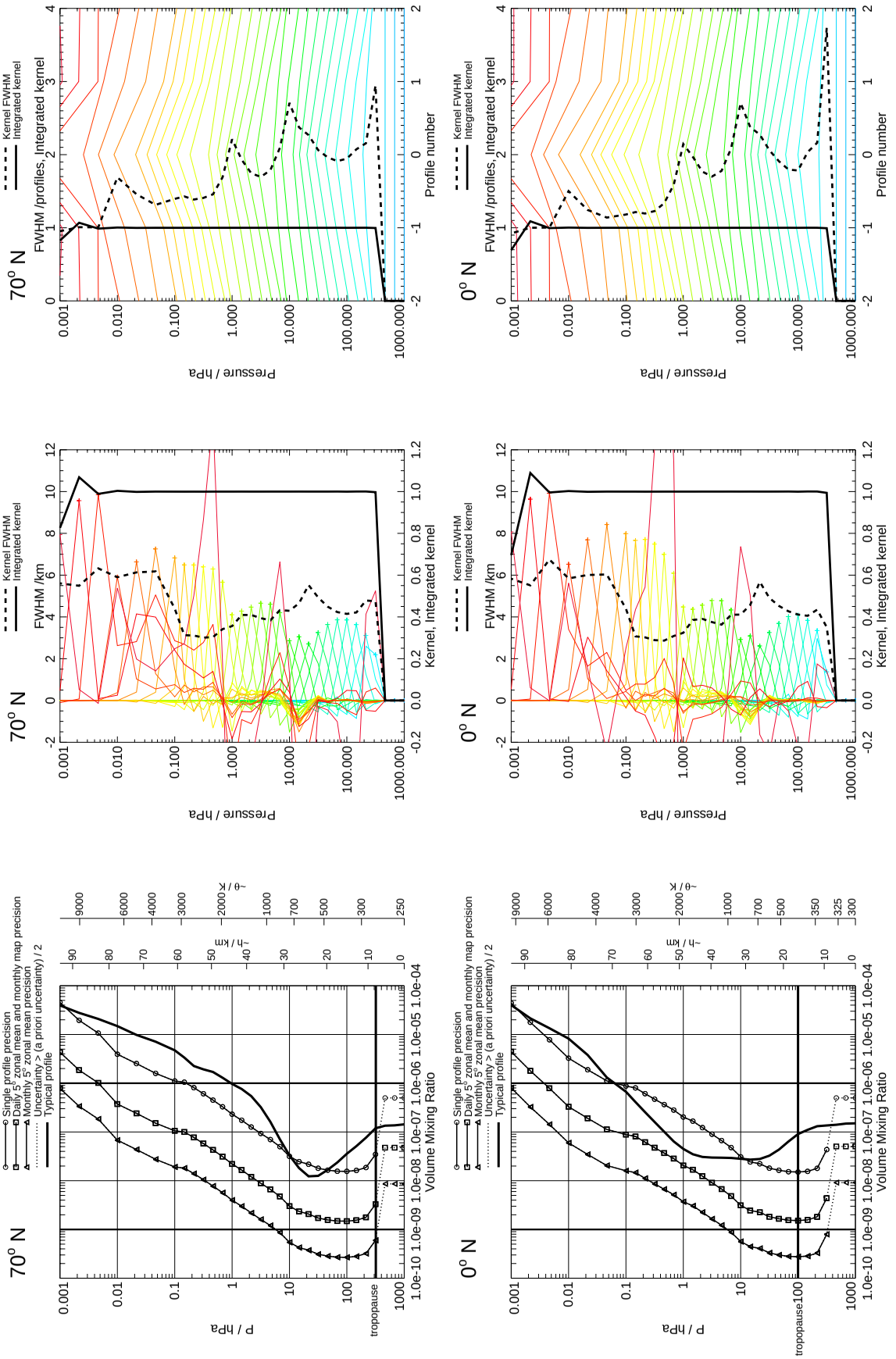

Figure 19: CO precision and averaging kernels, with V1.4 regularisation. V1.4 phase CorePlusR3.

CO

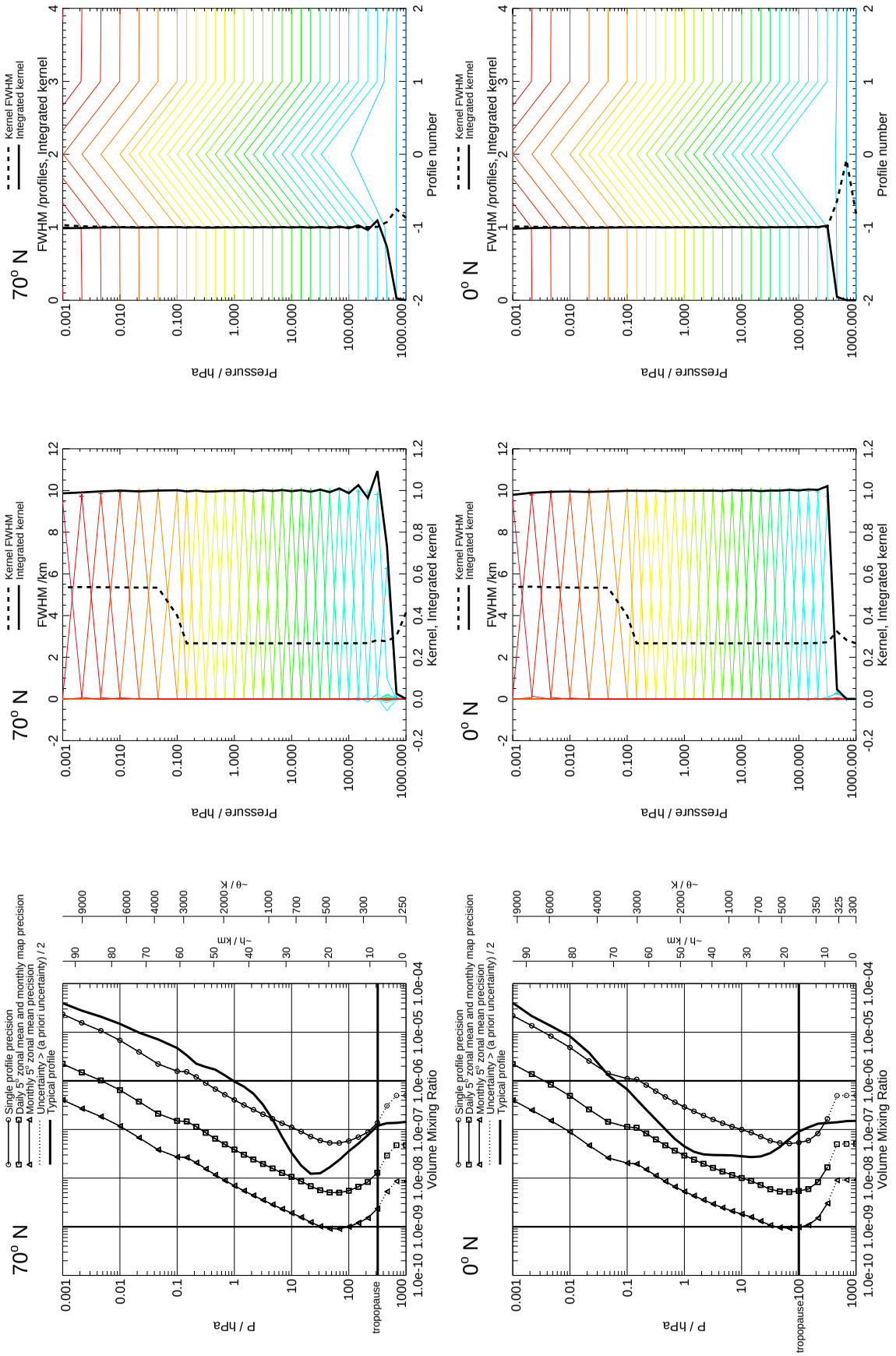

Figure 20: CO precision and averaging kernels, with no regularisation. Touchstone phase CorePlusR3.

GPH

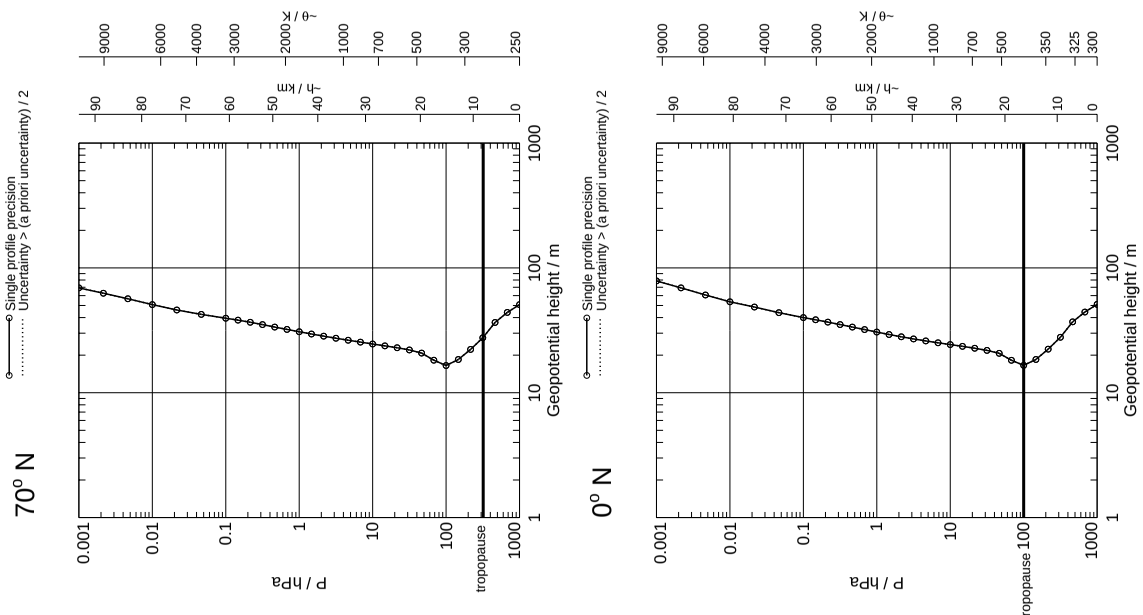

Figure 21: Geopotential height precision for Single Profile only, with V1.4 regularisation. V1.4 phased retrieval. No averaging kernels are generated for this product which is derived from temperature and reference geopotential.

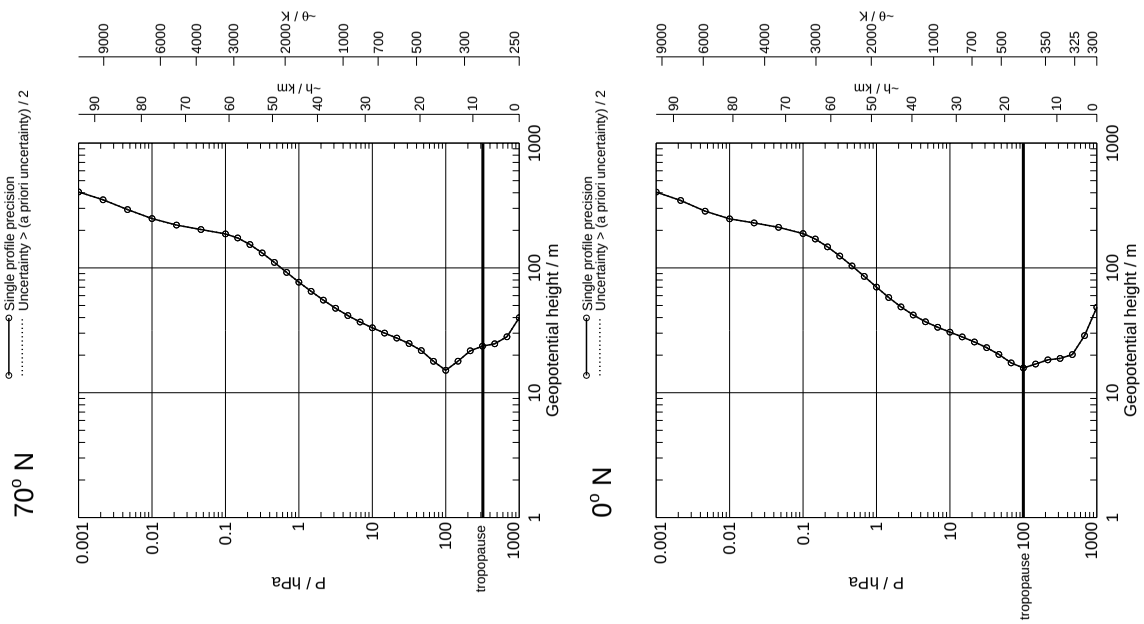

Figure 22: Geopotential height precision for Single Profile only, with no regularisation. Touchstone retrieval. No averaging kernels are generated for this product which is derived from temperature and reference geopotential.

GPH

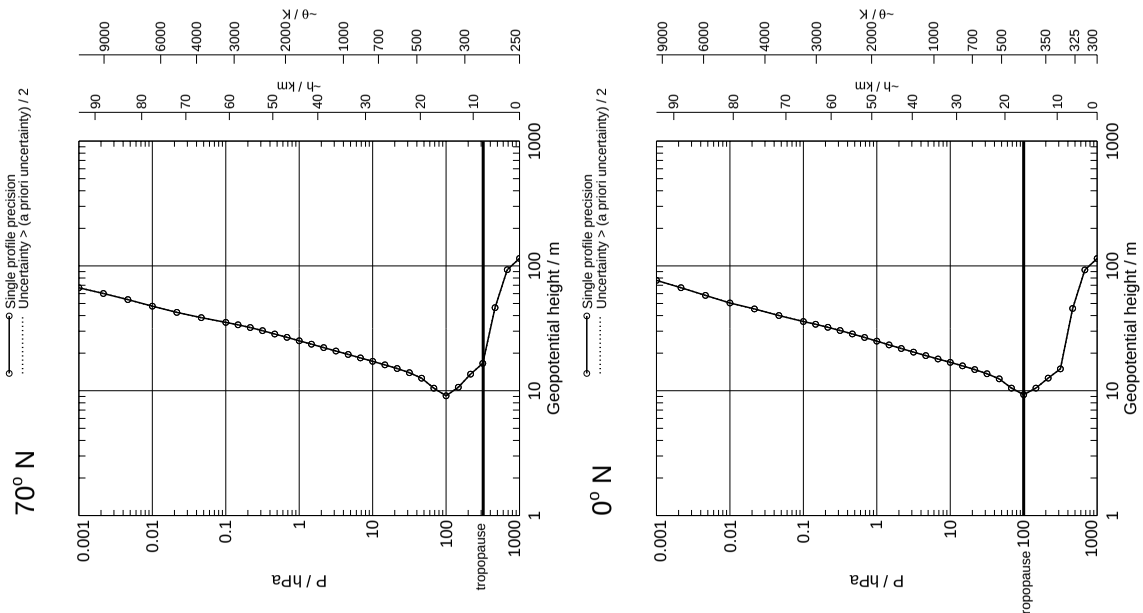

Figure 23: Geopotential height precision for Single Profile only, with V1.4 regularisation. V1.4 phase CorePlusR2. No averaging kernels are generated for this product which is derived from temperature and reference geopotential.

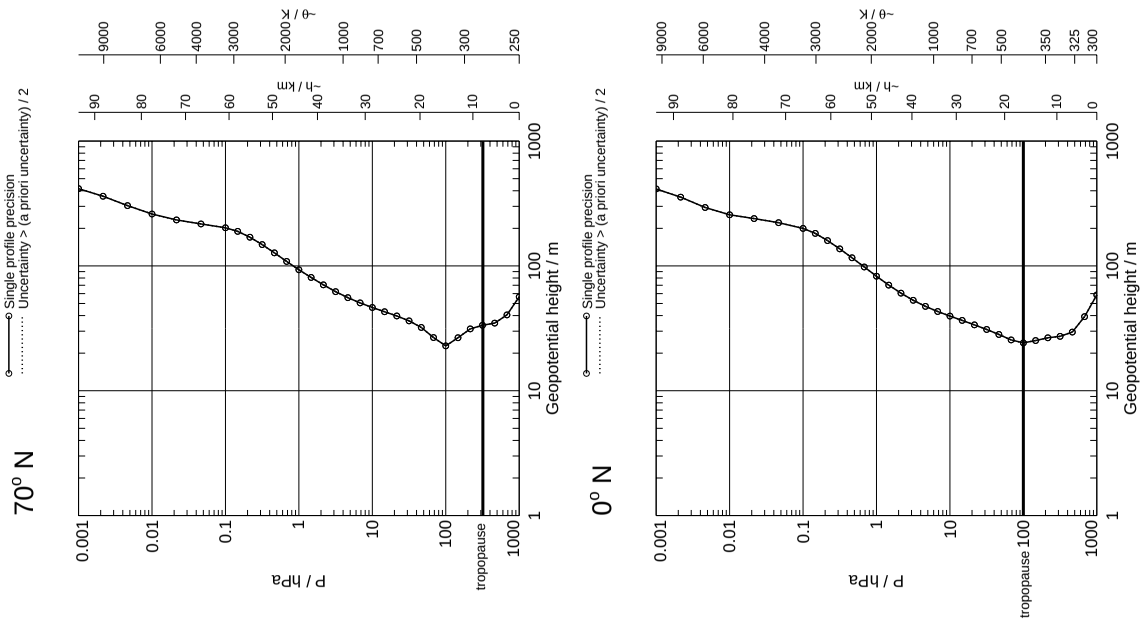

Figure 24: Geopotential height precision for Single Profile only, with no regularisation. Touchstone phase CorePlusR2. No averaging kernels are generated for this product which is derived from temperature and reference geopotential.

GPH

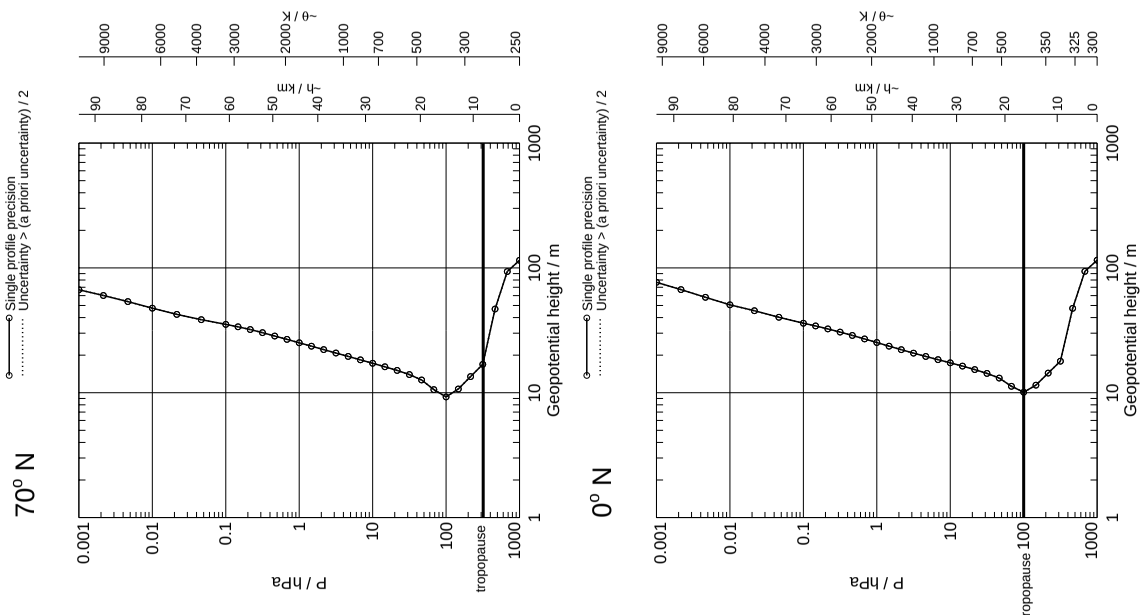

Figure 25: Geopotential height precision for Single Profile only, with V1.4 regularisation. V1.4 phase CorePlusR3. No averaging kernels are generated for this product which is derived from temperature and reference geopotential.

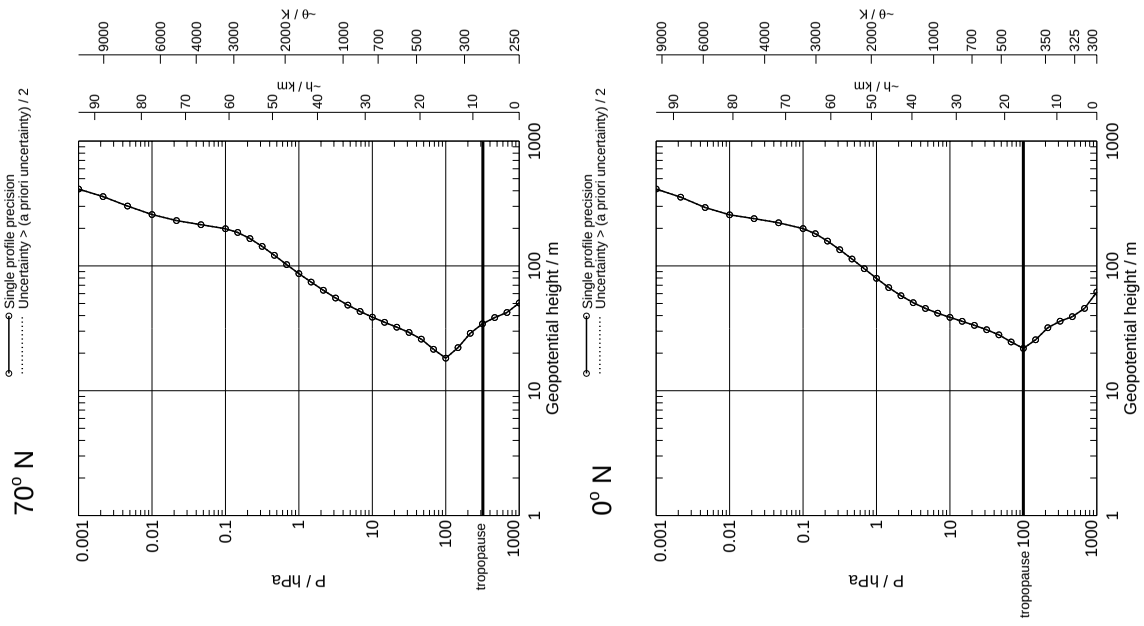

Figure 26: Geopotential height precision for Single Profile only, with no regularisation. Touchstone phase CorePlusR3. No averaging kernels are generated for this product which is derived from temperature and reference geopotential.

GPH

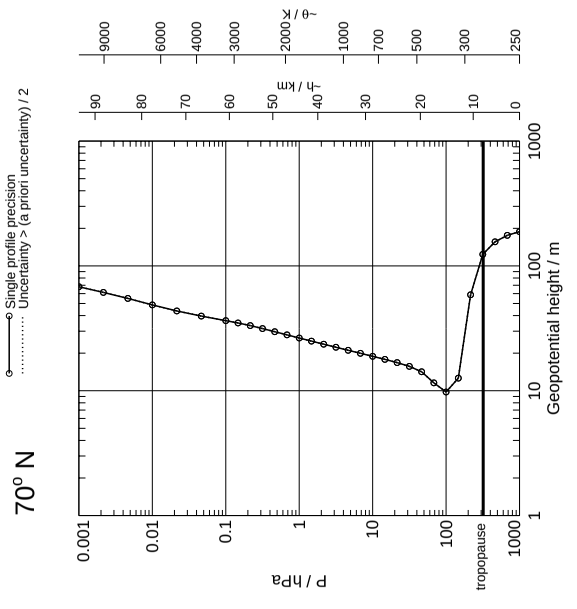

Figure 27: Geopotential height precision for Single Profile only, with V1.4 regularisation. V1.4 phase CorePlusR4. No averaging kernels are generated for this product which is derived from temperature and reference geopotential.

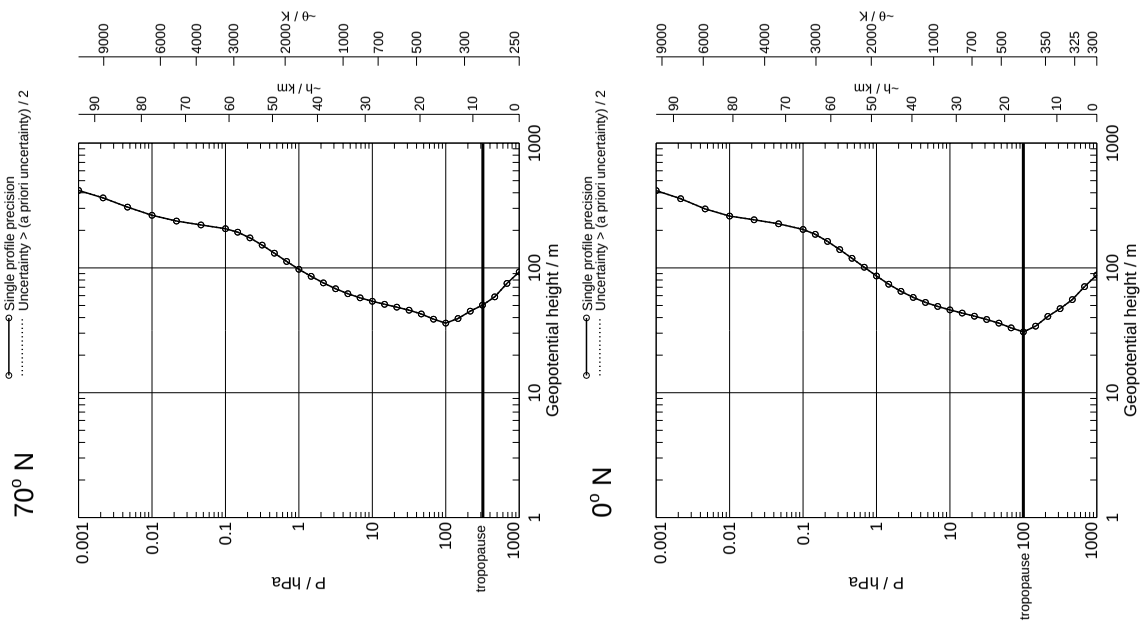

Figure 28: Geopotential height precision for Single Profile only, with no regularisation. Touchstone phase CorePlusR4. No averaging kernels are generated for this product which is derived from temperature and reference geopotential.

GPH

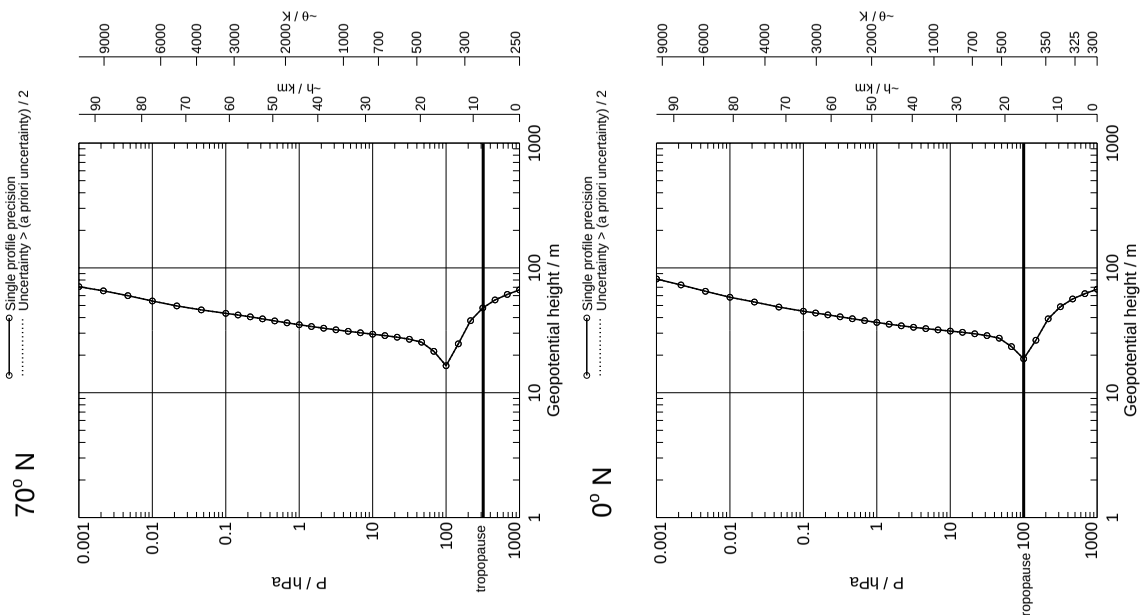

Figure 29: Geopotential height precision for Single Profile only, with V1.4 regularisation. V1.4 phase CorePlusR5. No averaging kernels are generated for this product which is derived from temperature and reference geopotential.

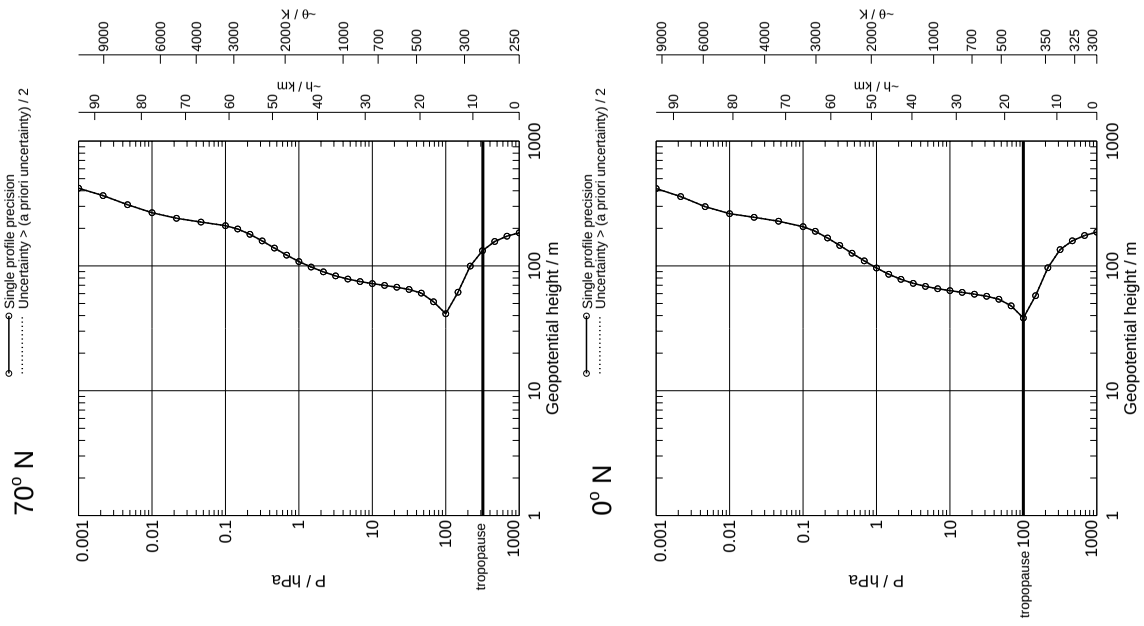

Figure 30: Geopotential height precision for Single Profile only, with no regularisation. Touchstone phase CorePlusR5. No averaging kernels are generated for this product which is derived from temperature and reference geopotential.

GPH

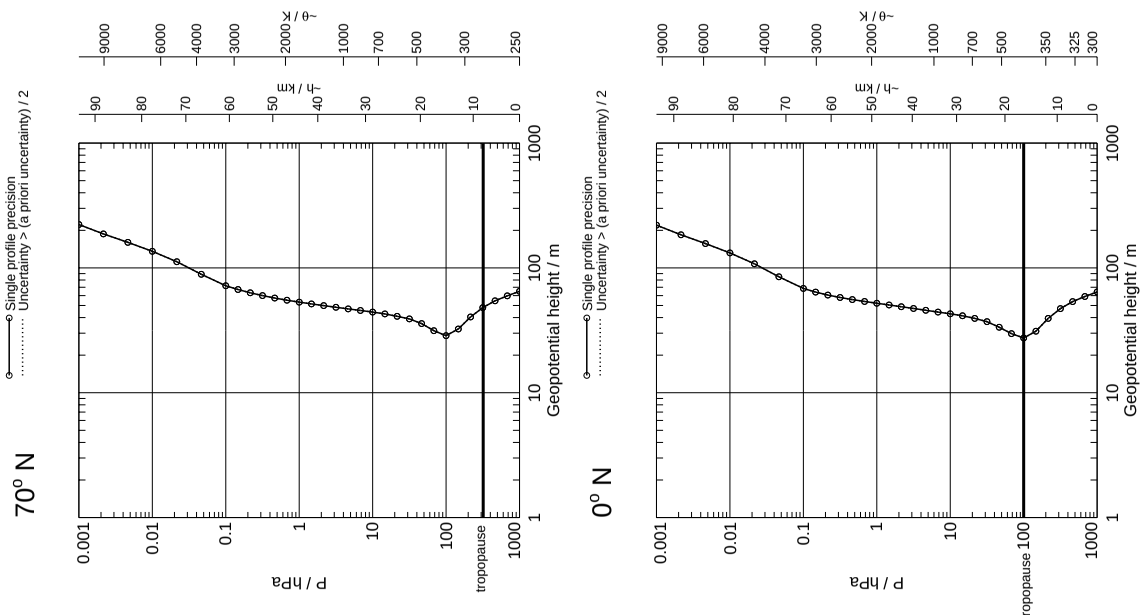

Figure 31: Geopotential height precision for Single Profile only, with V1.4 regularisation. V1.4 phase InitPtan. No averaging kernels are generated for this product which is derived from temperature and reference geopotential.

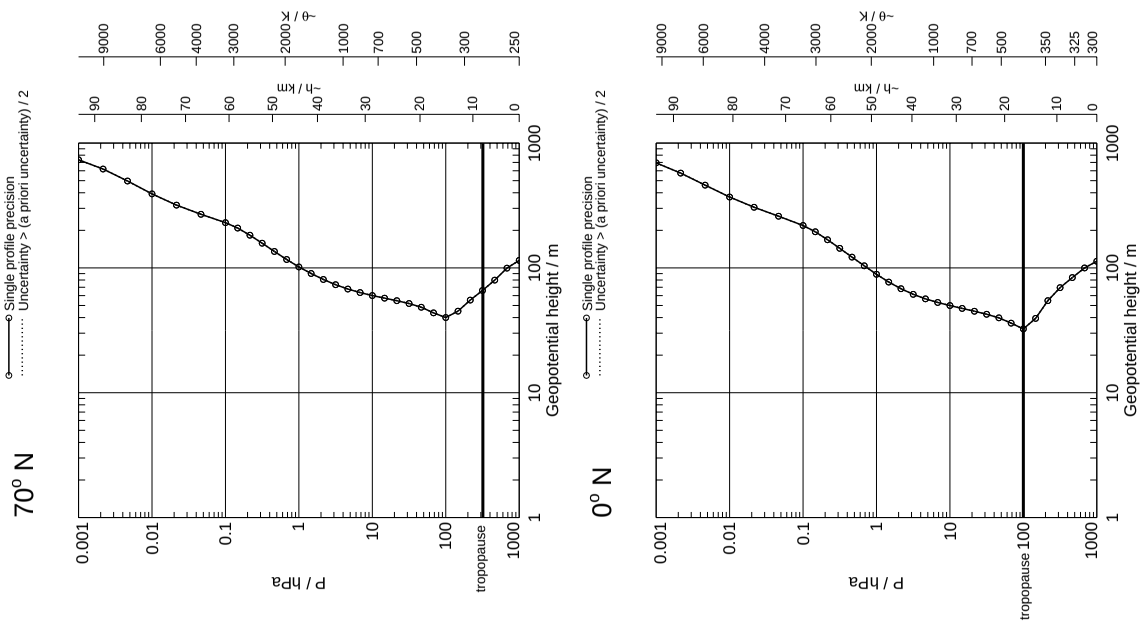

Figure 32: Geopotential height precision for Single Profile only, with no regularisation. Touchstone phase InitPtan. No averaging kernels are generated for this product which is derived from temperature and reference geopotential.

GPH

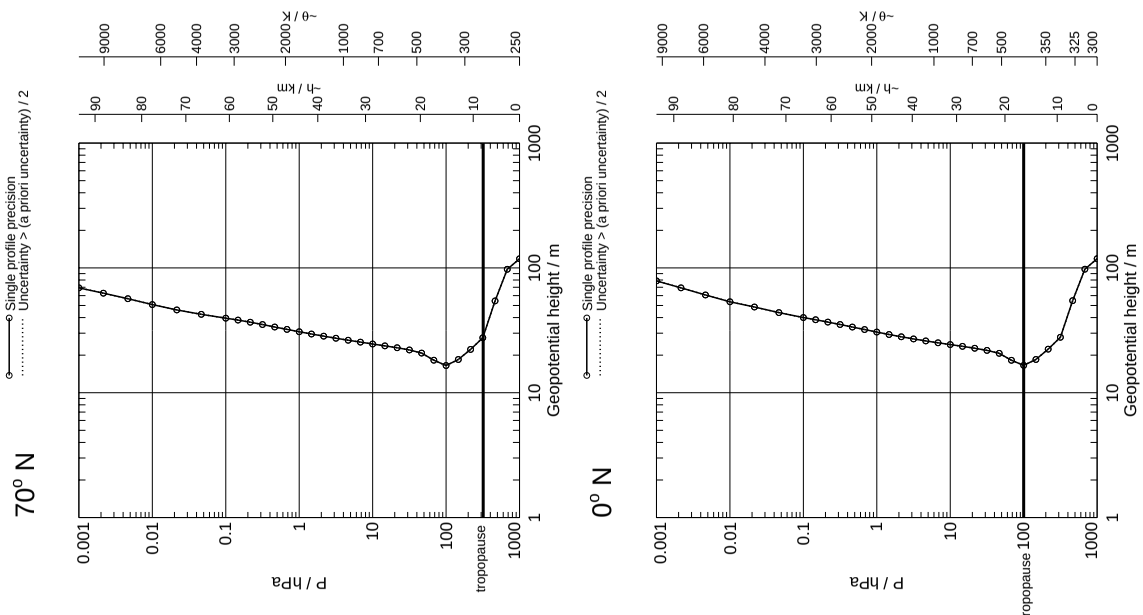

Figure 33: Geopotential height precision for Single Profile only, with V1.4 regularisation. V1.4 phase UpdatePtan. No averaging kernels are generated for this product which is derived from temperature and reference geopotential.

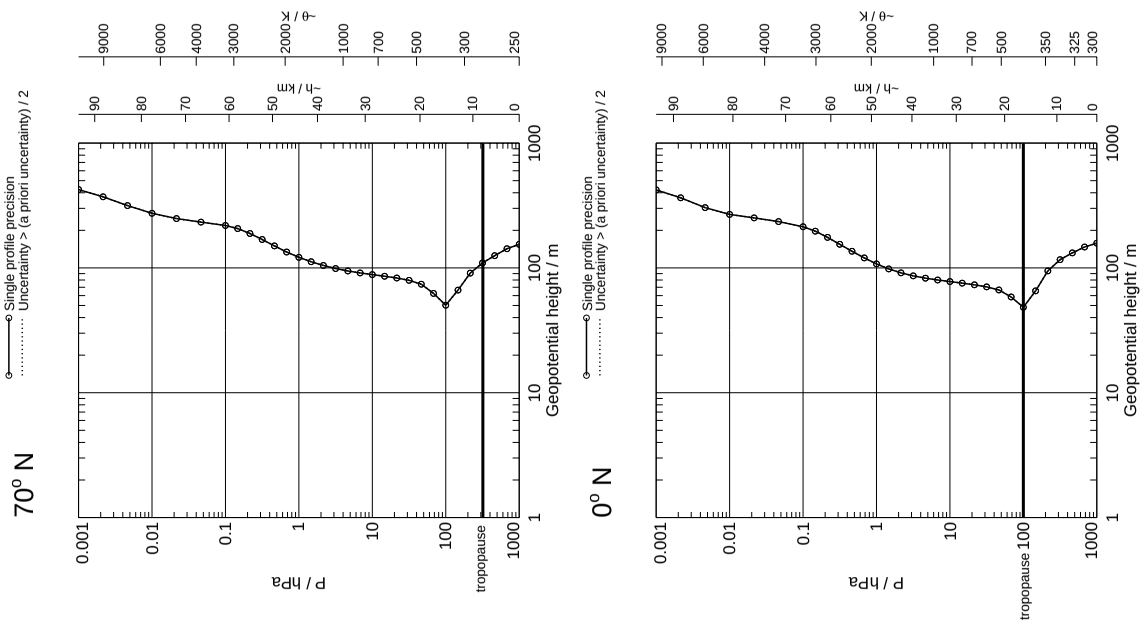

Figure 34: Geopotential height precision for Single Profile only, with no regularisation. Touchstone phase UpdatePtan. No averaging kernels are generated for this product which is derived from temperature and reference geopotential.

GPH

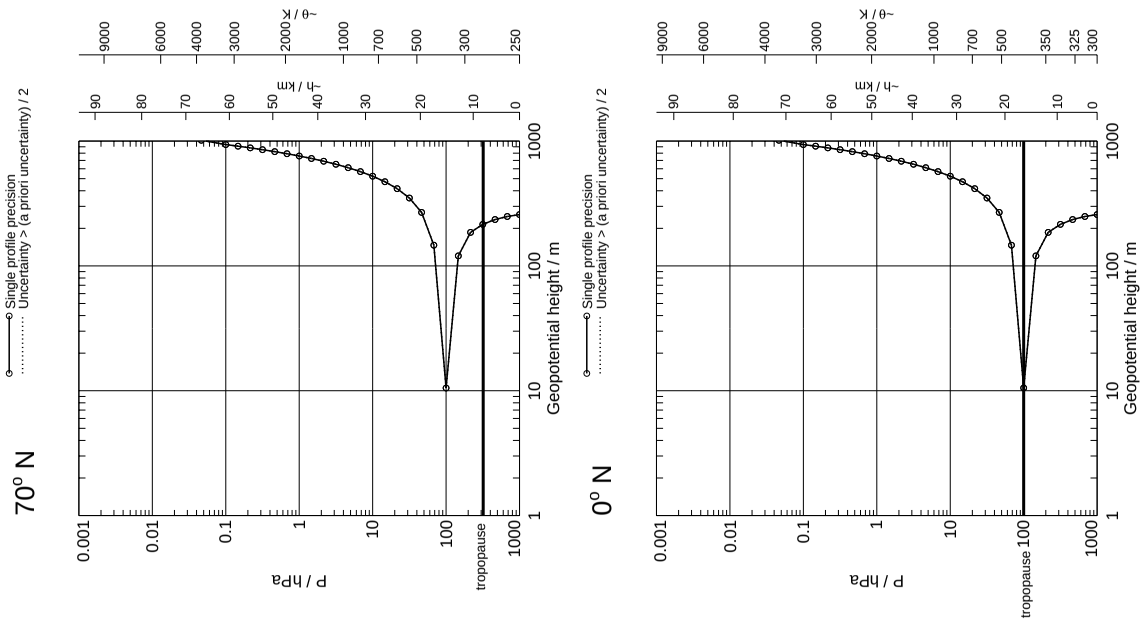

Figure 35: Geopotential height precision on high resolution grid, for Single Profile only, with V1.4 regularisation. V1.4 phased retrieval. No averaging kernels are generated for this product which is derived from temperature and reference geopotential.

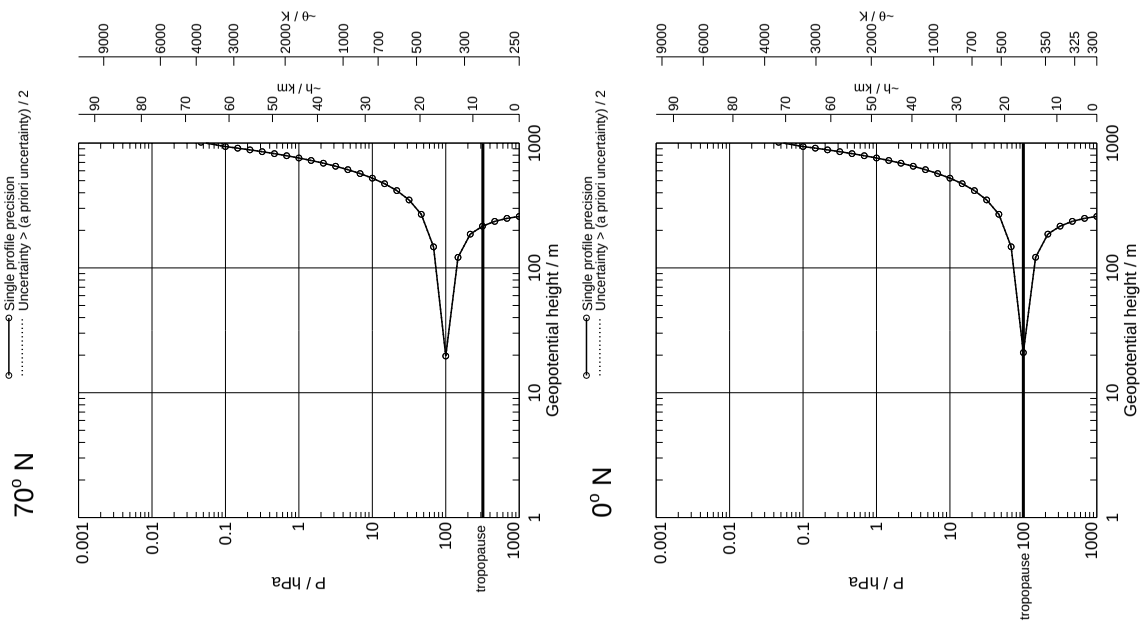

Figure 36: Geopotential height precision on high resolution grid, for Single Profile only, with no regularisation. Touchstone retrieval. No averaging kernels are generated for this product which is derived from temperature and reference geopotential.

GPH

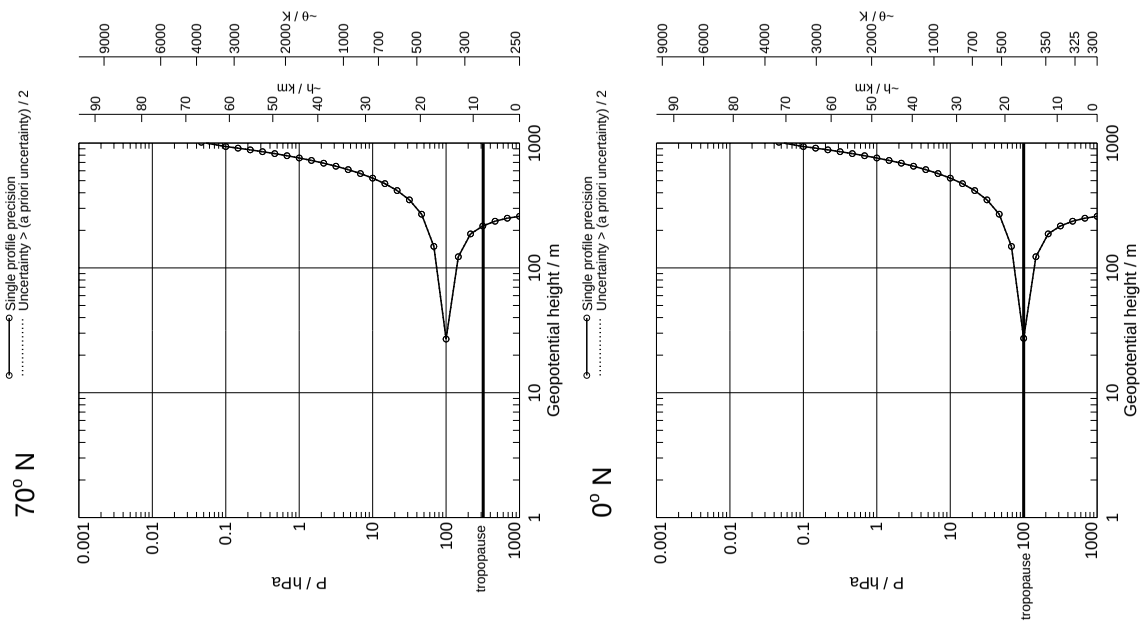

Figure 37: Geopotential height precision on high resolution grid, for Single Profile only, with no regularisation. Touchstone phase CorePlusR2. No averaging kernels are generated for this product which is derived from temperature and reference geopotential.

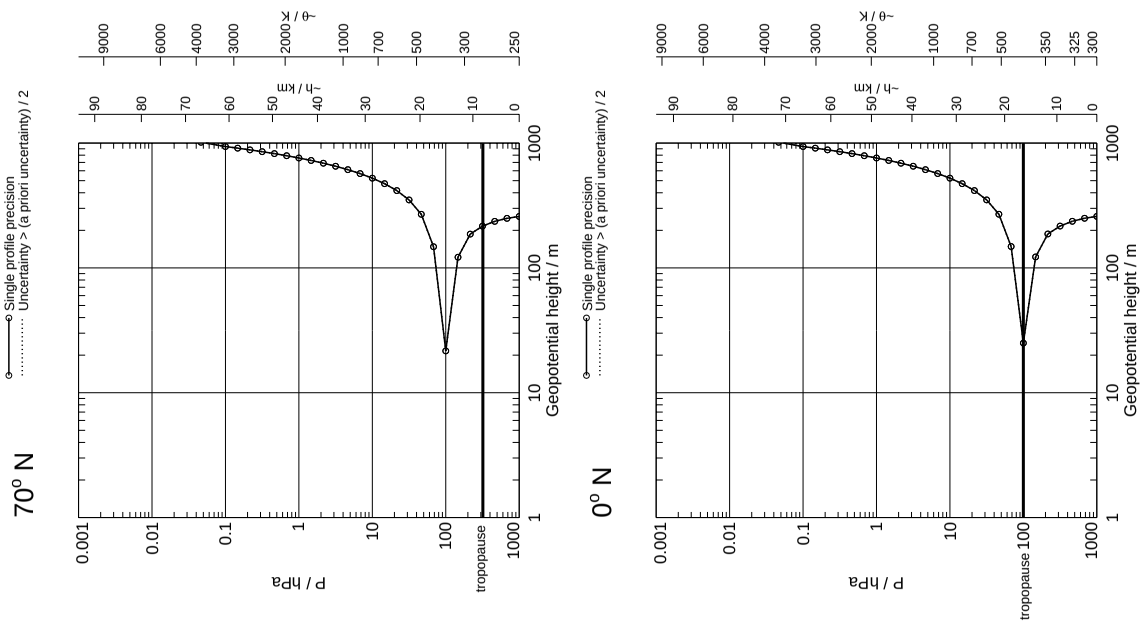

Figure 38: Geopotential height precision on high resolution grid, for Single Profile only, with no regularisation. Touchstone phase CorePlusR3. No averaging kernels are generated for this product which is derived from temperature and reference geopotential.

GPH

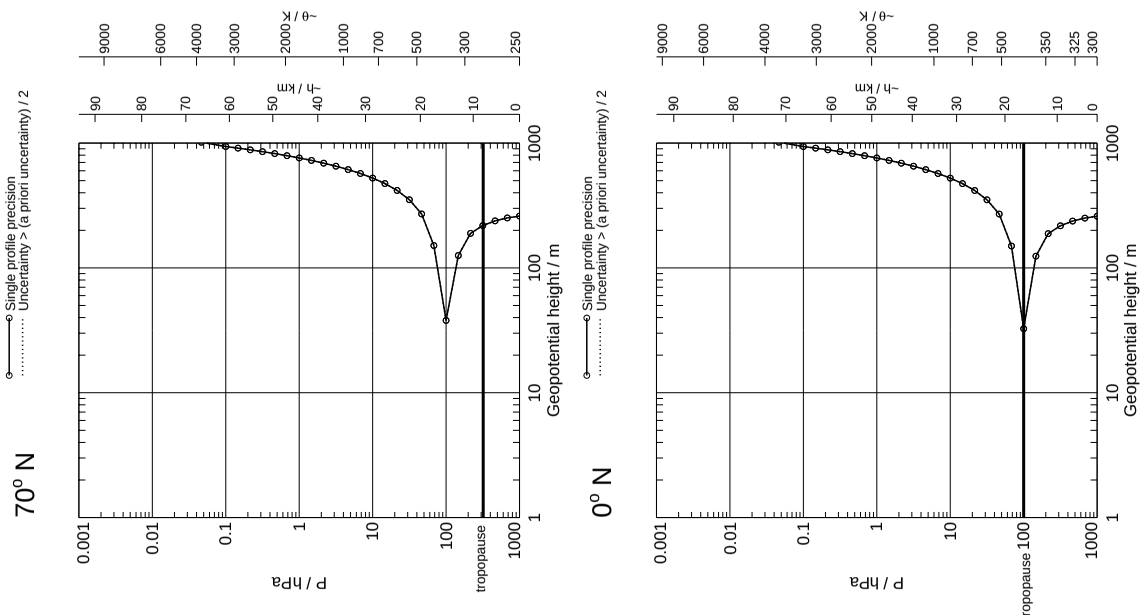

Figure 39: Geopotential height precision on high resolution grid, for Single Profile only, with no regularisation. Touchstone phase CorePlusR4. No averaging kernels are generated for this product which is derived from temperature and reference geopotential.

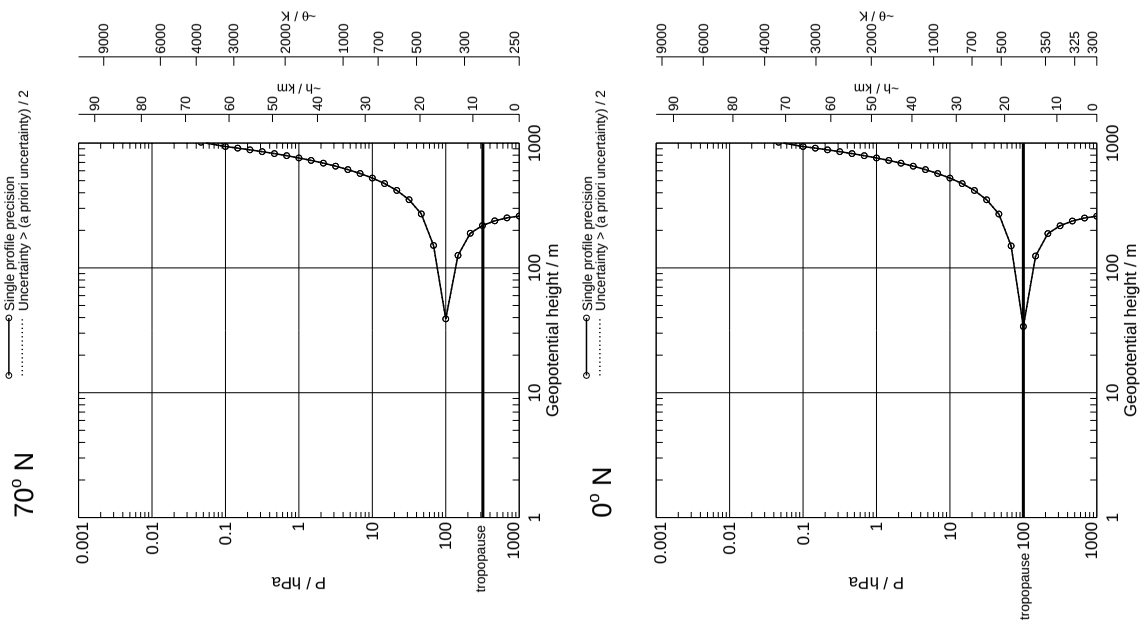

Figure 40: Geopotential height precision on high resolution grid, for Single Profile only, with no regularisation. Touchstone phase InitPtan. No averaging kernels are generated for this product which is derived from temperature and reference geopotential.

GPH

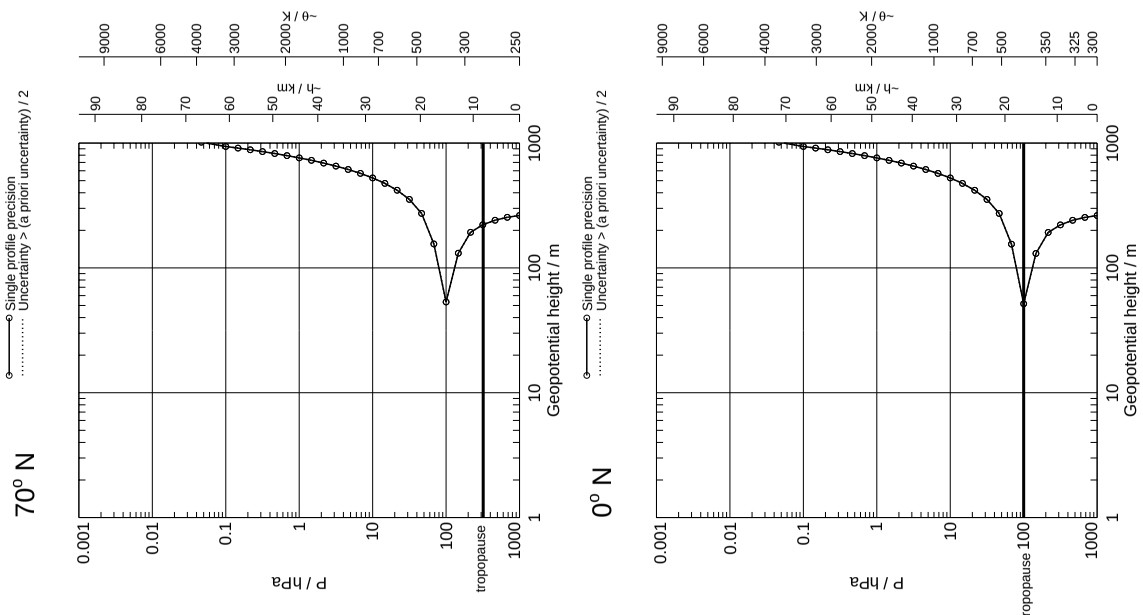

Figure 41: Geopotential height precision on high resolution grid, for Single Profile only, with no regularisation. Touchstone phase UpdatePtan. No averaging kernels are generated for this product which is derived from temperature and reference geopotential.

Blank page

GPH

H_2O

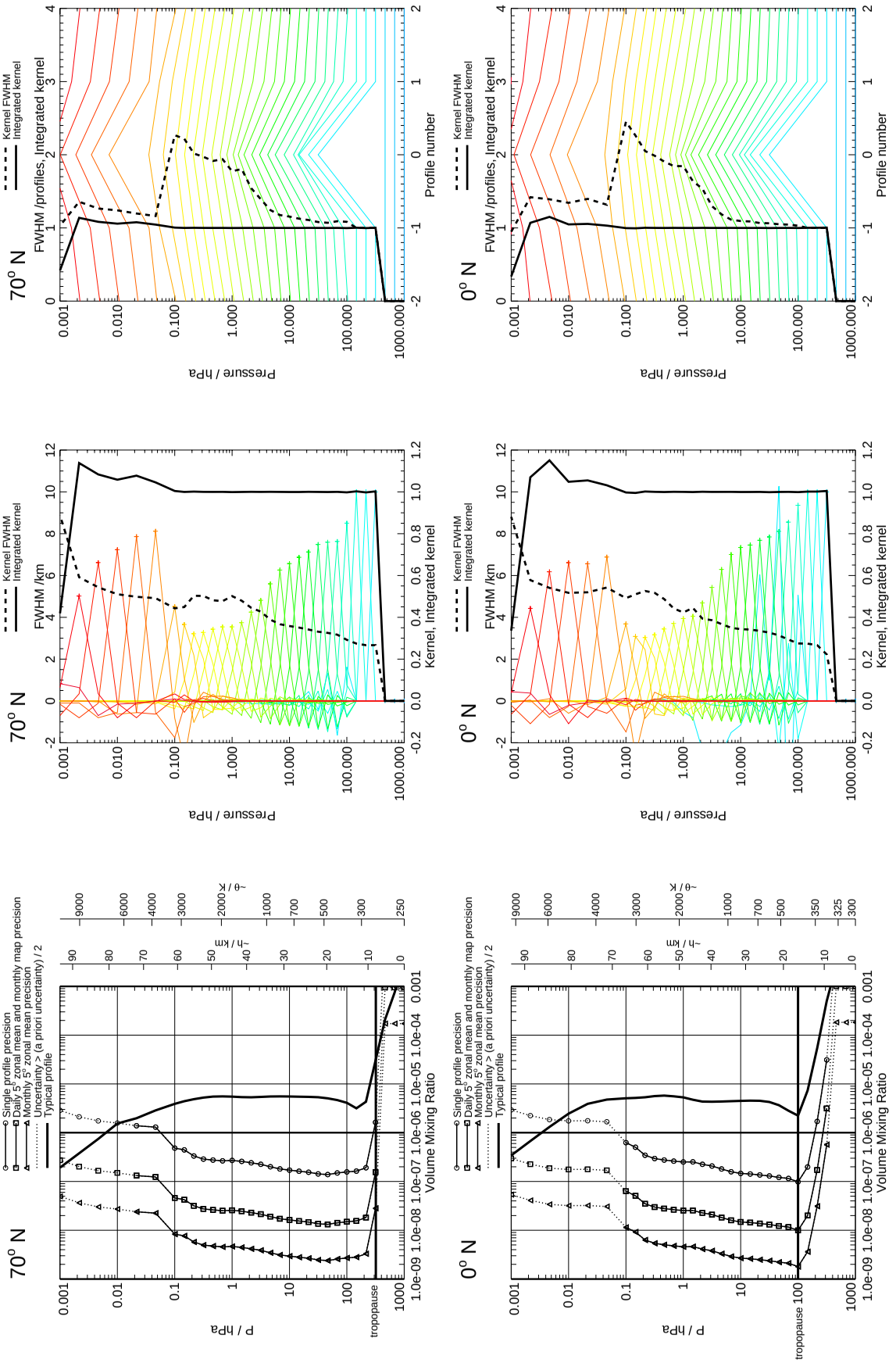

Figure 42: H_2O precision and averaging kernels, with V1.4 regularisation. V1.4 phased retrieval.

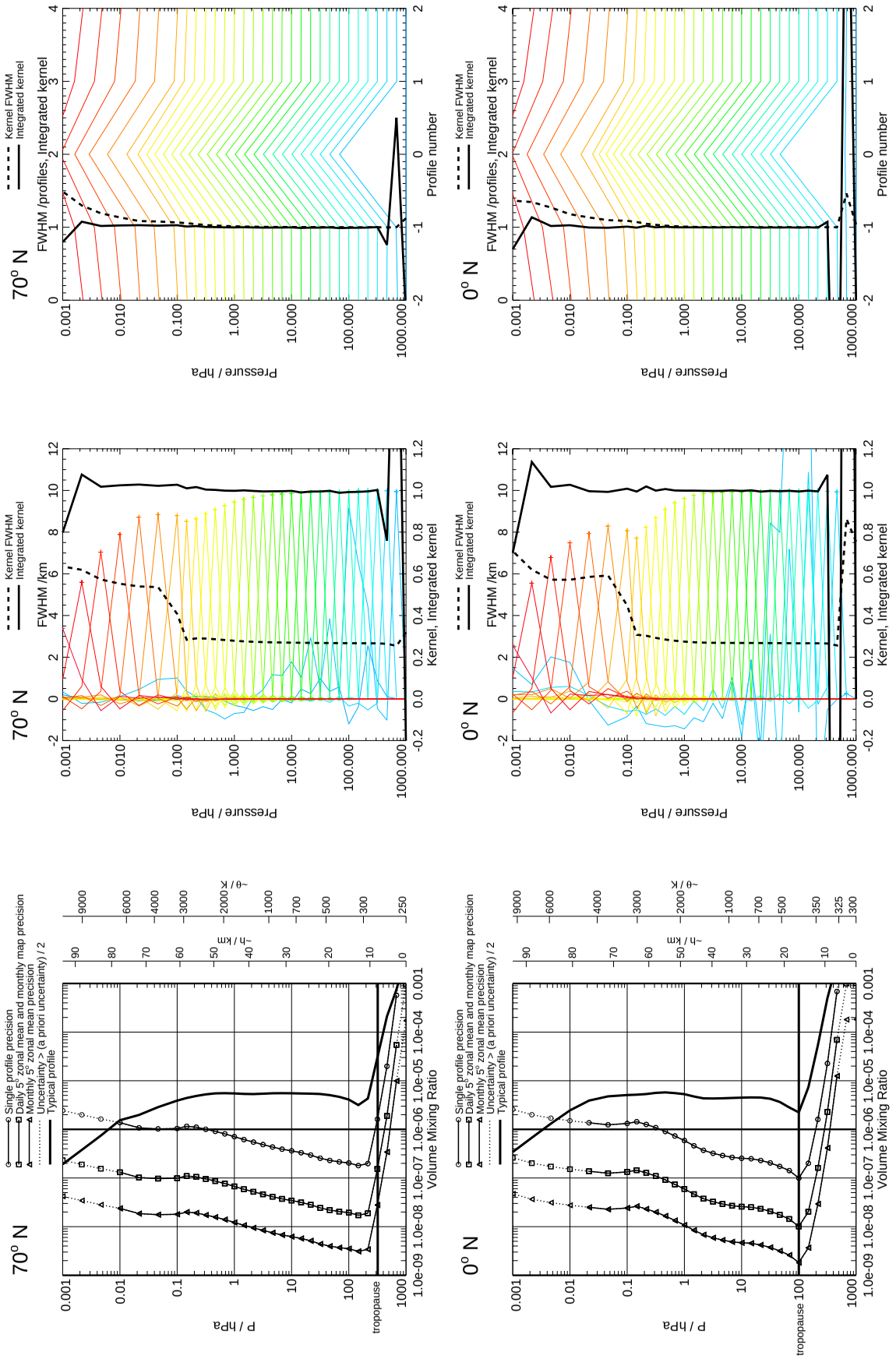

H_2O

Figure 43: H_2O precision and averaging kernels, with no regularisation. Touchstone retrieval.

H_2O

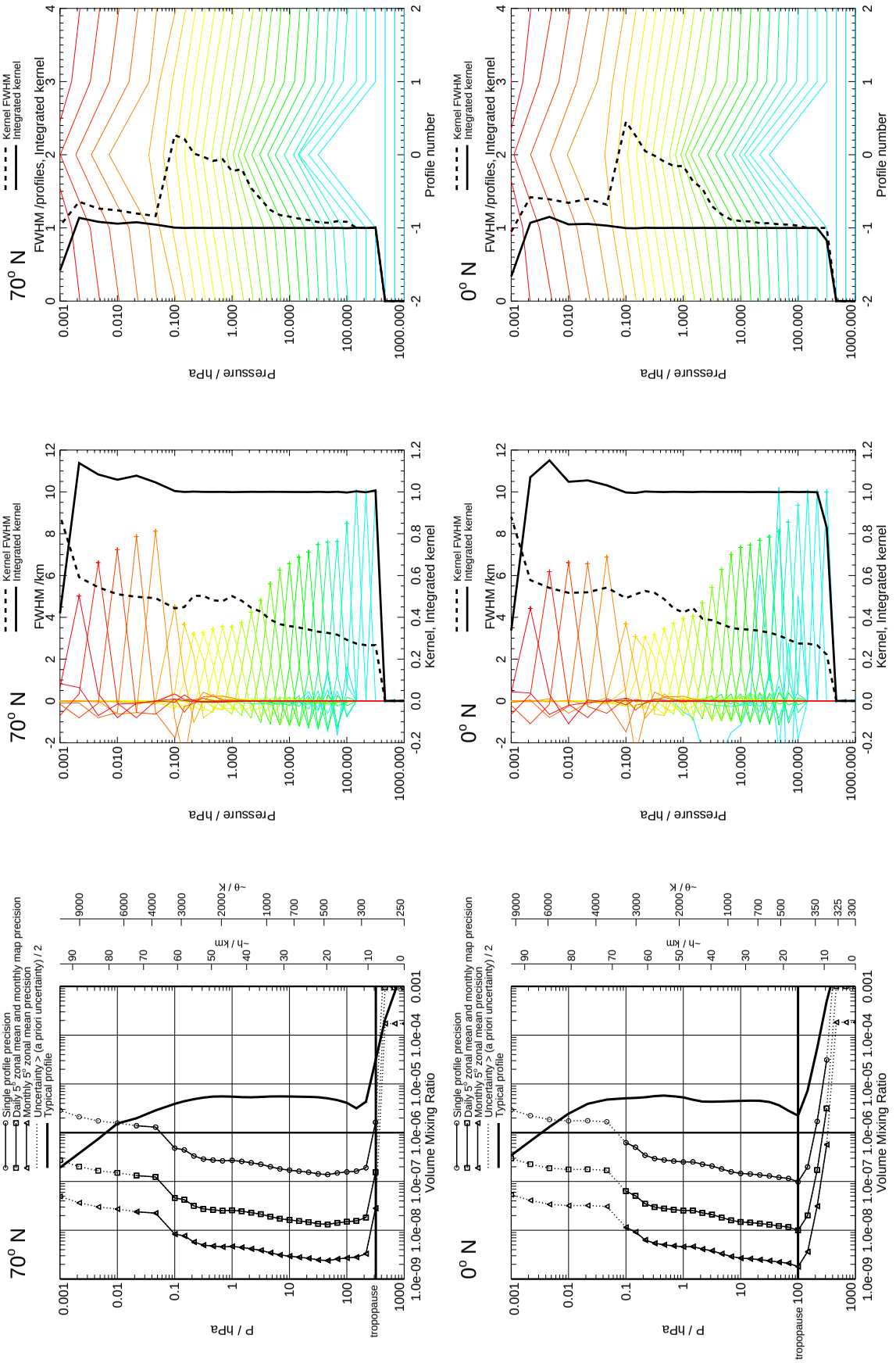

Figure 44: H_2O precision and averaging kernels, with V1.4 regularisation. V1.4 phase CorePlusR2.

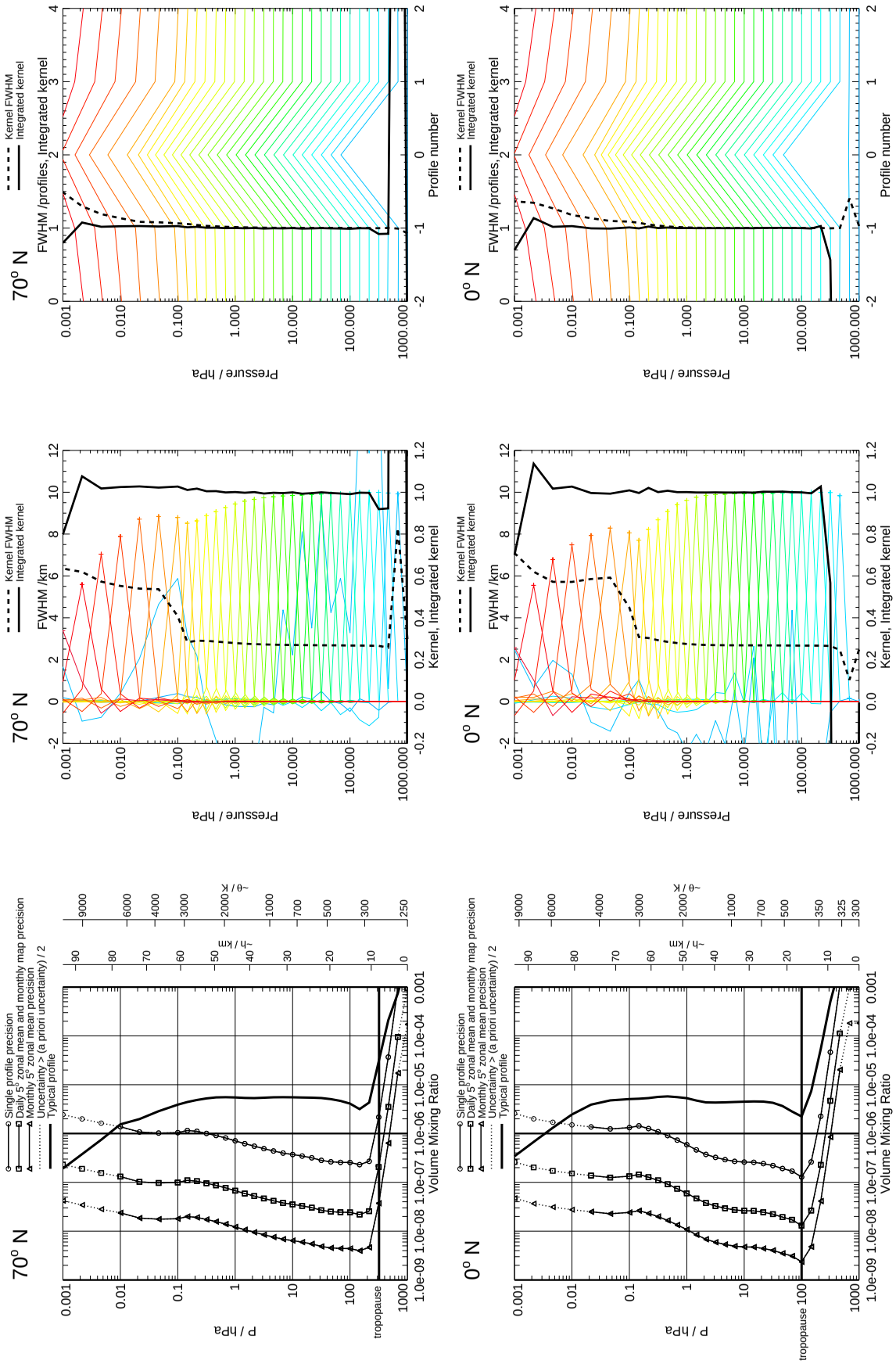

Figure 45: H_2O precision and averaging kernels, with no regularisation. Touchstone phase CorePlusR2.

H_2O

H_2O

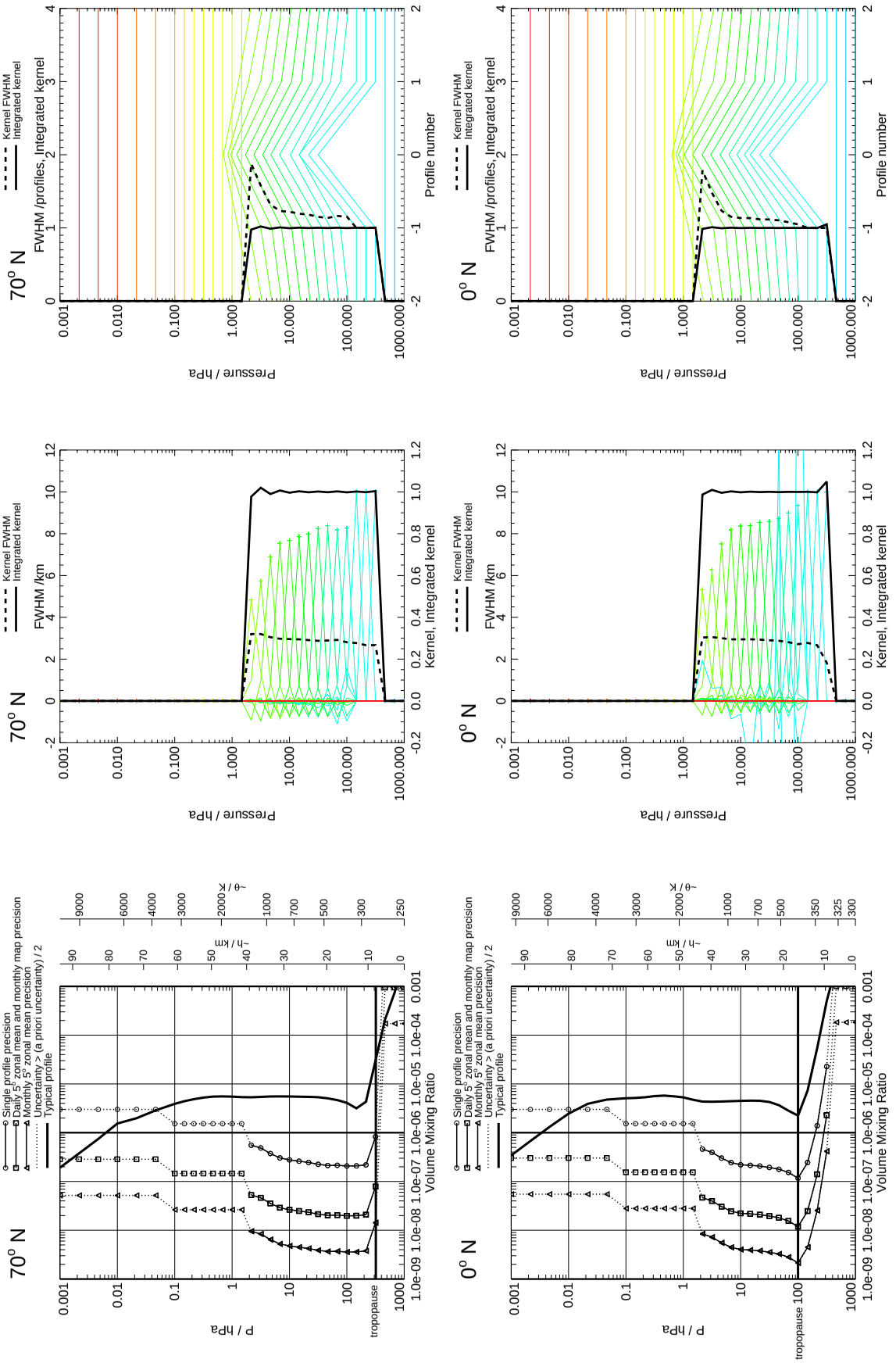

Figure 46: H_2O precision and averaging kernels, with V1.4 regularisation. V1.4 phase InitUTH.

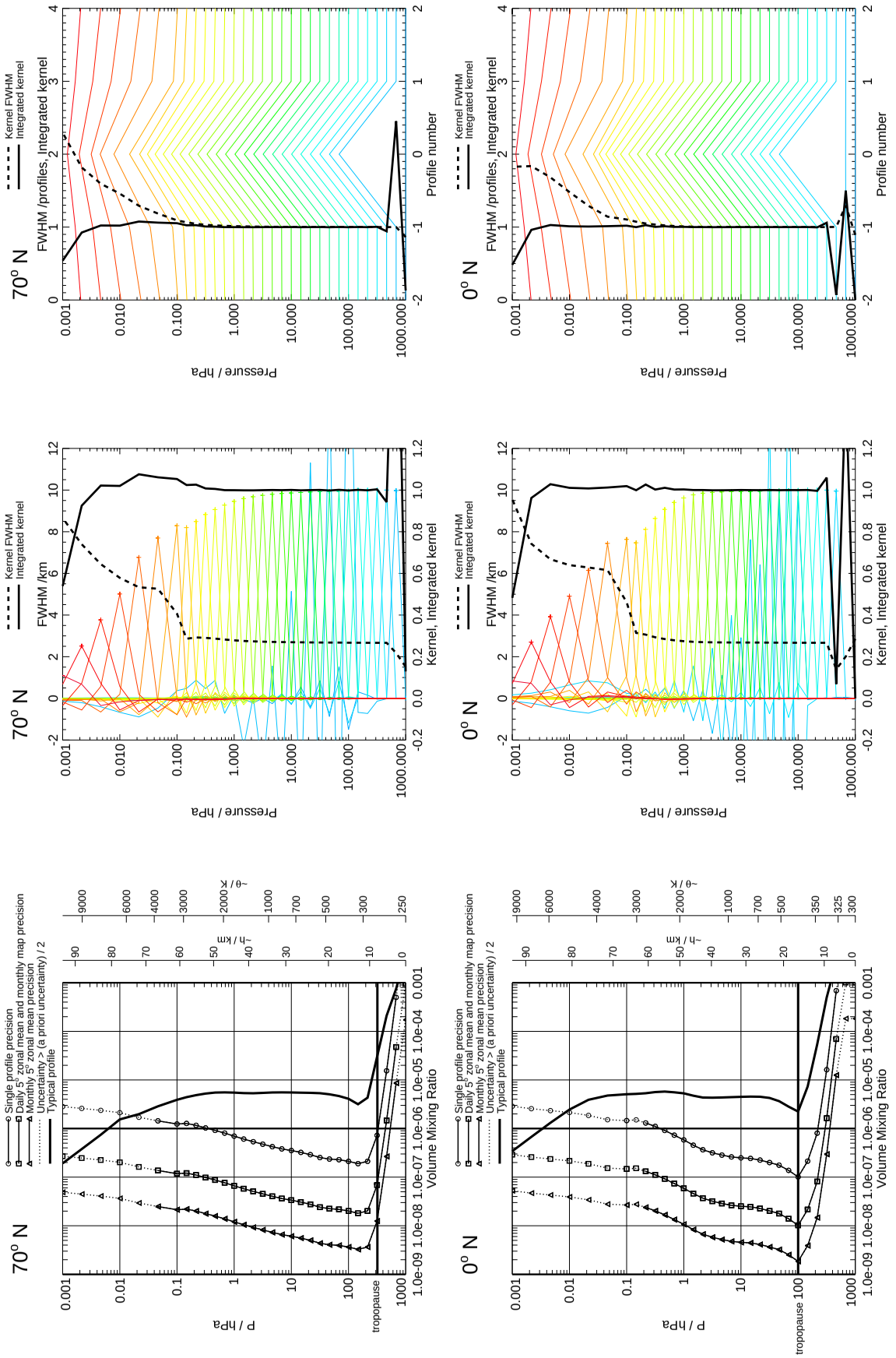

Figure 47: H_2O precision and averaging kernels, with no regularisation. Touchstone phase InitUTH.

H_2O

H_2O

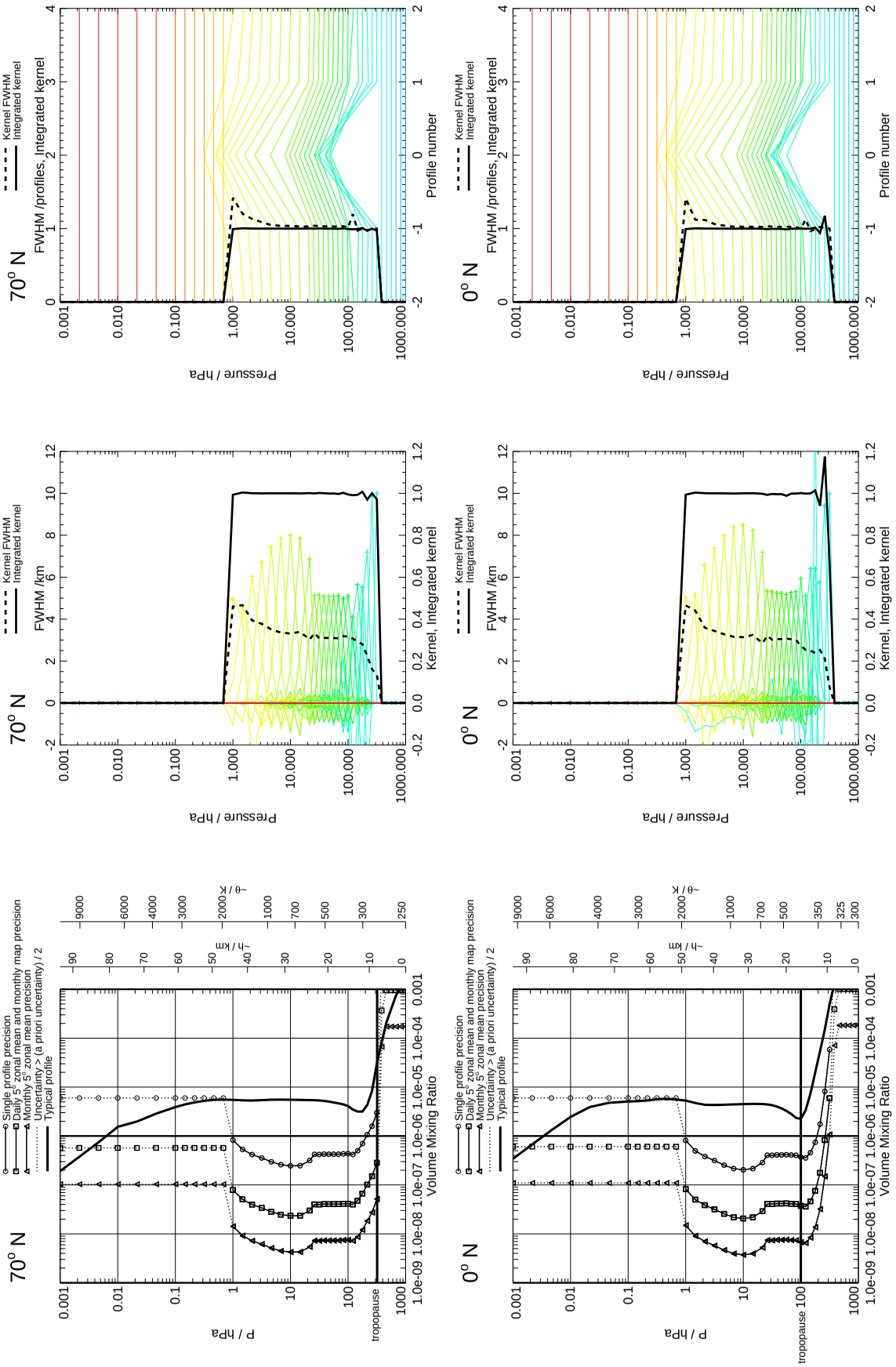

Figure 48: H_2O precision and averaging kernels on high resolution grid, with V1.4 regularisation. V1.4 phased retrieval.

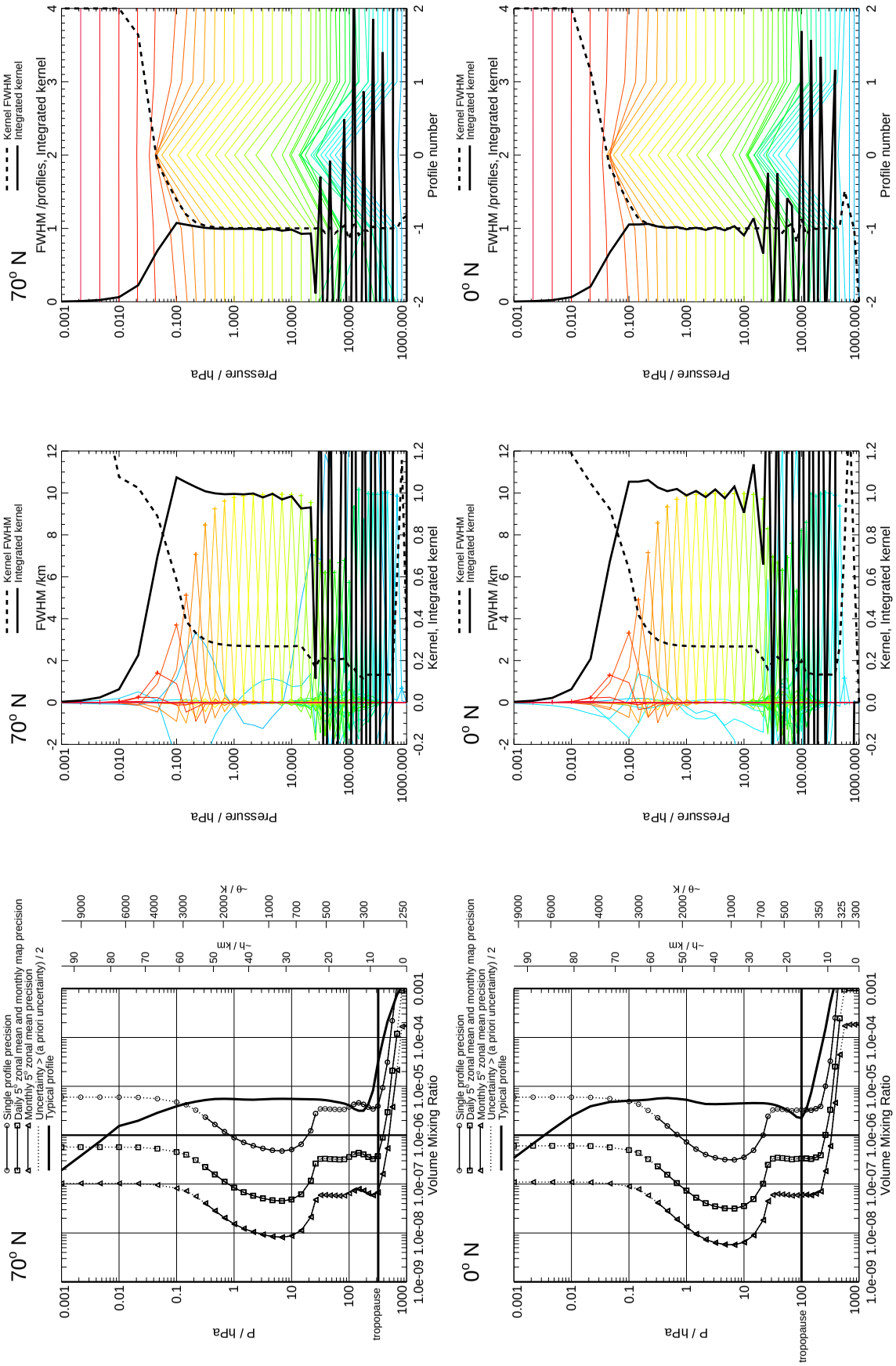

H_2O

Figure 49: H_2O precision and averaging kernels, on high resolution grid, with no regularisation. Touchstone retrieval. The oscillations in the integrated kernel for this retrieval (and the other Touchstone high resolution retrievals) indicate that retrieval of H_2O at 12/decade resolution is not possible.

H_2O

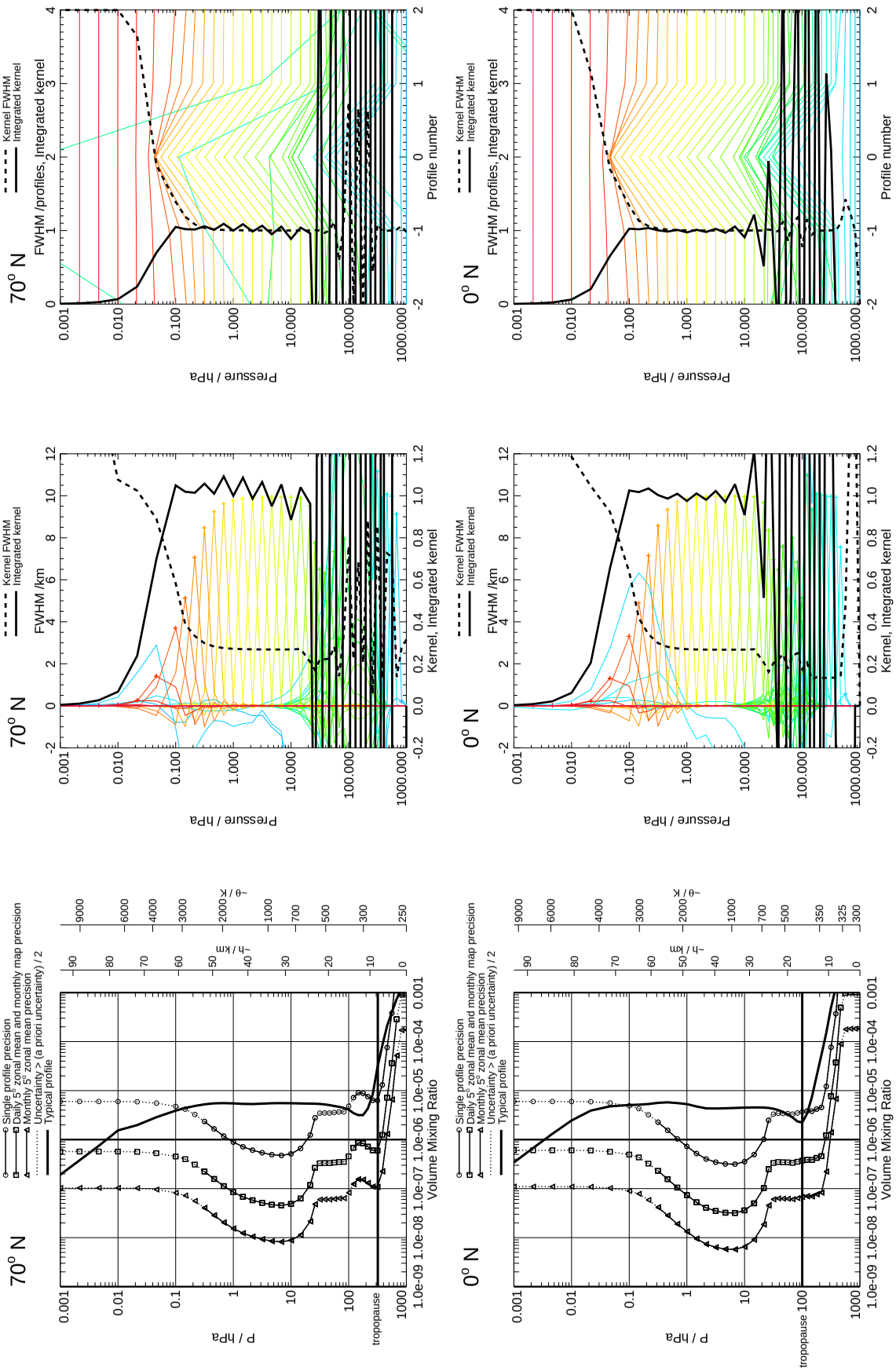

Figure 50: H_2O precision and averaging kernels, on high resolution grid, with no regularisation. Touchstone phase CorePlusR2.

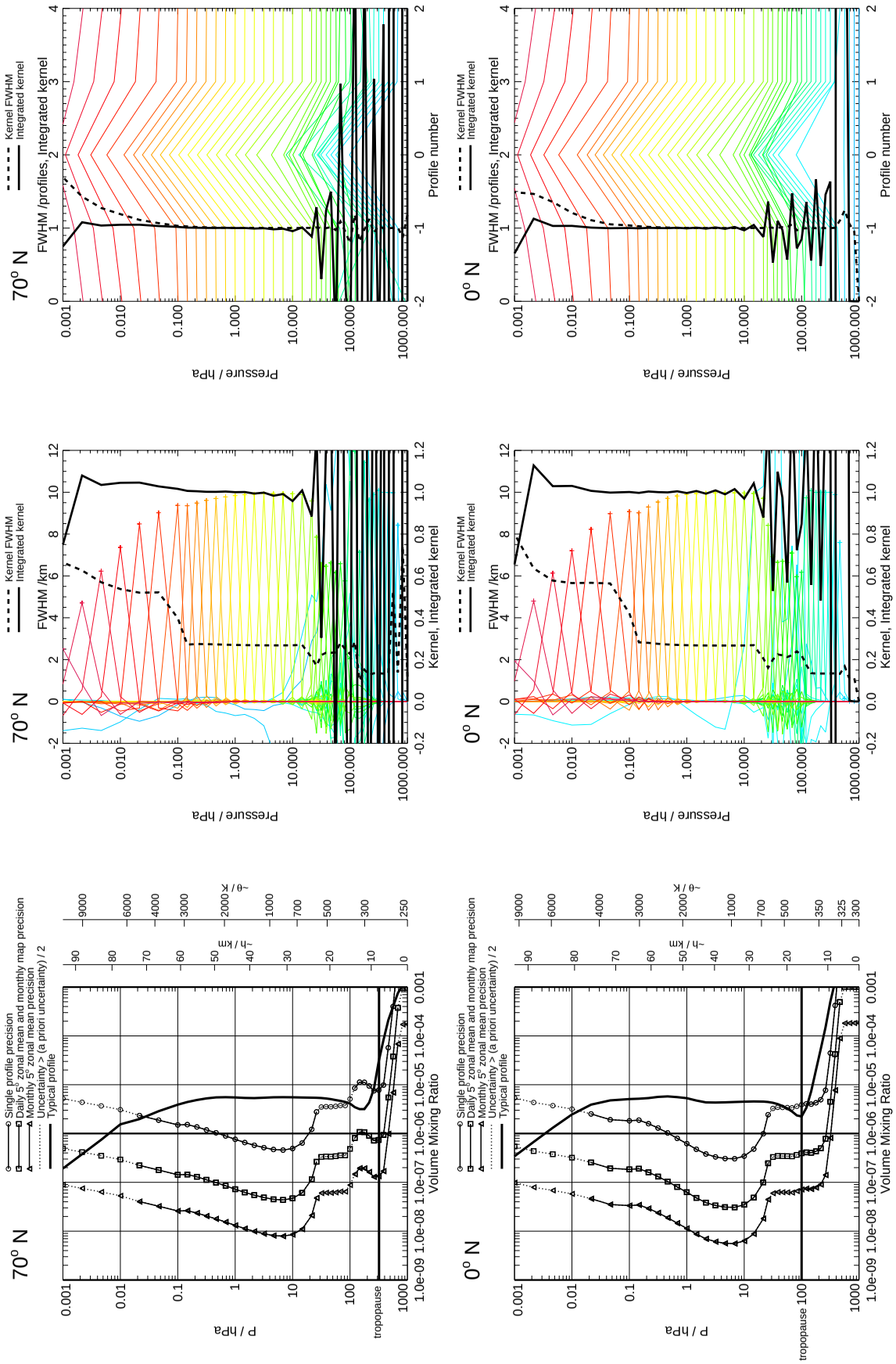

H_2O

Figure 51: H_2O precision and averaging kernels, on high resolution grid, with no regularisation. Touchstone phase InitUTH.

HCl

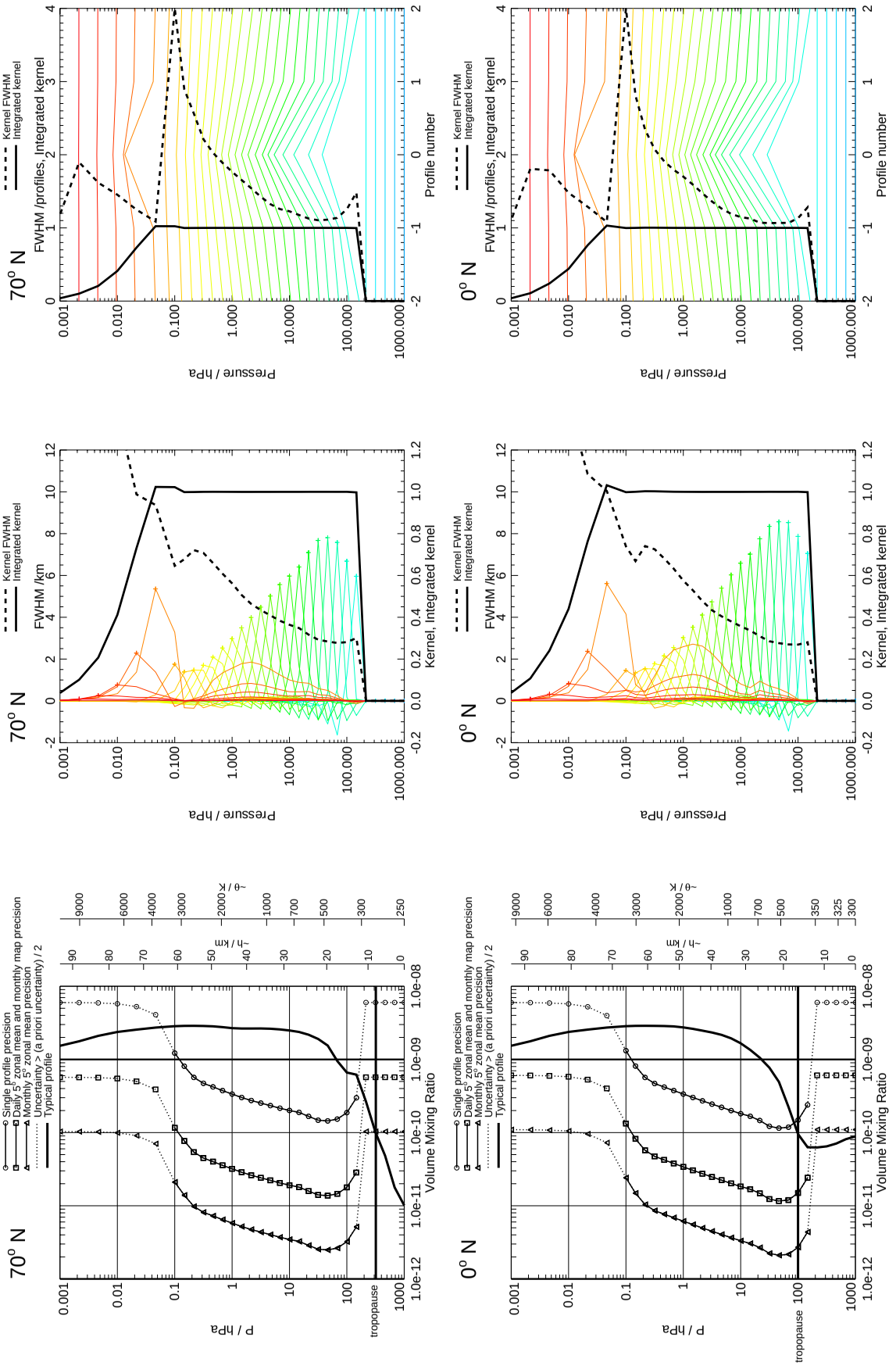

Figure 52: HCl precision and averaging kernels, with V1.4 regularisation. V1.4 phased retrieval.

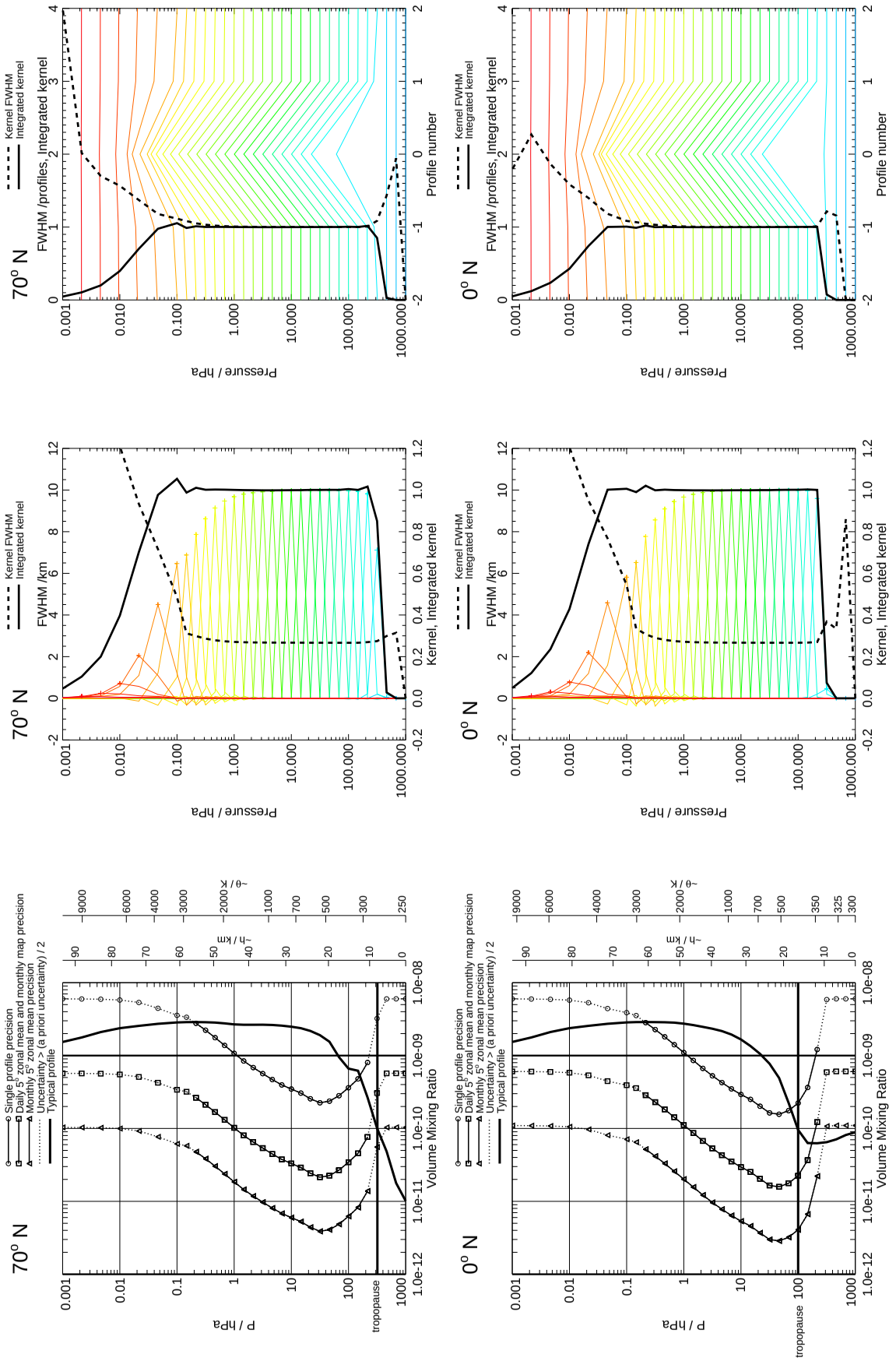

Figure 53: HCl precision and averaging kernels, with no regularisation. Touchstone retrieval.

HCl

HCl

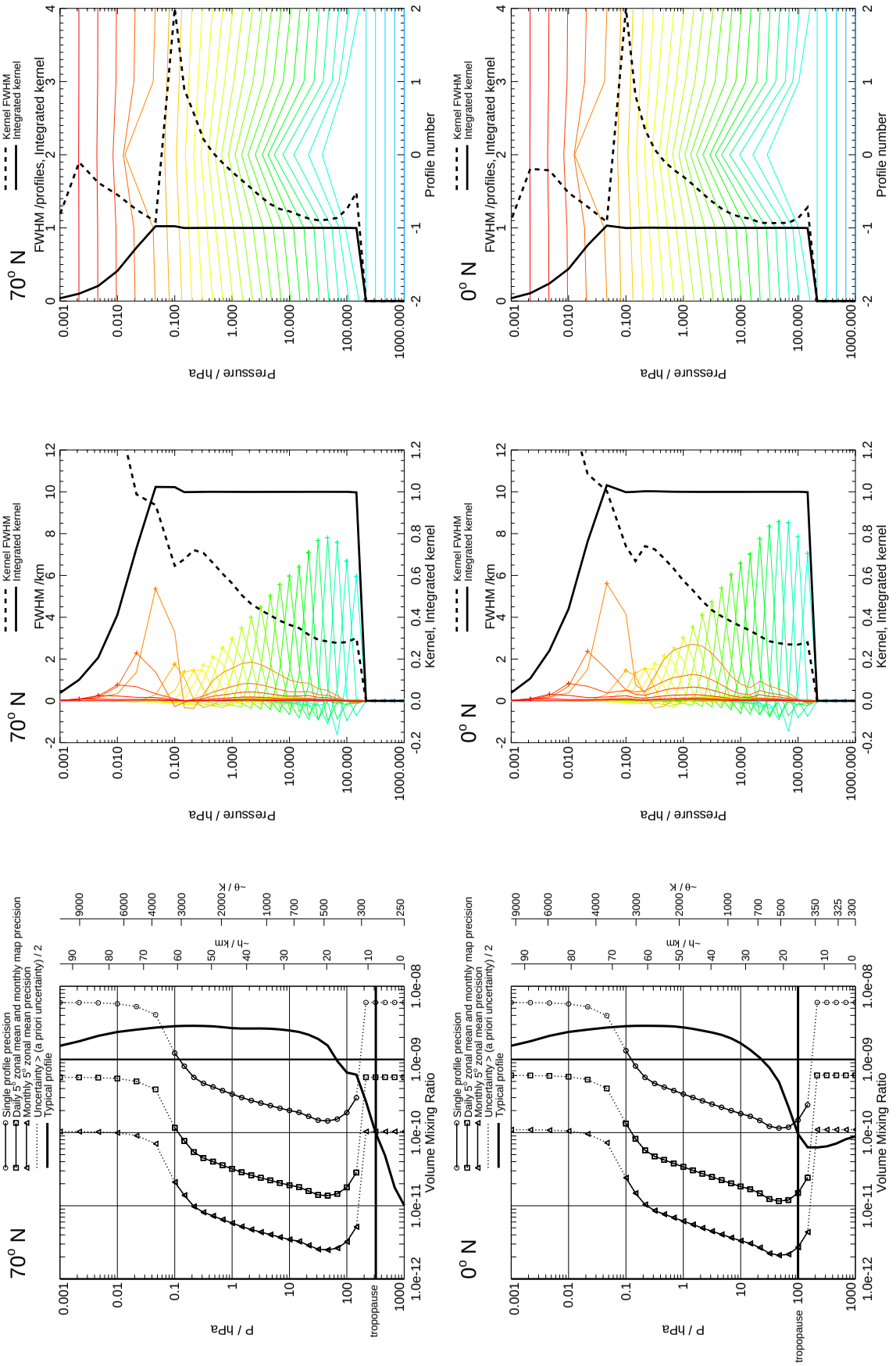

Figure 54: HCl precision and averaging kernels, with V1.4 regularisation. V1.4 phase CorePlusR4.

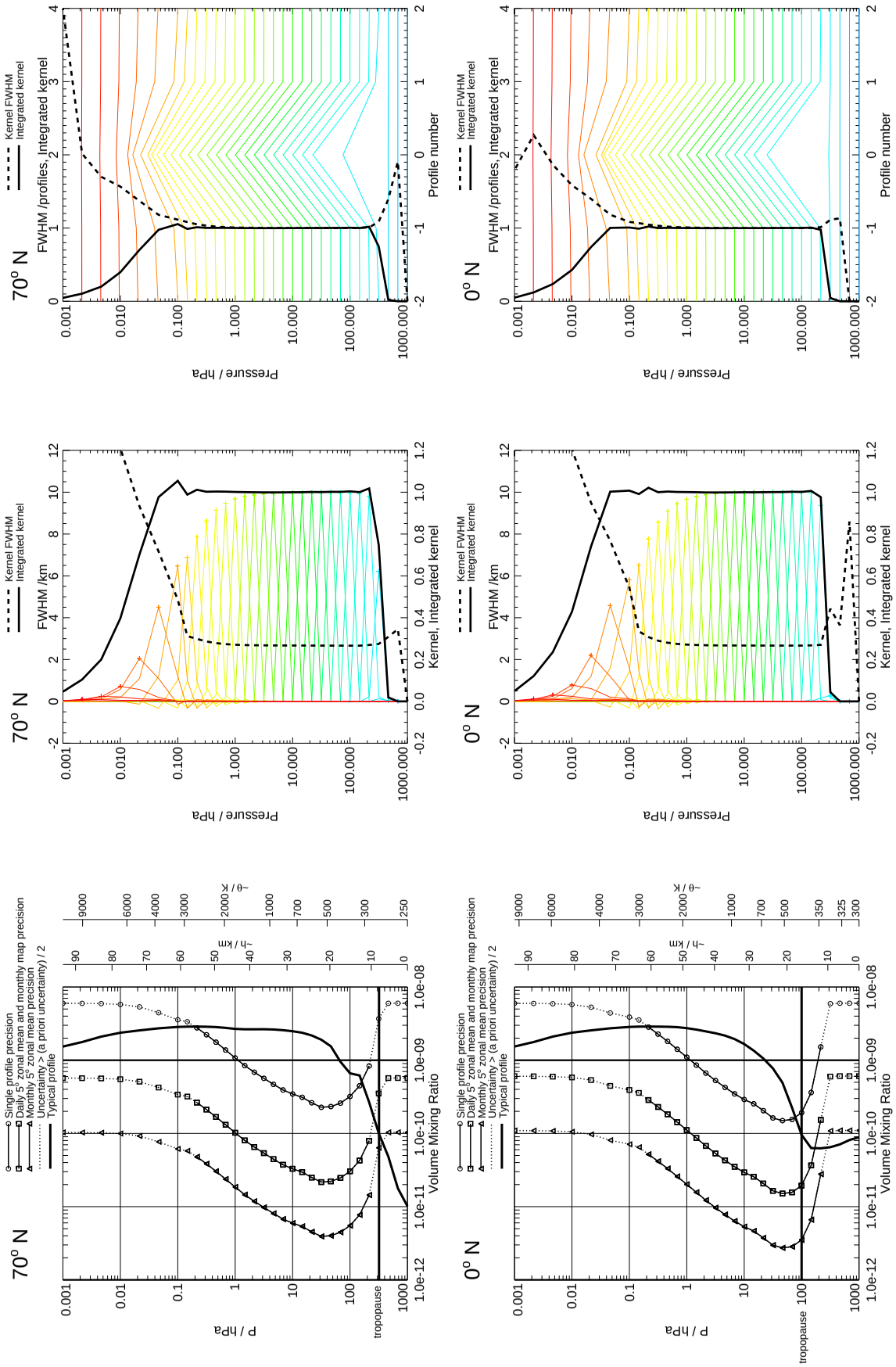

HCl

Figure 55: HCl precision and averaging kernels, with no regularisation. Touchstone phase CorePlusR4.

HCN

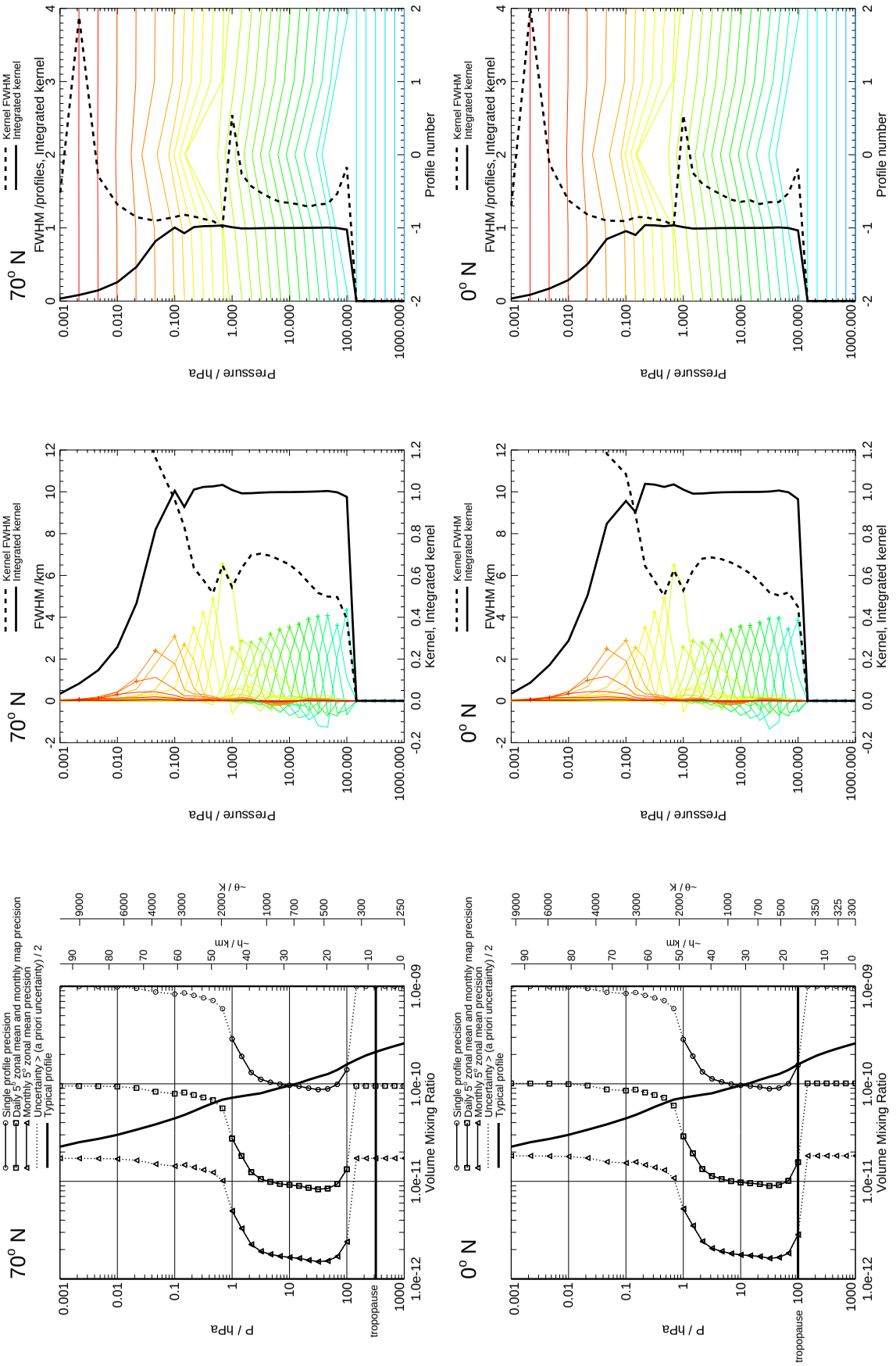

Figure 56: HCN precision and averaging kernels, with V1.4 regularisation. V1.4 phased retrieval.

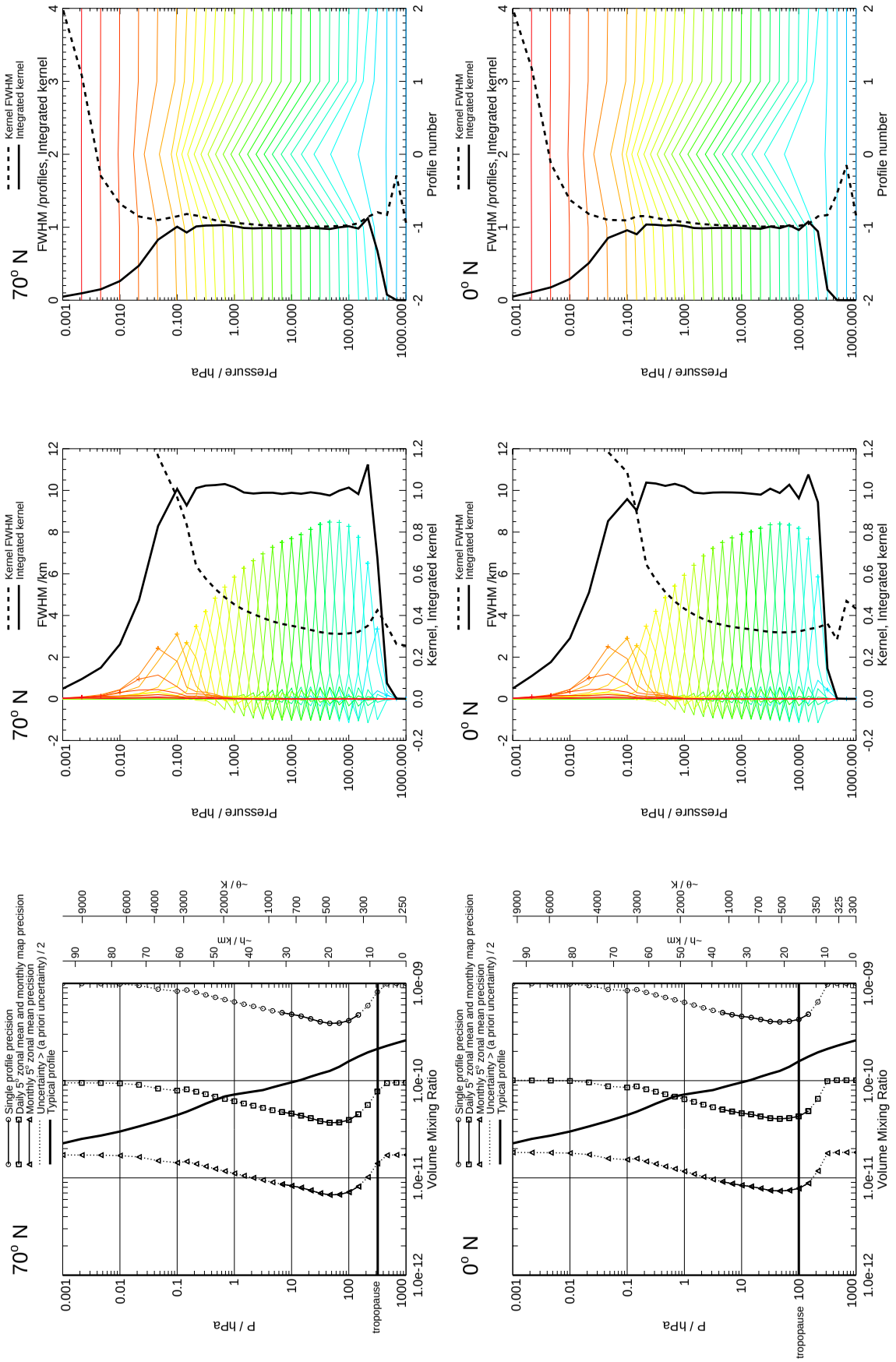

HCN

Figure 57: HCN precision and averaging kernels, with no regularisation. Touchstone retrieval.

HCN

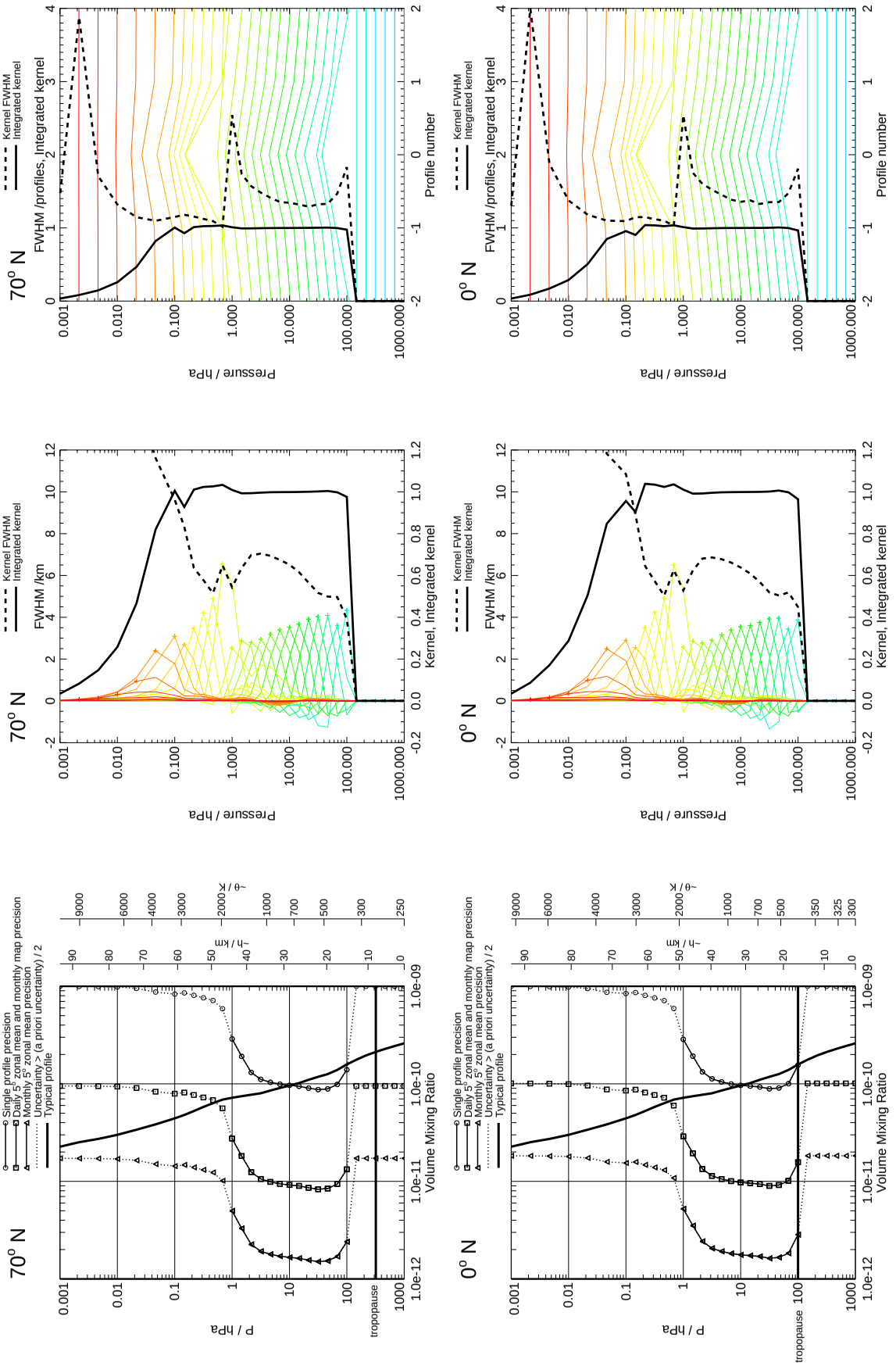

Figure 58: HCN precision and averaging kernels, with V1.4 regularisation. V1.4 phase CorePlusR2.

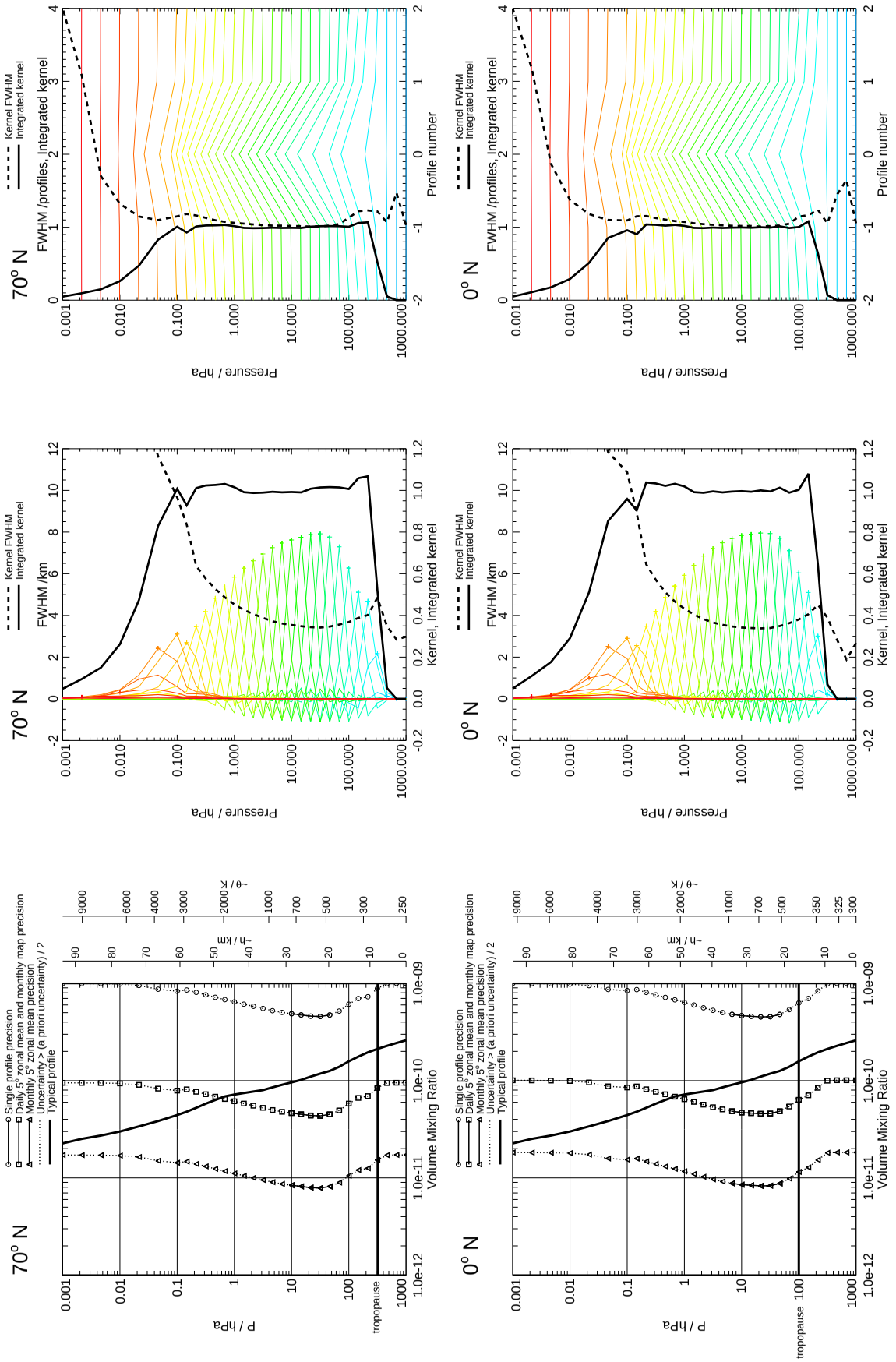

Figure 59: HCN precision and averaging kernels, with no regularisation. Touchstone phase CorePlusR2.

HCN

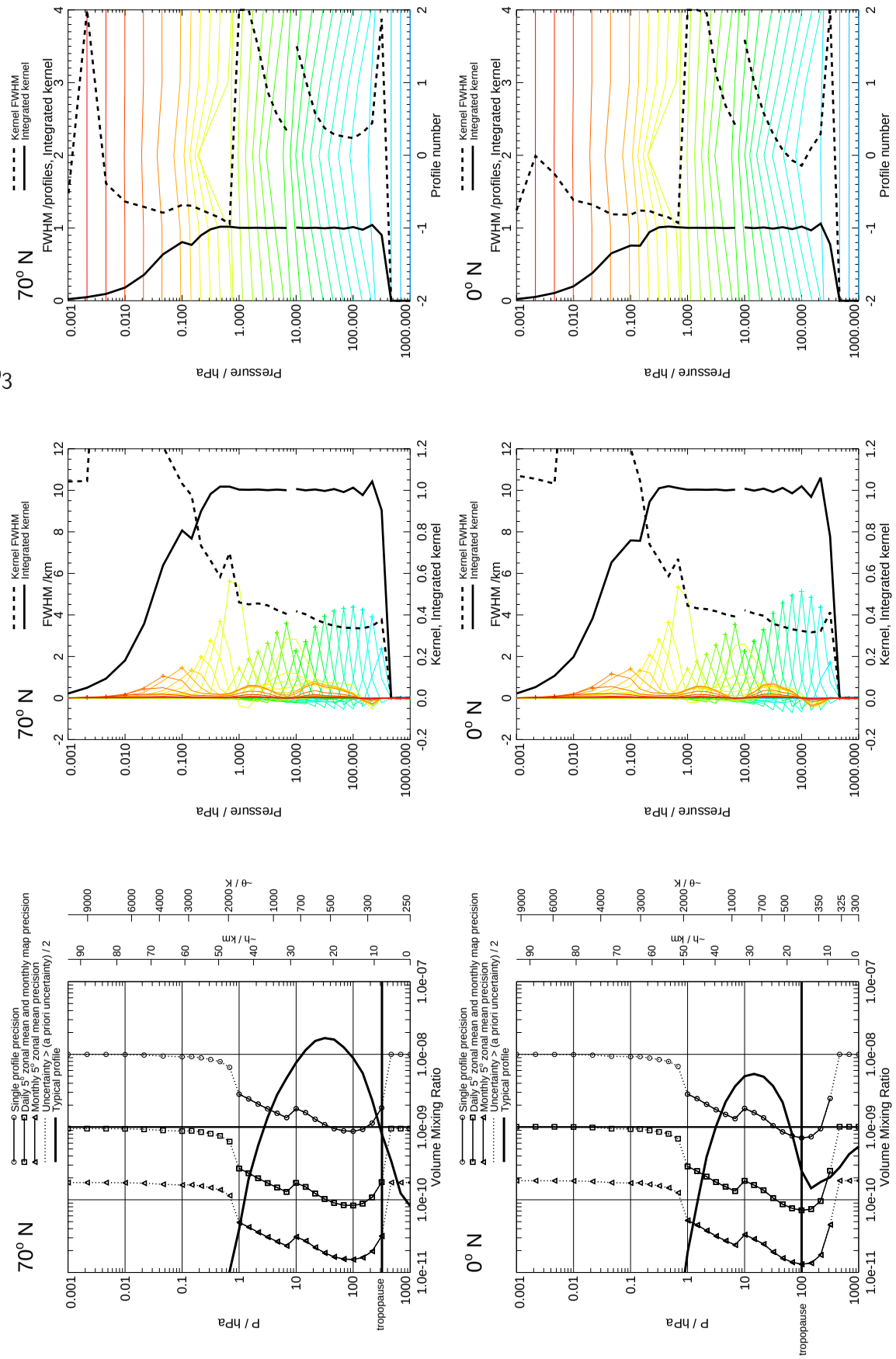

Figure 60: HNO_3 precision and averaging kernels, with V1.4 regularisation. V1.4 phased retrieval. The HNO_3 standard product is a combination of the results from CorePlusR3 (at and below 10 hPa) and CorePlusR2 (above 10 hPa). The results from these phases/ranges are displayed together in these plots.

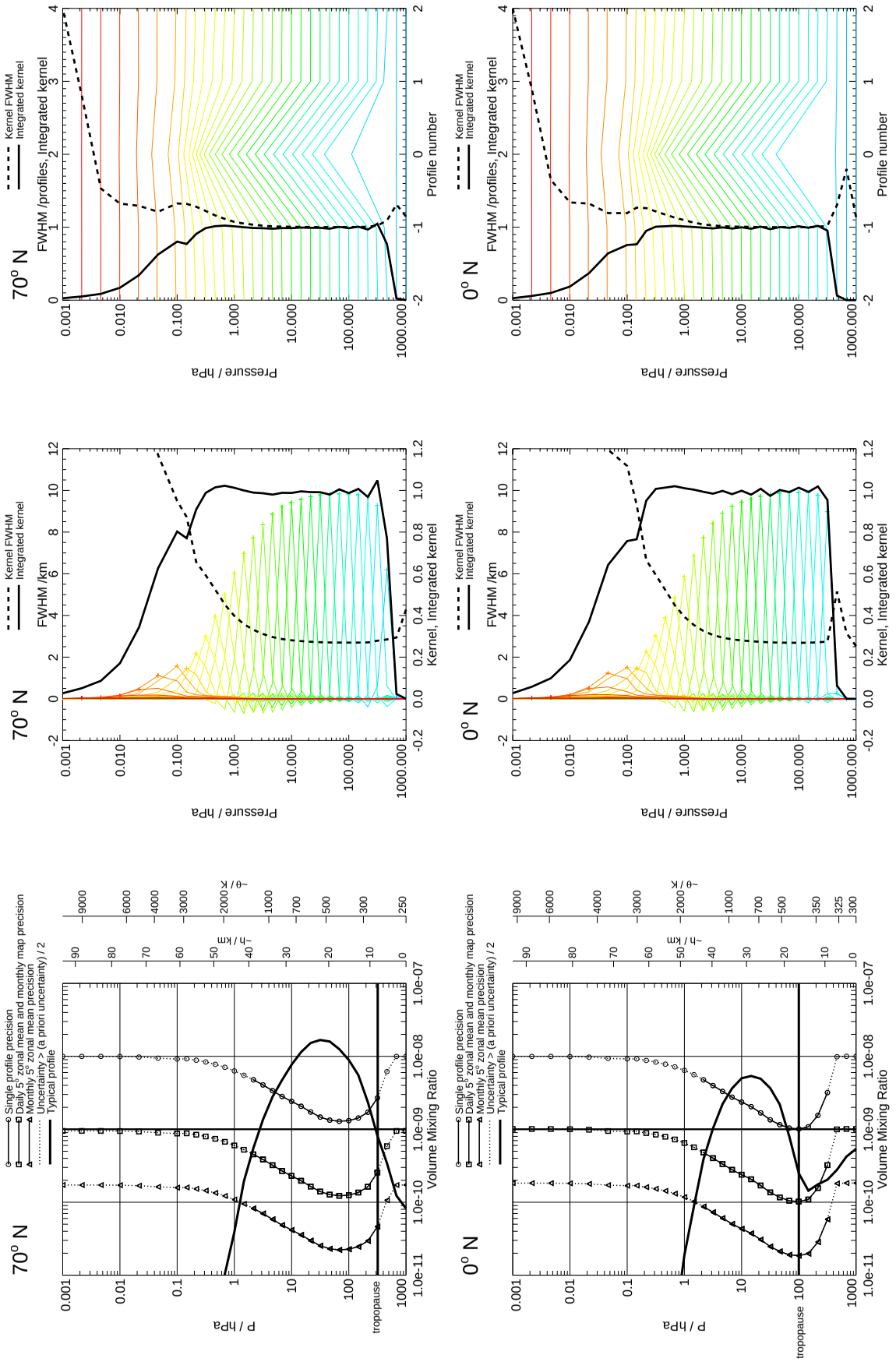

Figure 61: HNO_3 precision and averaging kernels, with no regularisation. Touchstone retrieval.

HNO_3

HNO_3

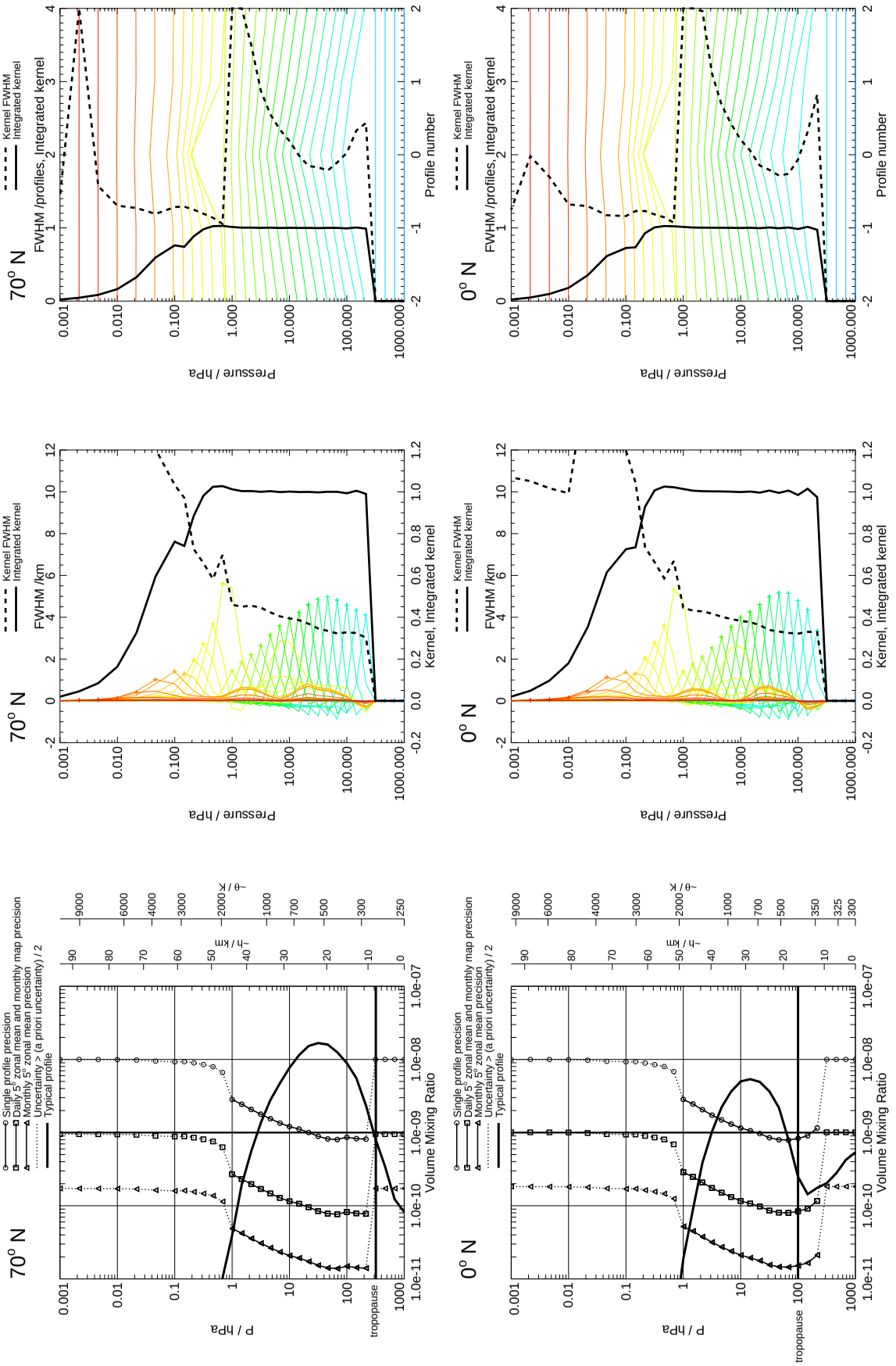

Figure 62: HNO_3 precision and averaging kernels, with V1.4 regularisation. V1.4 phase CorePlusR2.

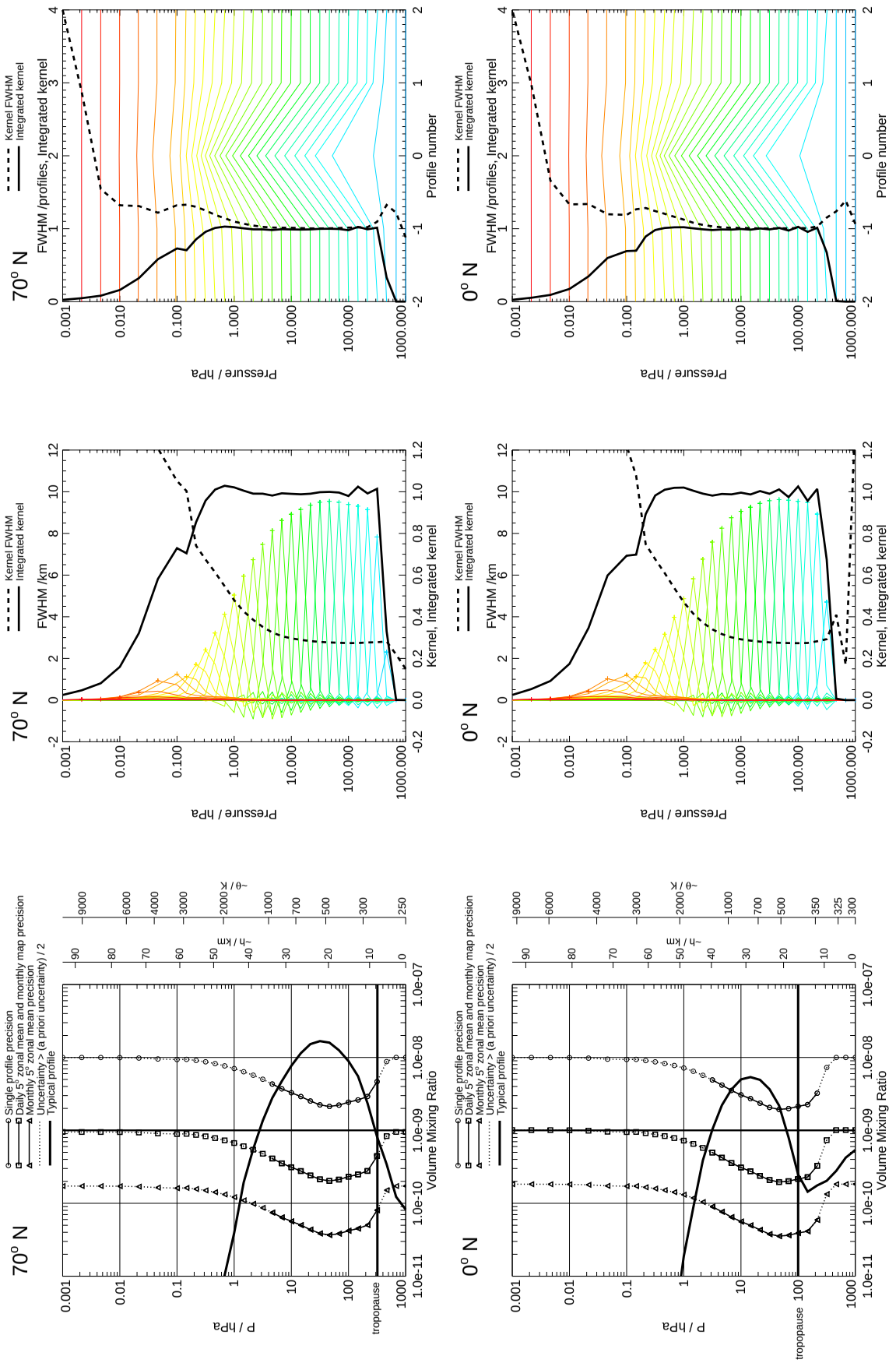

HNO_3

Figure 63: HNO_3 precision and averaging kernels, with no regularisation. Touchstone phase CorePlusR2.

HNO_3

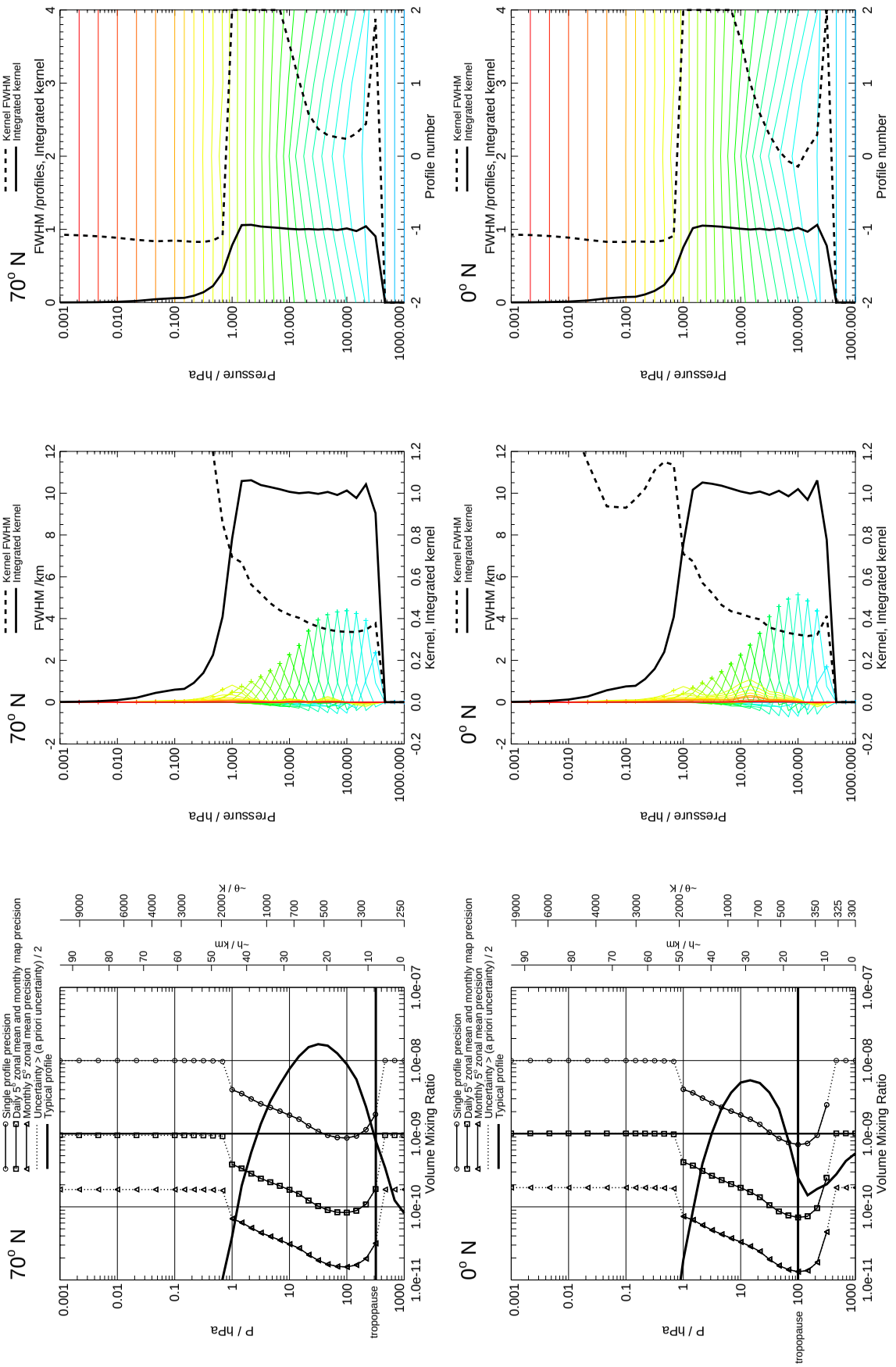

Figure 64: HNO_3 precision and averaging kernels, with V1.4 regularisation. V1.4 phase CorePlusR3.

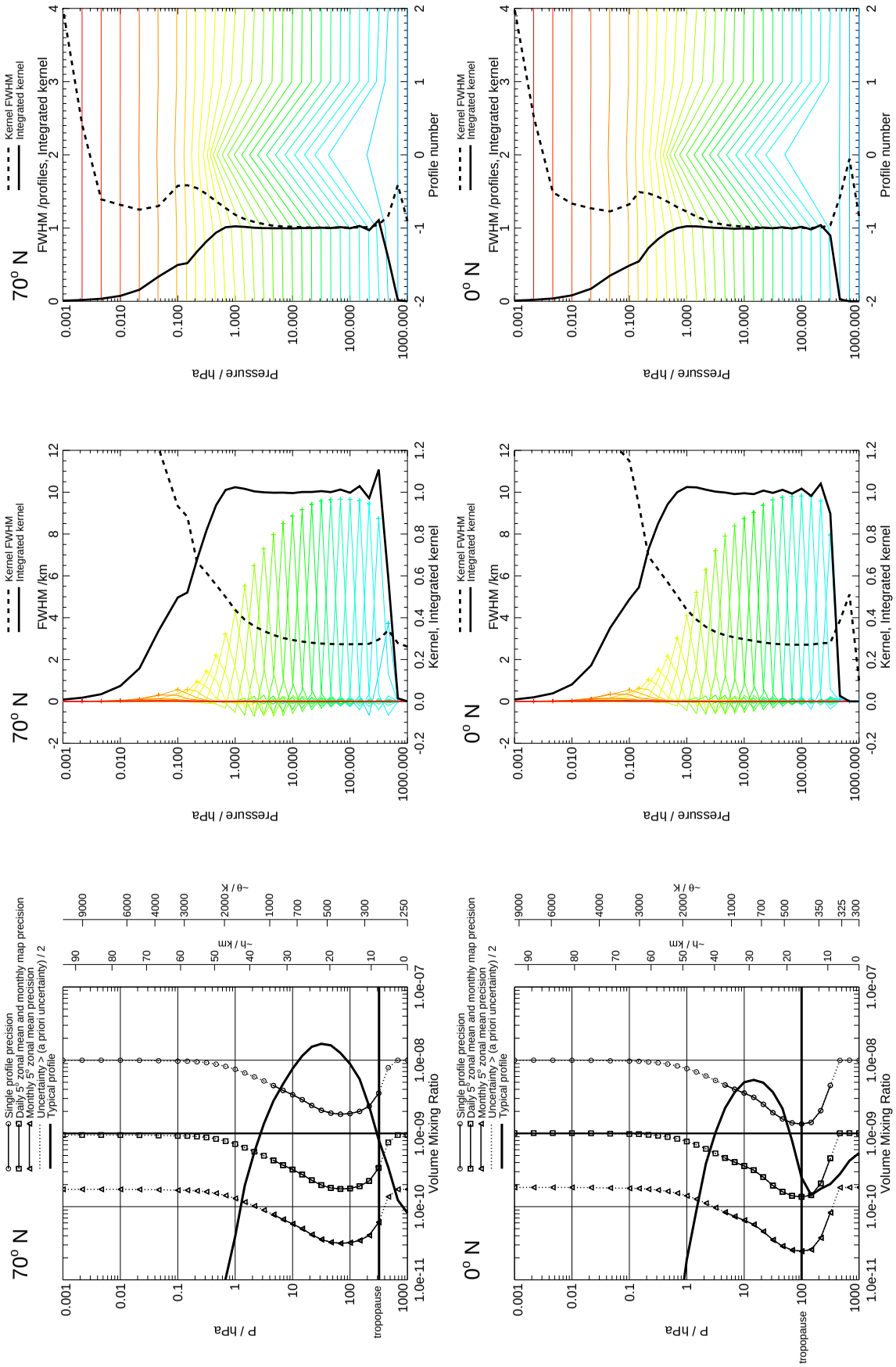

HNO_3

Figure 65: HNO_3 precision and averaging kernels, with no regularisation. Touchstone phase CorePlusR3.

HNO_3

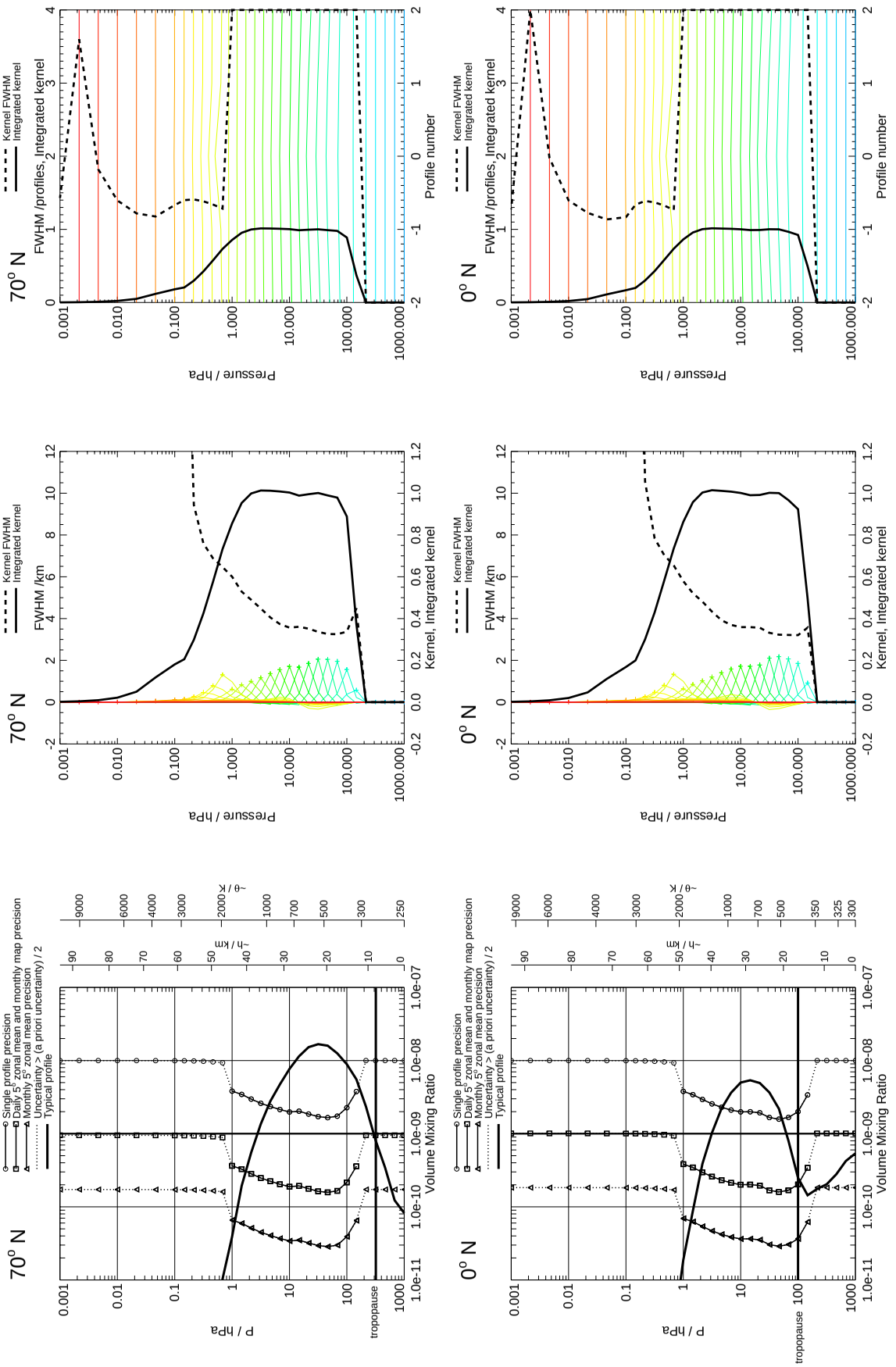

Figure 66: HNO_3 precision and averaging kernels, with V1.4 regularisation. V1.4 phase CorePlusR4.

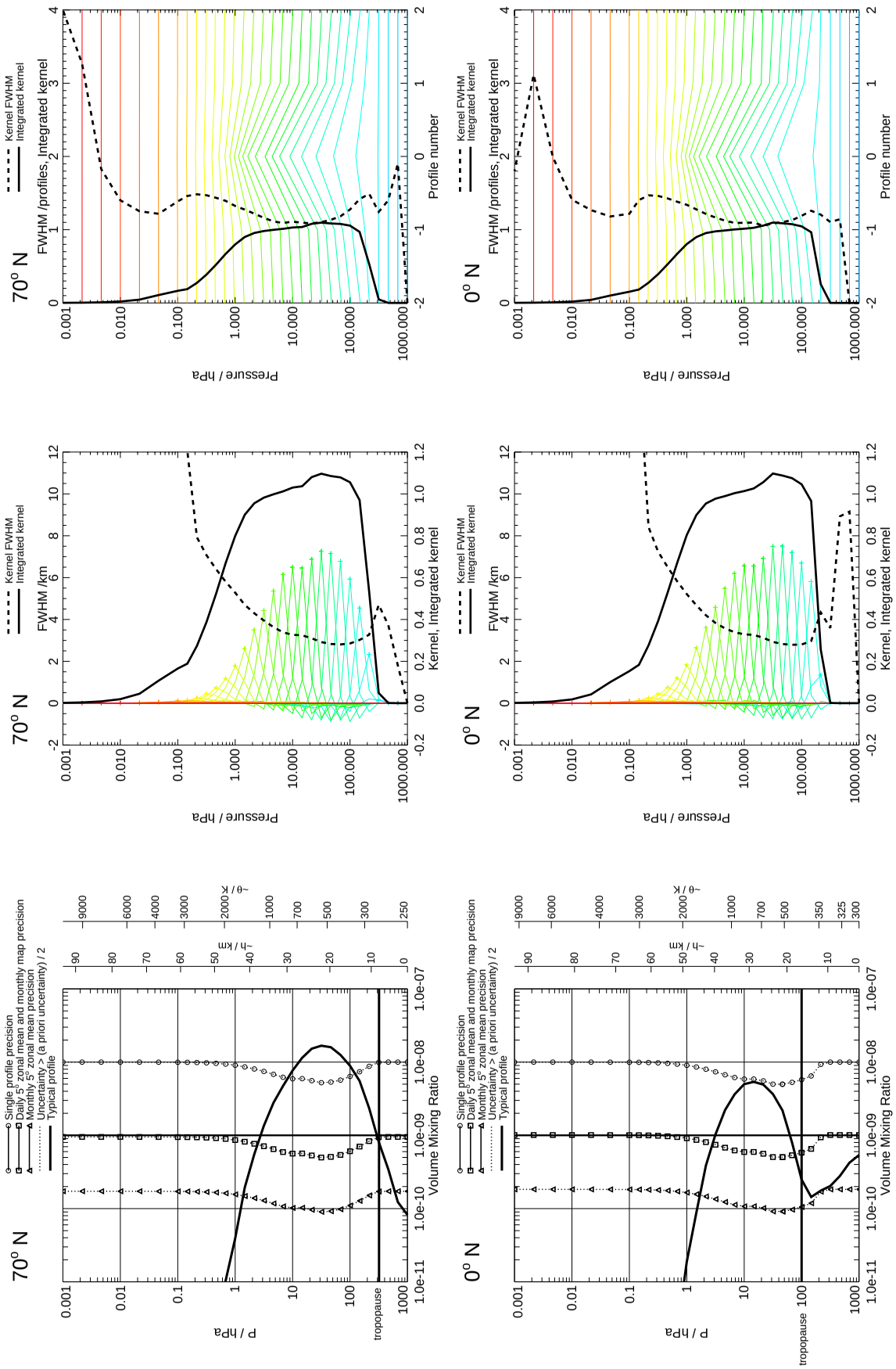

Figure 67: HNO_3 precision and averaging kernels, with no regularisation. Touchstone phase CorePlusR4.

HNO_3

HO_2

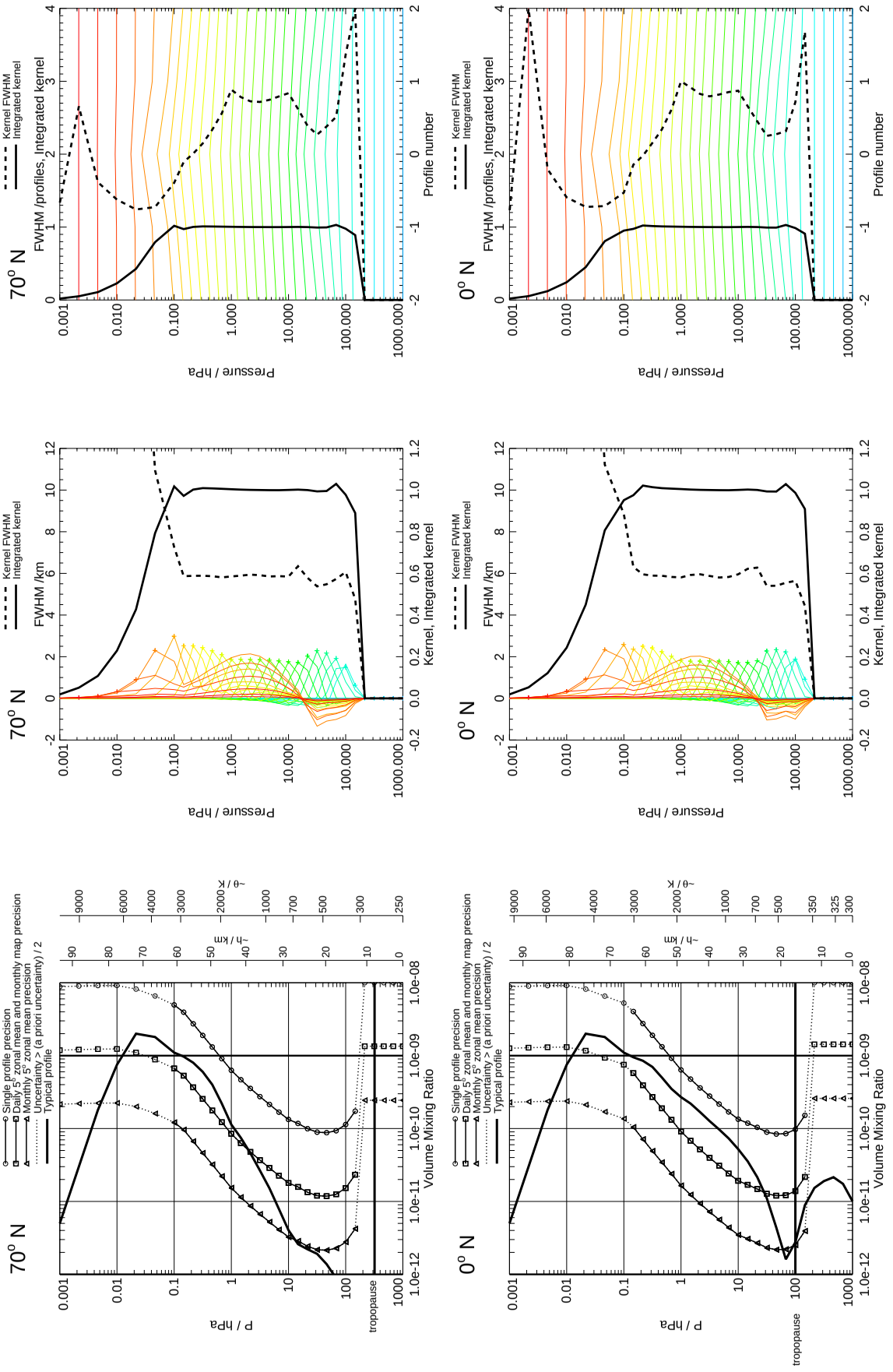

Figure 68: HO_2 precision and averaging kernels, with V1.4 regularisation. V1.4 phased retrieval.

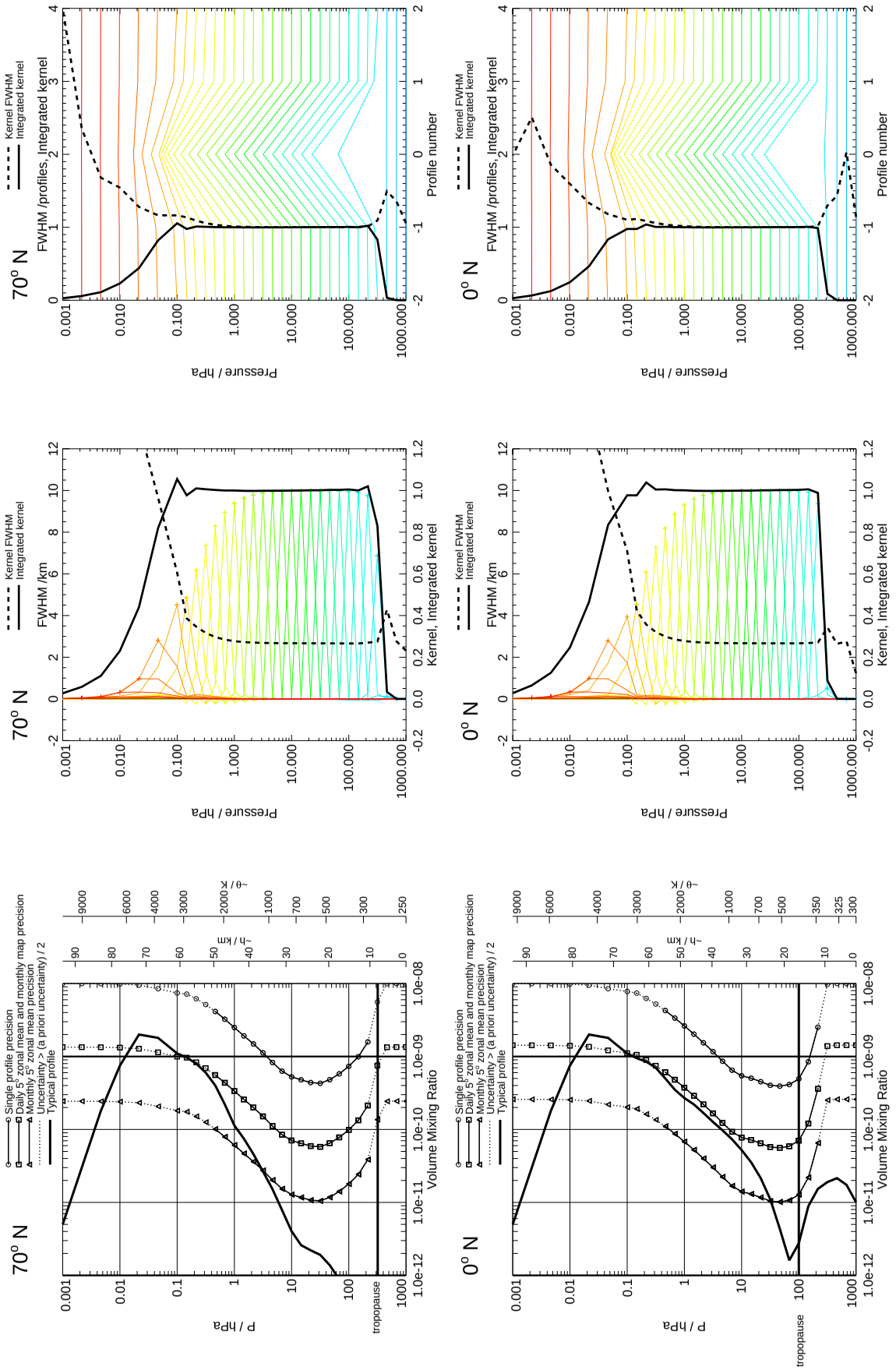

Figure 69: HO_2 precision and averaging kernels, with no regularisation. Touchstone retrieval.

HO_2

HO_2

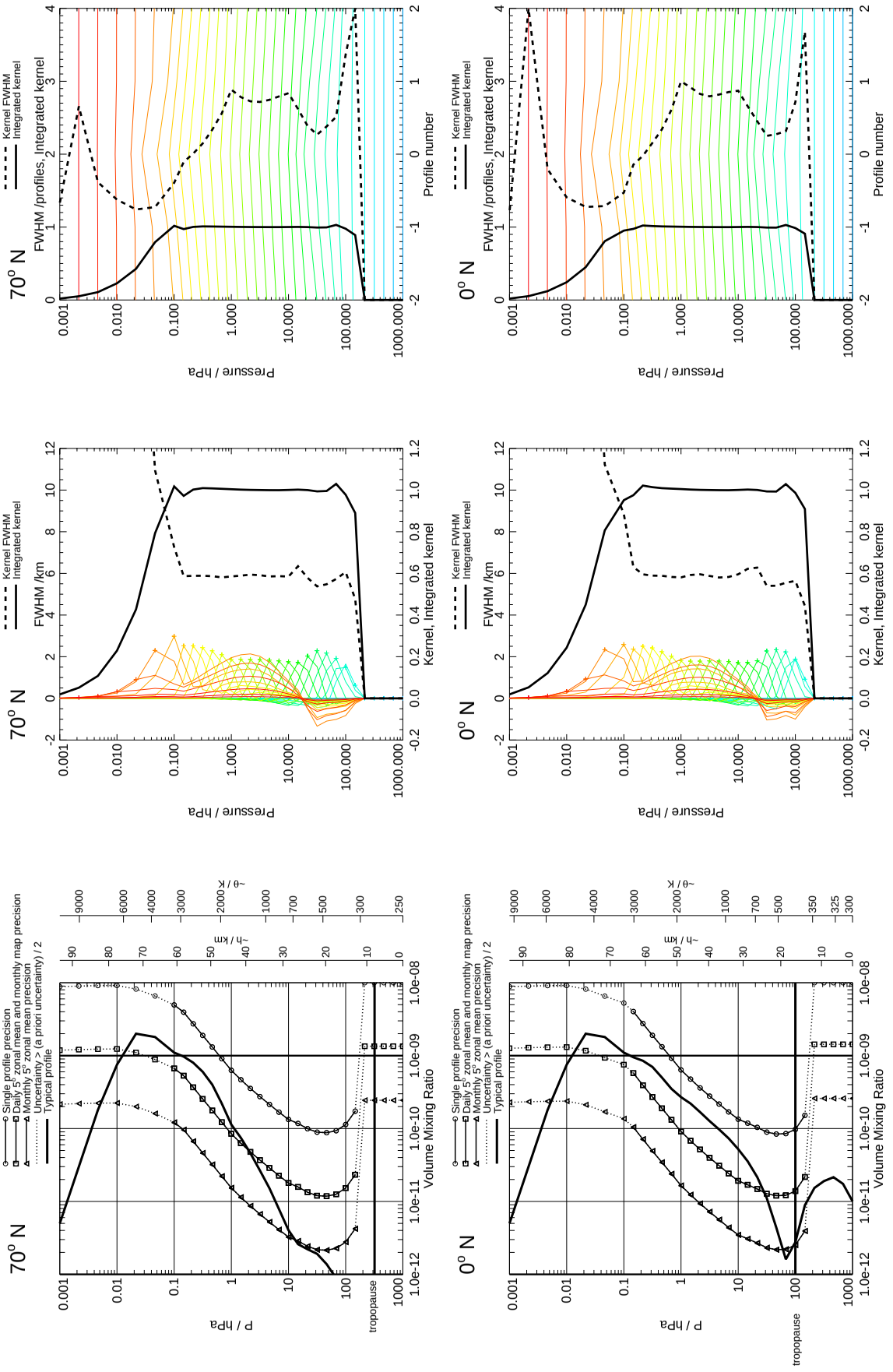

Figure 70: HO_2 precision and averaging kernels, with V1.4 regularisation. V1.4 phase CorePlusR4.

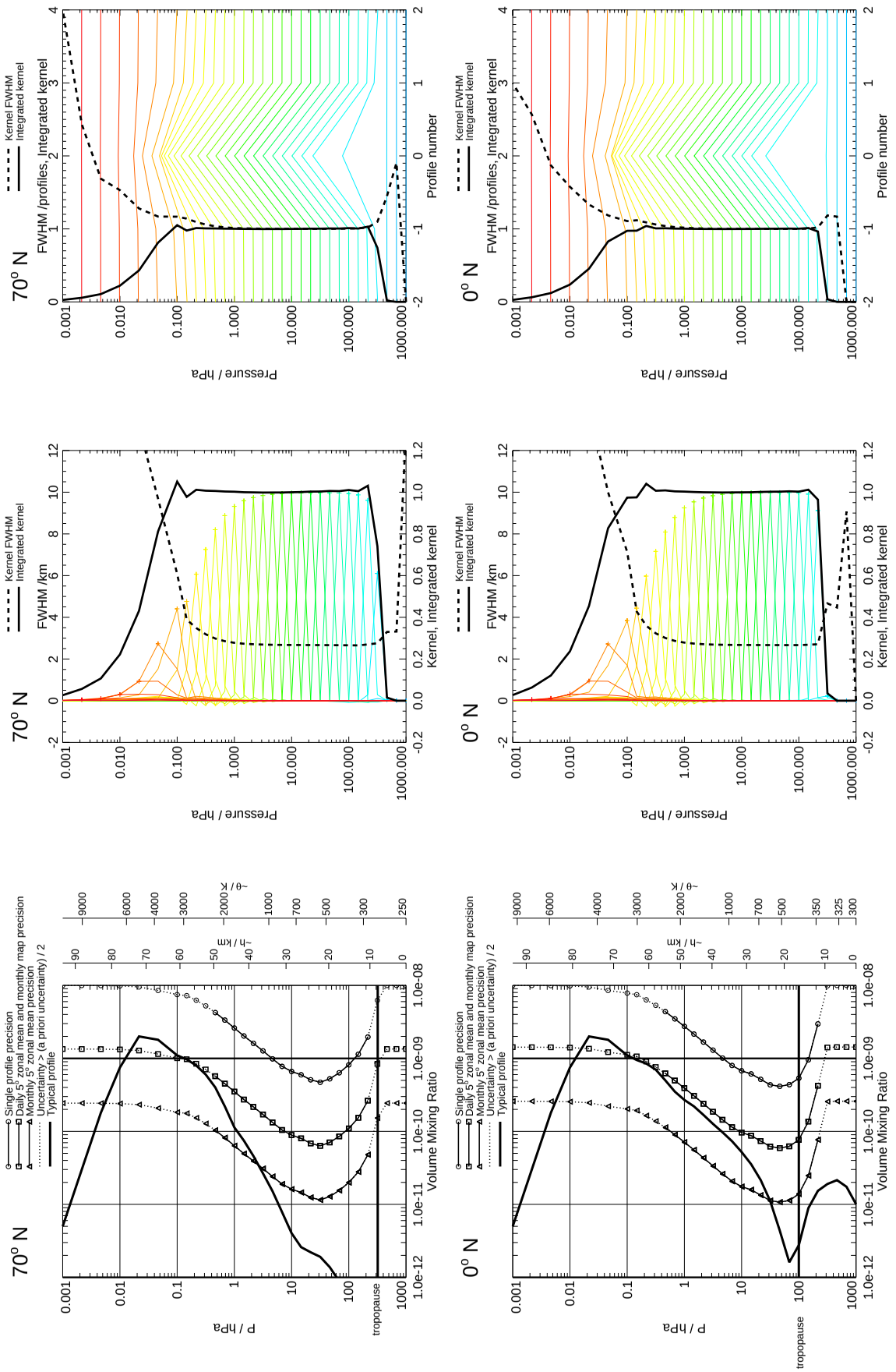

Figure 71: HO_2 precision and averaging kernels, with no regularisation. Touchstone phase CorePlusR4.

HO_2

HOCl

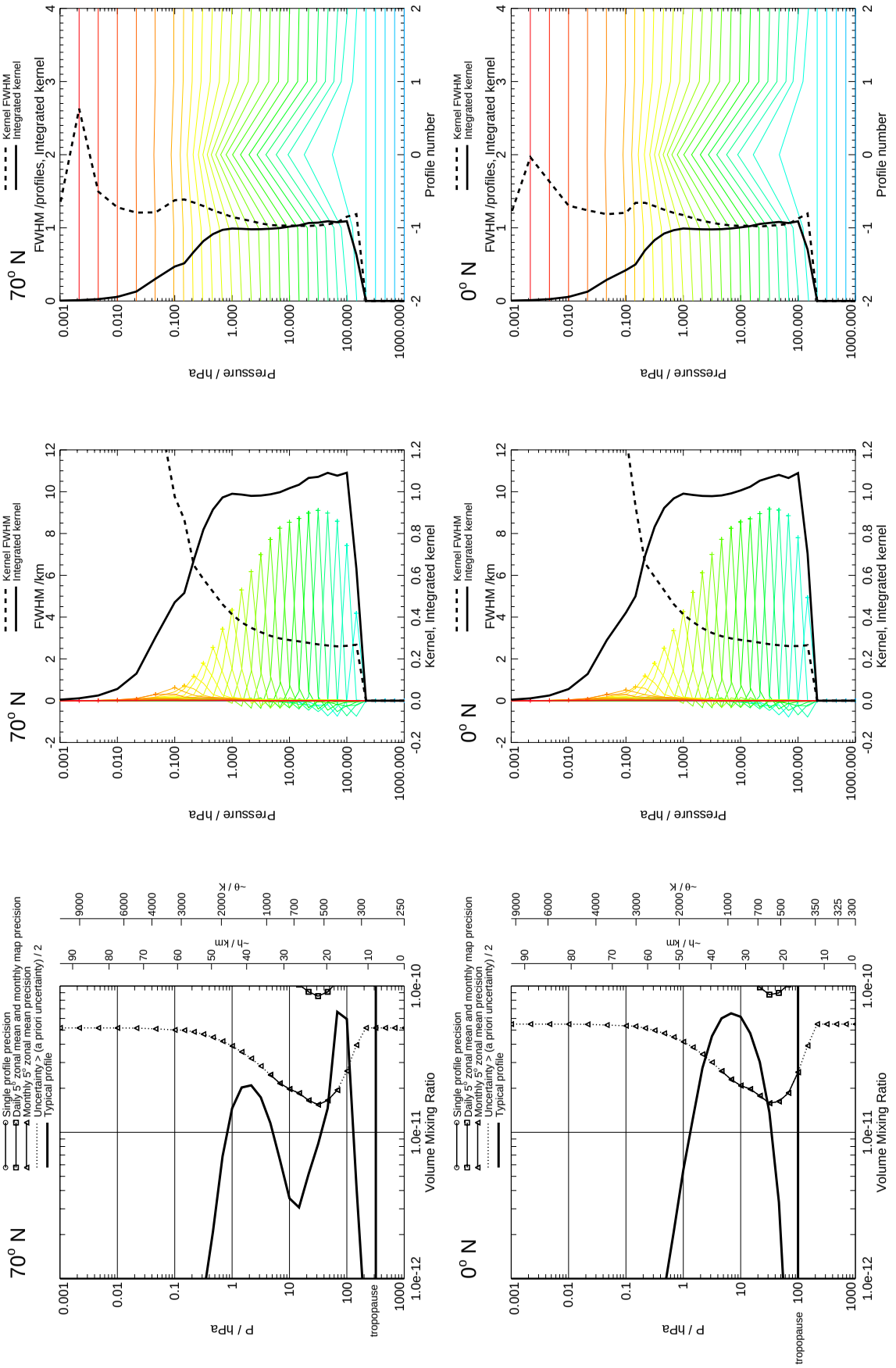

Figure 72: HOCl precision and averaging kernels, with V1.4 regularisation. V1.4 phased retrieval.

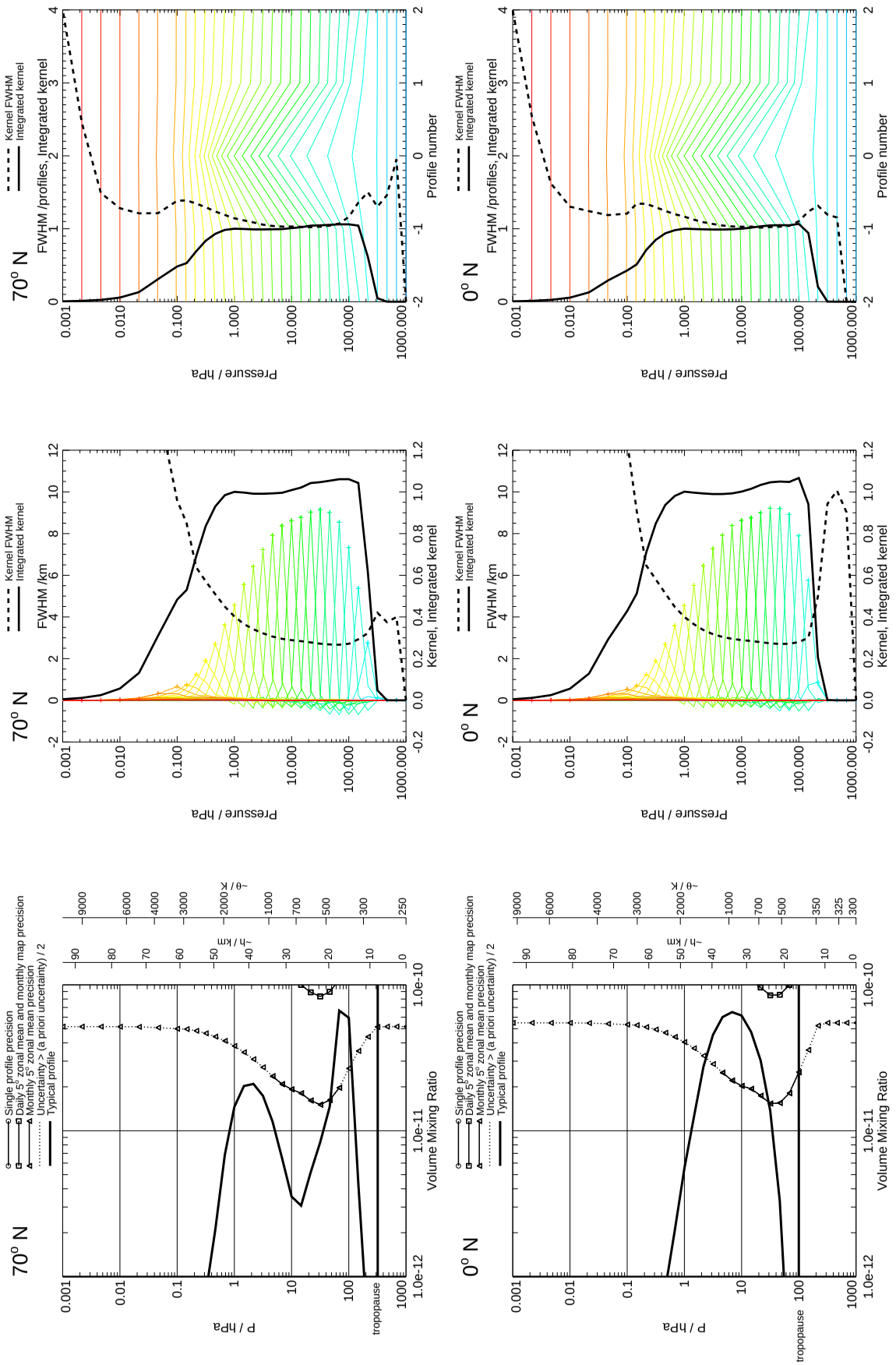

Figure 73: HOCl precision and averaging kernels, with no regularisation. Touchstone retrieval.

HOCl

HOCl

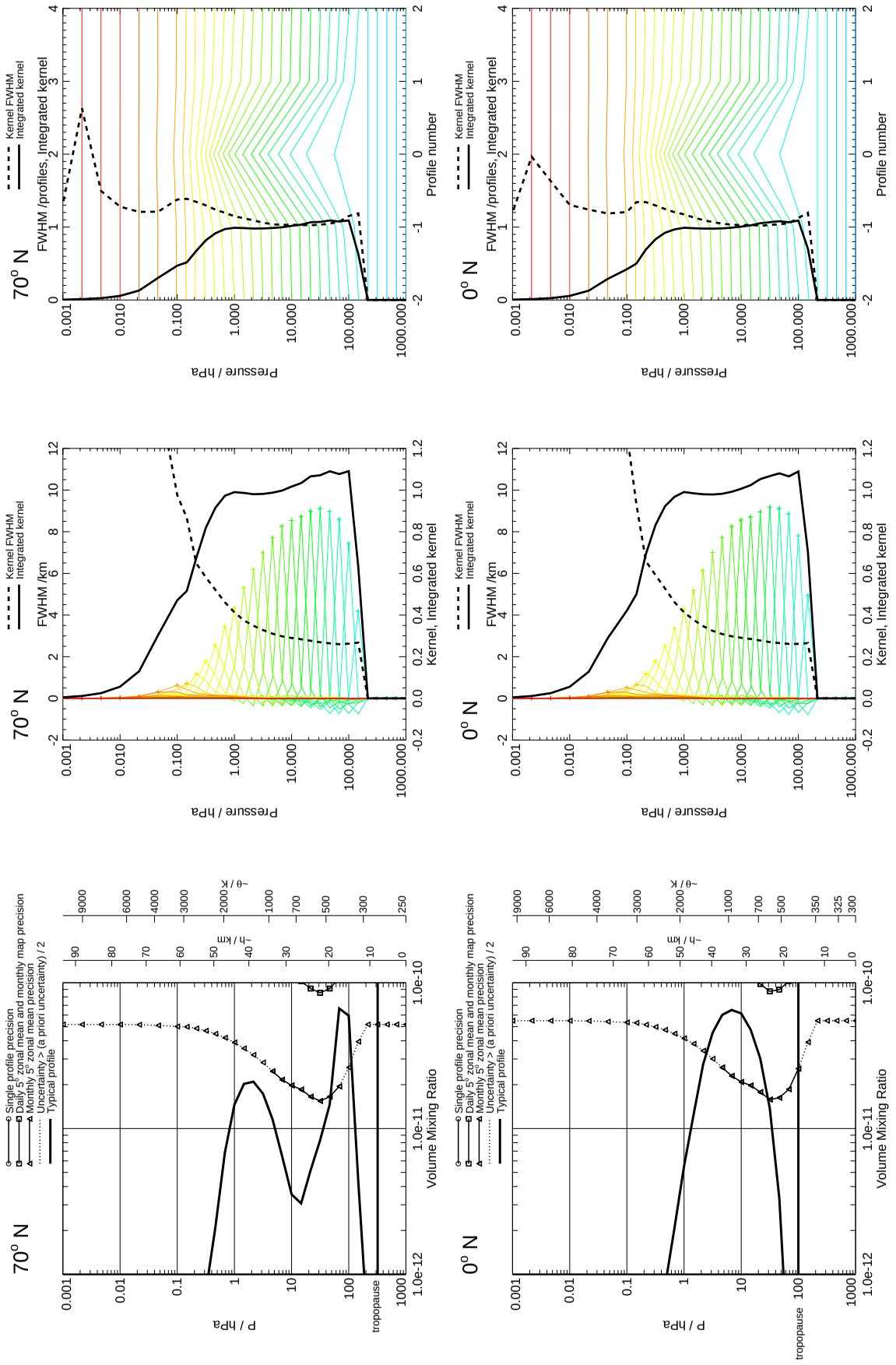

Figure 74: HOCl precision and averaging kernels, with V1.4 regularisation. V1.4 phase CorePlusR4.

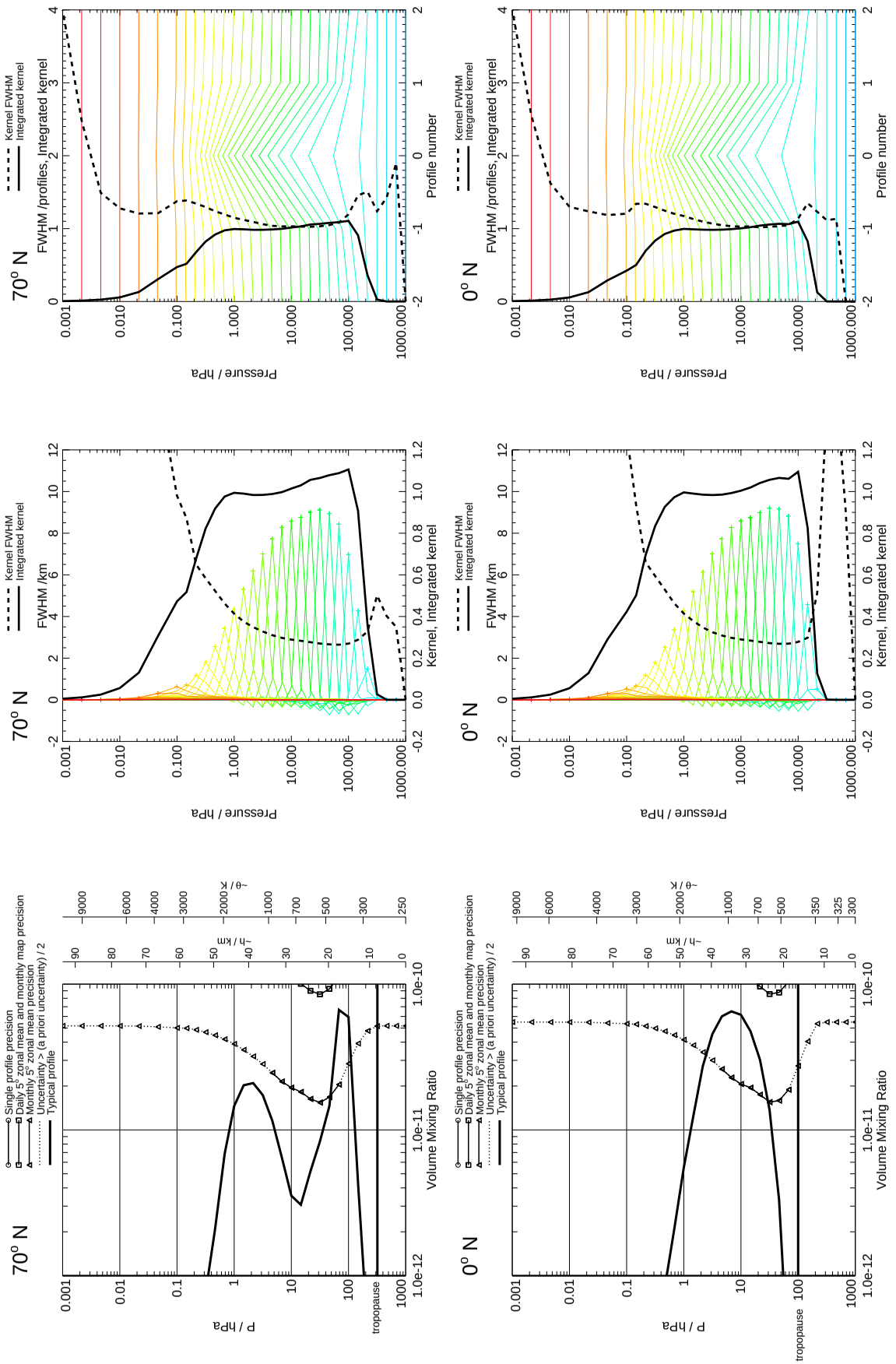

Figure 75: HOCl precision and averaging kernels, with no regularisation. Touchstone phase CorePlusR4.

N_2O

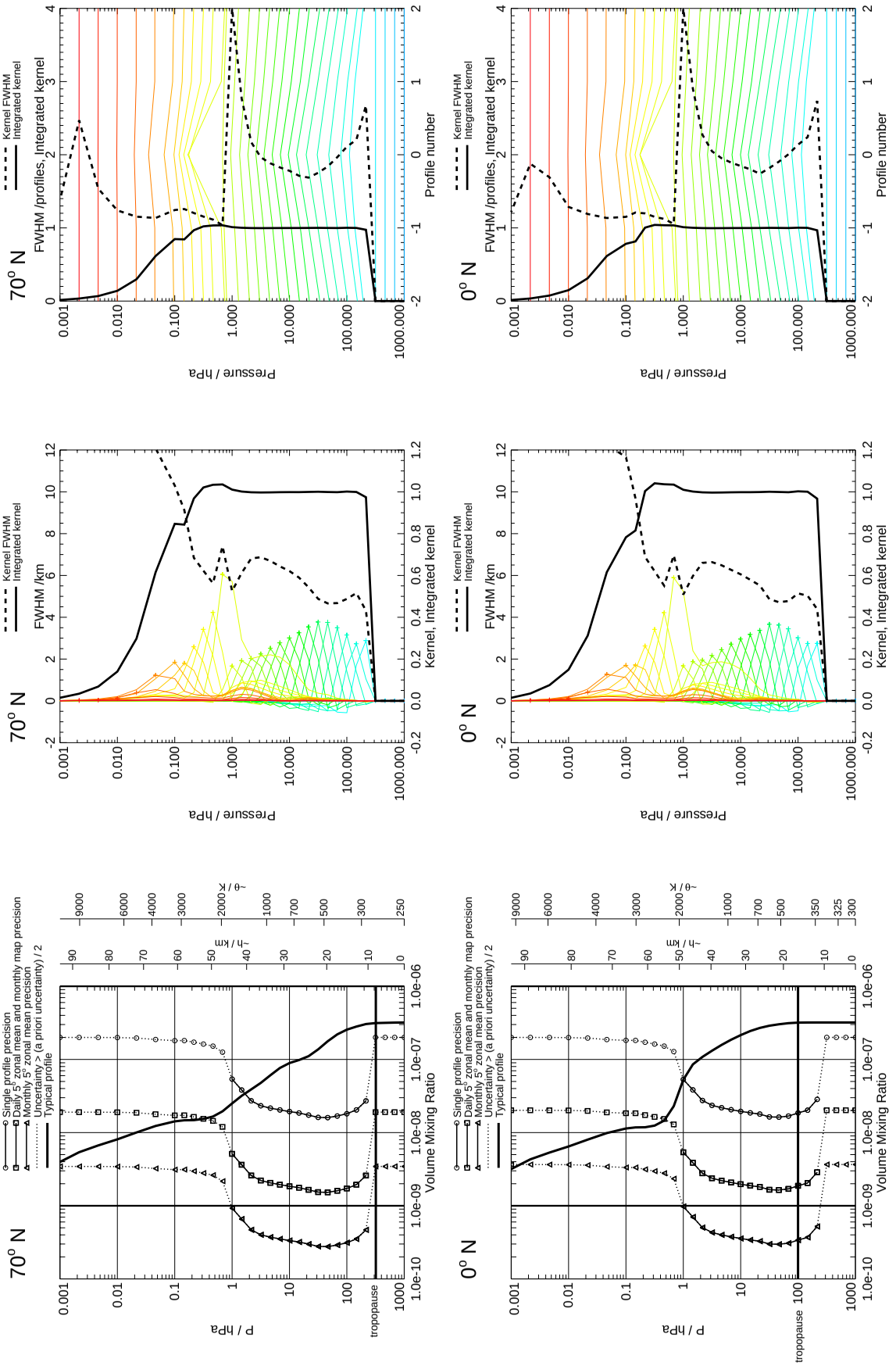

Figure 76: N_2O precision and averaging kernels, with V1.4 regularisation. V1.4 phased retrieval.

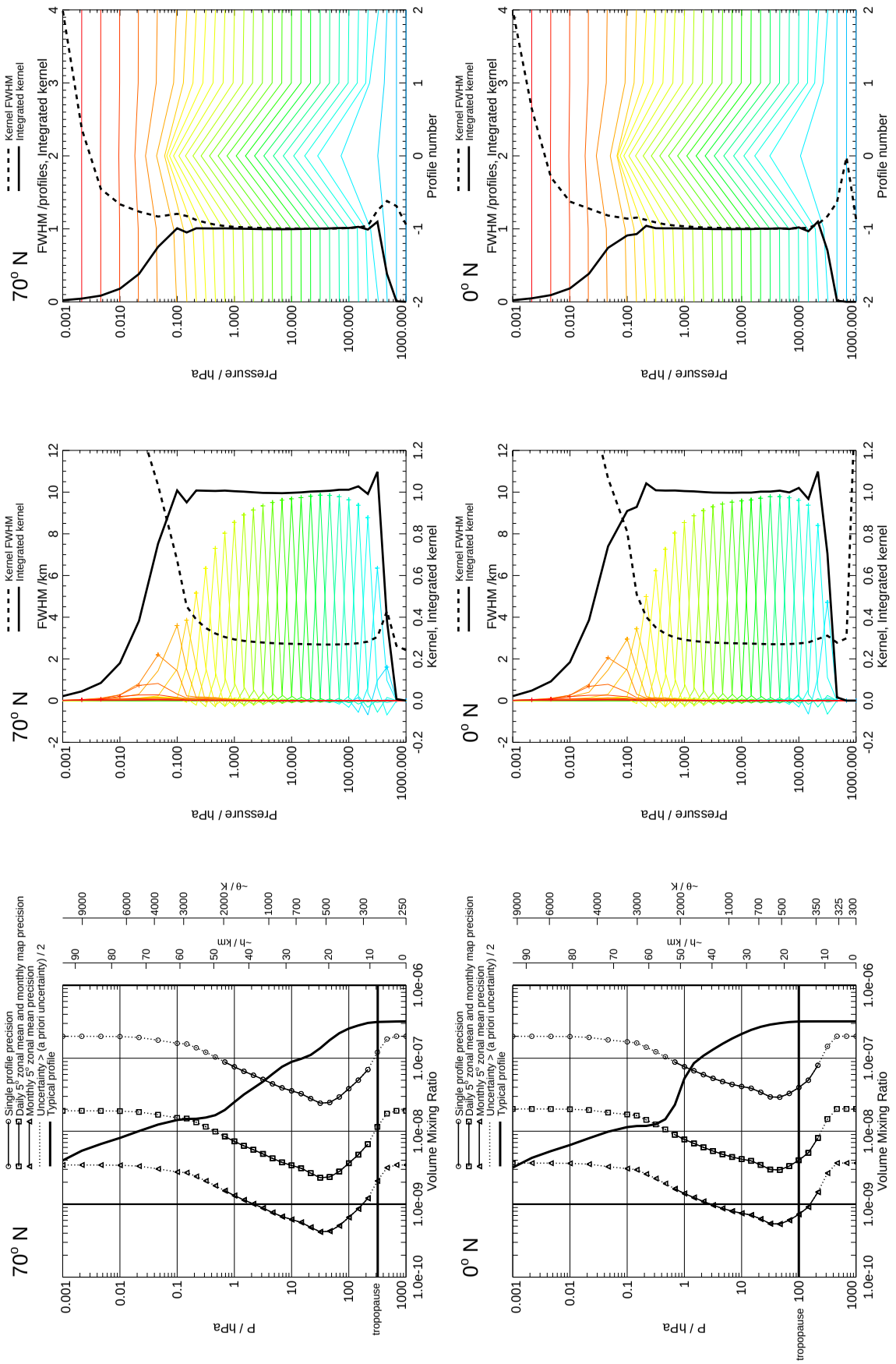

Figure 77: N_2O precision and averaging kernels, with no regularisation. Touchstone retrieval.

N_2O

N_2O

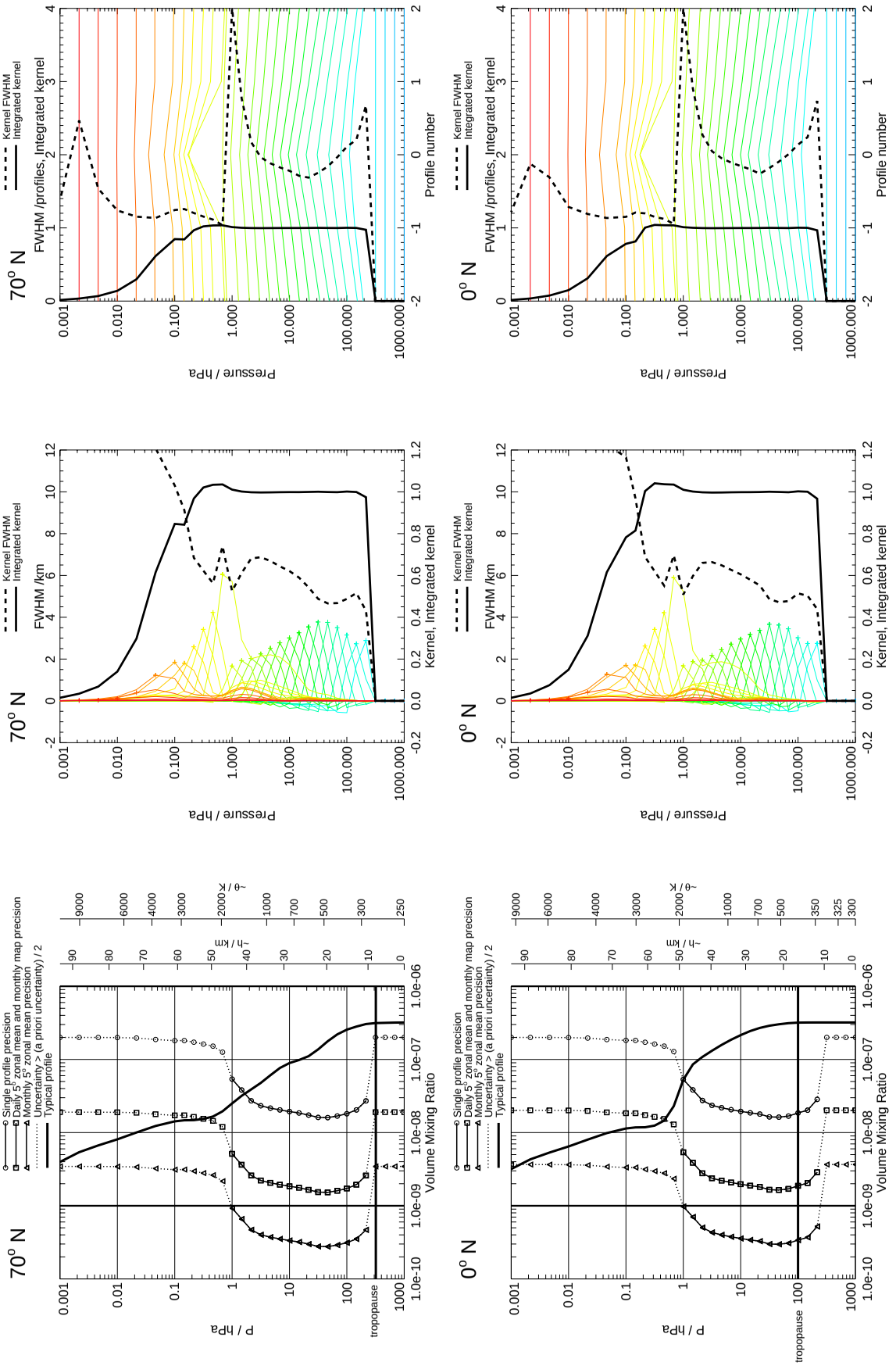

Figure 78: N_2O precision and averaging kernels, with V1.4 regularisation. V1.4 phase CorePlusR2.

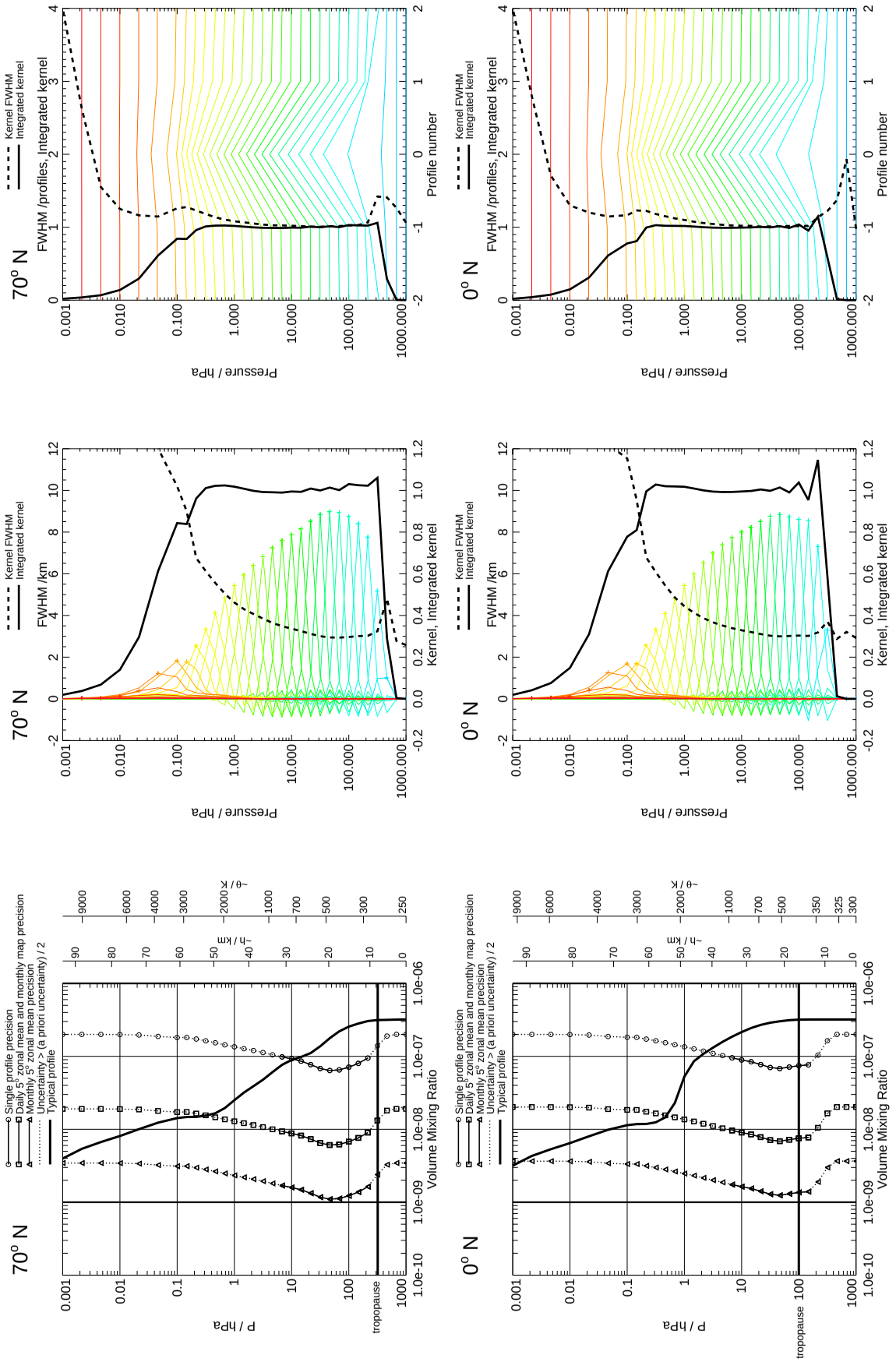

Figure 79: N_2O precision and averaging kernels, with no regularisation. Touchstone phase CorePlusR2.

N_2O

N_2O

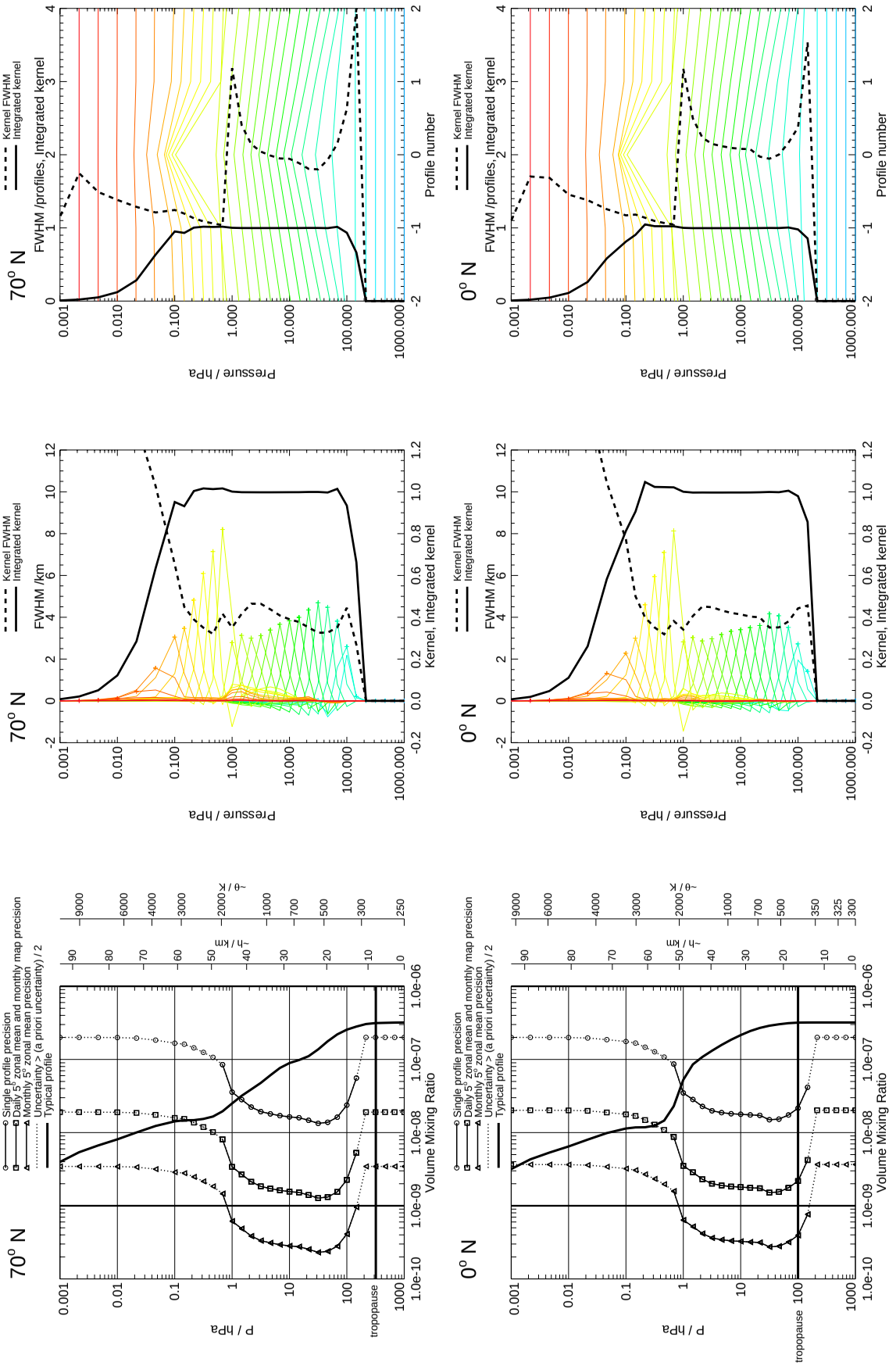

Figure 80: N_2O precision and averaging kernels, with V1.4 regularisation. V1.4 phase CorePlusR4.

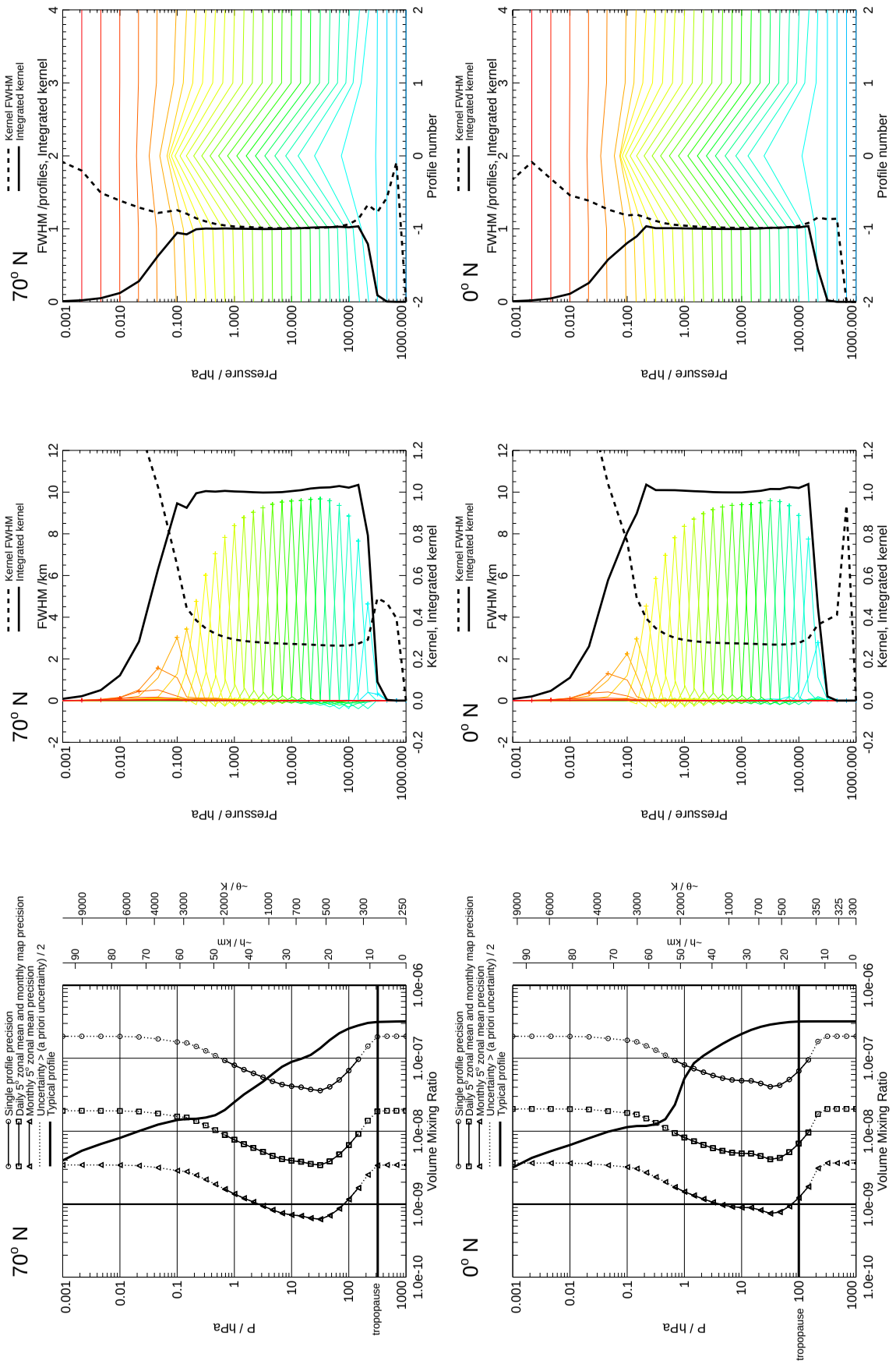

Figure 81: N_2O precision and averaging kernels, with no regularisation. Touchstone phase CorePlusR4.

N_2O

O_3

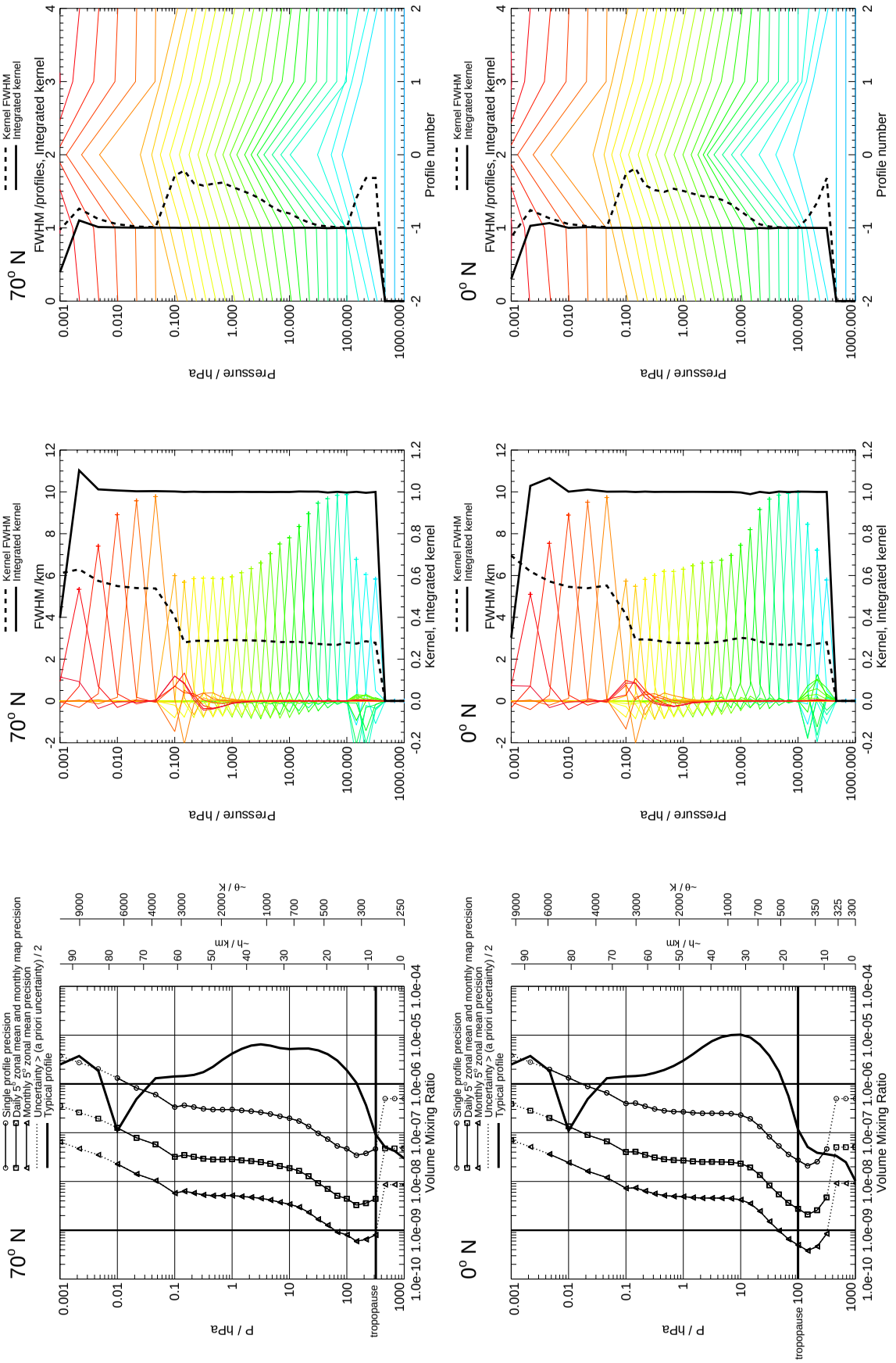

Figure 82: O_3 precision and averaging kernels, with V1.4 regularisation. V1.4 phased retrieval.

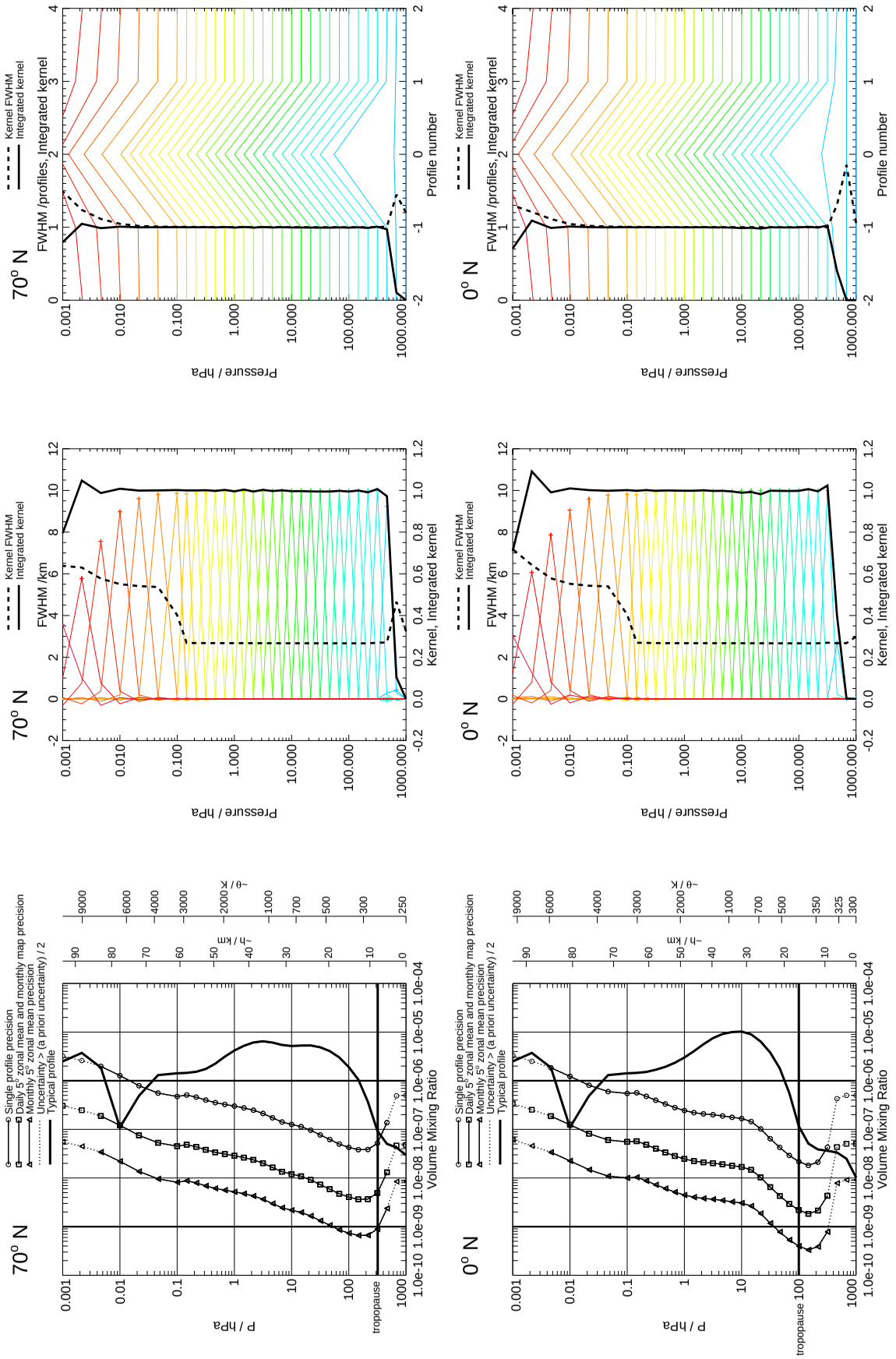

Figure 83: O_3 precision and averaging kernels, with no regularisation. Touchstone retrieval.

O_3

O_3

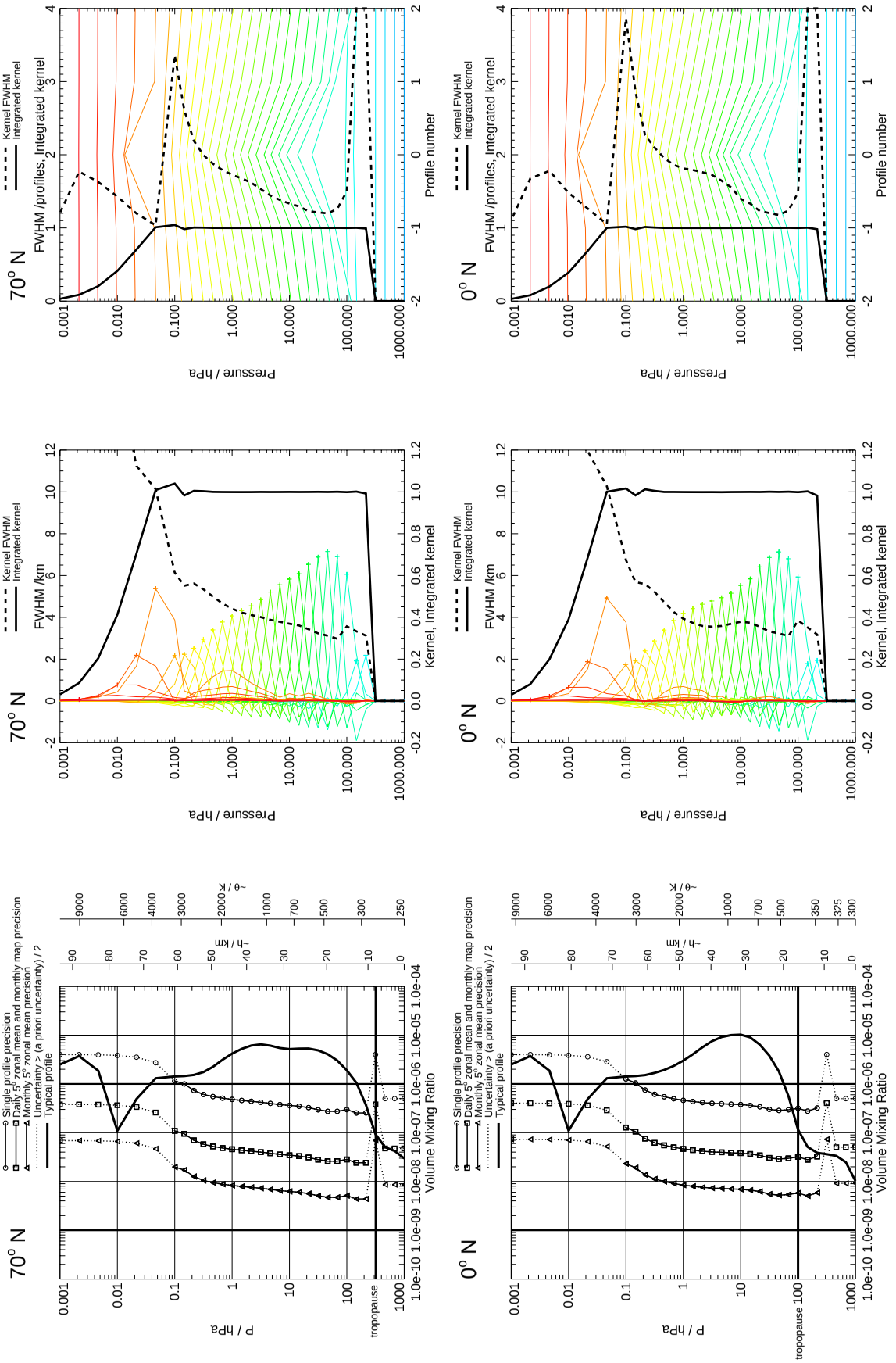

Figure 84: O_3 precision and averaging kernels, with V1.4 regularisation. V1.4 phase CorePlusR2.

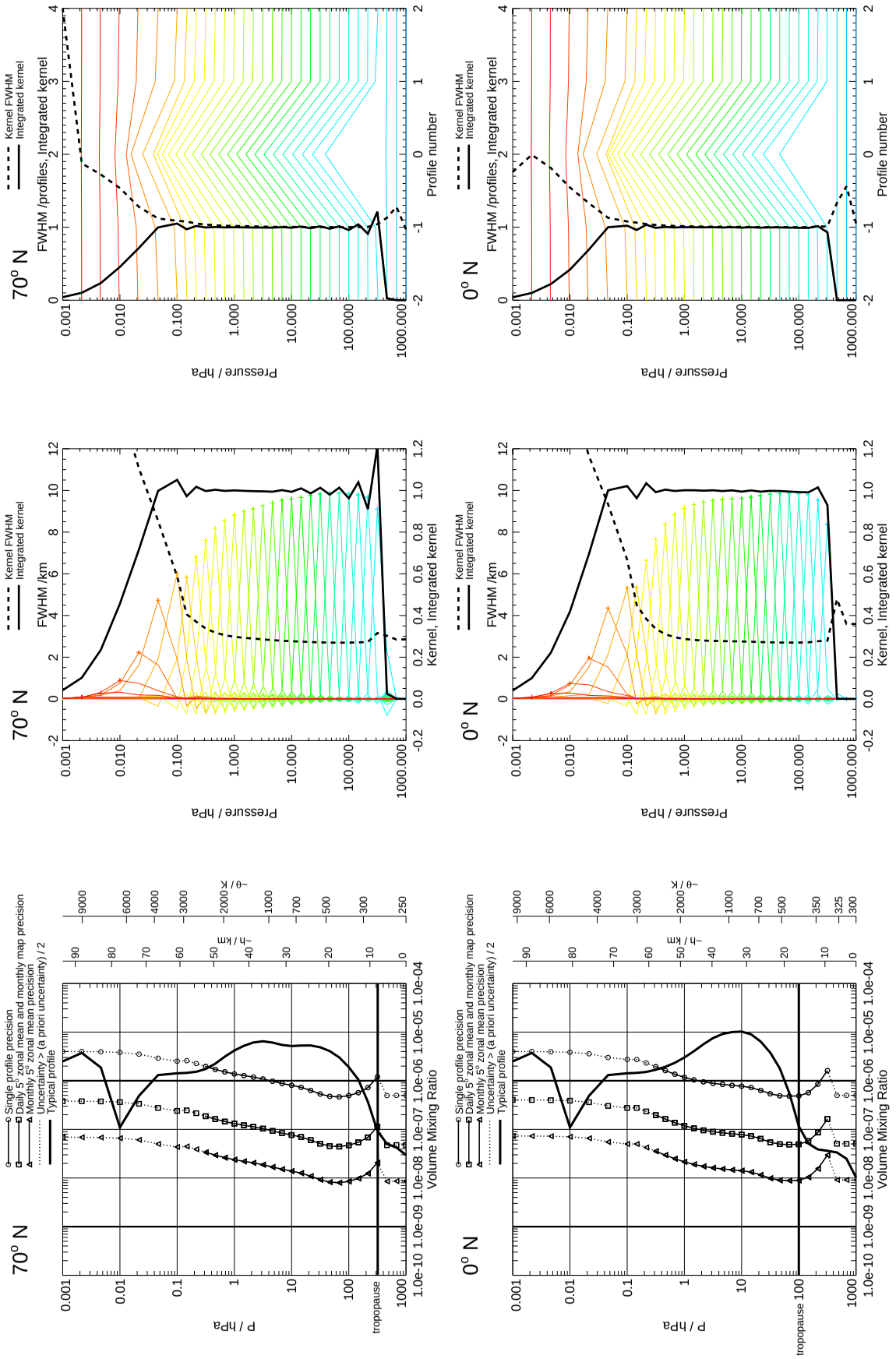

Figure 85: O_3 precision and averaging kernels, with no regularisation. Touchstone phase CorePlusR2.

O_3

O_3

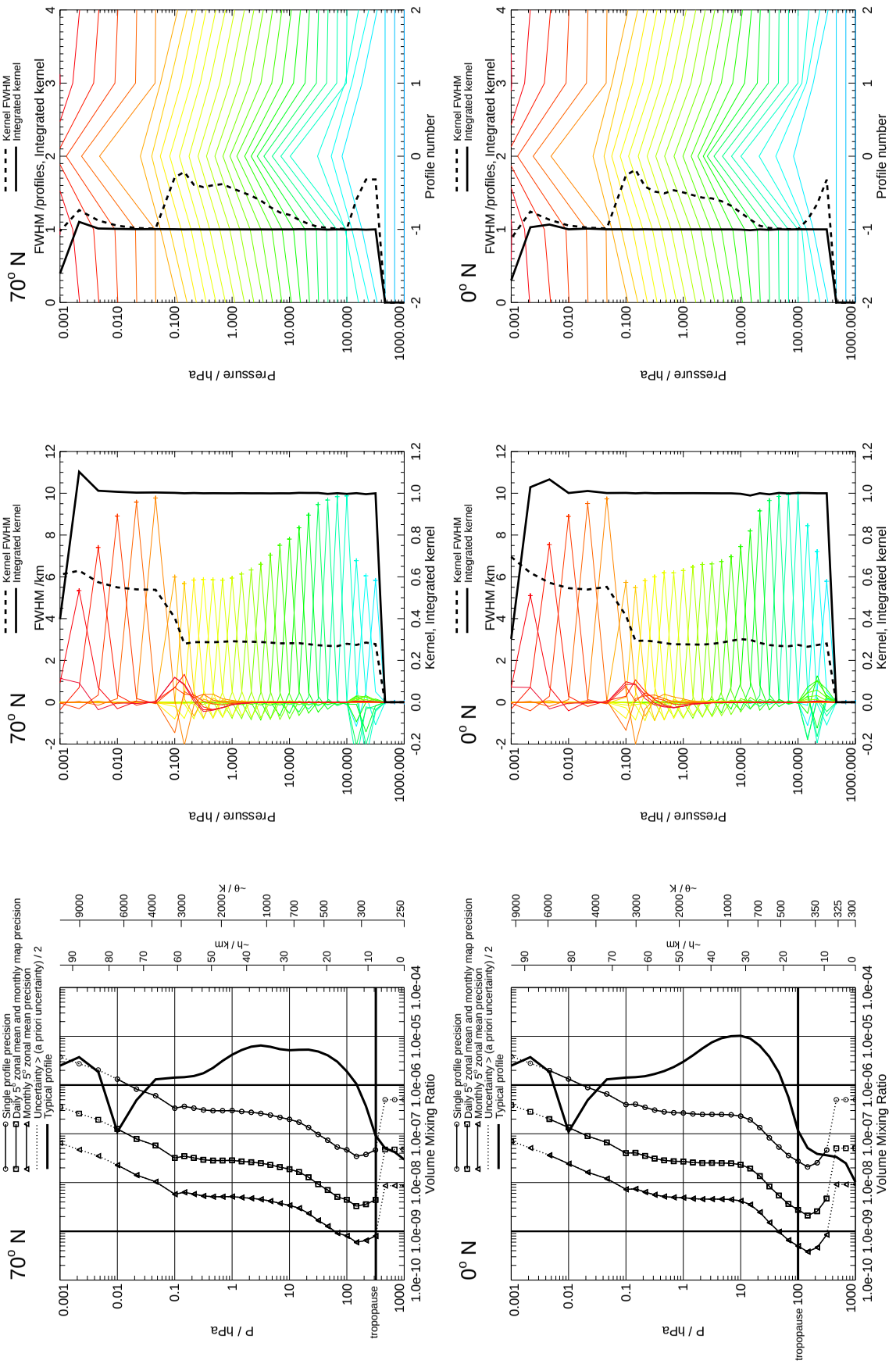

Figure 86: O_3 precision and averaging kernels, with V1.4 regularisation. V1.4 phase CorePlusR3.

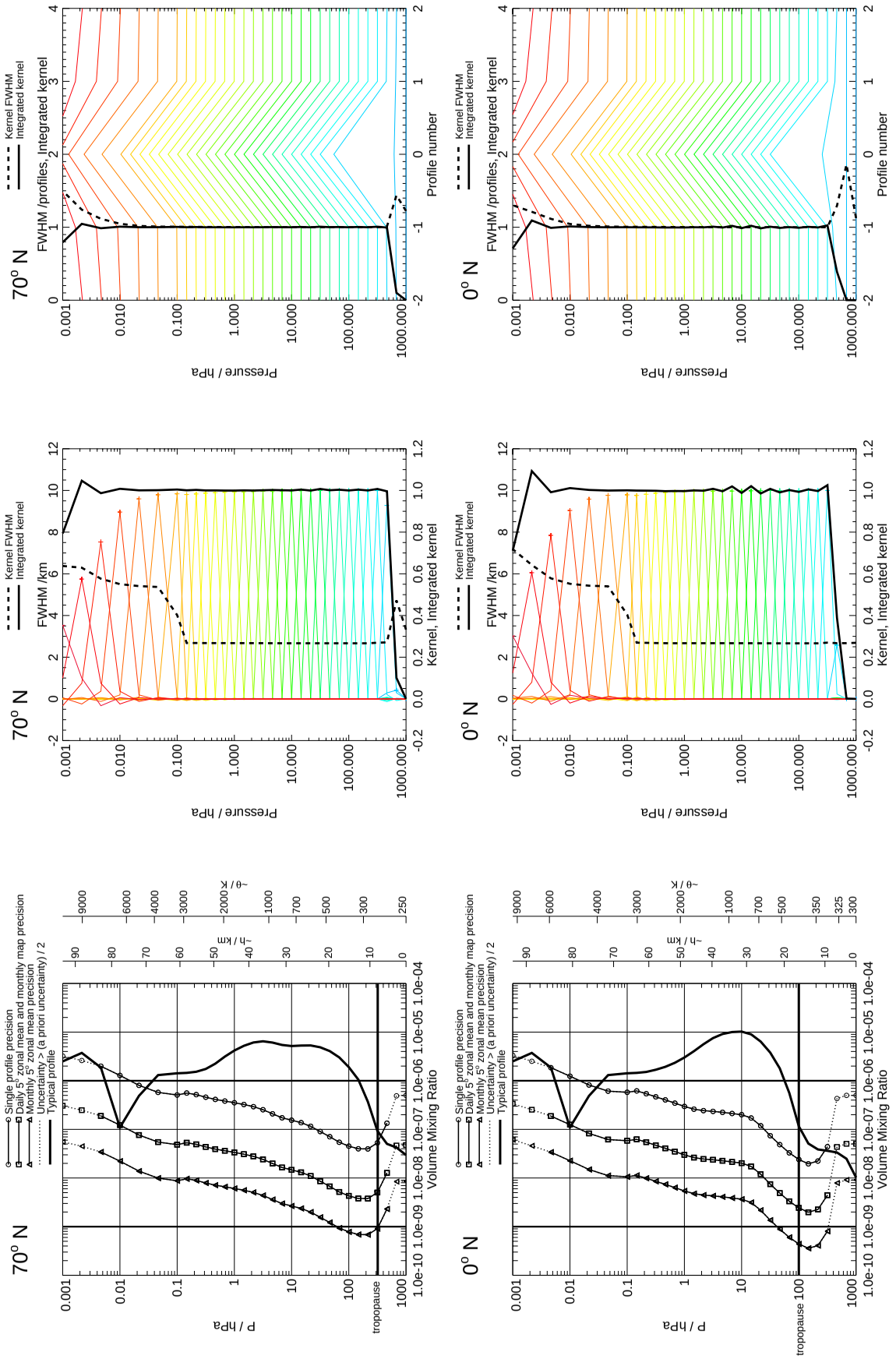

Figure 87: O_3 precision and averaging kernels, with no regularisation. Touchstone phase CorePlusR3.

O_3

O_3

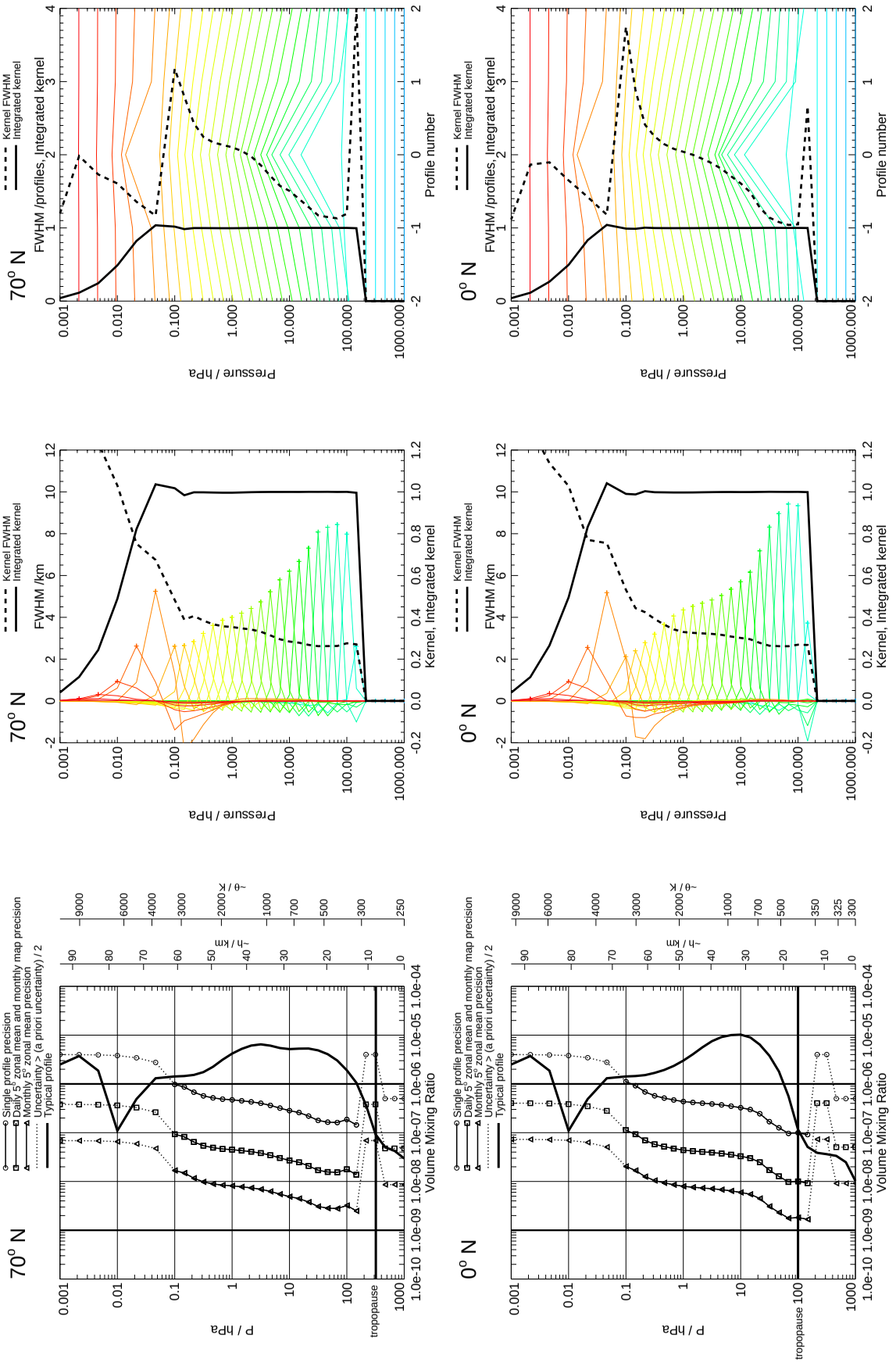

Figure 88: O_3 precision and averaging kernels, with V1.4 regularisation. V1.4 phase CorePlusR4.

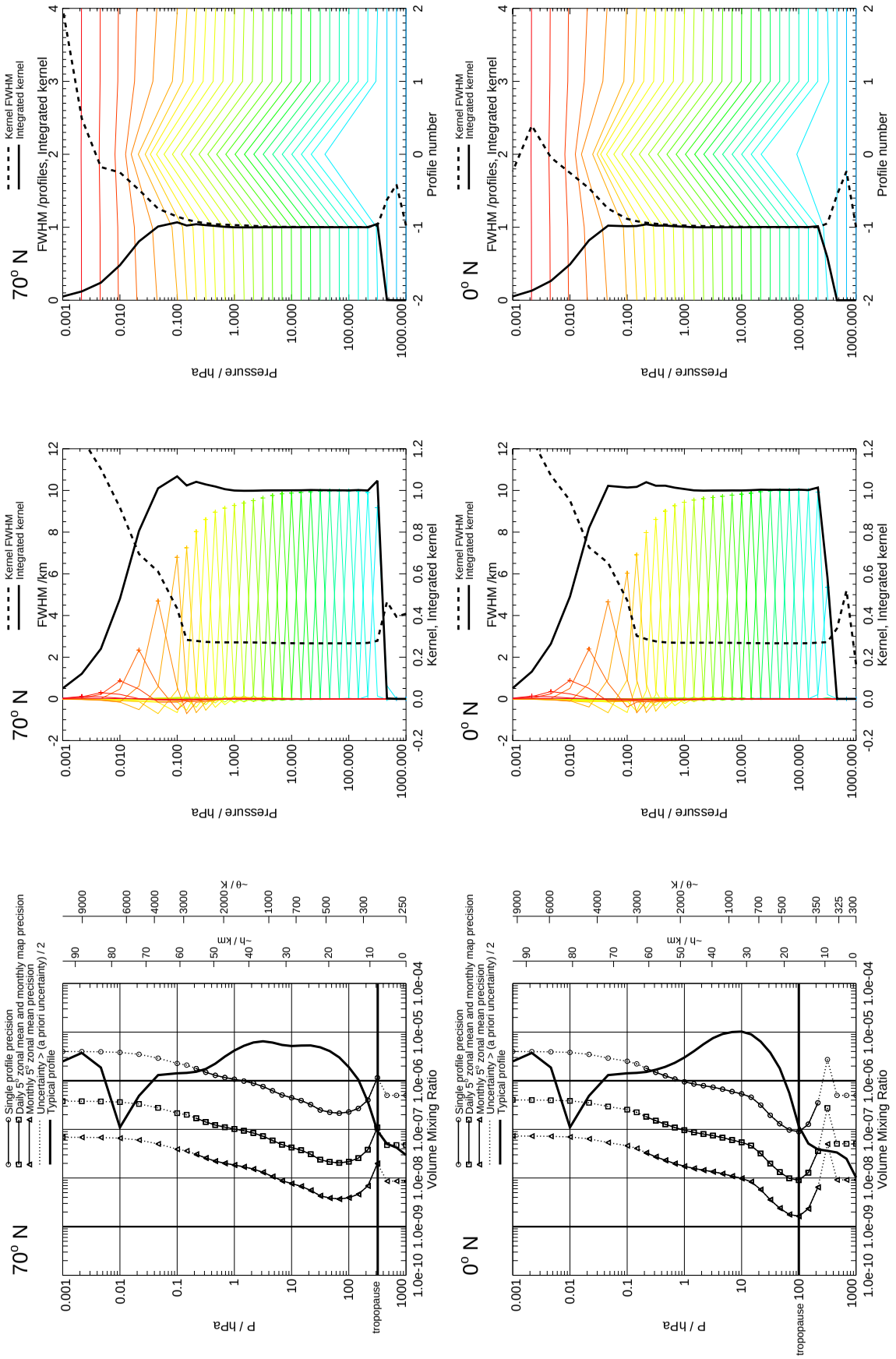

Figure 89: O_3 precision and averaging kernels, with no regularisation. Touchstone phase CorePlusR4.

O_3

O_3

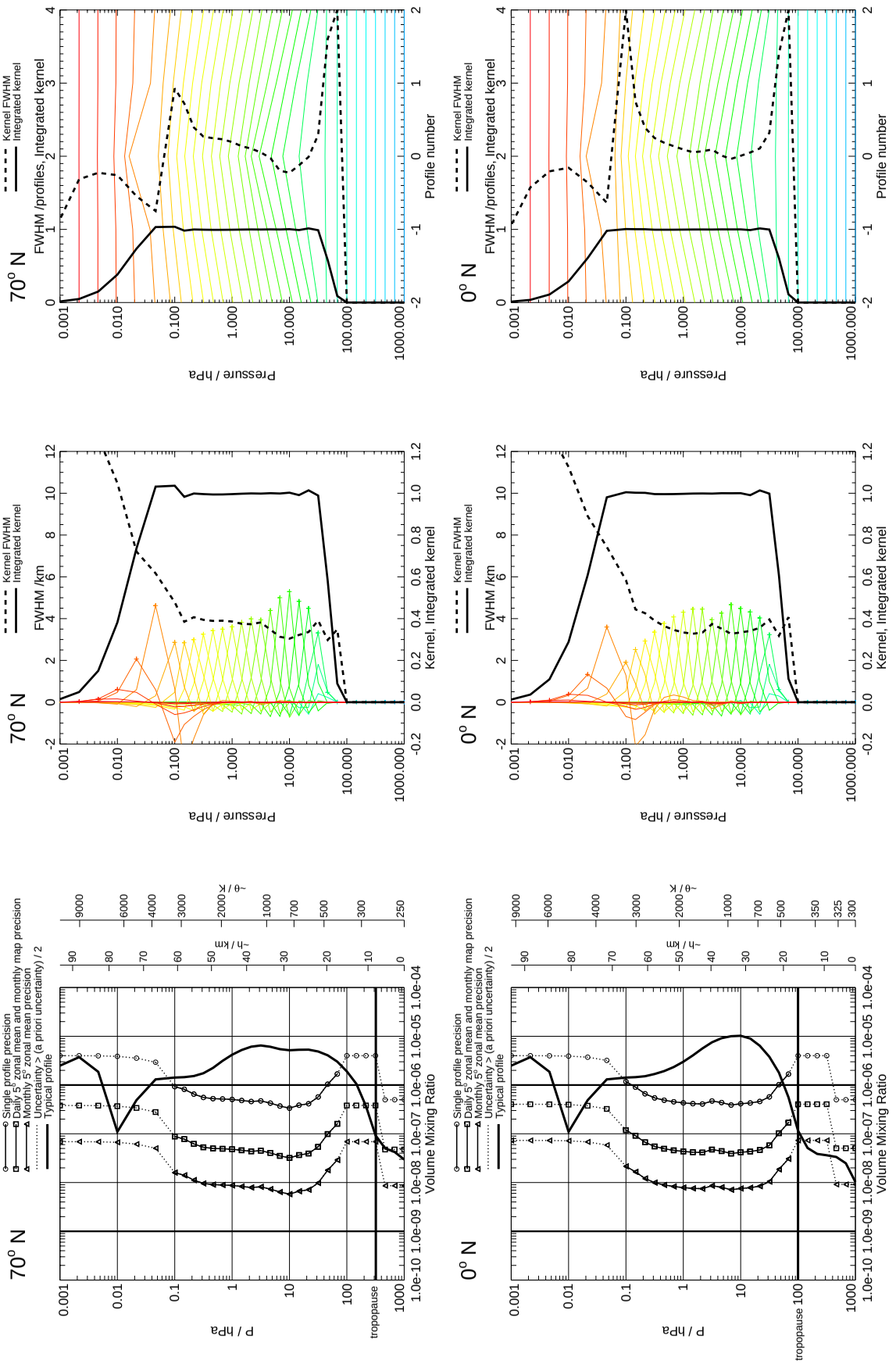

Figure 90: O_3 precision and averaging kernels, with V1.4 regularisation. V1.4 phase CorePlusR5.

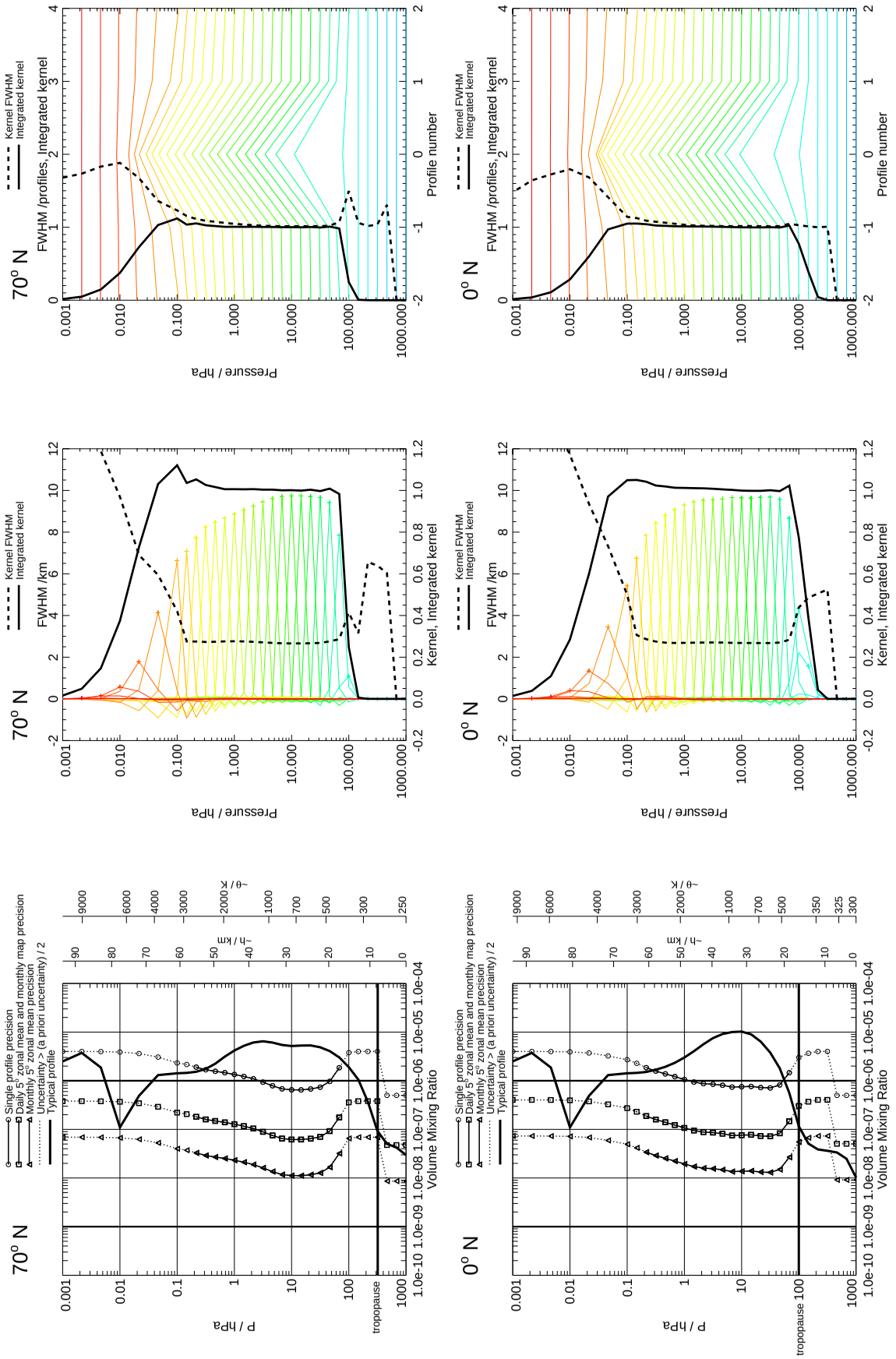

Figure 91: O_3 precision and averaging kernels, with no regularisation. Touchstone phase CorePlusR5.

O_3

O_3

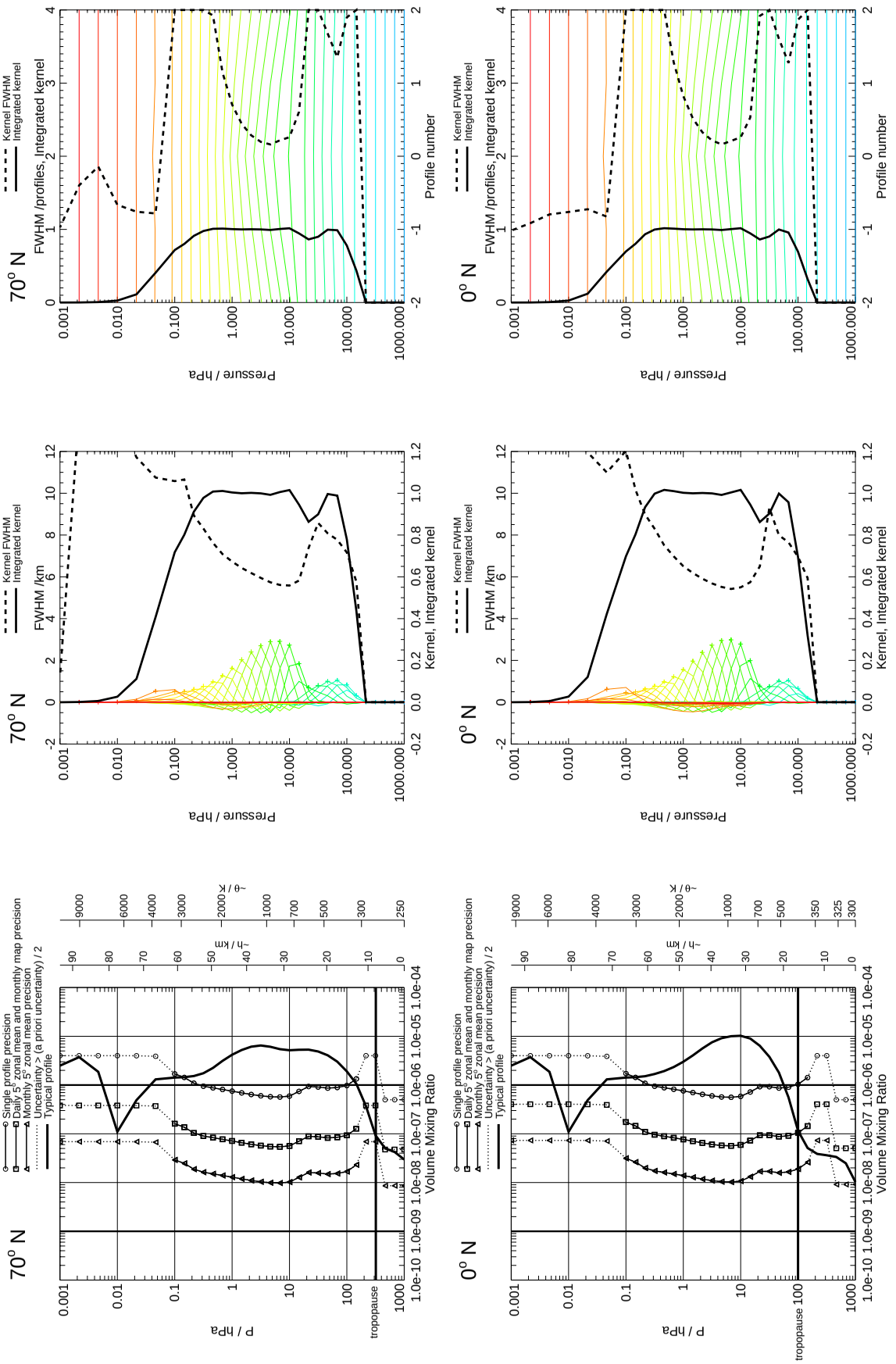

Figure 92: O_3 precision and averaging kernels, with V1.4 regularisation. V1.4 phase UpdatePtan.

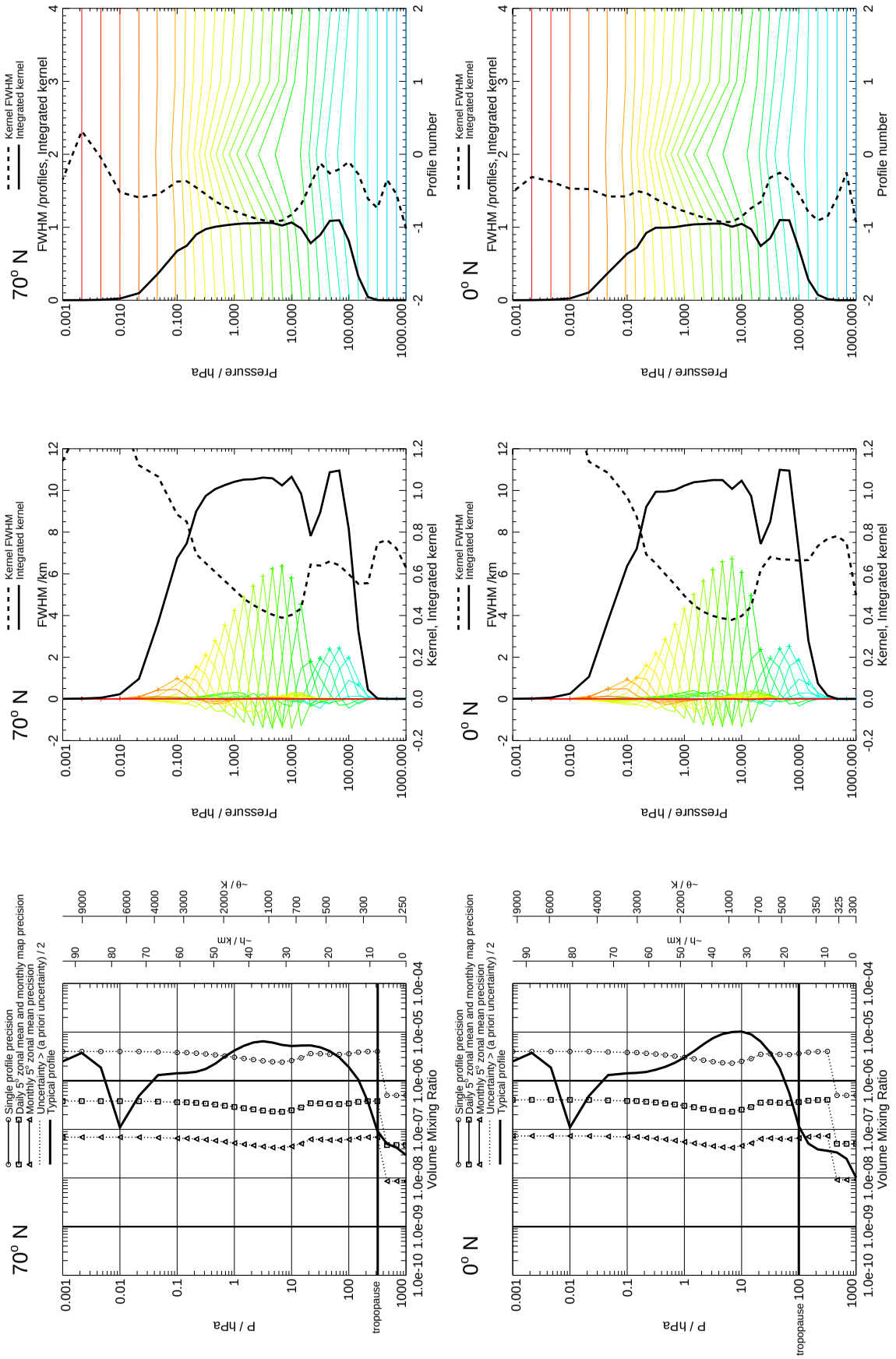

Figure 93: O_3 precision and averaging kernels, with no regularisation. Touchstone phase UpdatePtan.

O_3

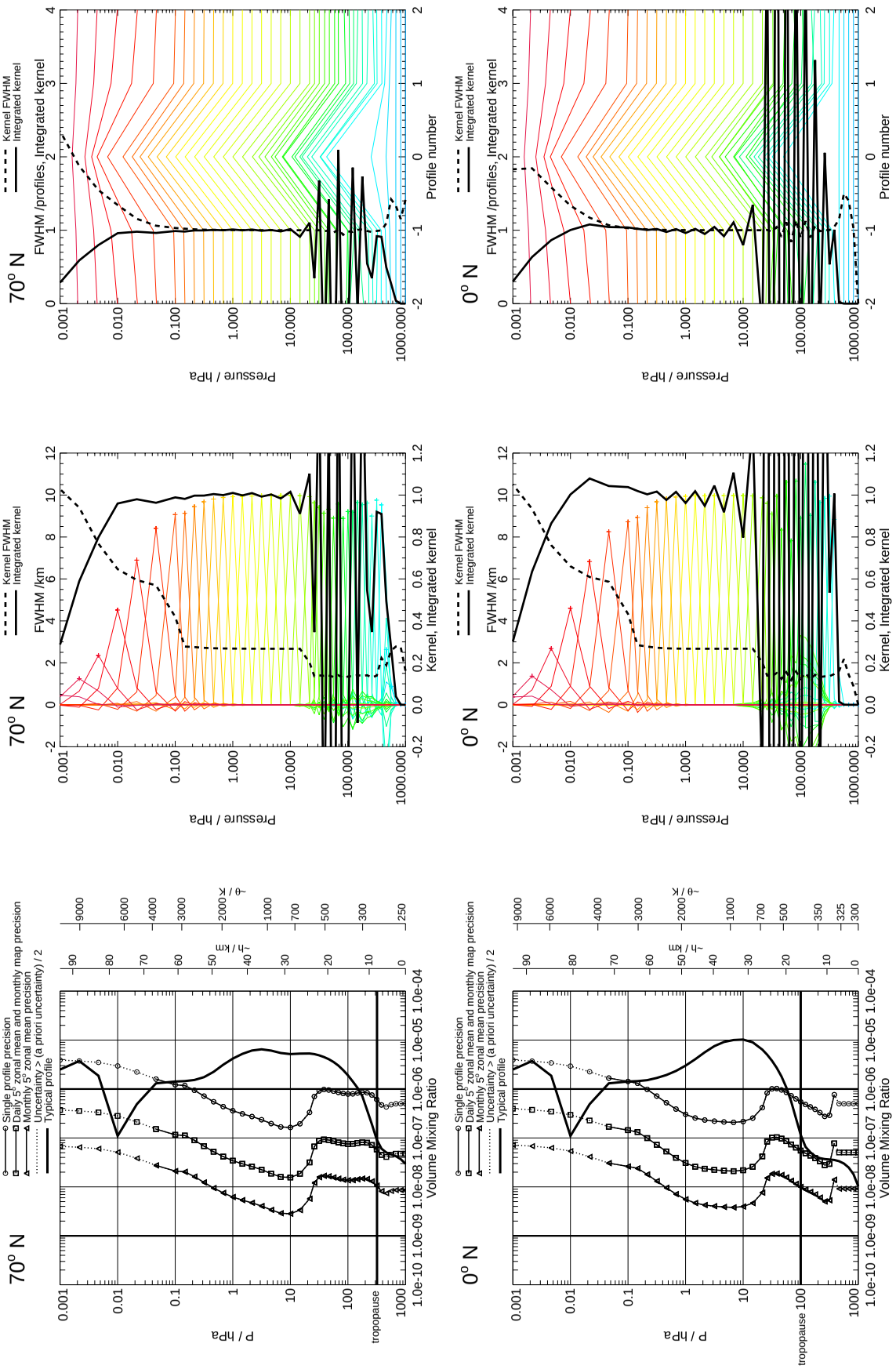

Figure 94: O_3 precision and averaging kernels, on high resolution grid, with no regularisation. Touchstone retrieval. Oscillations in the integrated kernel are also present for the CorePlusR3 and (to a lesser extent) CorePlusR2 phases but not in the CorePlusR4. Thus a O_3 at retrieval 12/decade resolution may be possible by using R4 alone.

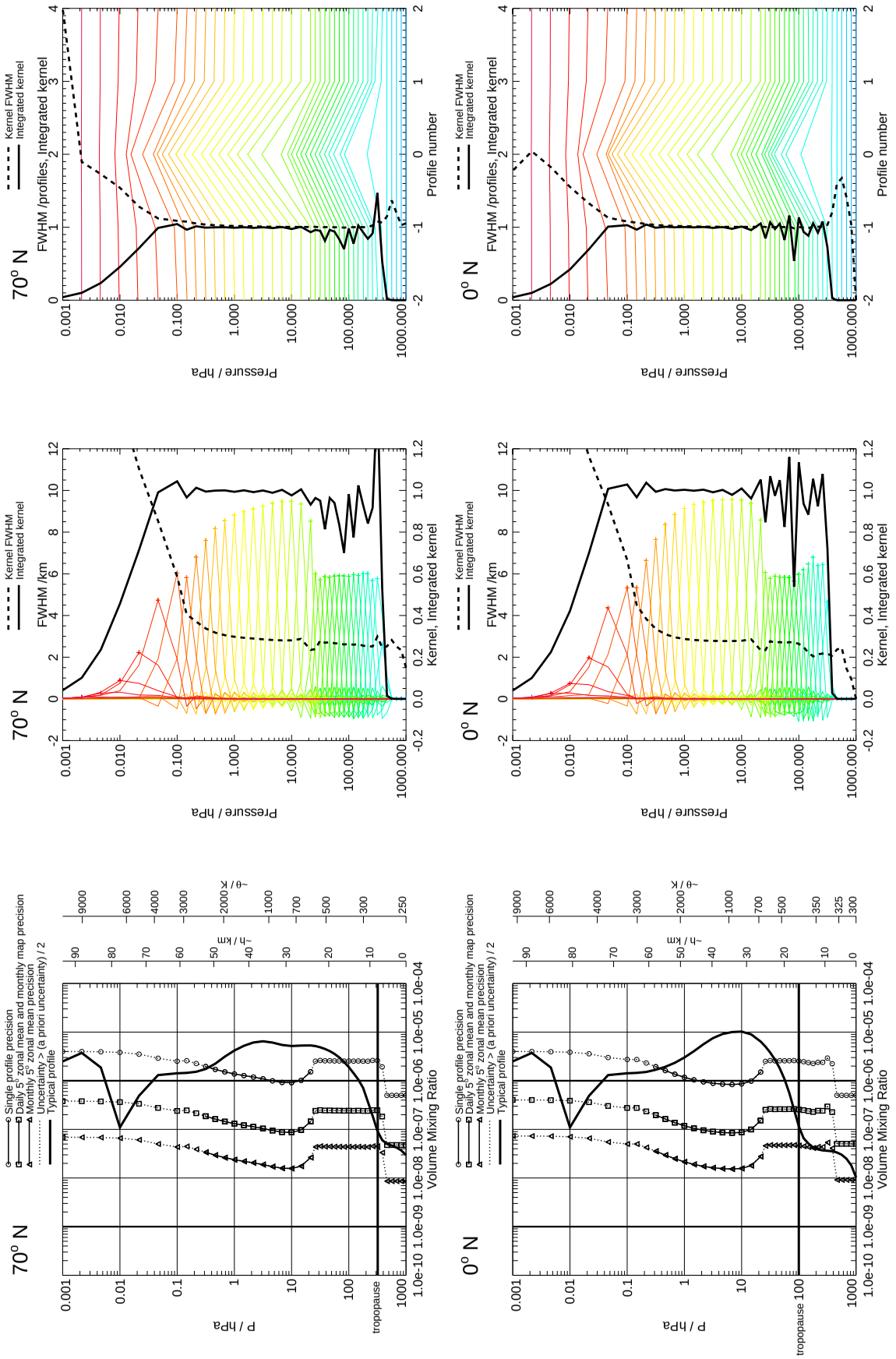

Figure 95: O_3 precision and averaging kernels, on high resolution grid, with no regularisation. Touchstone phase CorePlusR2.

O_3

O_3

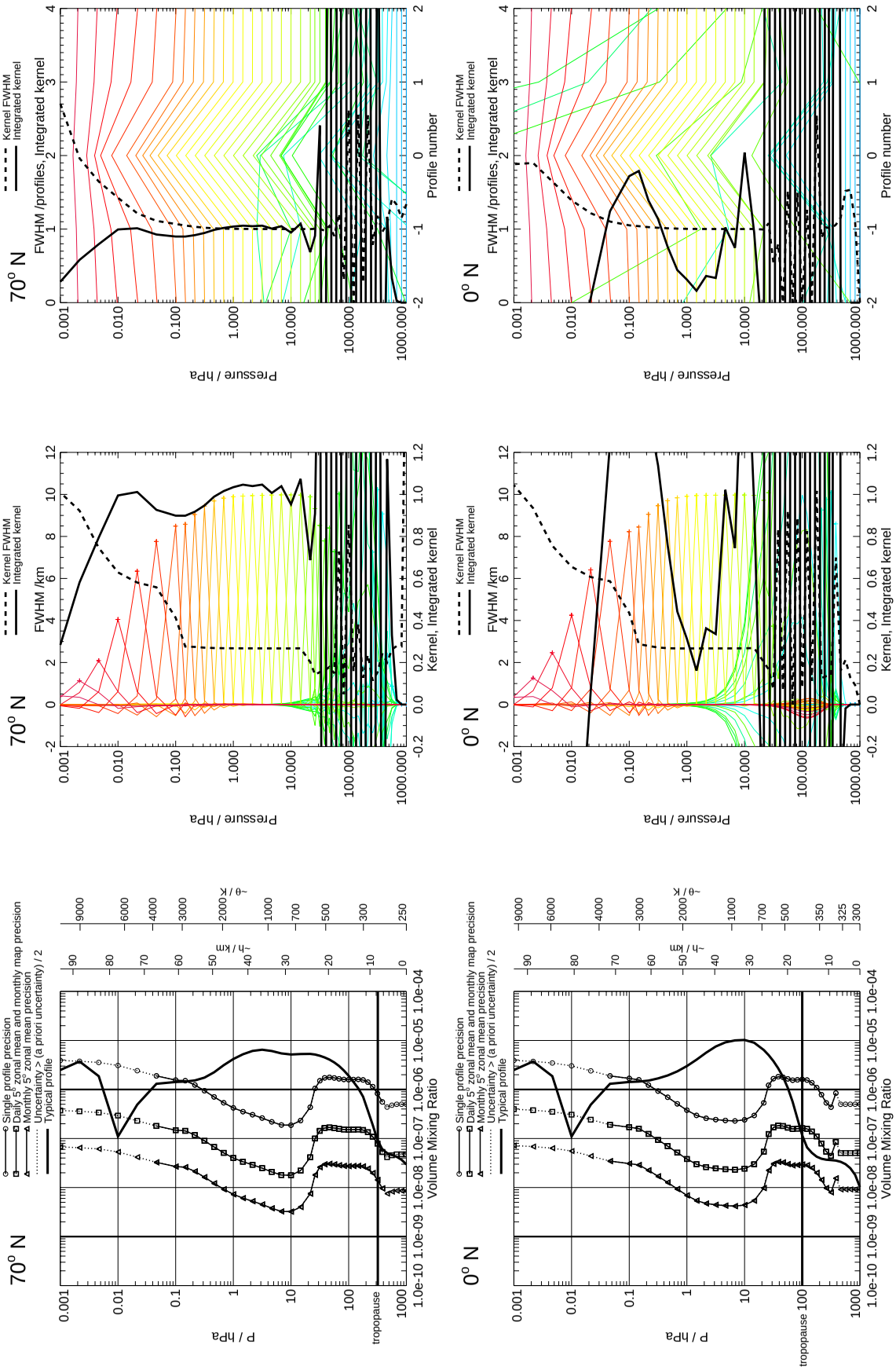

Figure 96: O_3 precision and averaging kernels, on high resolution grid, with no regularisation. Touchstone phase CorePlusR3.

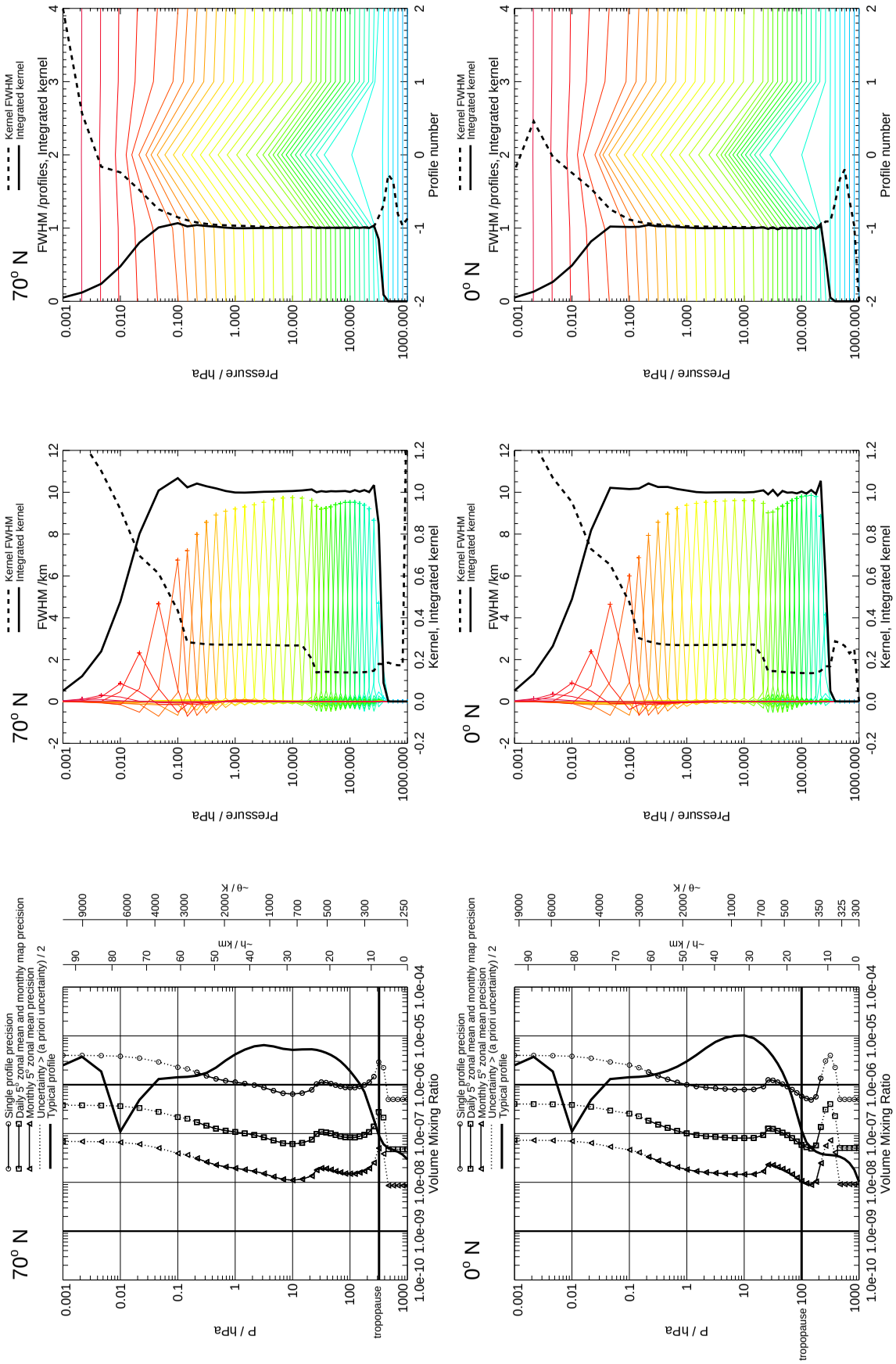

Figure 97: O_3 precision and averaging kernels, on high resolution grid, with no regularisation. Touchstone phase CorePlusR4.

O_3

O_3

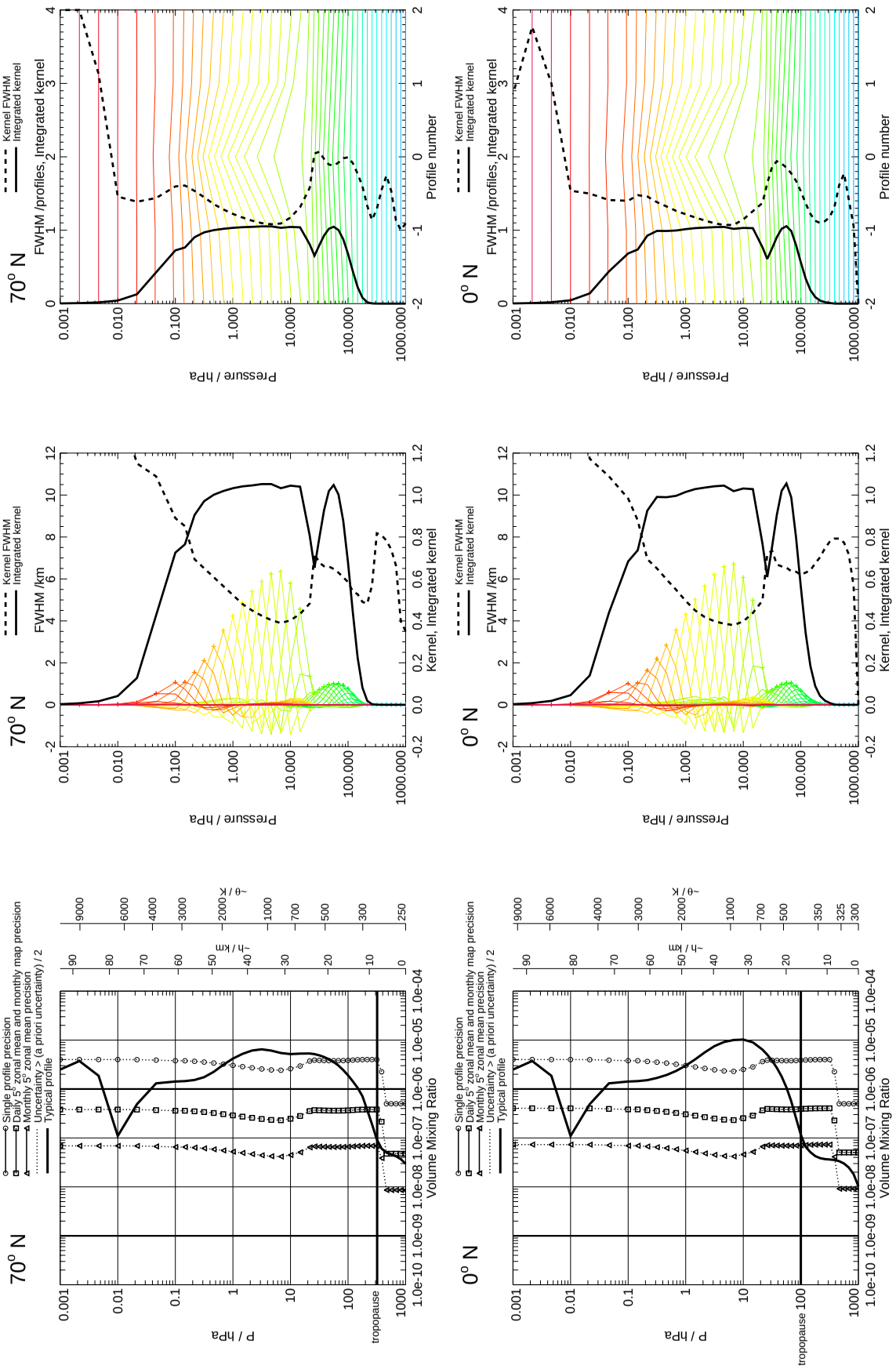

Figure 98: O_3 precision and averaging kernels, on high resolution grid, with no regularisation. Touchstone phase UpdatePtan.

Blank page

OH

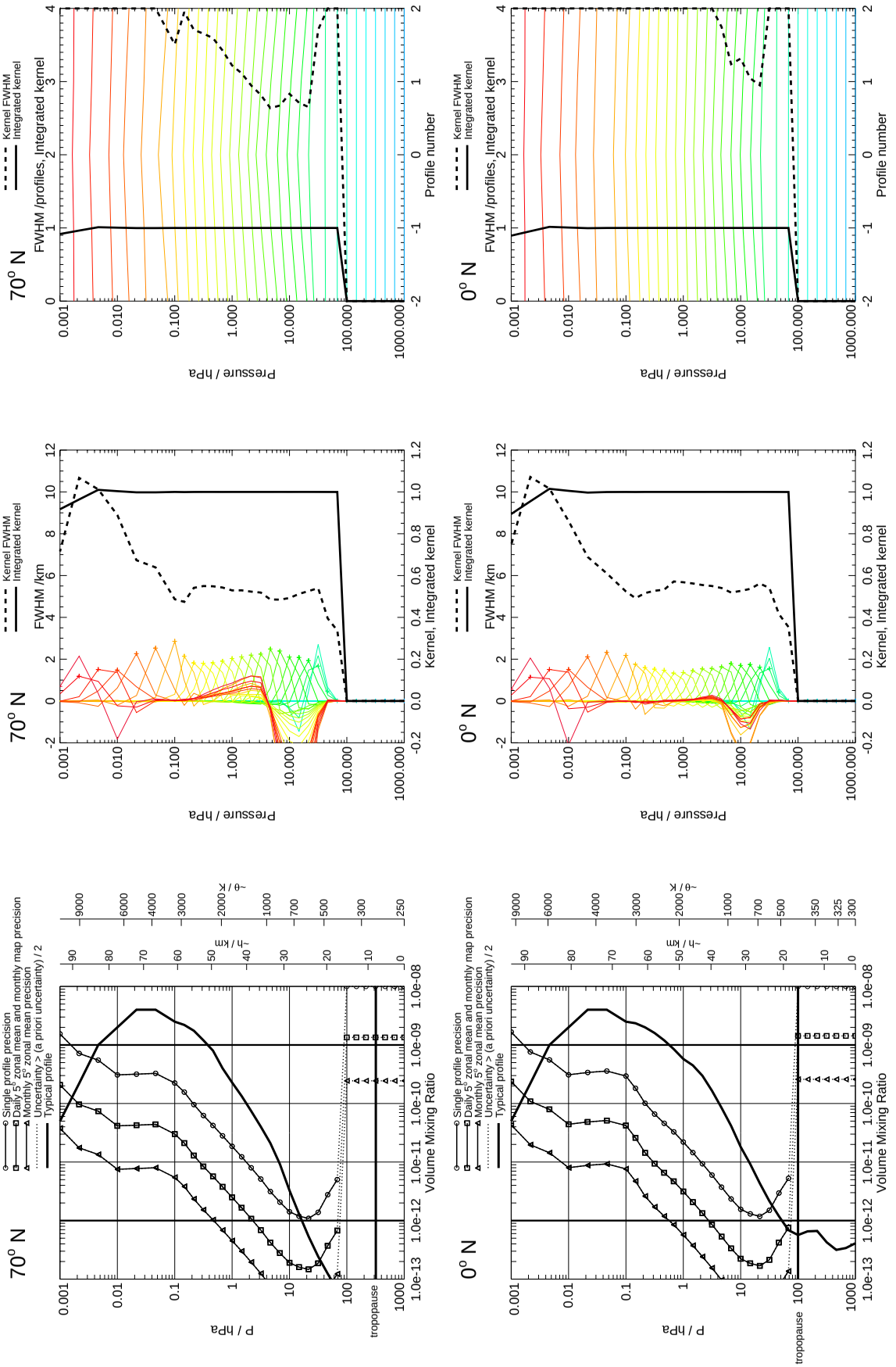

Figure 99: OH precision and averaging kernels, with V1.4 regularisation. V1.4 phased retrieval.

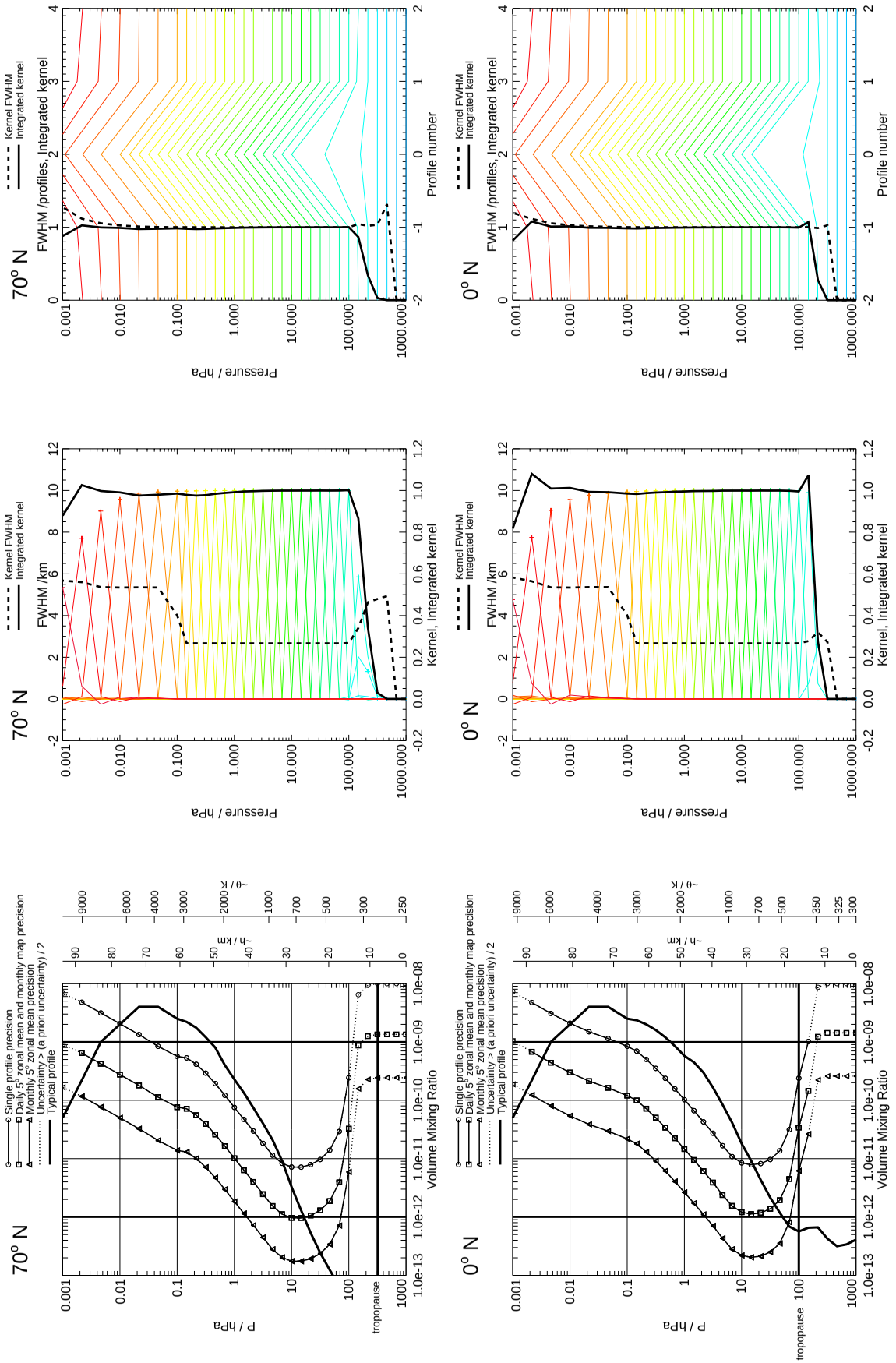

OH

Figure 100: OH precision and averaging kernels, with no regularisation. Touchstone retrieval.

OH

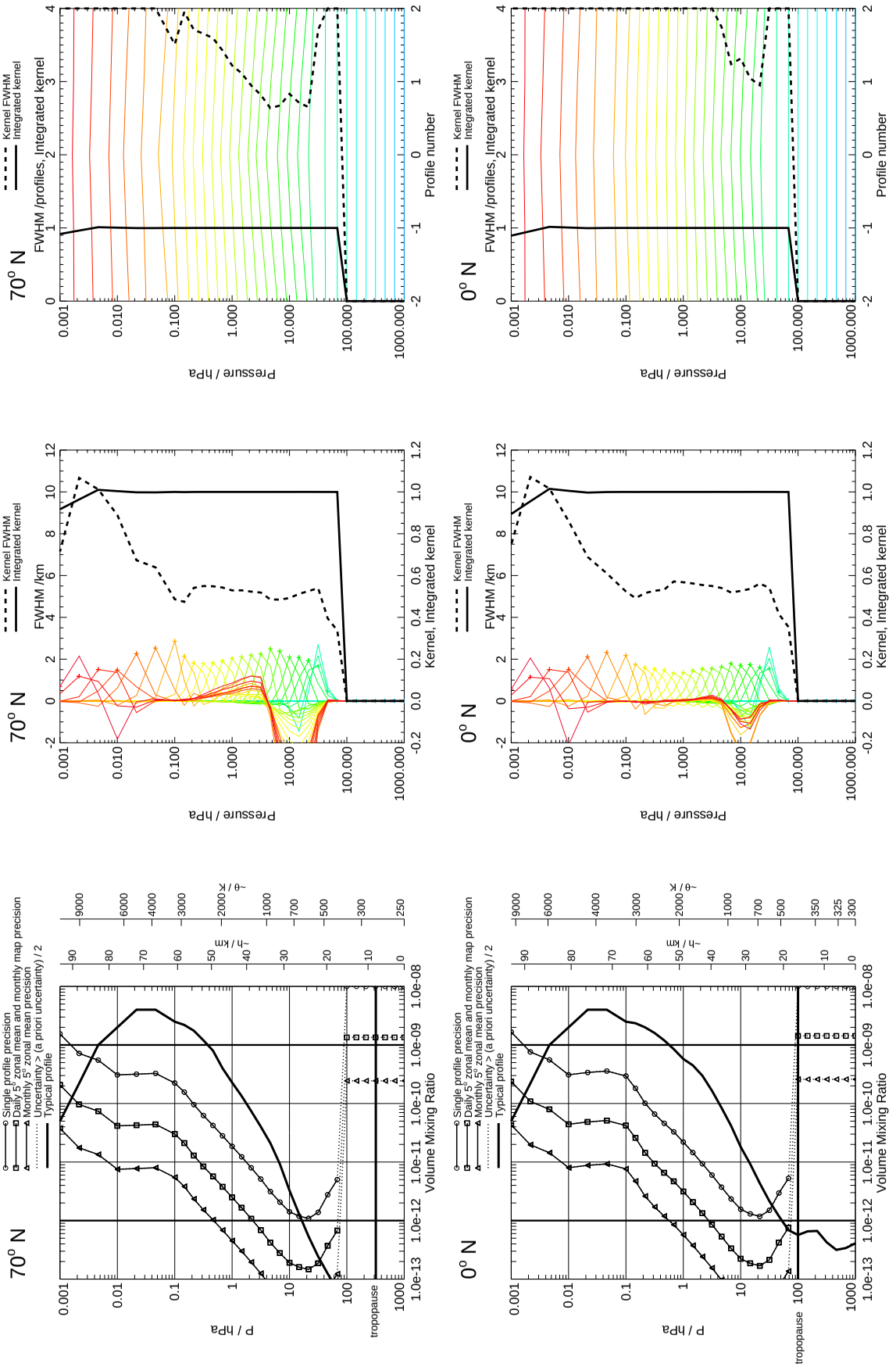

Figure 101: OH precision and averaging kernels, with V1.4 regularisation. V1.4 phase CorePlusR5.

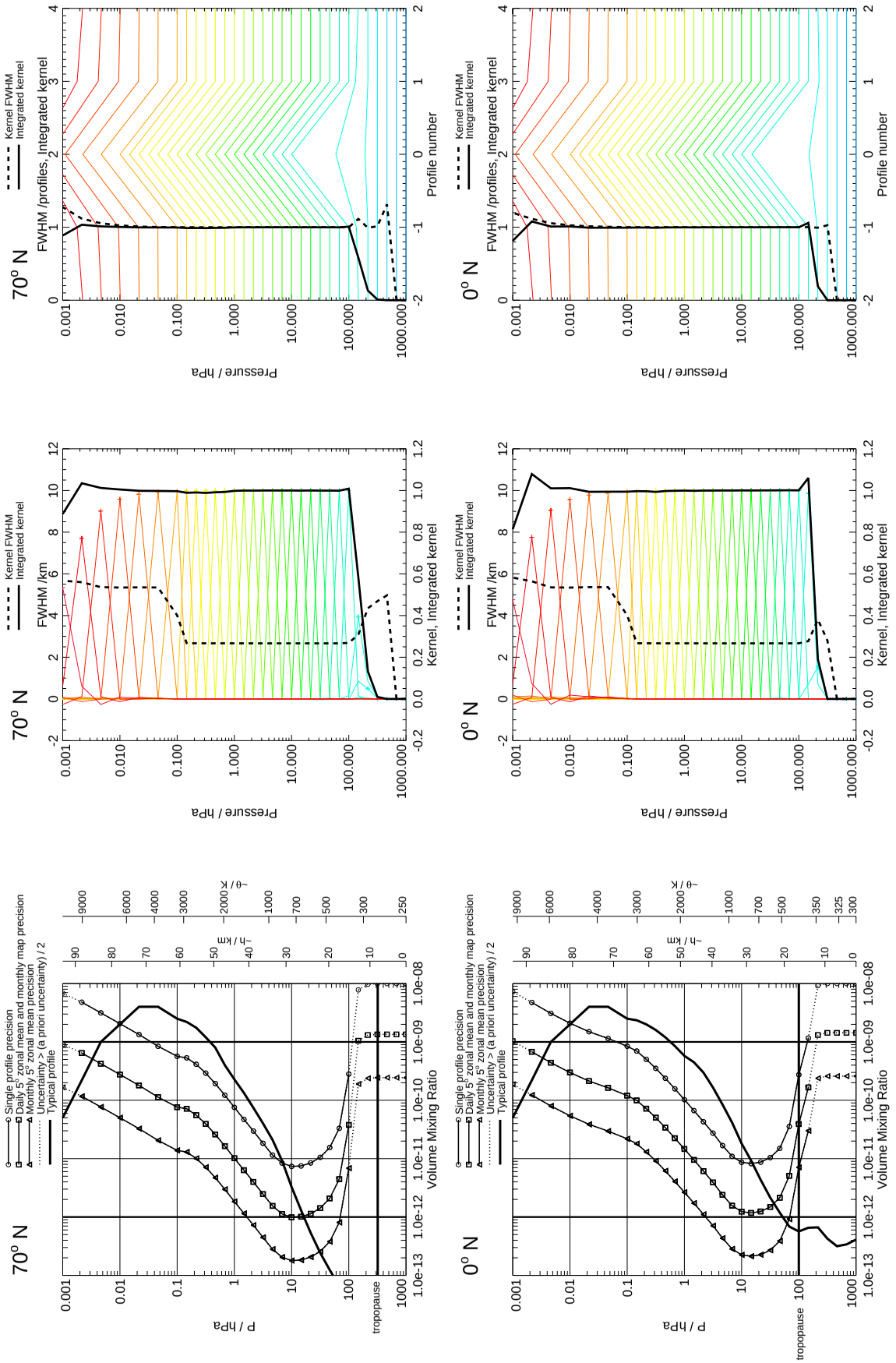

Figure 102: OH precision and averaging kernels, with no regularisation. Touchstone phase CorePlusR5.

OH

RHI

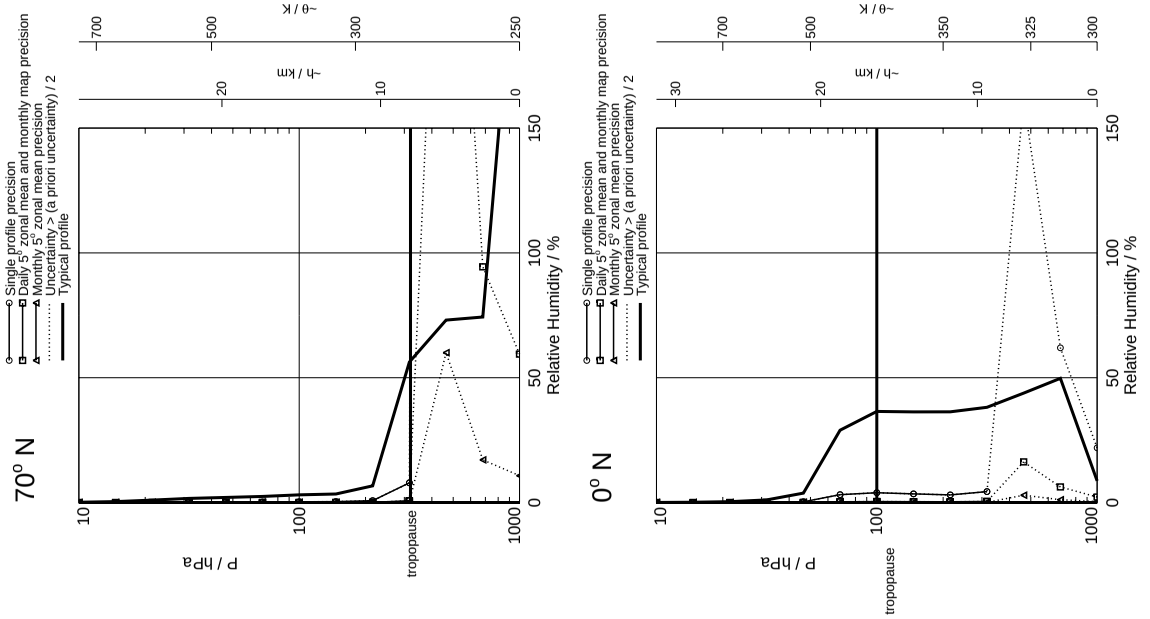

Figure 103: Relative humidity precision, with V1.4 regularisation. V1.4 phased retrieval. No averaging kernels are generated for this product which is derived from temperature and H_2O.

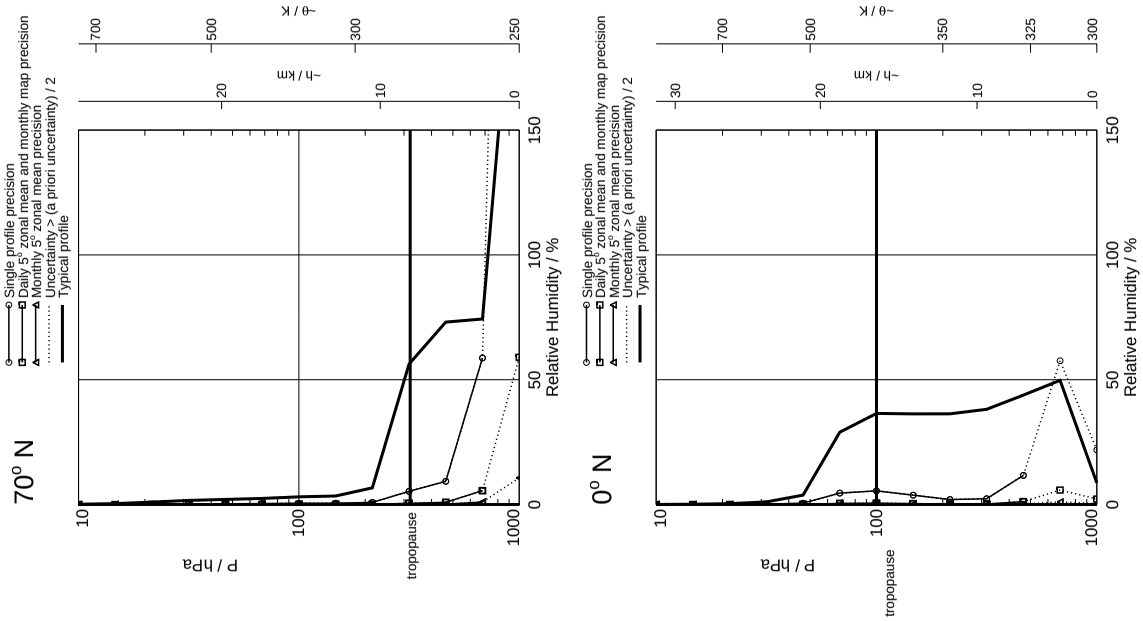

Figure 104: Relative humidity precision, with no regularisation. Touchstone retrieval. No averaging kernels are generated for this product which is derived from temperature and H_2O.

RHI

RHI

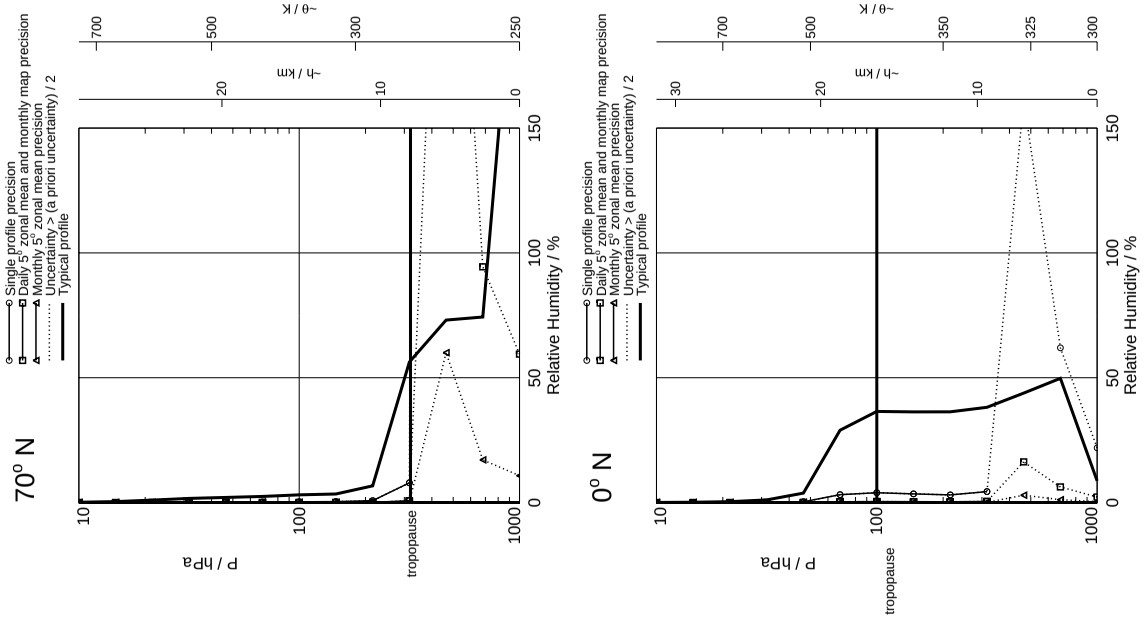

Figure 105: Relative humidity precision, with V1.4 regularisation. V1.4 phase CorePlusR2. No averaging kernels are generated for this product which is derived from temperature and H_2O.

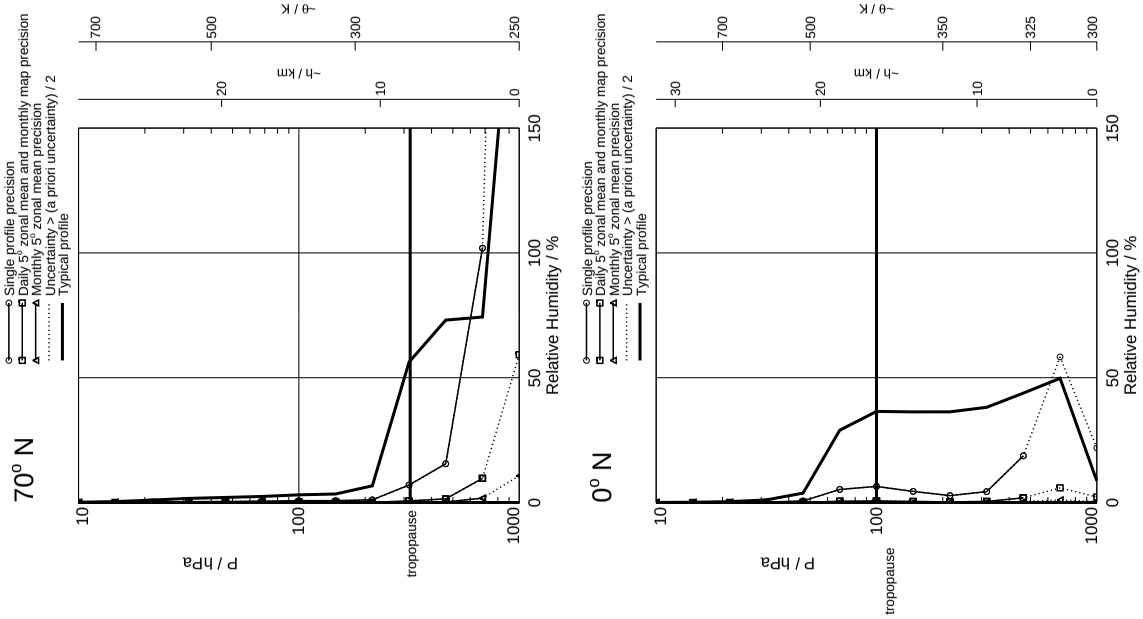

Figure 106: Relative humidity precision, with no regularisation. Touchstone phase CorePlusR2. No averaging kernels are generated for this product which is derived from temperature and H_2O.

RHI

RHI

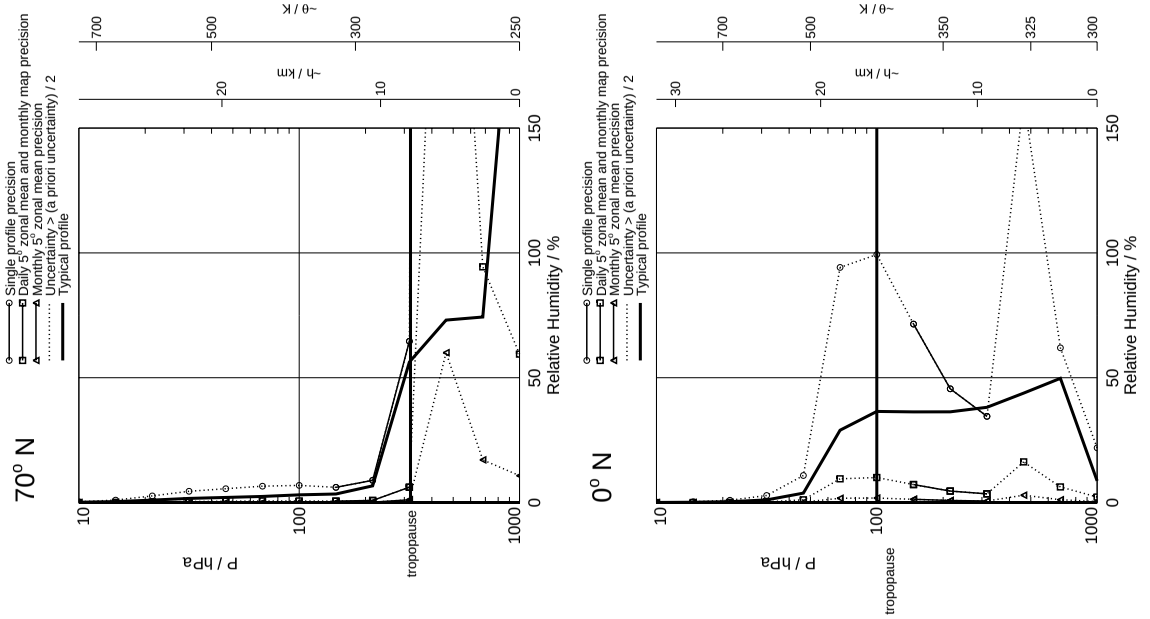

Figure 107: Relative humidity precision, with V1.4 regularisation. V1.4 phase InitUTH. No averaging kernels are generated for this product which is derived from temperature and H_2O.

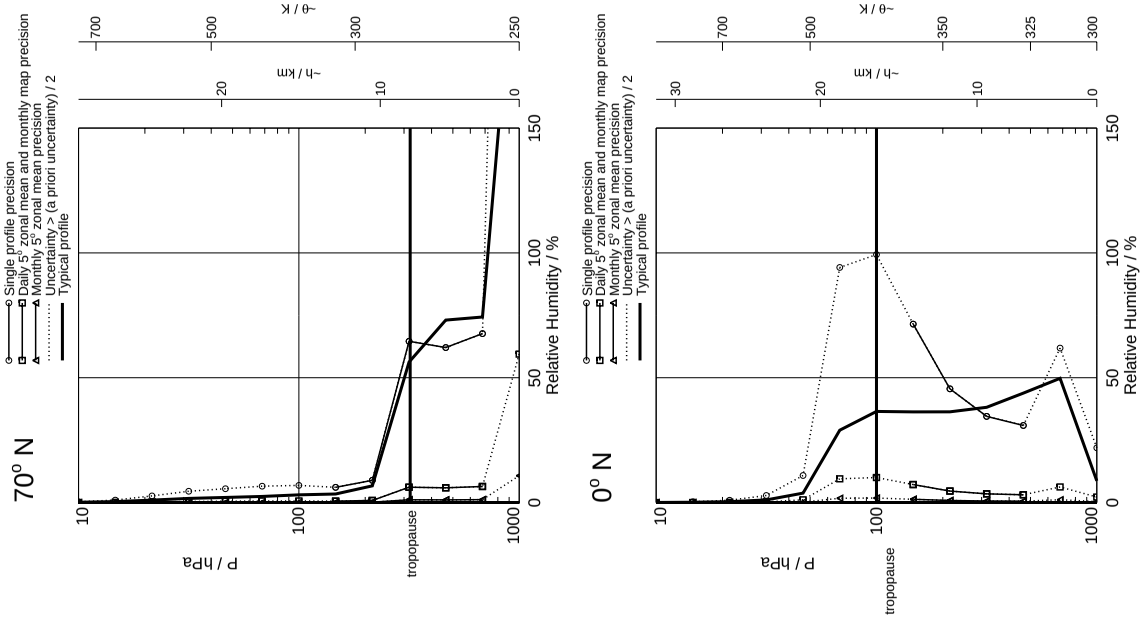

Figure 108: Relative humidity precision, with no regularisation. Touchstone phase InitUTH. No averaging kernels are generated for this product which is derived from temperature and H_2O.

RHI

RHI

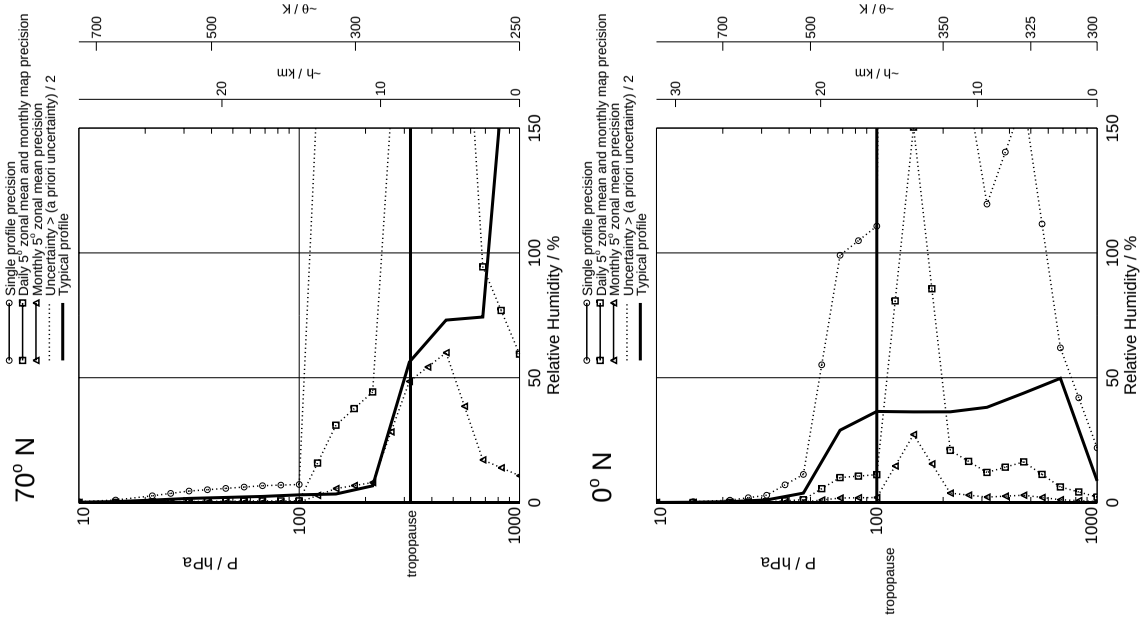

Figure 109: Relative humidity precision, on high resolution grid, with V1.4 regularisation. V1.4 phased retrieval. No averaging kernels are generated for this product which is derived from temperature and H_2O.

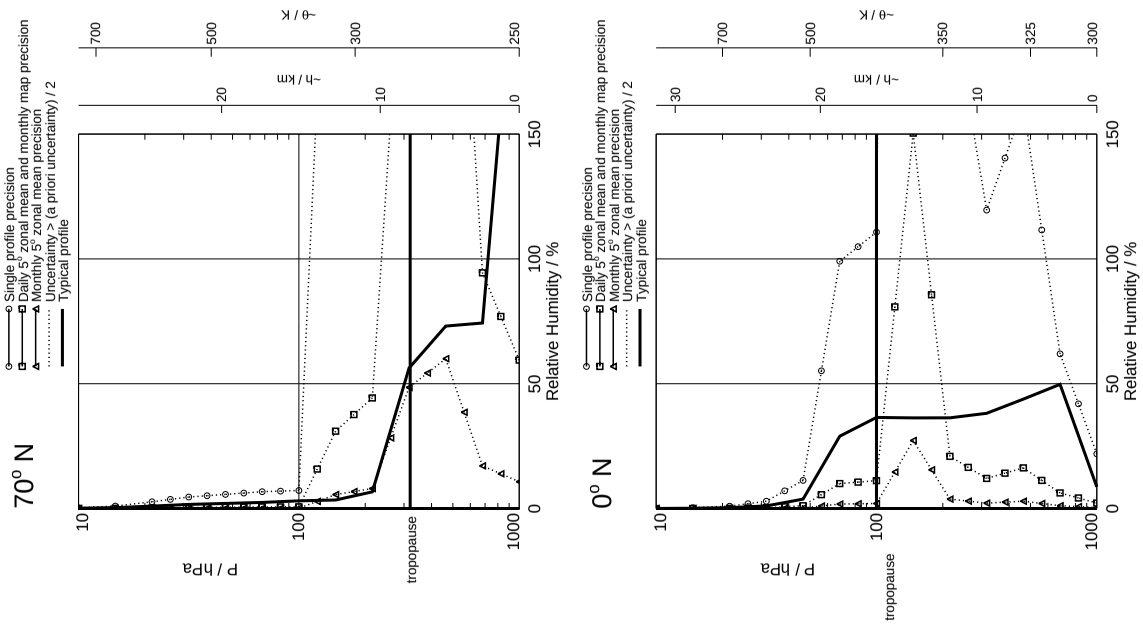

Figure 110: Relative humidity precision, on high resolution grid, with no regularisation. Touchstone retrieval. No averaging kernels are generated for this product which is derived from temperature and H_2O.

RHI

RHI

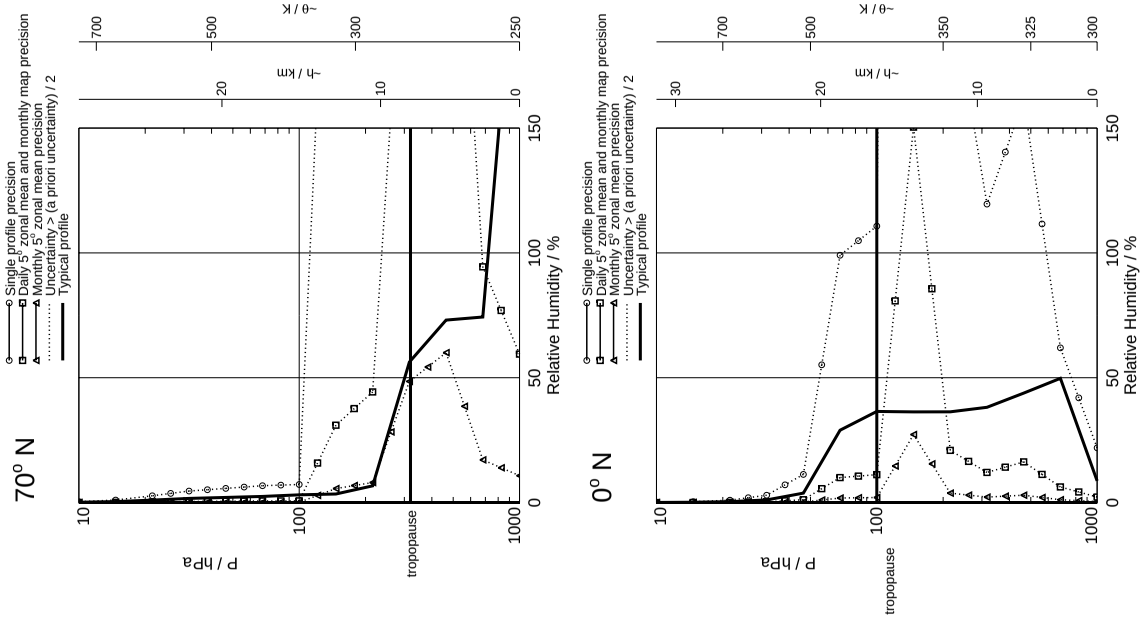

Figure 111: Relative humidity precision, on high resolution grid, with no regularisation. Touchstone phase CorePlusR2. No averaging kernels are generated for this product which is derived from temperature and H_2O.

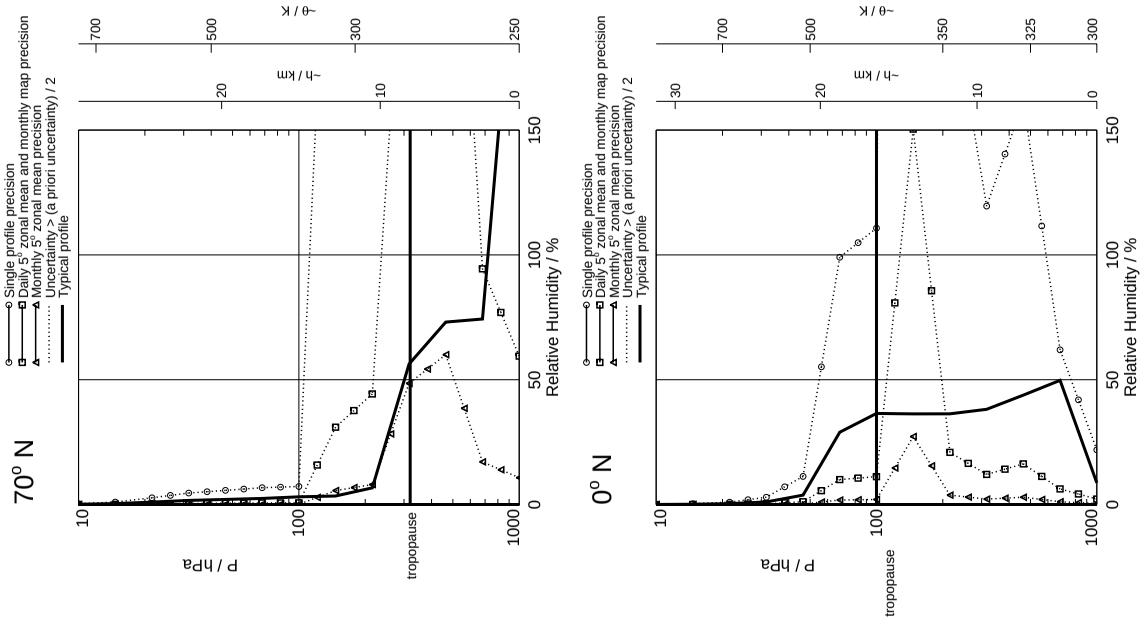

Figure 112: Relative humidity precision, on high resolution grid, with no regularisation. Touchstone phase InitUTH. No averaging kernels are generated for this product which is derived from temperature and H_2O.

RHI

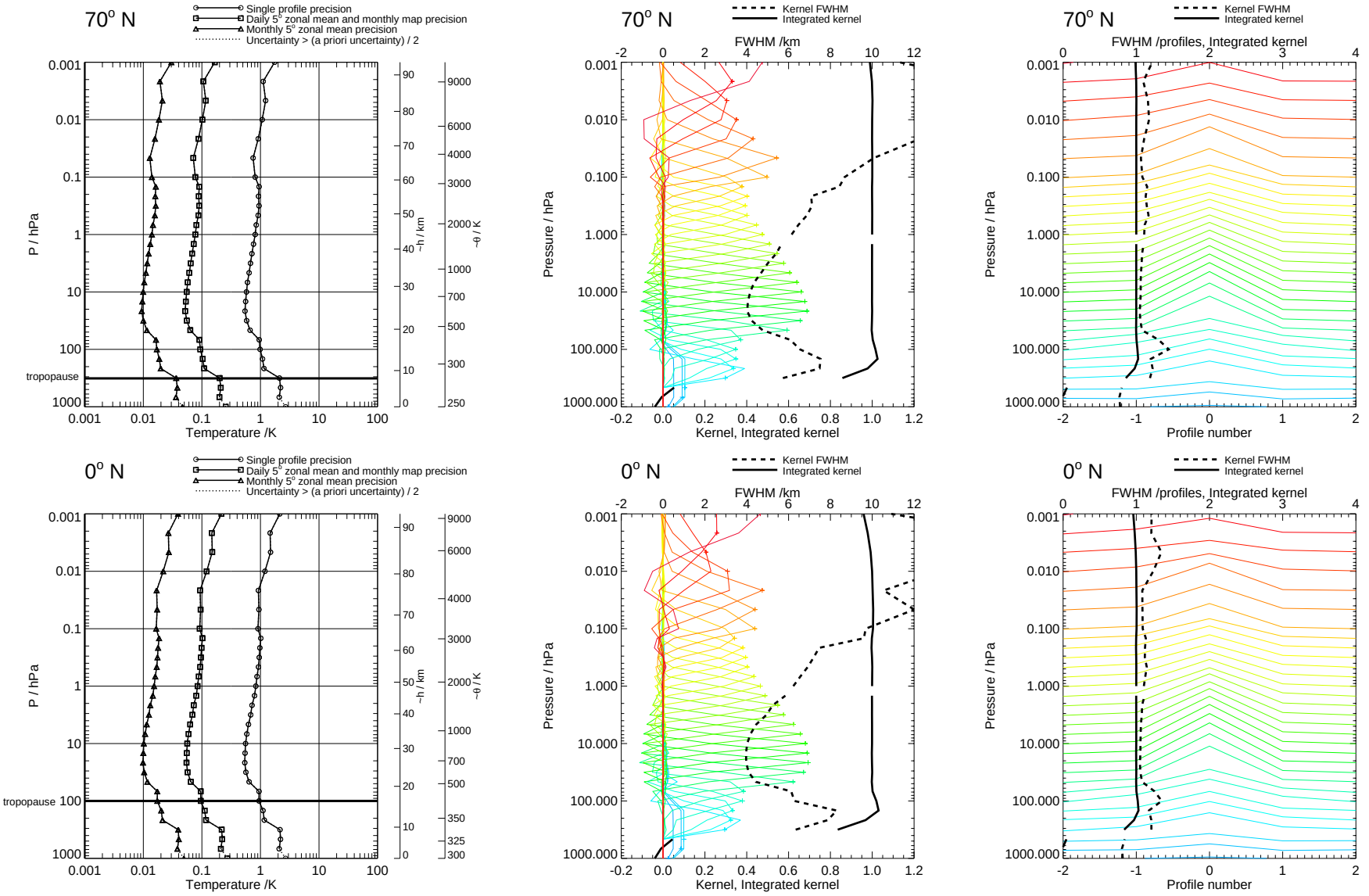

Figure 113: Temperature precision and averaging kernels, with V1.4 regularisation. V1.4 phased retrieval. The temperature standard product is a combination of the results from InitPtan (at and below 464 hPa), UpdatePtan (316 to 1.47 hPa) and CorePlusR2 (1 hPa and above). The results from these phases/ranges are displayed together in these plots.

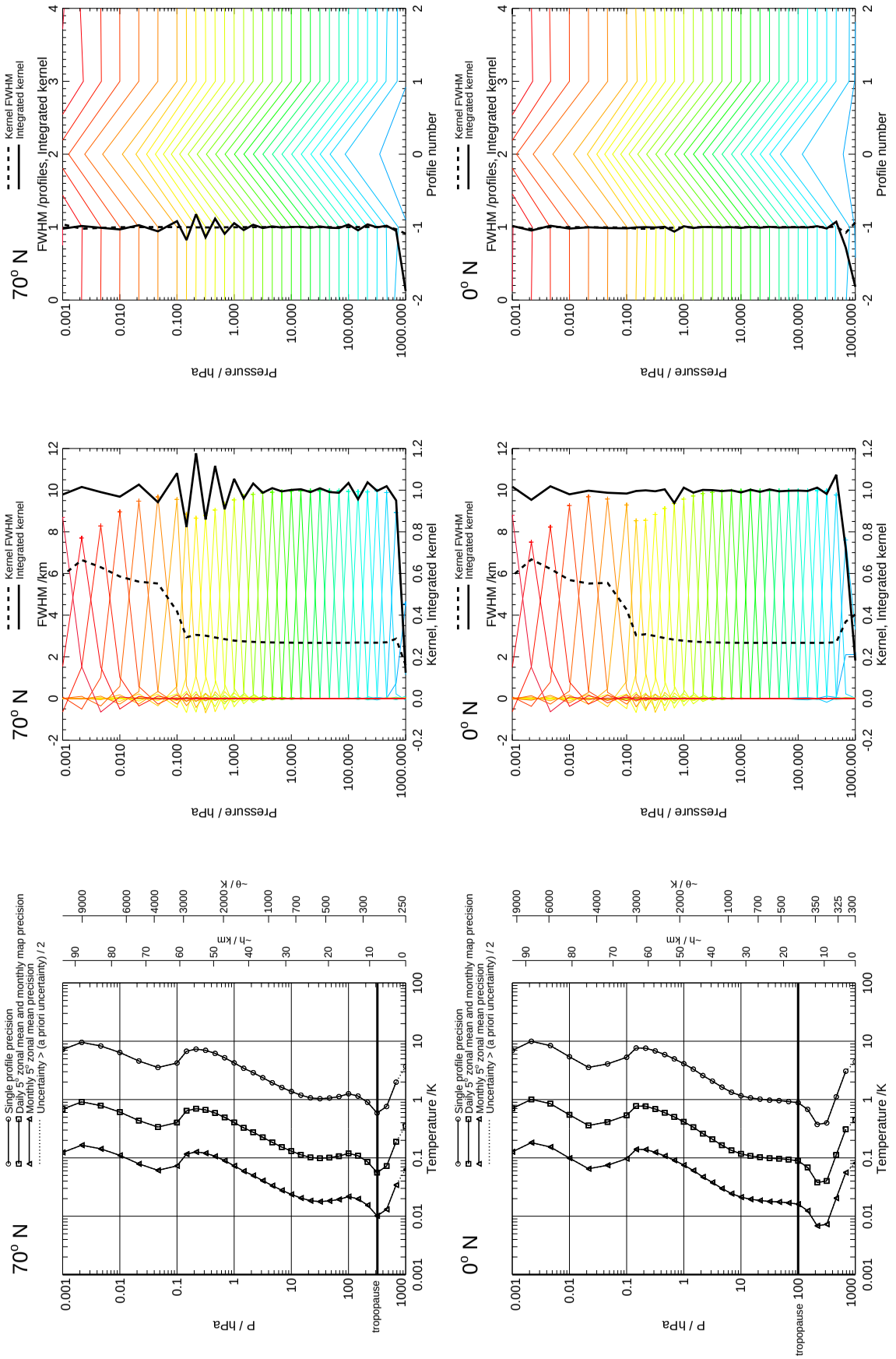

Figure 114: Temperature precision and averaging kernels, with no regularisation. Touchstone retrieval.

T

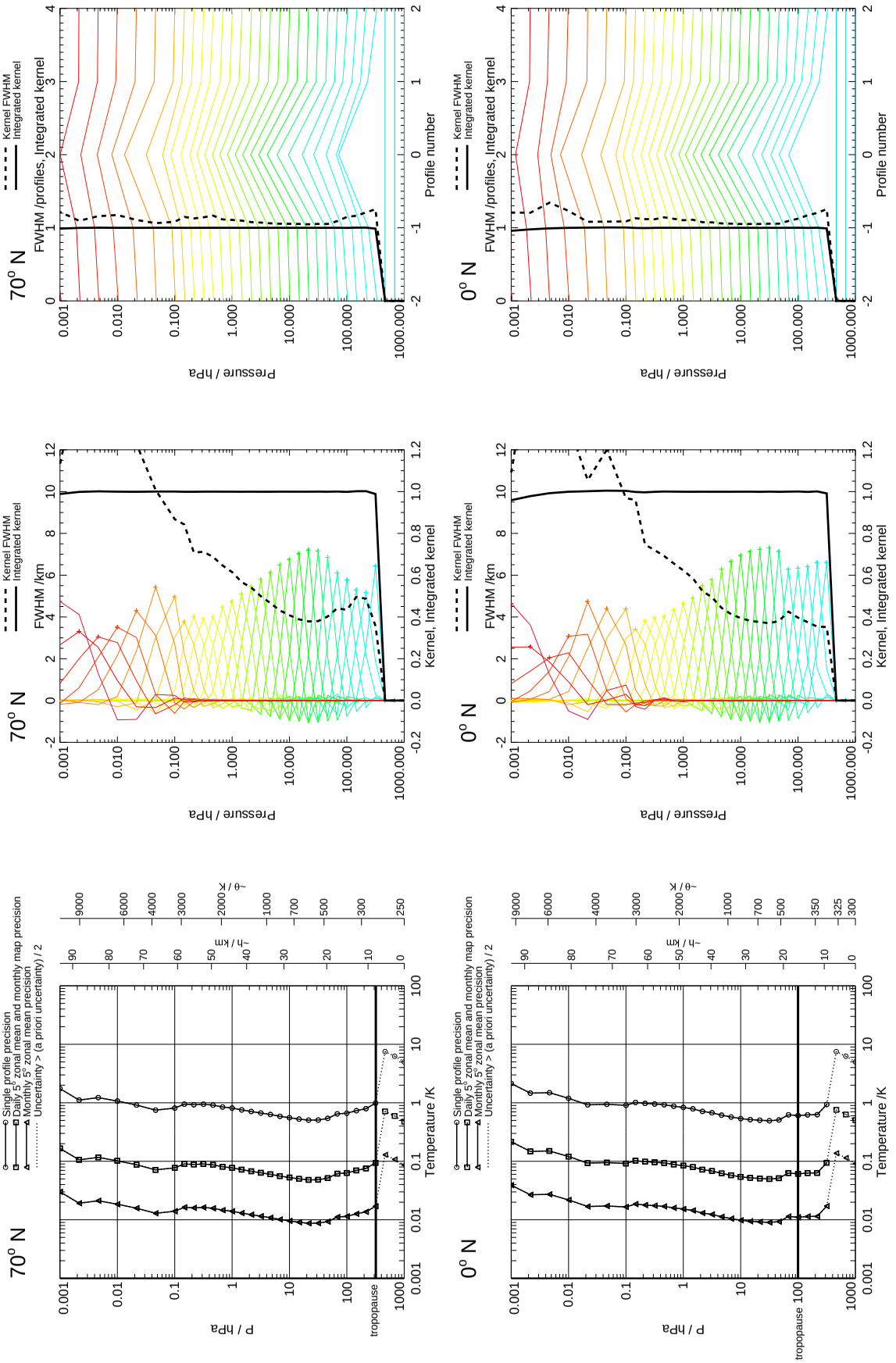

Figure 115: Temperature precision and averaging kernels, with V1.4 regularisation. V1.4 phase CorePlusR2.

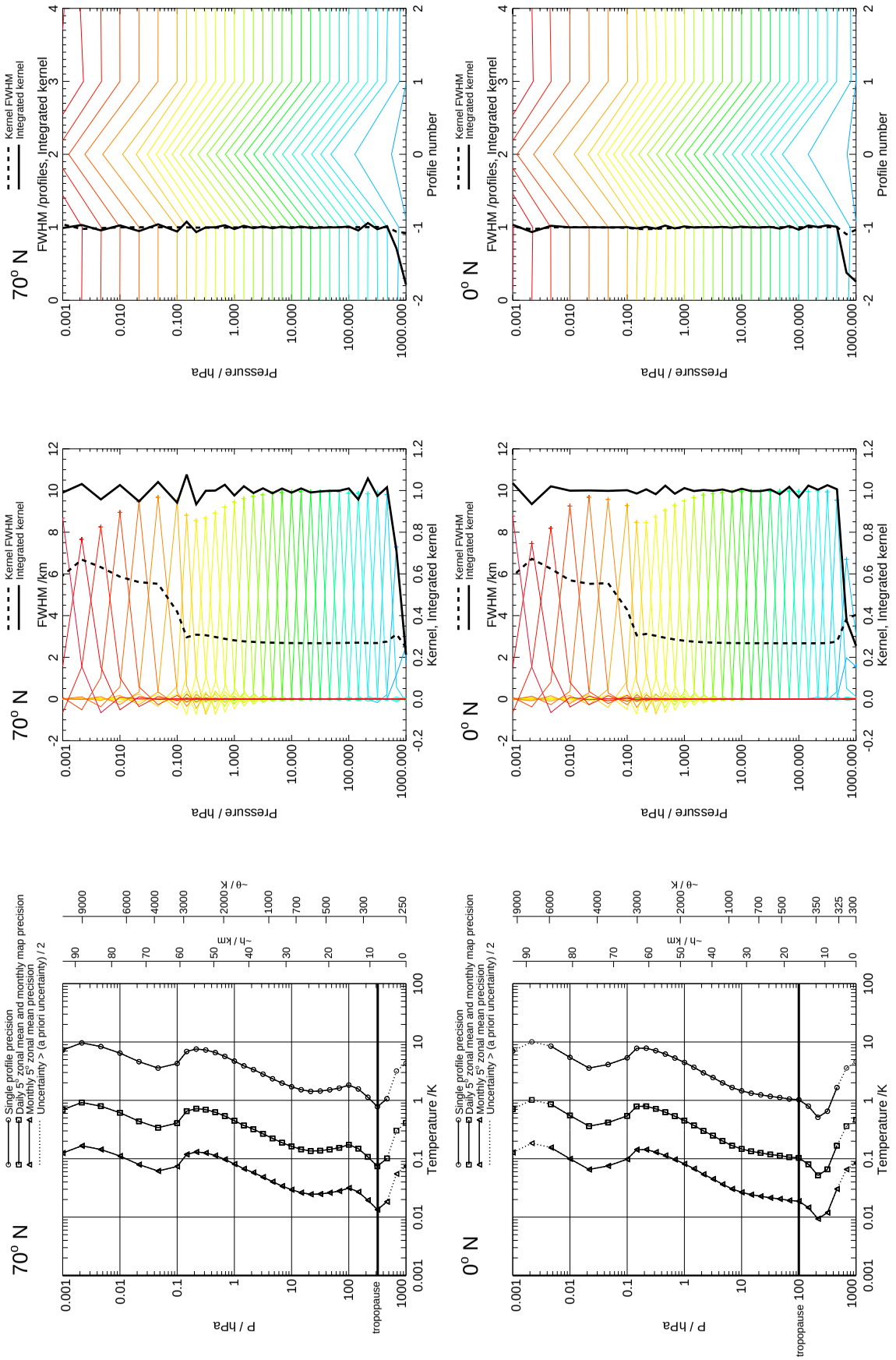

Figure 116: Temperature precision and averaging kernels, with no regularisation. Touchstone phase CorePlusR2.

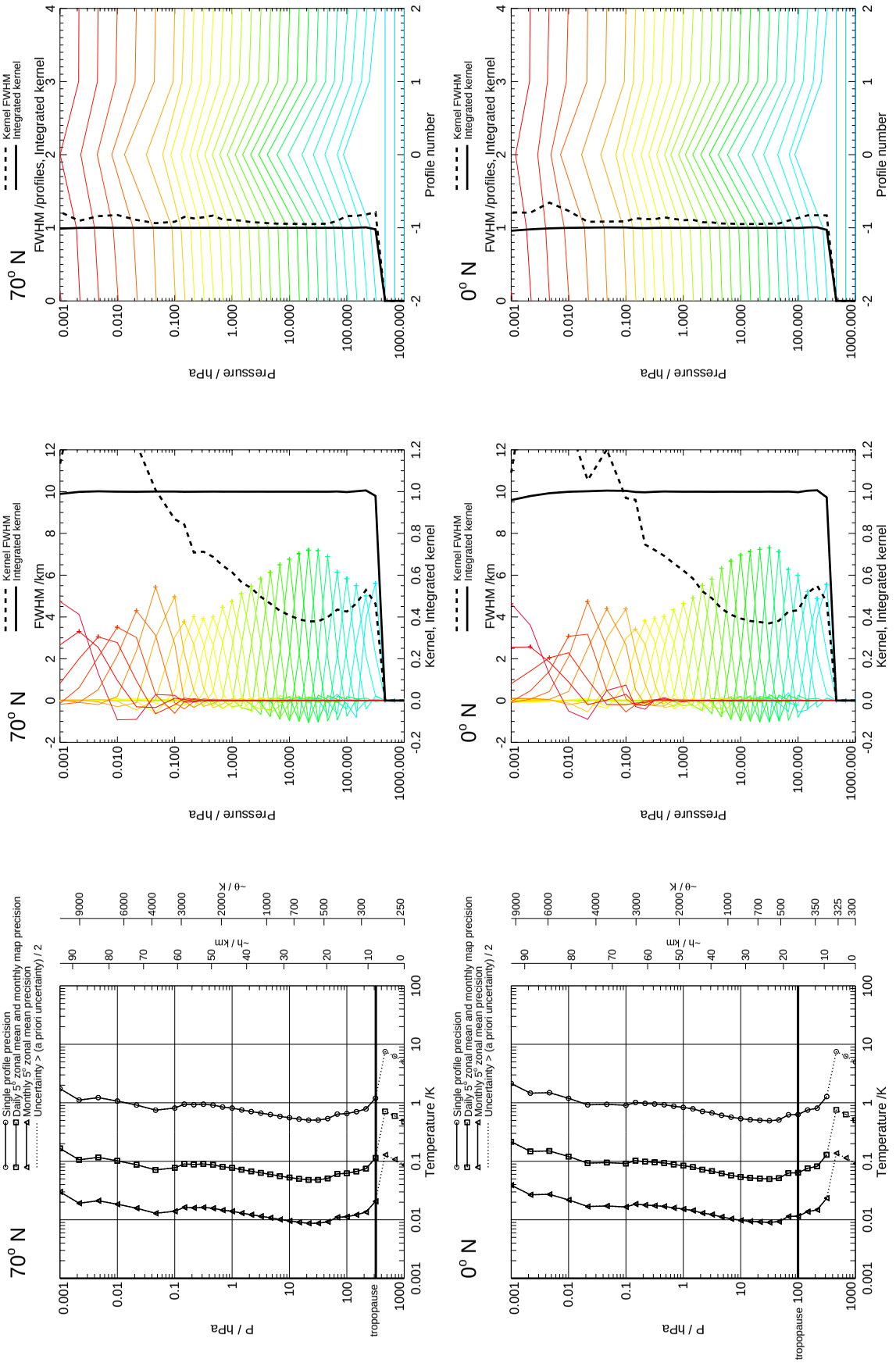

Figure 117: Temperature precision and averaging kernels, with V1.4 regularisation. V1.4 phase CorePlusR3.

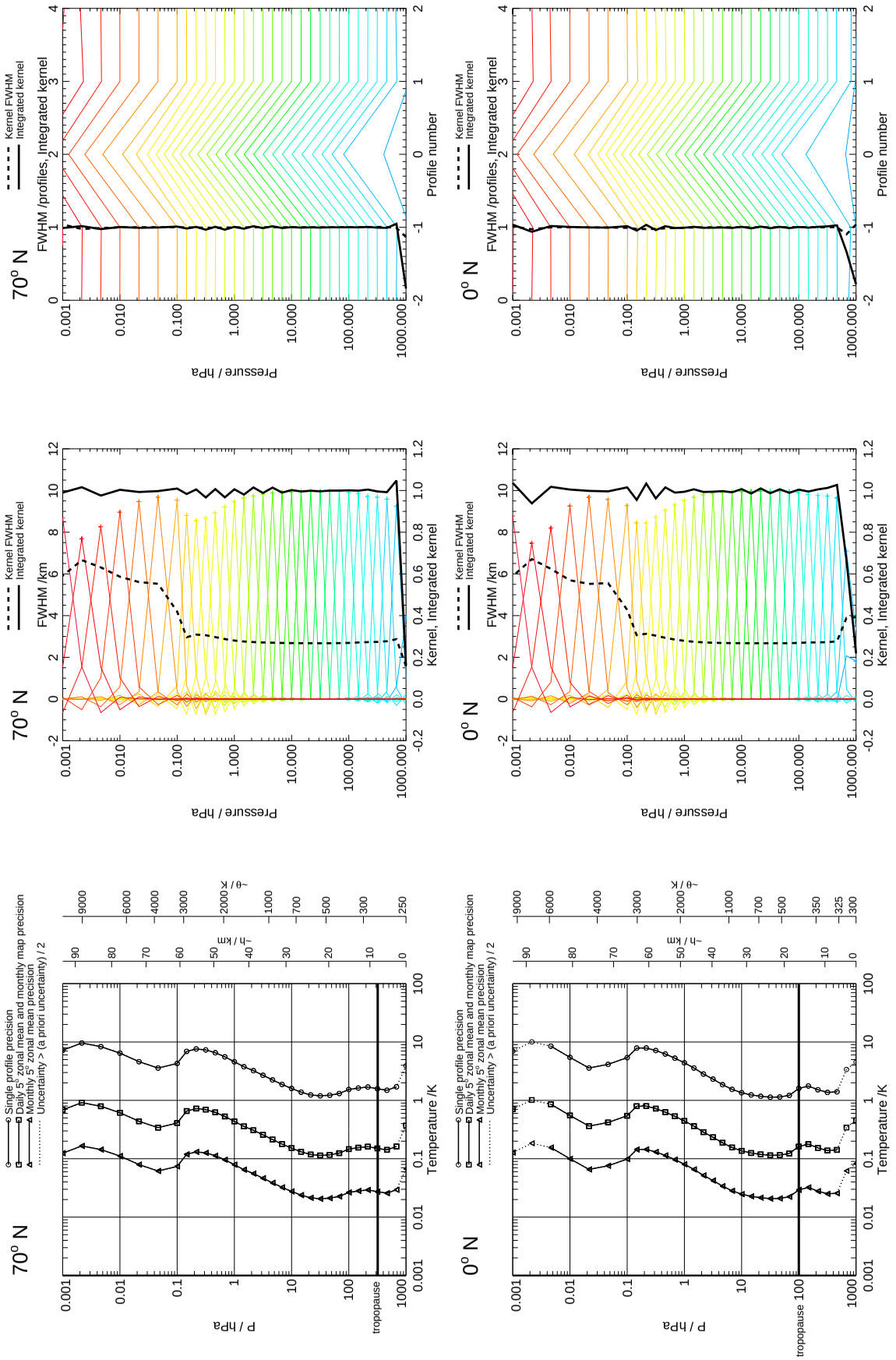

Figure 118: Temperature precision and averaging kernels, with no regularisation. Touchstone phase CorePlusR3.

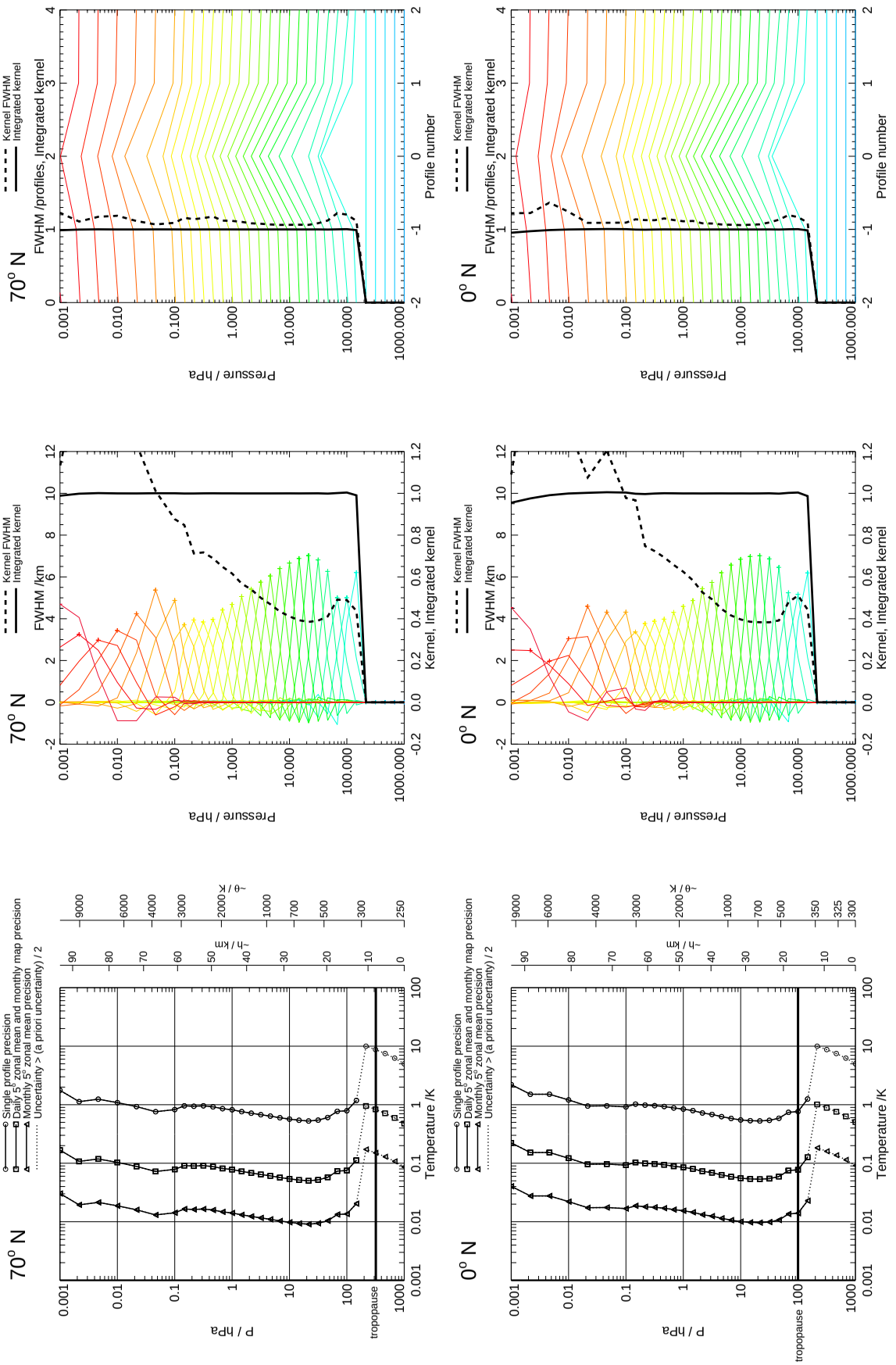

Figure 119: Temperature precision and averaging kernels, with V1.4 regularisation. V1.4 phase CorePlusR4.

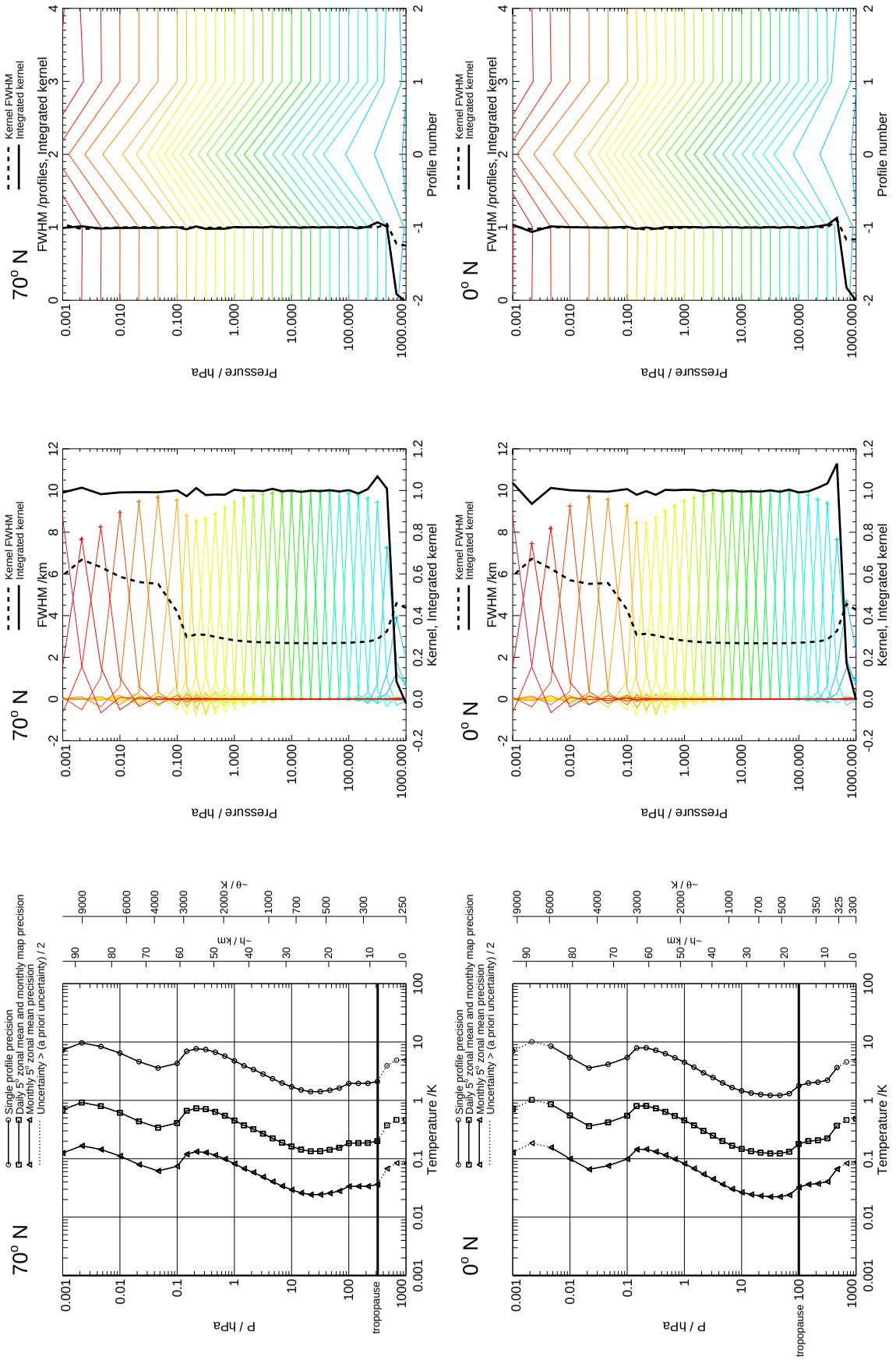

Figure 120: Temperature precision and averaging kernels, with no regularisation. Touchstone phase CorePlusR4.

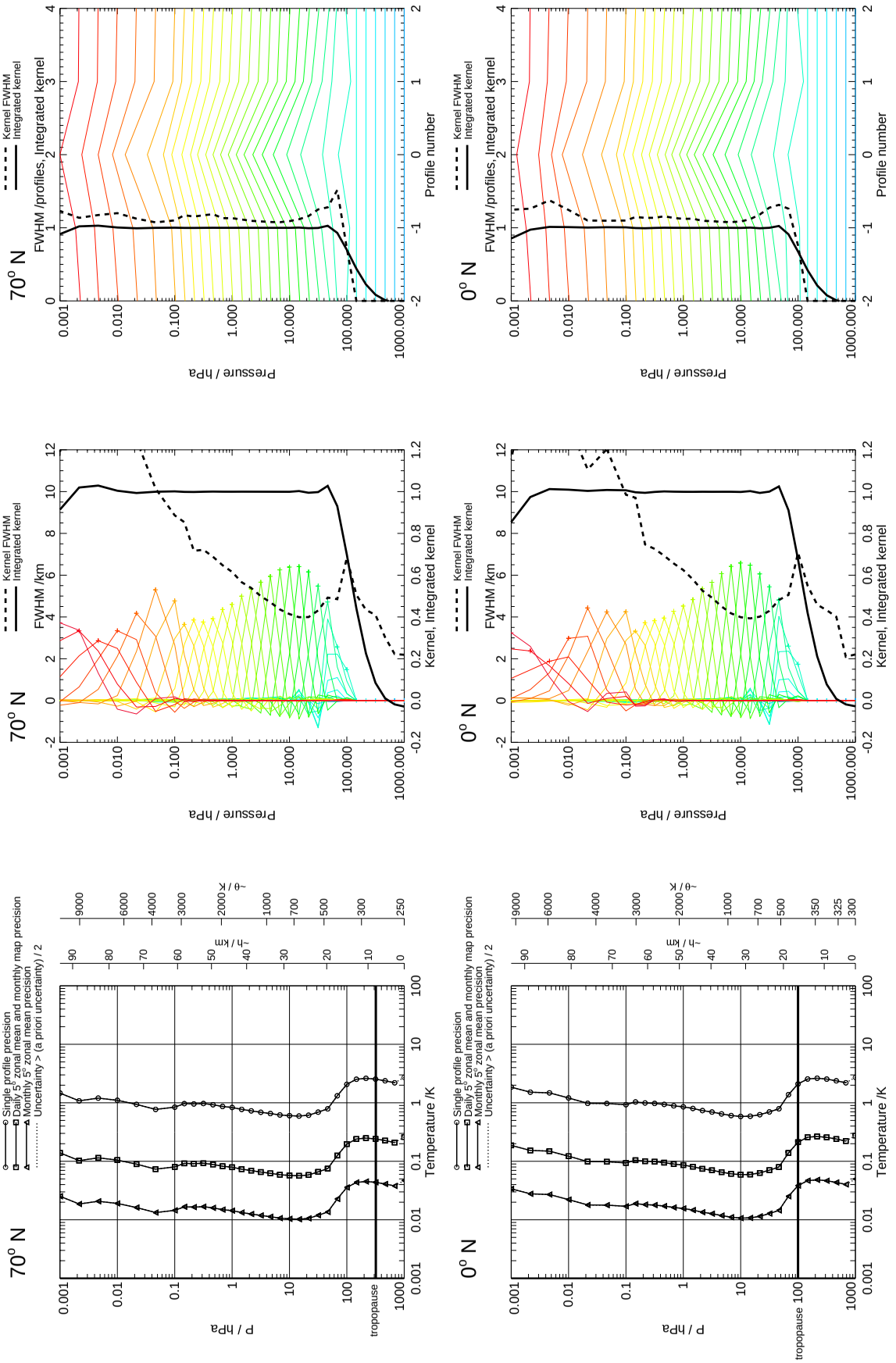

Figure 121: Temperature precision and averaging kernels, with V1.4 regularisation. V1.4 phase CorePlusR5.

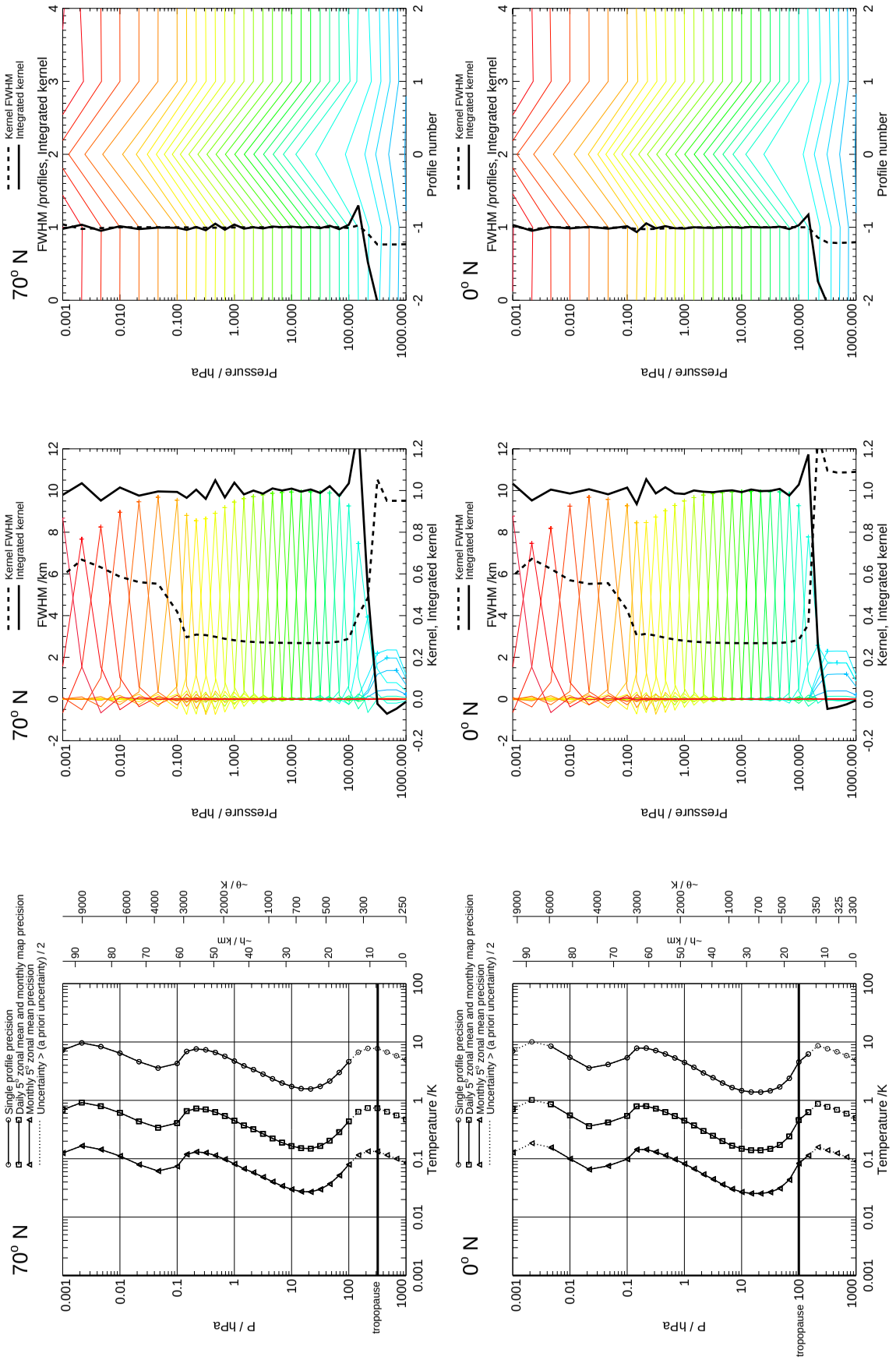

Figure 122: Temperature precision and averaging kernels, with no regularisation. Touchstone phase CorePlusR5.

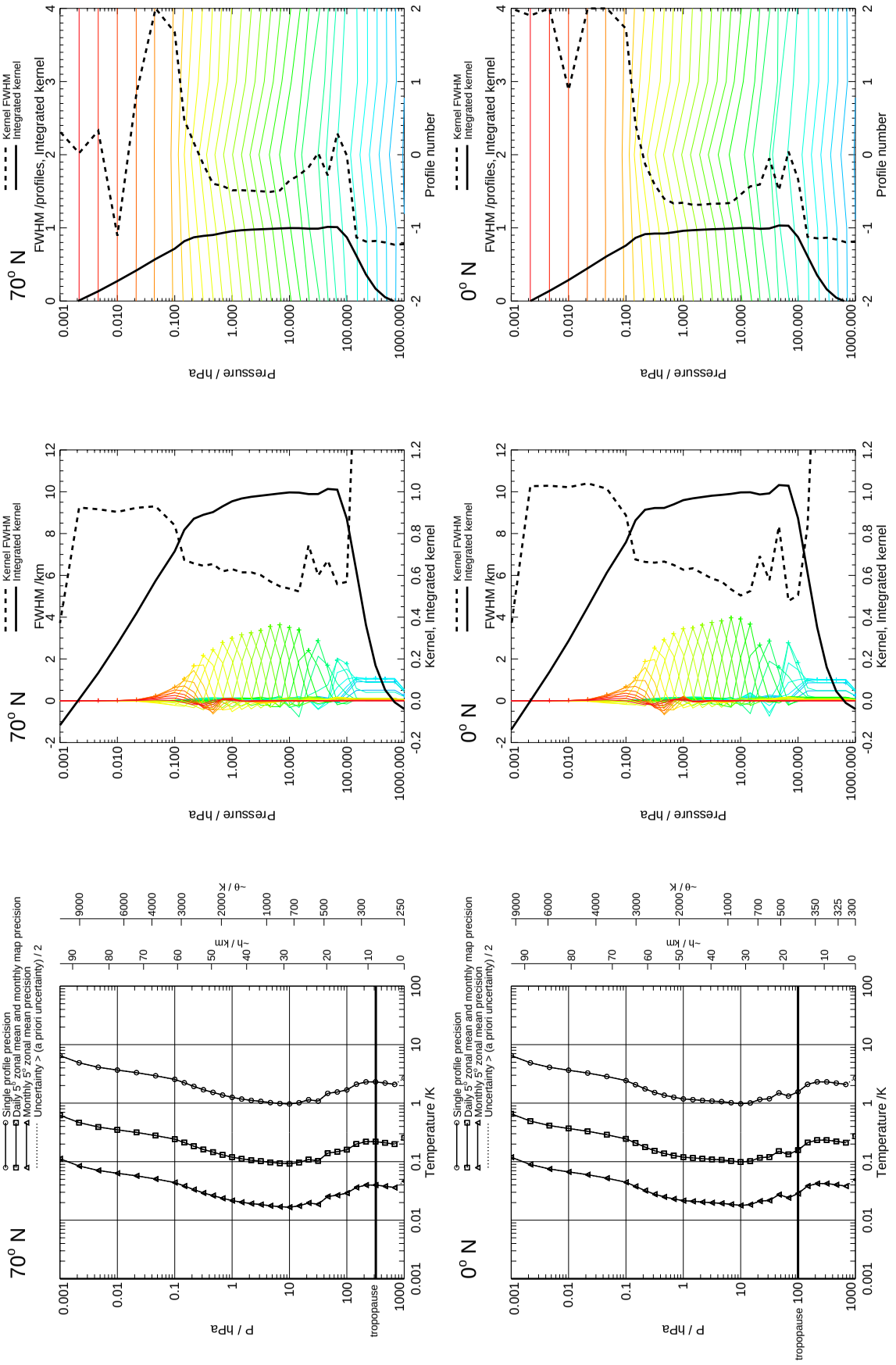

Figure 123: Temperature precision and averaging kernels, with V1.4 regularisation. V1.4 phase InitPtan.

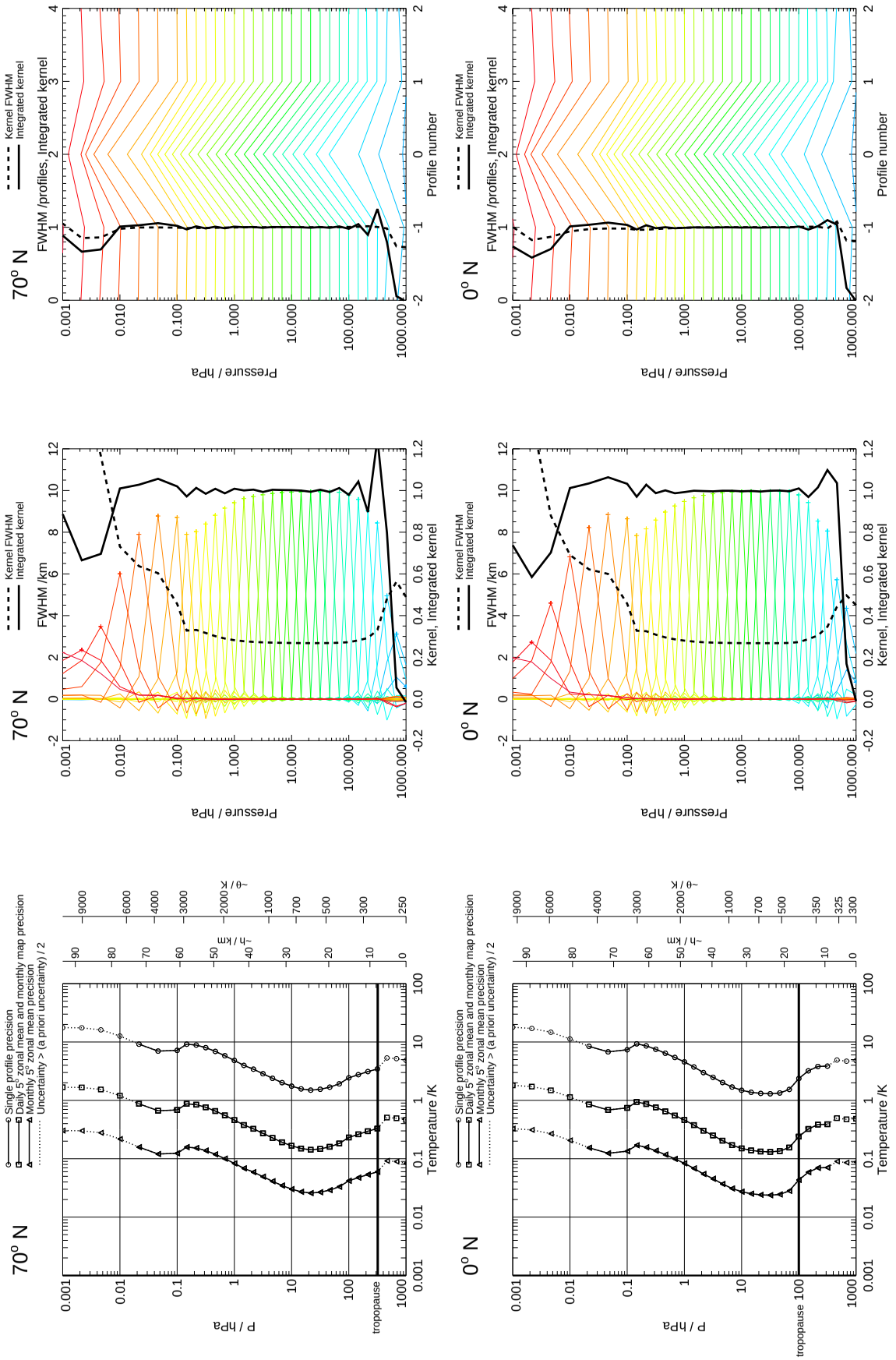

Figure 124: Temperature precision and averaging kernels, with no regularisation. Touchstone phase InitPtan.

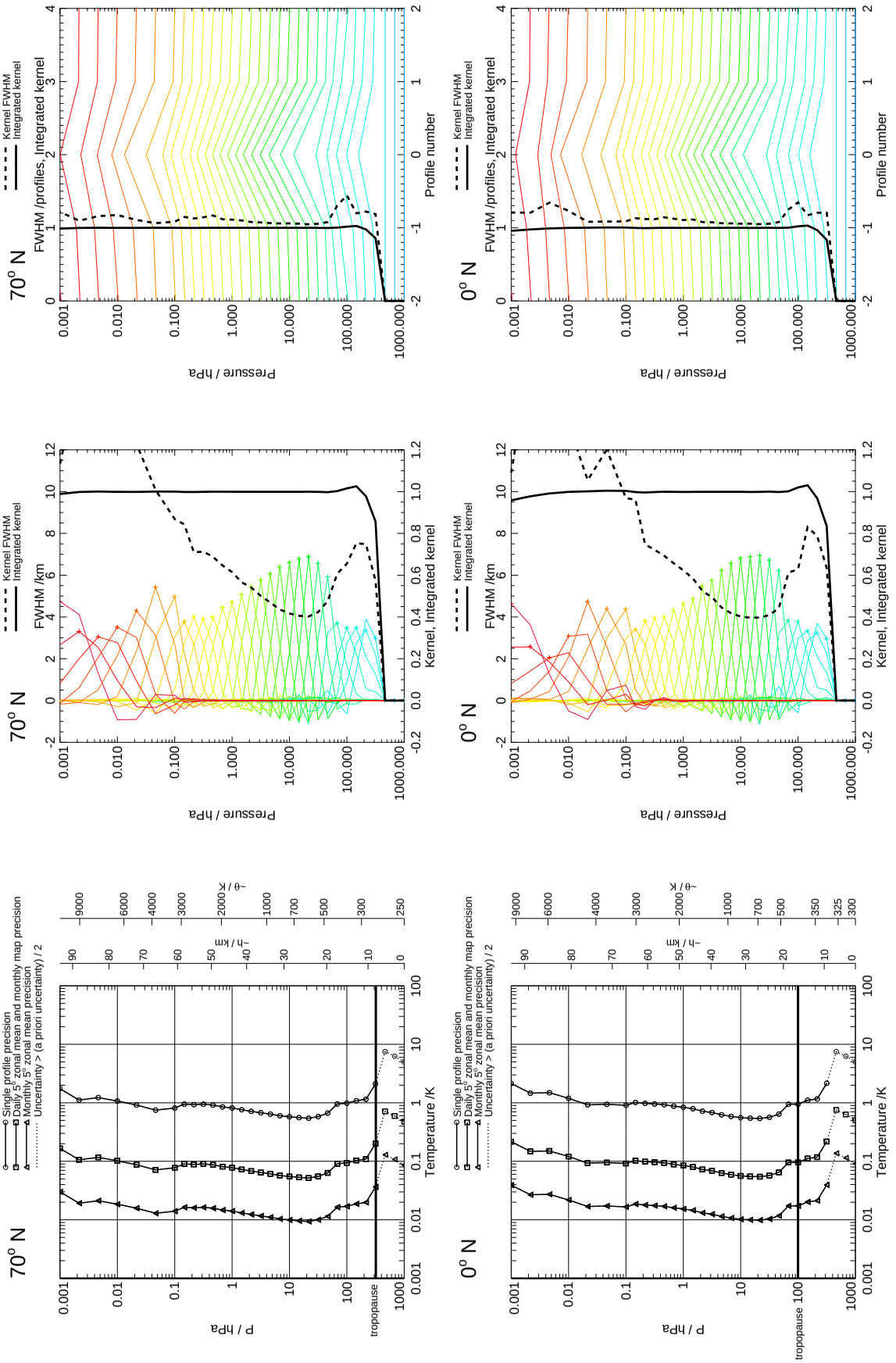

Figure 125: Temperature precision and averaging kernels, with V1.4 regularisation. V1.4 phase UpdatePtan.

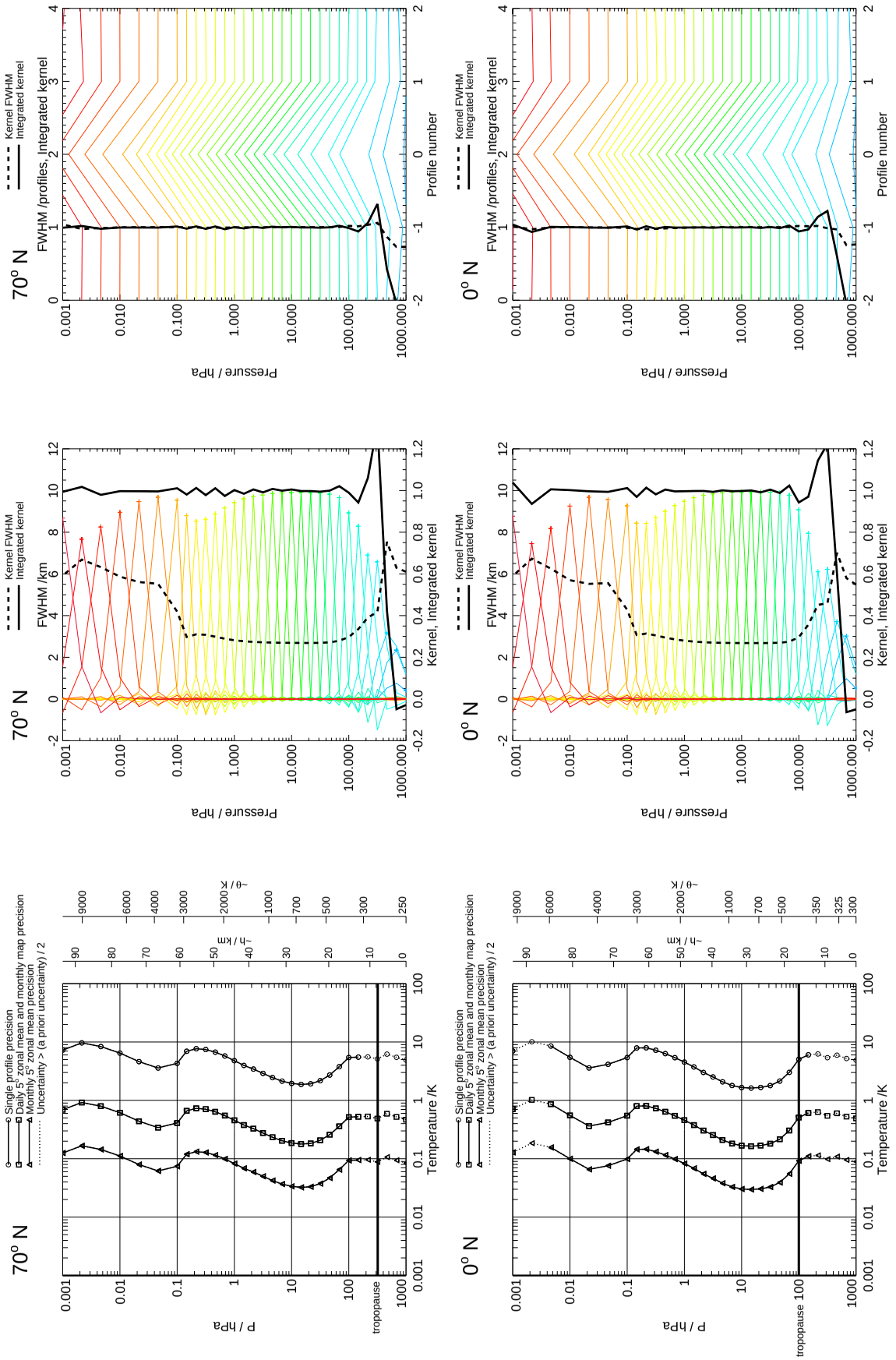

Figure 126: Temperature precision and averaging kernels, with no regularisation. Touchstone phase UpdatePtan.

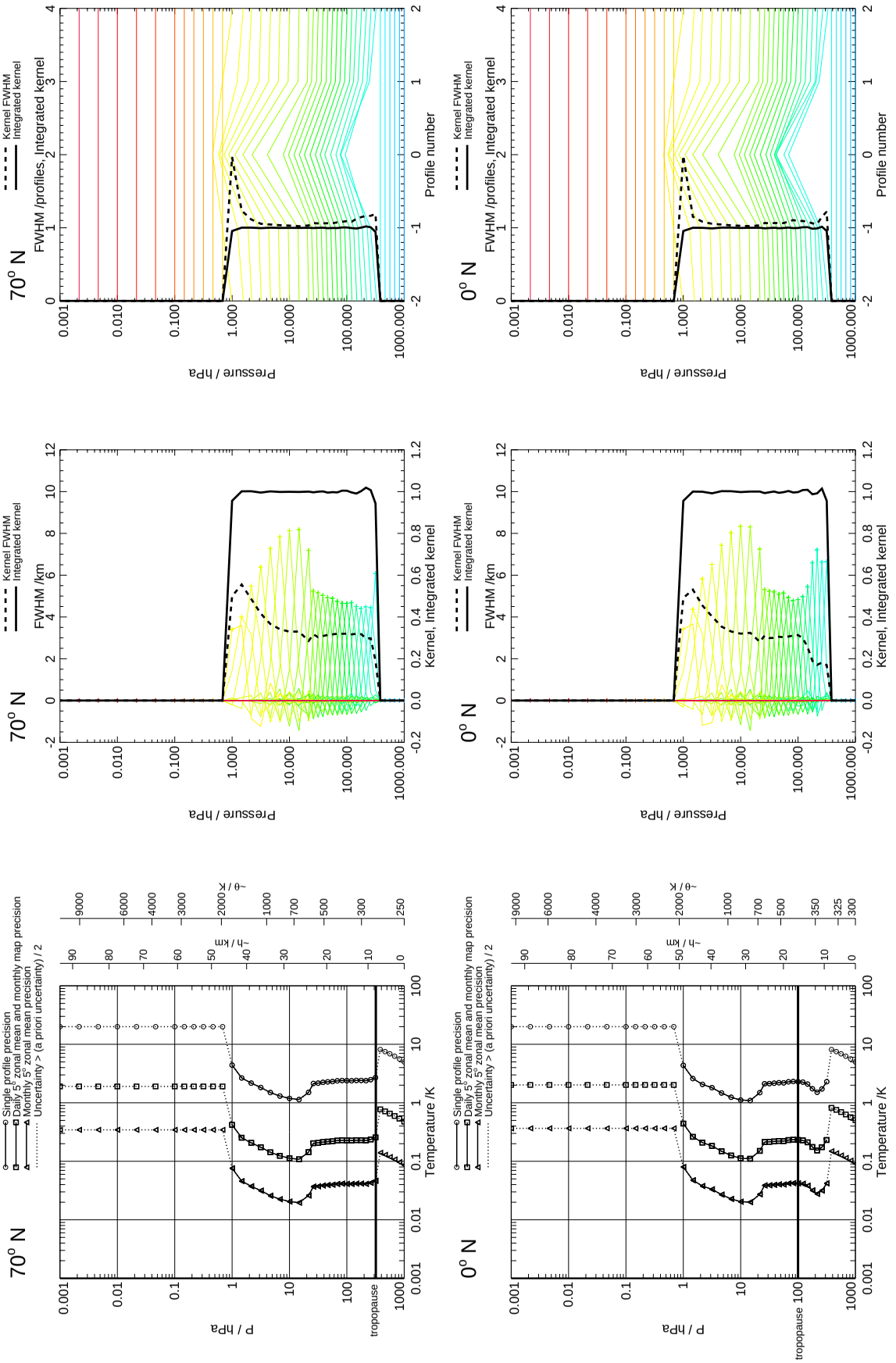

Figure 127: Temperature precision and averaging kernels, on high resolution grid, with V1.4 regularisation. V1.4 phased retrieval.

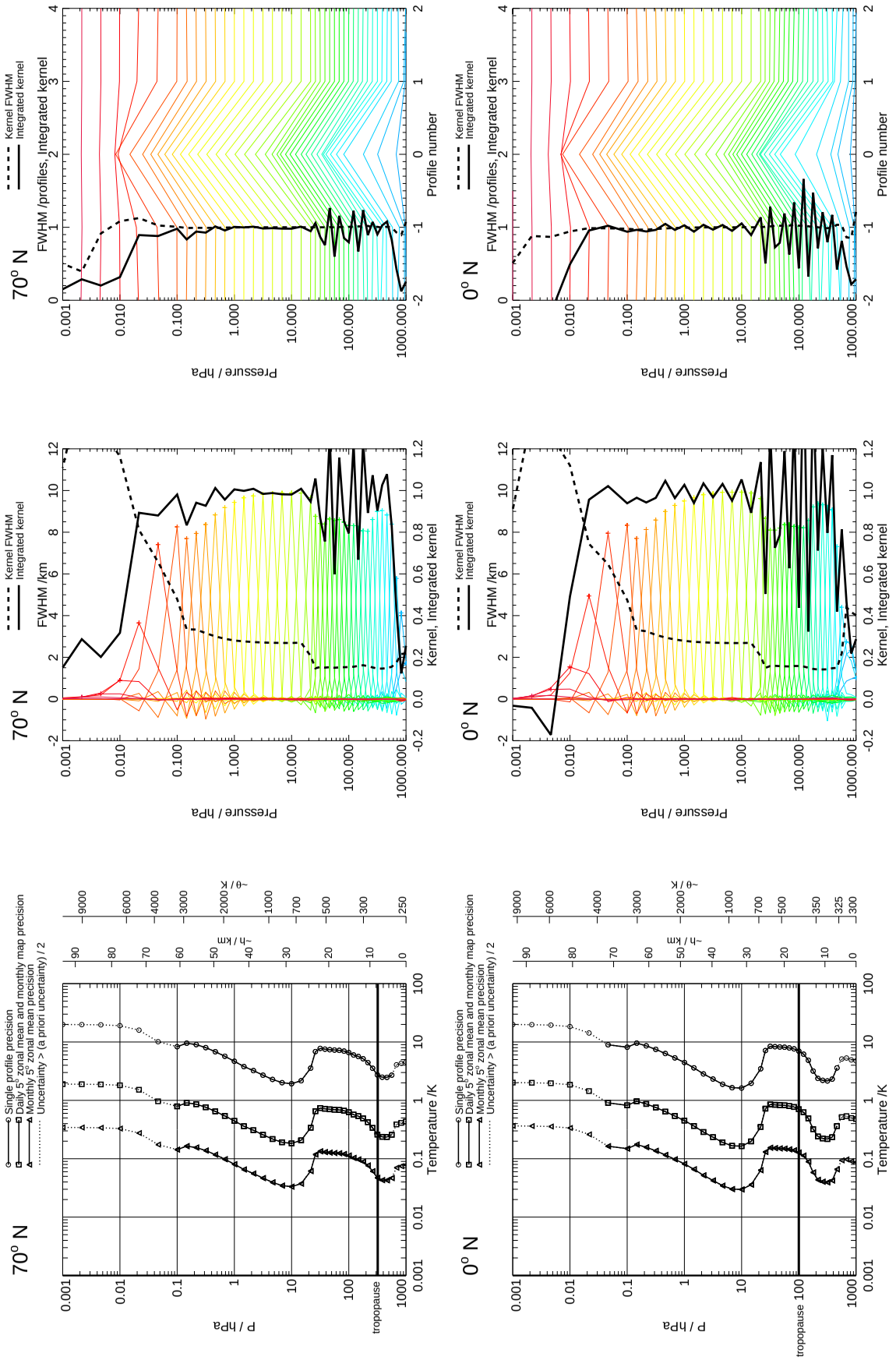

Figure 128: Temperature precision and averaging kernels, on high resolution grid, with no regularisation. Touchstone retrieval.

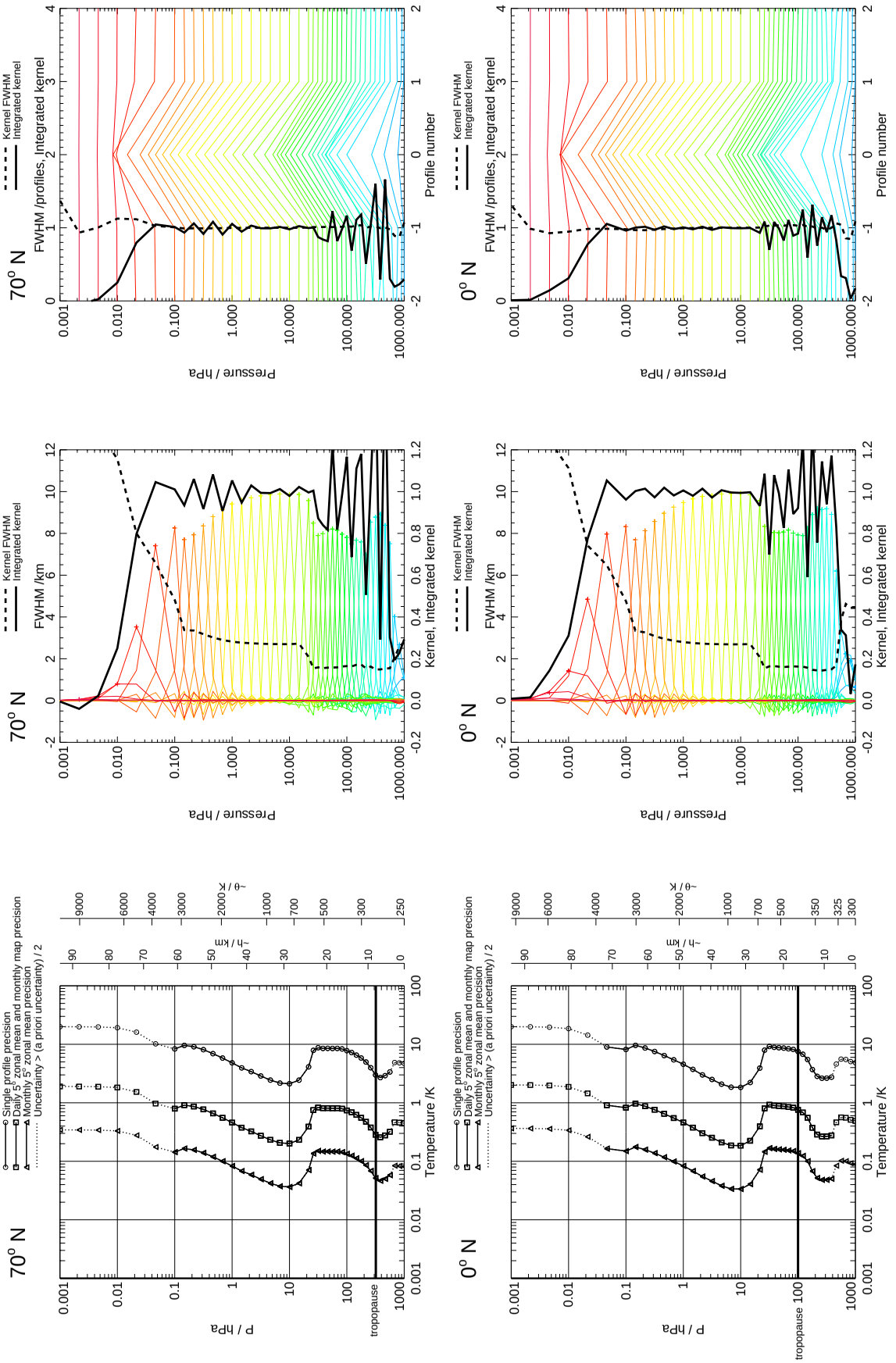

Figure 129: Temperature precision and averaging kernels, on high resolution grid, with no regularisation. Touchstone phase CorePlusR2.

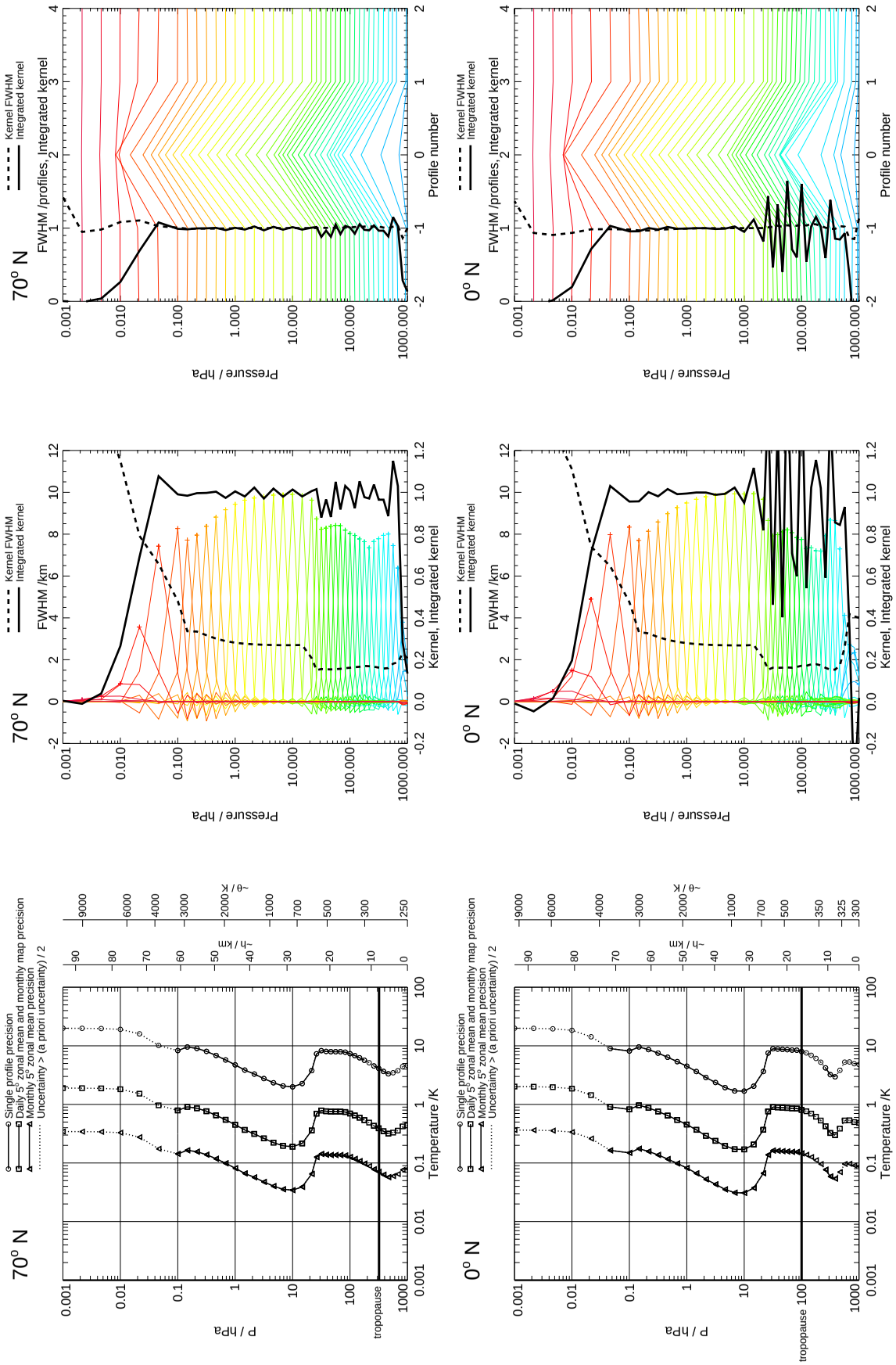

Figure 130: Temperature precision and averaging kernels, on high resolution grid, with no regularisation. Touchstone phase CorePlusR3.

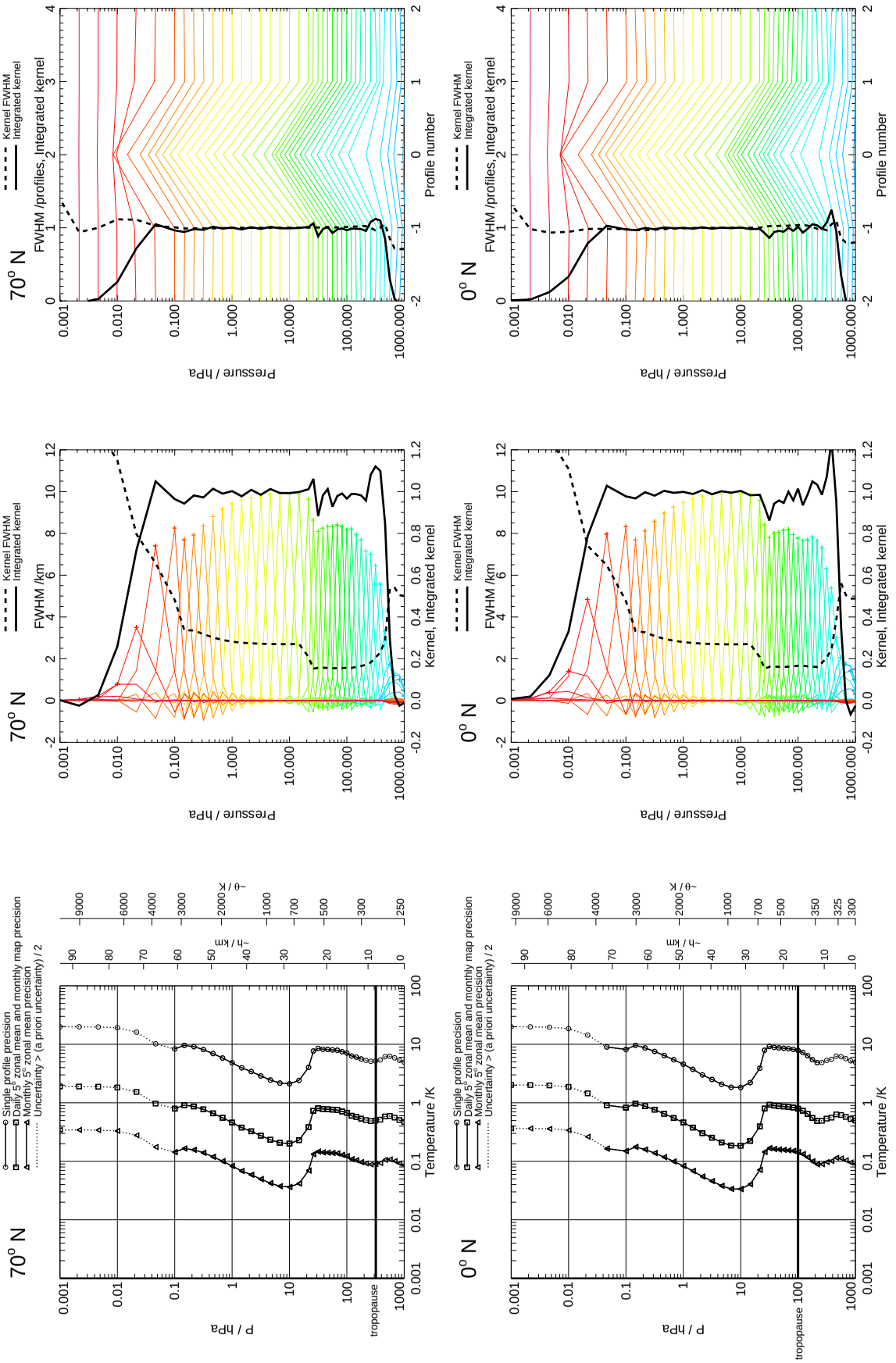

Figure 131: Temperature precision and averaging kernels, on high resolution grid, with no regularisation. Touchstone phase CorePlusR4.

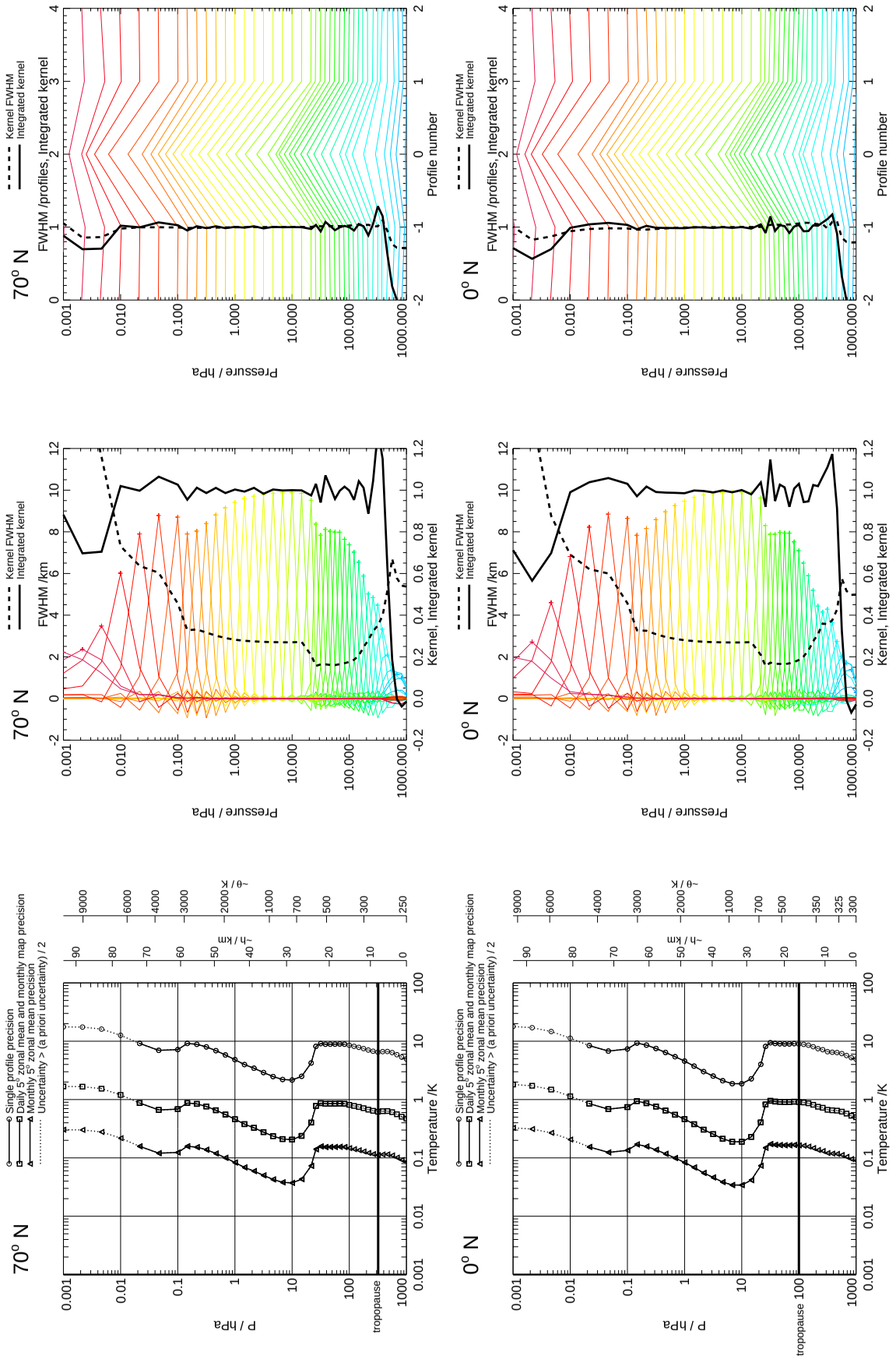

Figure 132: Temperature precision and averaging kernels, on high resolution grid, with no regularisation. Touchstone phase InitPtan.

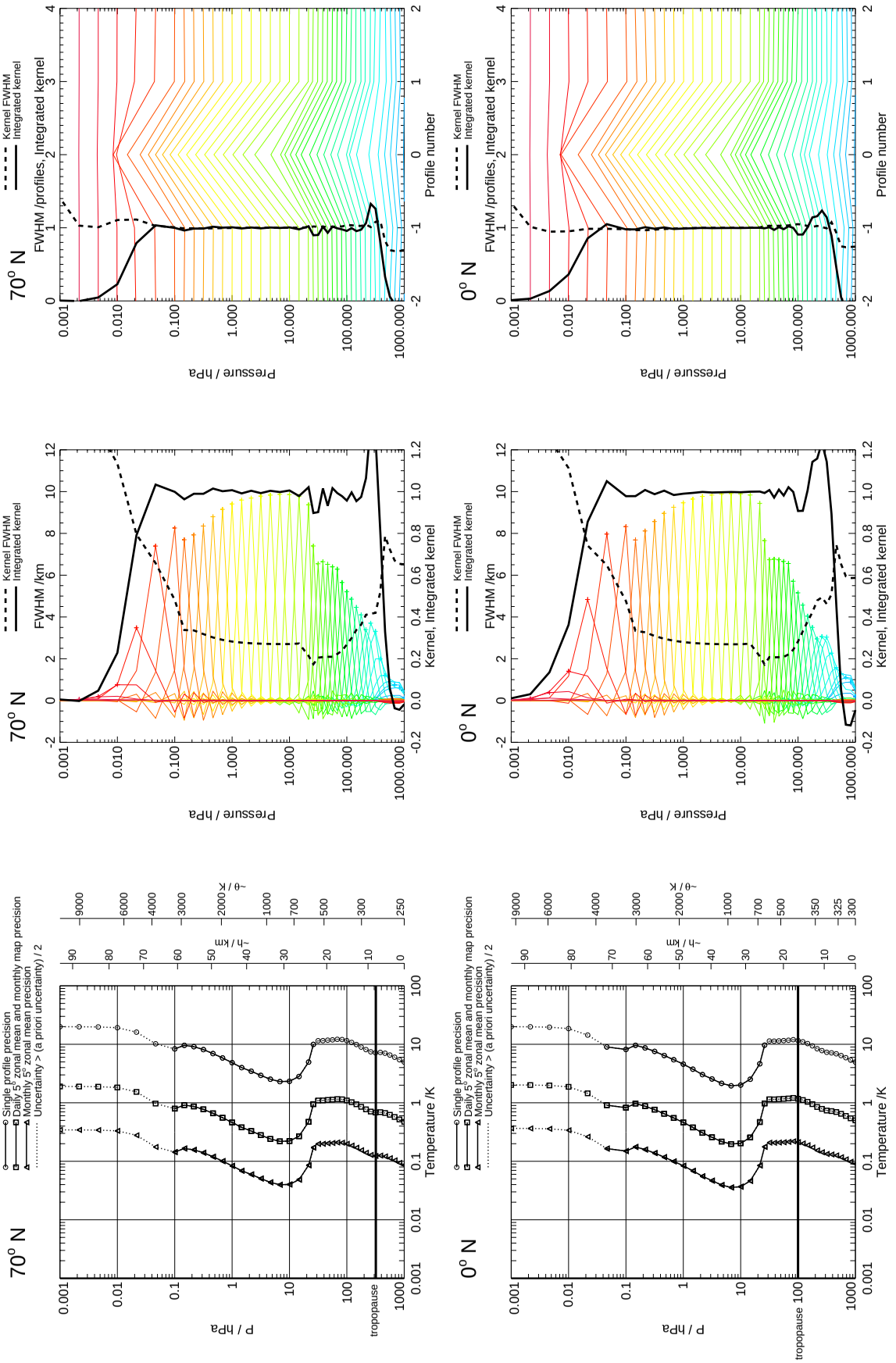

Figure 133: Temperature precision and averaging kernels, on high resolution grid, with no regularisation. Touchstone phase UpdatePtan.

Acronyms

ATBD	Algorithm Theoretical Basis Document
DACS	Digital Auto-Correlator Spectrometer
DU	Dobson Unit
EOS	Earth Observing System
FOV	Field of View
IWC	Ice Water Content
MLS	Microwave Limb Sounder
UARS	Upper Atmosphere Research Satellite

References

AFGL, 'Handbook of Geophysics and the Space Environment', 1985.

D.R. Allen, J.L. Stanford, N. Nakamura, M.A. Lopez-Valverde, M. Lopez-Puertas, F.W. Taylor, J.J. Remedios, 'Antarctic polar descent and planetary wave activity observed in ISAMS CO from April to July 1992', Geophys. Res. Lett., 27(5), 665–668, 2000.

G. Brasseur and S. Solomon, 'Aeronomy of the Middle Atmosphere', 2nd ed., D. Reidel, Dordrecht, 1986.

W. J. Collins, D. S. Stevenson, C. E. Johnson, R. G. Derwent, 'Tropospheric ozone in a global-scale three-dimensional Lagrangian model and its response to NO_X emission controls', J. Atmos. Chem., 26, 223–274, 1997.

A.E. Hedin, MSISE Model, 1990.

R.F. Jarnot, H.M. Pickett and M.J. Schwartz, 'EOS MLS Level 1 Data Processing Algorithm Theoretical Basis', JPL D-15210, Version 2.0, 22 June 2004.

J.S. Kinnersley and R.S. Harwood, 'An isentropic two-dimensional model with an interactive parametrization of dynamical and chemical planetary-wave fluxes', Quart. J. Roy. Meteorol. Soc., 119, 1167–1193, 1993.

N.J. Livesey and W. Van Snyder, 'EOS MLS Retrieval Processes Algorithm Theoretical Basis', JPL D-16159, Version 1.3, 21 June 2004.

J.A. Logan, 'An analysis of ozonesonde data for the troposphere: recommendations for testing 3-D models and development of a gridded climatology for tropospheric ozone', J. Geophys. Res., 104(D13) 16115–16149, 1999.

A.H. Oort, 'Global Atmospheric Circulation Statistics', NOAA Professional Paper 14, Rockville, 1983.

H.M. Pickett, R.L. Poynter and E.A. Cohen, 'Submillimeter, Millimeter, and Microwave Spectral Line Catalogue', JPL Publication 80-23, Rev. 3, 1992.

H.C. Pumphrey, 'Future measurements of ozone in the MLT', poster presented at AURA Science Team Meeting, April 2002.

H.C. Pumphrey, D. Rind, J. M. Russell III and J. E. Harries, 'A preliminary zonal mean climatology of water vapour in the stratosphere and mesosphere', Adv. Space Res., 21(10), 1417–1420, 1998.

W.G. Read, Z. Shippony, and W. Van Snyder, 'EOS MLS Forward Model Algorithm Theoretical Basis Document', JPL D-18130, Version 1.3, 26 April 2004.

W.G. Read, L. Froidevaux and J.W. Waters, 'Microwave Limb Sounder measurement of stratospheric SO_2 from the Mt. Pinatubo volcano', Geophys. Res. Lett., 20(12), 1299–1302, 1993.

C.P. Rinsland, M.R. Gunson, R. Zander, M. Lopez-Puertas, 'Middle and upper-atmosphere pressure-temperature profiles and the abundances of CO_2 and CO in the upper-atmosphere from ATMOS SPACE-LAB 3 observations' J. Geophys. Res., 97(D18), 20479–20495, 1992.

C.D. Rodgers, 'Retrieval of atmospheric temperature and composition from remote measurements of thermal radiation', Rev. Geophys. Space. Phys., 14, 609–624, 1976.

C.D. Rodgers, 'Characterization and error analysis of profiles retrieved from remote sounding measurements', J. Geophys. Res., 95(D5), 5587–5595, 1990.

M.J. Schwartz, W. Van Snyder and W.G. Read, 'EOS MLS Mesosphere-Specific Forward Model Algorithm Theoretical Basis Document', JPL D-28534, Version 0.1, 30 April 2004.

T. Shimazaki, 'Minor Constituents in the Middle Atmosphere', Terra Scientific, Tokyo, 1985.

S. Solomon *et al.*, 'Photochemistry and transport of carbon monoxide in the middle atmosphere', J. Atmos. Sci., 42(10), 1072–1083, 1985.

W.-C. Wang, X.-Z. Liang, M.P. Dudek, D. Pollard, S.L. Thompson, 'Atmospheric ozone as a climate gas', Atmos. Res. 37, 247–256, 1995.

J.W. Waters and L. Froidevaux, 'An Overview of the EOS MLS Experiment', JPL D-15745, Version 2.0, 2 April 2004 draft.

J.W. Waters *et al.*, 'Validation of UARS Microwave Limb Sounder ClO measurements', J. Geophys. Res., 101(D6), 10091–10127, 1996.

D.L. Wu and J.H. Jiang, 'EOS MLS Algorithm Theoretical Basis for Cloud Measurements', JPL D-19299, Version 0.9, 26 April 2004.